January 2017

A Radioelement Analysis Of The Northern Black Hills, South Dakota, U.S.A.

Dylan Wade Young

A RADIOELEMENT ANALYSIS OF THE NORTHERN BLACK HILLS, SOUTH DAKOTA, U.S.A.

by

Dylan Wade Young
Bachelor of Science, University of North Dakota, 2014

A Thesis

Submitted to the Graduate Faculty

of the

University of North Dakota

in partial fulfillment of the requirements

for the degree of

Master of Science

Grand Forks, North Dakota

December
2017

This thesis, submitted by Dylan Young in partial fulfillment of the requirements for the Degree of Master of Science from the University of North Dakota, has been read by the Faculty Advisory Committee under whom the work has been done and is hereby approved.

Dr. William Gosnold

Dr. Stephan Nordeng

Dr. Dexter Perkin

This thesis is being submitted by the appointed advisory committee as having met all of the requirements of the School of Graduate Studies at the University of North Dakota and hereby approved.

Dean of the School of Graduate Studies

December 6, 2017

Date

PERMISSION

Title A Radioelement Analysis of the Northern Black Hills, South Dakota, U.S.A.

Department Harold Hamm School of Geology and Geological Engineering

Degree Masters of Science

In presenting this thesis in partial fulfillment of the requirements for a graduate degree from the University of North Dakota, I agree that the library of this University shall make it freely available for inspection. I further agree that permission for extensive copying for scholarly purposes may be granted by the professor who supervised my thesis work or, in his absence, by the Chairperson of the department or the dean of the School of Graduate Studies. It is understood that any copying or publication or other use of this thesis or part thereof for financial gain shall not be allowed without my written permission. It is also understood that due recognition shall be given to me and to the University of North Dakota in any scholarly use which may be made of any material in my thesis.

Dylan Young

Date 12/06/2017

TABLE OF CONTENTS

LIST OF FIGURES

FIGURE Page

LIST OF TABLES

LIST OF APPENDICES

APPENDIX Page

LIST OF ACRONYMS

3D	Third Dimensional
α	Alpha decay/particle
β	Beta decay/particle
β^+	Positron decay/emission
β^-	Beta minus decay/electron capture
BH	Black Hills
BSE	Bulk Silicate Earth
cm	Centimeter
DUNE	Deep Underground Neutrino Experiment
DUSEL	Deep Underground Science and Engineering Laboratory
e^-	Electron
ε_v	Antineuntrino Luminosity (particles emitted per mg per second)
Elev.	Elevation
ft	Foot(feet)
Fm	Formation(s)
γ	Gamma decay/particle, photon
g	Gram
GPS	Global Positioning System
GRS	Gamma-ray Spectrometer/Spectrometry
Ge	Germanium
HGM	Homestake Gold Mine

HHSGGE	Harold Hamm School of Geology and Geological Engineering
IDW	Inverse Distance Weighted
K	Potassium
Kg	Kilogram
Km	Kilometer
LBNE	Long Baseline Neutrino Experiment
Lv	Luminosity
M	Mass
m	Meters
MeV	1,000,000 (M) electron volts (eV)
$mg^{-1}s^{-1}$	Per milligram per second
mm	Millimeter
MW	Megawatt
mW	Milliwatt
mW/m^2	Milliwatts per meter squared
µW	Microwatt
$µW/m^3$	Microwatts per meter cubed
n	Neutron
NBH	Northern Black Hills
ρ	Proton
pct	Percentage
ppm	Part Per Million

Q	Radiogenic heat
q	Heat flow
REE	Rare Earth Element(s)
Rn	Radon
Rxn	Reaction
SD	South Dakota
SDev	Standard deviation
SDSTA	South Dakota Science and Technology Authority
SED	Standard Electrode Detector
SMU	Southern Methodist University
SURF	Sanford Underground Research Facility
Th	Thorium
Tl	Thallium
TW	Terawatt
U	Uranium
UND	University of North Dakota
USGS	United States Geological Survey
$\boldsymbol{V}$	Neutrino
$\boldsymbol{\overline{\nu}}$	Antineutrino
$\boldsymbol{\overline{\nu}_e}$	Geoneutrino (electron antineutrino)
W	Watts
Yrs	Years

ACKNOWLEDGEMENTS

I would first like to sincerely thank all the members of my advisory committee (Dr. William Gosnold, Dr. Dexter Perkins, and Dr. Steven Nordeng) for all of their assistance, encouragement and guidance towards this research. I would like that thank the faculty at Harold Hamm School of Geology and Geological Engineering for all of their generosity. Appreciation to Dr. Anna Crowell, Dr. James Crowell, and Darin Buri for their kindness, assistance and feedback throughout the years. Special thanks to Dr. Ronald Matheney, Dr. Stacy Bjorgaard, and Dr. Dennis Taylor, for their critique during the development of this thesis. Cheers to Daniel (Burke) Brunson, Caitlin Hartig, Faye Ricker, and the other members of the UND Geothermal Team.

My research and thesis would not have completed without the financial assistance provided by the North Dakota Space Grant Consortium Graduate Fellowship and NASA, by the Harold Hamm Experience Fund from the Harold Hamm School of Geology and Geological Engineering, and by the Graduate Student Travel Funding at UND's Office of the Vice President for Research and Economic Development. I appreciate the financial assistance granted from Gran Sasso Science Institute to attend the 2016 Summer Institute for Particle Physicists and Geologists in L'Aquila, Italy to improve my understanding on the subject.

My research could not have been completed without the help and assistance of everyone at the Sanford Underground Research Facility, who operate the Homestake Gold Mine. My appreciation goes out to the (South Dakota Science and Technology

Authority (SDSTA) employees, Kathy Hart (geology consultant) and Tom Regan (guide-safety-assistant) for their assistance and guidance inside the Homestake Gold Mine. Additionally, special thanks is to Jaret Heise (Science Liaison Director at SURF) for permitting my survey, as well as providing guidance over the horrifying battle with paperwork.

Finally, I would like to thank my friends, family and colleagues for their optimism and encouragement which helped me to persist throughout college.

Dedicated to my family:

My father and mother, Kevin and Denise Young,

My little sister and brother-in-law, Haley and Evan Soulek,

And my older brother and sister-in-law, Mike and Sarah Young

ABSTRACT

The uranium, thorium, and potassium contents from 736 samples, within a 15-km radius of the Homestake Gold Mine and Sanford Underground Research Facility in the Northern Black Hills indicate the geoneutrino background may be higher than average for the continental crust. The radioactive element contents of igneous, metamorphic, and sedimentary rocks were determined by gamma ray spectrometry. Many rocks show hydrothermal and metamorphic alteration within the last ten Ma of the Tertiary period. Young alkali rich igneous rocks, such as rhyolite, phonolite and other volcanic rocks, have lower than average Th:U ratios. The radioelement content of 215 igneous rocks were determined. The radioelement contents of 143 metamorphic rocks were determined. This study also shows that metamorphic rocks were found to have low variable U:Th content when compared to content in igneous rocks. Sedimentary rocks, in general, have low U, Th, and K content. The radioelement content of 236 sedimentary rocks were determined.

Rocks present within the Homestake Gold Mine, are highly altered by hydrothermal and metamorphic activity, enriching U, and in some areas, Th content. The Homestake Gold Mine lies almost entirely within metamorphic rocks. Igneous rocks occur in the mine as veins and dikes. The dominant igneous rock present is rhyolite. Metamorphic rocks present inside the HGM, were divided by formation; Ellison Fm, Poorman Fm, Yates Unit [lower Poorman Fm], Homestake Fm, and Flagrock Fm. The finding of high radioelement content in the rocks suggests that the antineutrinos

background at the HGM will need to be considered and calibrated for, in future experiments conducted at the Sanford Underground Research Facility. A geoneutrino luminosity of $1.26x10^5$ ($mg^{-1}s^{-1}$) was calculated from the samples analyzed within the Homestake Gold Mine. A total geoneutrino luminosity of $4.44x10^5$ ($mg^{-1}s^{=1}$) was calculated from the sum of all analyses conducted in the Northern Black Hills.

CHAPTER I

RADIOACTIVITY IN NORTHERN BLACK HILLS, SOUTH DAKOTA

Purpose of the Research

This project seeks to determine radioactive heat production from uranium (U), thorium (Th), potassium (K), and to estimate geoneutrino luminosity in the area surrounding the Homestake Gold Mine (HGM) in the Northern Black Hills (NBH), of South Dakota (SD). This thesis study is key to the Sanford Underground Research Facility (SURF), which plans to install a geoneutrino detector as part of the Deep Underground Neutrino Experiment (DUNE) at the 4850-foot (ft) level of the HGM. The DUNE facility began excavation and construction on July 21, 2017, and should be operational by 2027 (DUNE).

An estimate of the background geoneutrino flux (flow of particles) can be determined from the U, Th, and K content in the rocks surrounding the HGM. Naturally occurring radioactivity in these three elements produces geoneutrino emissions. Igneous rocks from different eras, and metamorphic rocks from the Precambrian eon in the Black Hills, contain significant amounts of U, Th, and K.

Sampling at the crust's surface would only provide a two-dimensional section of a three-dimensional source. By providing a systematic model of the plutonic emplacement present in the NBH, and estimating the radioactive contribution of U, Th, and K within the pluton, plausible geoneutrino luminosity values can also estimate potential neutrino flux emissions.

Data collection in this study focused on igneous and metamorphic rocks within a 15-kilometer (km) radius of the HGM and included a gamma ray survey inside the HGM. Data were analyzed in the Geothermal Laboratory facilities using associated computational resources at the University of North Dakota (UND).

A related goal of this project is to understand the role of heat production in the Black Hills where heat flow is abnormally low ($q= 24.4\pm5.4$ mW m^{-2}, N=9) (Gosnold, 1999). Regional heat flow, excluding the Black Hills, averages 62.1 ± 10.5 mW m^{-2} (N=95) and is typical for the continental crust (Gosnold, 1999).

Hypothesis

The Deep Underground Neutrino Experiment (DUNE) will use the 4850-ft level of the former Homestake Gold Mine in the Black Hills of South Dakota for installation of the neutrino detector. Accurate neutrino detection requires a separation of the neutrino source flux and the experiment neutrino emission. Antineutrinos, also known as geoneutrinos, are emitted during radioactive decay of ^{235}U, ^{238}U, ^{232}Th, and ^{40}K which occur naturally in Earth's crust and mantle. The concentrations of these radioactive elements correlate with silica content (Table 1) and are highest in young aphanitic, intrusive rocks (Adams, 1959; Whitefield, 1959).

Table 1. Average % of silica content in various igneous rocks (Ehlers, 1982)

% SiO_2	Terminology	Rock Type
>66	Felsic	Granite-Rhyolite
52-66	Intermediate	Diorite-Andesite
45-52	Mafic	Gabbro-Basalt
<45	Ultra-mafic	Dunite-Peridotite

The Black Hills were uplifted during the Laramide Orogeny (Paleogene Period). Plutonic intrusions followed this uplift, allowing for REE and heavy elements to be introduced. Laramide uplift and Cenozoic plutonic intrusion may have allowed the radioactive element content of the Black Hills to be higher than crustal norms. Previous studies of crustal radioactivity in North America indicated the highly radioactive parts of the intrusive series are within the upper one to two km of the crust (Roy et al., 1972) or at most the upper six km of the crust (Phair and Gottfried; 1964).

This study was designed to determine if the radioelement contents of igneous and metamorphic rocks within a 15-km radius of the DUNE site would be higher than continental norms. My hypothesis is: The radioelement content present in the Northern Black Hills has been enriched allowing for a higher neutrino background when compared to global averages.

Research in the Black Hills and the Homestake Gold Mine

The geology of the Black Hills has been studied for more than 150 years (Stillwell, 1895; Vickers, 1954; Ziegler, 1914). The BH are considered an unspoiled location to host particle physics research, specifically inside the HGM (SURF, 2016). Raymond Davis conducted early particle physics experiments deep inside the HGM in the 1960s (McDonough, 2012). These experiments uncovered and established the idea of neutrino oscillations and various “flavor” states of neutrinos (McDonough, 2012). After the success of Davis’ experiment, mining continued inside HGM for the next four decades until 2001, when all the mining operations were shut down. In 2006, the closed HGM was converted to the Sanford Underground Research Facility.

During the years of 2013 to 2014, Eric Zimny (MS-UND) examined the radioactive contribution and geoneutrino luminosity present in massive igneous outcrops in the NBH (Zimny, 2014). This preliminary study was conducted on an 18-km radius surrounding the HGM (Zimny, 2014). Zimny (2014) collected 41 rock samples with the results shown in Table 2.

Table 2. Average U, Th, and K content in Zimny's samples from the Black Hills

Radioactive Averages	**U (ppm)**	**Th (ppm)**	**K (pct)**
	2.8 ± 1.9	13.4 ± 14.5	1.9 ± 0.7

(Zimny, 2014)

Zimny's research consisted largely of rhyolite or other volcanic, silica-rich rocks. Estimations of radioelement abundances and SiO_2 content in rocks in continental crust are present in Tables 3.

Table 3. Radioelement Abundances in Earth's Continental Crust.

Radioelemental Abundances in Continental Crust					
	U (ppm)	**Th (ppm)**	**K (pct)**	**Th:U Ratio**	**SiO_2 (pct)**
Taylor & McLennan, 1995	0.9	5.5	1.3	6.1	57.1
Rudnick & Fountain, 1995	1.4	5.6	1.9	4.0	-
Rudnick & Gao, 2003	-	-	-	-	60.6

Bulk silicate Earth (BSE) refers to the primitive mantle composition of Earth's silicate section prior to differentiation of the first crust (Pinti, 2014). BSE models estimate the abundance of U, Th, and K present on Earth by relying on cosmogenic abundances of the radioelements combined with global sampling (McDonough, 1995).

Estimates of the radioelement content of Earth's upper crust (Wollenberg, 1987) are present in Table 4.

Table 4. Radioelement Concentrations of Earth's Upper Crust (Wollenberg, 1987)

	U (ppm)	**Th (ppm)**	**K (pct)**	**Heat Production (μWm^{-3})**
Mean Sedimentary Rocks	4.0	9.1	1.4	2.2
Metasedimentary Rocks	3.0	12.0	2.2	2.5
Mean Igneous Rocks	10.0	32.6	2.5	4.8
Mean Igneous Rocks (*excluding alkali feldspathic rocks*)	2.7	10.2	1.9	2.1
Metaigneous Rocks	4.0	14.8	2.5	3.1

Results from Zimny's investigation bring into question whether the assumed radioactivity present around HGM should not be based on the BSE model. Zimny's study provided GIS-based maps of the igneous rock intrusion surrounding the HGM (Zimny, 2014). Zimny's (2014) maps indicate both high and low radioactivity concentrations in the surrounding region. The abundance of U, Th, and K were higher in Zimny's (2014) study than what the BSE models (McDonough, 1995) predict near the HGM. This signifies a need for a comprehensive analysis of the radioactivity present in the NBH, in order to determine the background neutrino flux which may interfere with DUNE's detector results.

Natural radioactive decay is present in all rock types across Earth. During each beta decay, according to Fermi's theory, both a beta particle and a neutrino are emitted with complimentary kinetic energy, to satisfy the first law of thermodynamics (conservation of energy) (Fermi, 1934; Faure, 1977). This natural geoneutrino generation, is thus influenced by the local geology present at the HGM and the NBH. Any unknown variations and distribution in radioactivity and local geological contributions may hinder

the outcomes of the DUNE research. There are uncertainties regarding the overall content of radioactivity and current estimates of the radiogenic contributions need further improvement.

Earth's thermal history is important in understanding the total internal heat present due to radioactive decay; however, many uncertainties are present specifically concerning the total abundance of U, Th, and K in Earth's interior (Sramek, 2012). Consequently, radioactive decay produces heat (radiogenic heat), and is one of the contributors to heat flow in Earth's interior.

CHAPTER II

RADIOACTIVITY AND EARTH'S INTERNAL HEAT CONTRIBUTION

Fundamentals of Earth's Internal Heat and Influence of Radioactivity

The main contributors to radiogenic heat are ^{232}Th, ^{235}U, ^{238}U, and ^{40}K (Milsom and Eriksen, 2015; Beardsmore, 2001). The linear relationship between heat flow and heat production suggests that U and Th are concentrated in the upper 10 km of Earth's continental crust (Roy et al., 1968). U, Th, and K are all lithophile elements and correlate with silica content and the emplacement depth of plutonic rocks (Roy et al., 1972; Roy et al., 1968). Lachenbrunch (1970) proposed that the heat flow/heat production relationship is best explained by an exponential decrease of radioactivity with depth. Large igneous intrusions may affect the surrounding Earth's crust and modify the contingent U and Th content and its distribution (Roy et al., 1972). Current estimates suggest an average Th:U ratio between 6:1 (Taylor & McLennan, 1995) and 3:1 (Palme and O'Neill, 2003) on Earth (see Table 1 & 2). The BSE model suggests that the Th:U ratio ranges from approximately 3.0 (Palme and O'Neill, 2003) to 3.9 (McDonough, 1995).

Estimates of Earth's internal heat are derived dependent on radioactive contribution and calculated heat flow from dispersed locations in Earth's interior through various geophysical methods (Birch et al., 1968). Disparities between heat sources and influences (i.e., varying topographies, geological, and climatic histories) challenge many measurements, since essential factors in continental and oceanic crusts are unknown or are poorly understood (Birch et al., 1968). Heat flow may be impacted by mixtures of the disparities and measuring the heat flow has difficulties.

Heat flow measurements may end up limited and costly. Practical measurements require many calibrations for reasonable accuracy (Birch et al., 1968). The distribution of heat flow observations and measurements are also greatly uneven when comparing oceanic and continental data (Beardsmore and Cull, 2001). Opportunities for continental and marine observations are largely limited to cost, with continental observations generally inadequately funded (Beardsmore and Cull, 2001). Marine observations are a fraction of the price of continental drilling for heat flow observations (Beardsmore and Cull, 2001). Continental measurements must be taken from deep boreholes in bedrock, with the temperature measurements being discrete and allowing for proper calibrations and determination of the mean temperature gradient (Birch et al., 1968). Lastly, there should be a general dispersion of thermal conductivity (Birch et al., 1968).

Even with accurately measured and calibrated heat flow determinations, some "conspicuous" anomalies are present (i.e., the high heat flow values present in the Basin and Range province in North American) (Birch et al., 1968). The local radioactive contribution must be taken into consideration when measuring heat flow and estimating heat production (Birch et al., 1968).

Current constraints, like mentioned above, make it impossible to directly measure the heat production in the Earth's mantle (Jaupart, 2011). Earth's heat flux derives from several sources: secular cooling, convective and advective mantle flows, and radioactive heat production from U, Th, and K in both the mantle and crust. Radioactive heat production contributes approximately 28 terawatts (TW) (Anderson, 2007) of Earth's total estimated surface heat flux of 47 TW (Davies & Davies, 2010). Radioactive heat is a major contribution to the total heat present on Earth. Mantle heat flow estimates range from 10 mW m^{-2} to 45 mW m^{-2} (Thakur and Blackwell, 2014) depending on the geological setting. Radiogenic heat production estimations of Earth's crust range from 4.46 x 10^{12} μW m^{-3} (McDonough and Sun, 1995) to 1.79 x 10^{12} μW m^{-3} (Anderson, 2007). Secular cooling contribution estimates range from 9 TW to 15 TW of the total surface flux on Earth (Anderson, 2007).

The large ranges in estimating total surface heat flux, mantle heat flow, crustal radioactivity, and the subsequent controversies over the heat flow/heat production relationship in the continental crust (Vedanti et al., 2014) are primarily due to inadequate data. Estimates of the total heat flux from Earth's interior increased from 32 ± 3 TW in 1965 (Lee and Uyeda, 1965) to 47 TW ± 2 TW in 2010 (Davies and Davies, 2010) as the number of heat flow data points increased from a few thousand to 58,536 data points, and analytical methods improved. The supplemental data necessary to improve understanding of the overall radiogenic contributions, has not increased as needed. Only 2,088 of 37,299 continental heat flow observation points on Earth include data on radioactive heat production. A simple test of the linear relation between heat flow and radioactive heat production yields a weak positive correlation (based on data provided by the International Heat Flow Commission) (Roy et al., 1972). There is inadequate data on igneous and metamorphic rocks from the heat flow observations (Roy et al., 1972). The correlation mixes the data from plutonic and metamorphic rocks. Both rock types have different compositions and formational histories; thus, the correlation cannot yield any comparative information.

The limitations associated with determining the total heat production on Earth have recently improved due to numerous observations from underground observatories being developed to detect natural and solar electron antineutrinos (geoneutrinos) (Jaupart, 2011; Fiorentini et al., 2005). McDonough and colleagues (2012) suggested that by measuring the flux of geoneutrinos from Earth's interior, it may be possible to independently determine the total U, Th, and K content in Earth's interior. Conversely, providing better constraints on heat flow may assist in designing experiments for geoneutrino detection (W. Gosnold, personal communication, 2017).

Neutrinos and Antineutrinos

Neutrinos and their antiparticles (antineutrinos) are produced by radioactive decay of elements in rocks present in Earth's interior (Jaupart, 2011). Geoneutrinos ($\bar{\nu}e$), also known as electron antineutrinos, are subatomic particles that are generated and emitted by the β^--decay of the radioelements ^{238}U, ^{235}U, ^{232}Th, and ^{40}K, or through electron capture of ^{40}K (Jaupart, 2011). Beta decay produces a daughter product, an electron, and an antineutrino. Electron capture produces a neutrino and a daughter product. The generation of geoneutrinos coincides with the emission of neutrinos. Both particles are "invisible" under normal circumstances. The particles are nearly weightless, travel near light speed through matter, and lack most measurable properties. Geoneutrinos, however, do interact with one type of force – weak nuclear force, which is the response of natural and non-natural (i.e., nuclear power) radioactive decay of U, Th, and K. Radioactive decay of U, Th, and K, only accounts for a fraction of the total neutrino flux present (Jaupart, 2011). The energy spectrum that is emitted from these three radioisotopes' decay is very distinctive, and the U and Th emissions can be easily spotted by neutrino

detectors (Jaupart, 2011). All the detectors currently in operation across Earth have sensitivity limitations which prevent ^{40}K antineutrinos from being detected due to their small size (Jaupart, 2011). The number of natural radiation events detected is limited; nuclear power plants also produce some neutrinos which contribute to global neutrino production. The nearest nuclear power plants to the NBH are in Welch, MN and Blaire, NE. Neutrinos, "undetectable particles," were originally hypothesized back in 1930 by Wolfgang Pauli to explain the missing energy of nuclear β-rays (β-decay) from emissions on the continuous energy spectrum (Usman, 2015).

β-decay is a process involving the emission of a β^- particle, associated with the conversion of a neutron in the β nucleus into a proton by the emission of an electron and an antiparticle (Aswathanarayana, 1985; Lilley, 2001). The following equations demonstrate how neutrinos and antineutrinos are generated through radioactive decay.

Equations 1 and 2:

$$n \rightarrow \rho + e^- + \bar{v} \text{ and } \rho \rightarrow n + e^+ + v$$

(Aswathanarayana, 1985; Lilley, 2001)

The symbol *n* represents the neutron being split by β-decay to a proton ρ, an electron e^-, and an antineutrino $\bar{v}$ (Aswathanarayana, 1985). Neutrinos (v) and antineutrinos ($\bar{v}$) are formed through a "weak nuclear force," resulting in delayed processes (Lilley, 2001). After 1930, numerous experiments identified and determined the presence of an additional particle collecting the energy, thereby providing agreement with the law of the conservation of mass. Enrico Fermi, in affiliation with the Manhattan Project, named the "undetectable particles," neutrinos (Lilley, 2001). Neutrinos are an uncharged fermion (particle) with almost nonexistent mass, and therefore are extremely

difficult to detect with previous equipment (Lilley, 2001). It was an additional twenty-five more years before neutrinos and antineutrinos were able to be detected and their existence proven by research conducted by Reins and Cowan in the mid 1950's (Lilley, 2001).

Another type of β^+ decay exists, known as electron capture, where a proton and electron are both transformed into a neutron and neutrino (Lilley, 2001). Equation 3 below demonstrates the β^+ decay process, based on Equation 1 & 2.

Equation 3:

$$p + e^- \rightarrow n + \bar{\nu}$$

(Lilley, 2001)

By measuring the emission energy levels of gamma-rays (γ-rays) from β-decay, scientists can accurately identify specific radioisotopes that are daughter products of the primordial U, Th, and K radioelements, enabling more unique applications to be applied in research (Lilley, 2001). By studying geoneutrinos and its relation to radioactivity, scientists can estimate the total radioactive content present within the Earth, as suggested by McDonough and colleagues (2012).

Currently in 2017, subatomic particles remain extremely difficult to detect. Only the most sophisticated equipment can detect any subatomic particles being emitted (McDonough, 2012). Today's equipment only recognizes a few counts of interaction with neutrinos per year (McDonough, 2012). Detection technology continues to improve over time, allowing for improved background calibrations (McDonough, 2012). By observing geoneutrinos over the past decade, scientists have determined better estimations of the total radiogenic heat production in Earth's interior, improving the calculated total heat

budget remaining for Earth (Enomoto et al., 2007; Jaupart, 2011; Mantovani et al., 2004). Radioactivity is a major component of Earth's internal heat flow. Subsequently, radioactivity is also a major contributor to the subatomic particles, neutrinos and antineutrinos, present within Earth's crust. The local geological contribution producing radioactivity must also be viewed in a similar manner.

CHAPTER III

GEOLOGIC HISTORY OF THE NORTHERN BLACK HILLS, SD

General Geology of the Black Hills

The BH are a "domelike" outlier of the Rocky Mountains, which uplifted during the Laramide orogeny in western North America (Vickers, 1954; Connolly, 1927). Precambrian rocks consist of various types of rocks (largely metamorphic), including amphibolite, schists, shales, slates, and some quartzite, all of which are cropping out of the central part of the Northern Black Hills (Vickers, 1954). Sedimentary rocks exposed in the BH range from Cambrian period through the Paleogene period (Vickers, 1954). Paleozoic sedimentary deposits range from 274 meters (m) thick in southern BH to 670 m thick in northern BH (Dewitt et al., 1986). Exposed intrusive and volcanic igneous rocks span from the Archean Era through the Cenozoic Era.

Prior to the Laramide orogeny, the Black Hills region was largely covered by Cretaceous embayment with deposition of sedimentary rocks between 850 m in southeast BH to 2130 m in northwest BH, on top of Precambrian metamorphic and igneous rocks (Dewitt et al, 1986; Vickers, 1954). A generic map of the BH geology is shown in Figure 1 (Karner ,1989; Karner, 1981; Gries, 1974; Lisenbee, 1978).

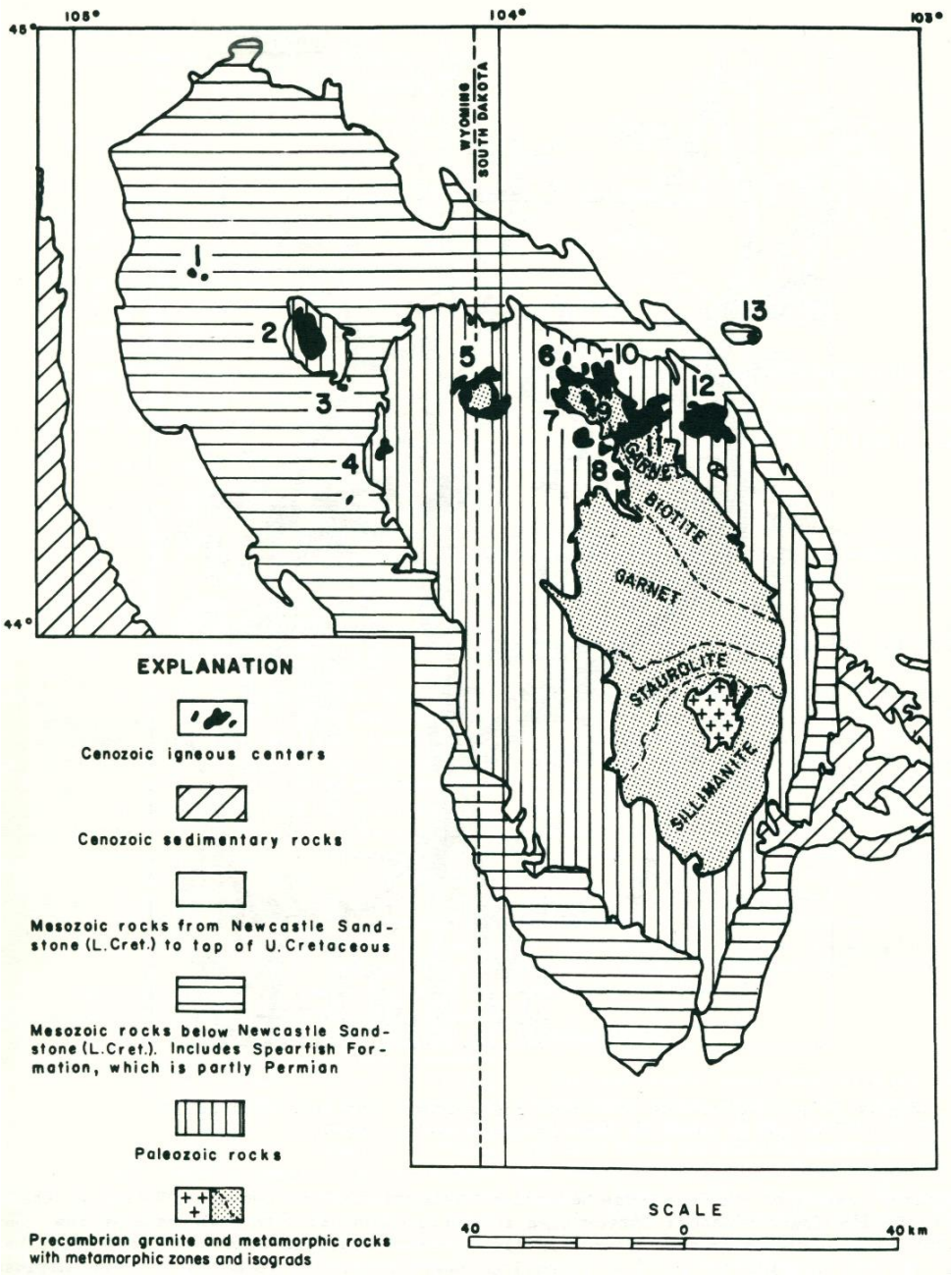

Figure 1. Generalized geology of the Black Hills, modified by (Karner, 1989). From (Gries, 1974), (Lisenbee, 1978) and (Karner, 1981). The numbers are igneous centers, including: 1.) Devils Tower; 2.) Bear Lodge Mtns; 3.) Sundance Mtn, 4.) Inyan Kara – Black Buttes; 5.) Mineral Hill – Tinton; 6.) Spearfish Carbonate; 7.) Terry Peak; 8.) Strawberry Hills – Custer; 9.) Cutting; 10.) Mount Roosevelt; 11.) Gilt Edge – Galena; 12.) Vanocker; 13.) Bear Butte.

During the Paleogene Period, alkali igneous rocks (i.e., rhyolite) intruded the Precambrian granite and pegmatite dikes. These later igneous events significantly enriched the BH with valuable economic ores and rare earth elements (REE) (Vickers, 1954). Numerous overlaying Mesozoic sedimentary deposits and Precambrian metamorphosed rocks developed in the BH (Vickers, 1954; Connolly, 1927). Four sedimentary formations (Fm) stand out due to Cenozoic plutonic intrusions and volcanic extrusions: the Deadwood (Cambrian), and the Whitewood limestone (Ordovician), Englewood (Devonian - Mississippian), and the Pahasapa Fm (Mississippian) (Vickers, 1954).

The Cenozoic igneous intrusions and extrusions include rhyolite, porphyritic trachyte, quartz-rich monzonite porphyries, grorudite, and phonolite (Vickers, 1954). The igneous rocks were rich in REE and other incompatible elements (due to unsuitable size and charge of ions and/or minerals) (Vickers, 1954). Approximately 65-60 Million Years Ago (Mya), these igneous bodies started to rise up from Earth's upper mantle and lower crust, uplifting Paleozoic and Mesozoic rocks (Dewitt, 1986; Paige, 1924). Almost all the ore-bearing deposits in the NBH are found in the Deadwood Fm (Lisenbee, 1986). Whitewood limestone also has REE ore occurrences, however, at a very low-grade (Lisenbee, 1986). The main exception to the lack of ore-bearing occurances in the NBH was the Homestake Fm, a metamorphic formation from the Paleoproterozoic Eon (Lisenbee, 1986). The stratigraphic sequence and types of metamorphic rocks present inside the HGM are listed in Table 4.

Table 5. Stratigraphic deposits of Precambrian Formations Present in Homestake Gold Mine (based on Paige, 1924; Connoly, 1925)

	Proterozoic Fm	**Rock Types**
Youngest	Grizzly	Metagraywacke, biotite schist
	Flag Rock	Biotite-sericite schist, graphitic schist
	Northwestern	(Biotite, quartz, sericite, garnet) schist
	Ellison	Quartzites, schist and phyllite
	Homestake	(Grunerite, siderite) schist, chert
	Poorman	(Biotite, carbonate) phyllite
Oldest	Yate Member	(Hornblende, plagioclase) schist

Precambrian formations (i.e., Homestake Fm), are rich with porphyritic gold-ore (Lisenbee, 1986). The REE-rich ore deposits in NBH are associated with mineralization of the Paleogene igneous bodies and the hydrothermal activity that occurred with the intrusions (Lisenbee, 1986; Vickers, 1954). A more detailed tectonic map of the Black Hills and igneous intrusions is shown in Figure 2 (Lisenbee, 1989). Additional information is available concerning the geology and REE ores present in the NBH and HGM is located on Connolly (1927) and Paige (1924), as well as the mineralogy and the mineral resources present in the Black Hills on Dewitt (1986).

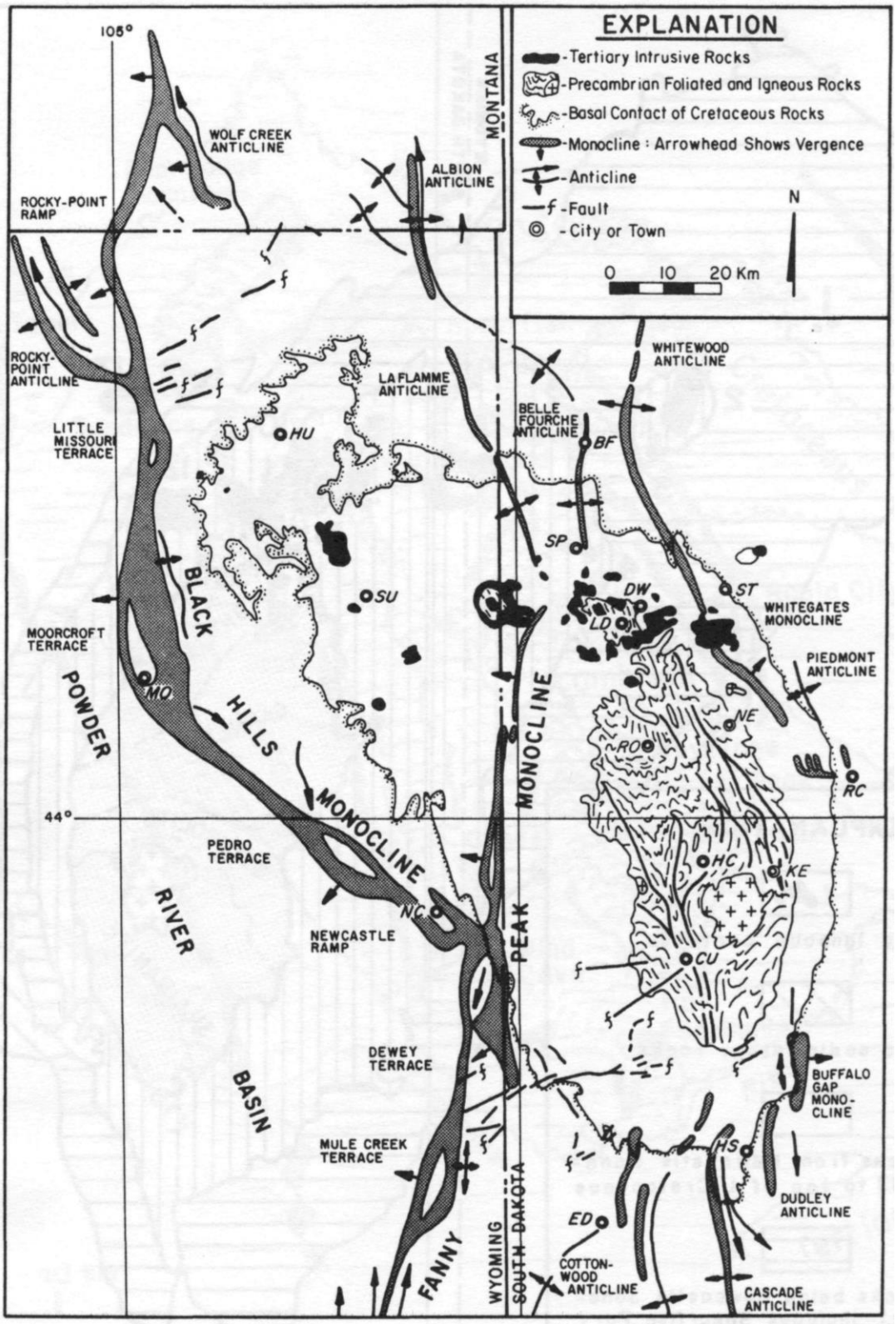

Figure 2. Tectonic Map of the Black Hills (Lisenbee, 1978; Lisenbee, 1985; Lisenbee, 1989).

Radioactivity in the Black Hills

Uranium, in the form of U-bearing mica was first reported in the NBH on Bald Mountain in 1895 by Stillwell (1895). In 1902, O'Harra mentions early U-bearing minerals in the BH, specifically in "torbernite" with copper and slate (Vickers, 1954). These U-bearing minerals are affiliated with porphyritic igneous rocks (Vickers, 1954). Ziegler (1914) studied torbernites at the Ross-Hannibal mine in the Lead district of Lawrence County, SD. Ziegler (1914) also discusses the mineral autumite (an uranium mineral) which was present in the phonolite porphyries at Annie Creek, in Spearfish Canyon, SD. From 1952 to 1954, numerous radioactive localities in the NBH were found during additional research conducted at Bald Mountain, in relation to exploration for REE and U-bearing deposits (Vickers, 1954). Abnormally high radioactive levels in intrusive rocks are present in the NBH, largely due to high Th content (Vickers, 1954). The radioactive occurrences were found in the altered conglomerates, siltstone and limestone present in the Deadwood Fm and Whitewood Fm, as well as some igneous intrusive rocks (Vickers, 1954).

U- and Th-bearing minerals are unable to exchange elements with minerals in common continental and oceanic rocks due to the large size ions of the radioelements (Vickers, 1954). Radioelements, like REE and ore minerals, travel with hydrothermal fluids (Vickers, 1954). Radioelements, however, are deposited at the edges of major REE ore accumulations (Dewitt, 1986; Paige, 1924; Vickers, 1954). There is a relationship between the zonal pattern of increased rare earth elements near gold accumulations and the U-bearing minerals near the edge of that zone (Vickers, 1954). Weathering of rocks

and soil leaching is much more frequent near the outer edges of zones of REE due to weaker ionic and molecular bonds (Vickers, 1954).

Aerial radiogenic surveys were also conducted in the BH for uranium exploration in the 1950's. As can be seen in airborne radioactive maps of the Nebraska Sand Hills to the southeast of the BH, ground covered by non-radioactive soils and clastic sediments mask gamma radiation. Data collected by airborne gamma-ray spectrometry surveys is limited to a maximum rock penetration depth of 30 cm (Bodorkos, et al., 2004; Hasterok and Chapman, 2011). The accuracy of aerial measurements is often hindered to depths of a couple cm by surface foliage and sedimentary coverage (Bodorkos, et al., 2004; Hasterok and Chapman, 2011). Most of the radioactive rocks in the BH have been covered by enough sand and foliage to affect aerial survey results.

Previous research on the radioactive content in the Black Hills may not be accurate. This study offers improved measurements on the localized geological contribution. The limitations which hindered previous research have been acknowledged and adjusted for, allowing for more accurate results. The data collection and methodology have been revised to accommodate specific rock types and rock formations present in the NBH.

CHAPTER IV

SAMPLE COLLECTION AND PREPARATION

Sampling

The initial sampling was conducted from early May until the end of June 2015. The region of this study was located mainly across Lawrence County and Meade County, SD. The radius of the study area is 15-km around SURF, which is centered on the Ross Shaft of HGM. This outer limit was set to quantify the natural radioactivity surrounding the HGM, and the known locations of Cenozoic igneous intrusions.

Figure 3. Google Earth view of the State of South Dakota. The Black Hills are in the Western portion on the map, with the study area highlighted in red.

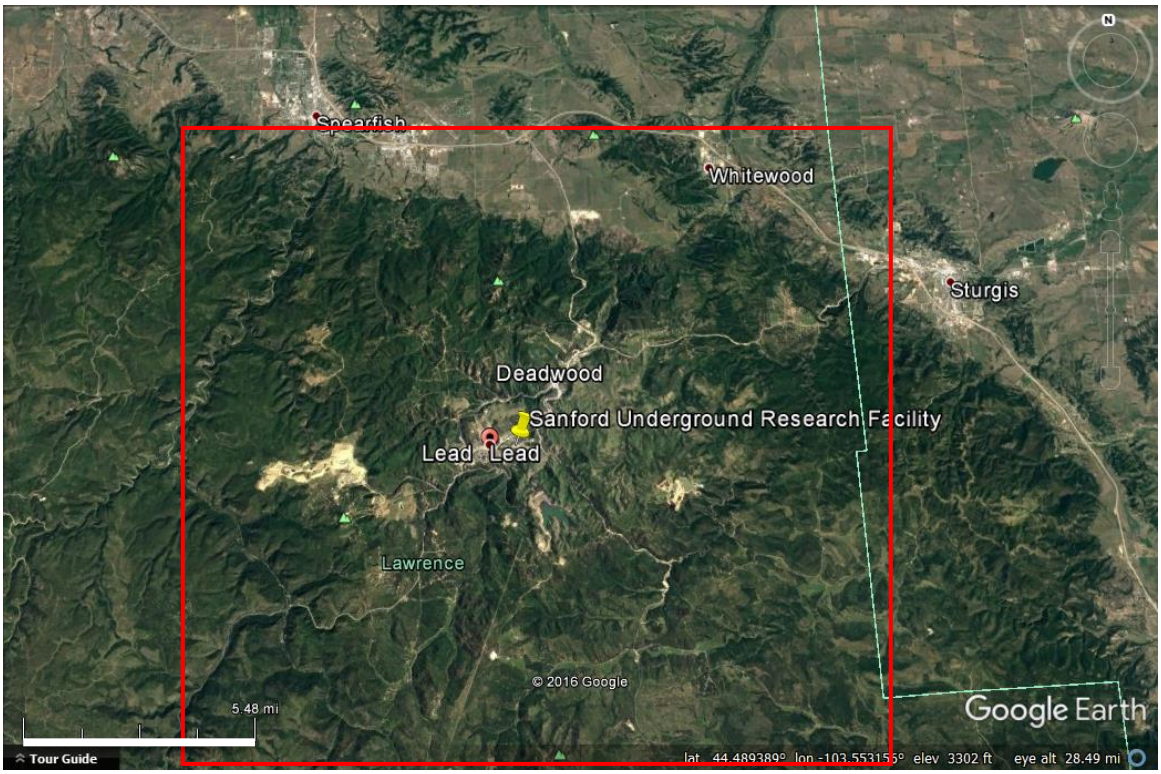

Figure 4. Closer Google Earth view of the Northern Black Hills, SD. The study area is highlighted in red.

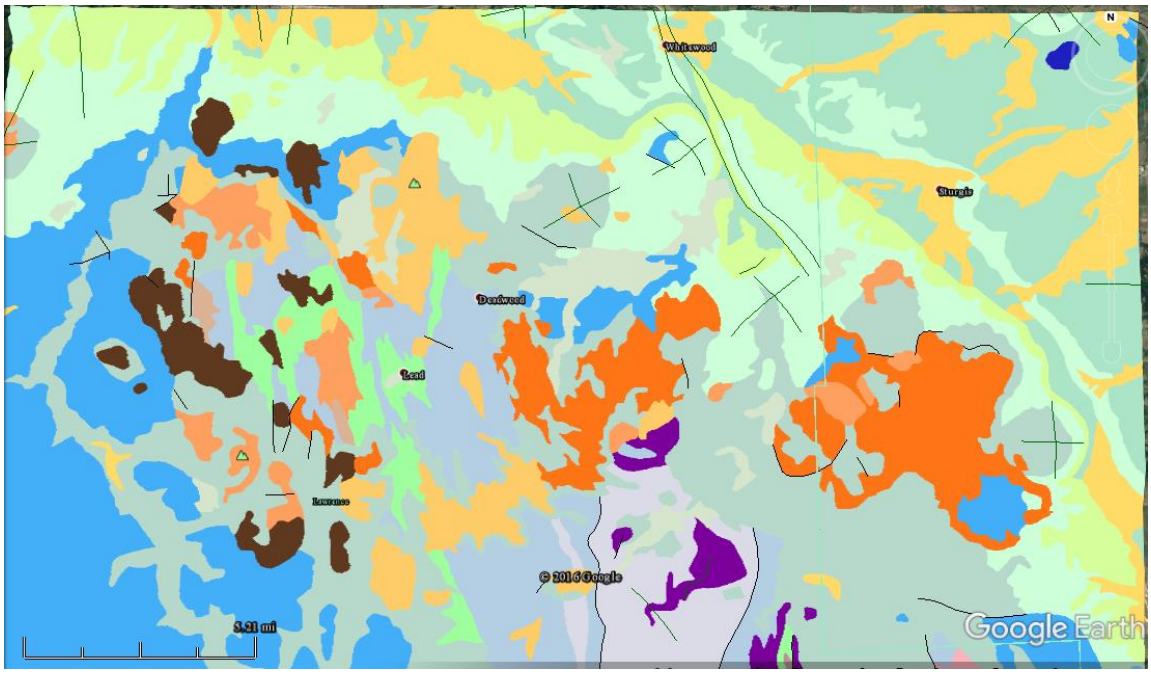

Figure 5. USGS Geological Map applied to Google Earth view of the Northern Black Hills, SD (Martin et al, 2004). See Fig. 6 for the lithology of the NBH.

Figure 6. Lithology of the Northern Black Hills, modified (Martin et al, 2004).

Lithology of Northern Black Hills			
Formation	***Age***	***Rock Types***	***Unit Color***
White River Group (Brule, Chadron, Chamberlain Pass, Slim Buttes)	Oligocene - Eocene	Claystone, siltstone, sandstone, conglomerates	
Phonolitic Intrusive Rocks	Eocene - Paleocene	Sills, laccoliths, and small stocks of phonolite, trachyphonolite and andesite	
Trachytic Intrusive Rocks	Eocene - Paleocene	Iron stained stocks, laccoliths, sills and dikes of trachyte, quartz trachyte	
Latitic Intrusive Rocks	Eocene – Paleocene	Laccoliths and sills of latite, latitic andesite, and quartz latite	
Rhyolitic Intrusive Rocks	Eocene - Paleocene	Stocks and laccoliths of rhyolite	
Inyan Kara Group (Fall River, Lakota)	Cretaceous	Variegated sandstone, siltstone and shale; silty shale, pebble conglomerate, bedded sandstone	
Morrison, Unkpapa Sandstone, Sundance, Gypsum Springs	Jurassic	Varied siliceous claystone, shale, siltstone & sandstone; bedded sandstone & limestone; massive gypsum w/ minor shale	
Spearfish	Jurassic – Permian	Red sandy shale, siltstone, sandstone, minor limestone, and interbedded gypsum	
Minnekahta Limestone & Opeche Shale	Permian	Bedded limestone, interbedded red shale, red siltstone and sandstone	
Minnelusa	Permian – Pennsylvanian	Interbedded sandstone, siltstone, shale, limestone, dolostone, chert & breccia	
Madison Group (Pahasapa, Englewood)	Mississippian - Devonian	Limestone, dolostone, dolomitic limestone	
Whitewood Limestone, Winnipeg, Deadwood	Ordovician - Cambrian	Fossiliferous limestone & dolostone, conglomerates, glauconitic sandstone and shale	

Figure 6. Cont.

Metagraywacke, metaconglomerate, metamorphosed black shale	Paleoproterozoic	Siliceous mica schist, impure quartzite, massive chert beds	
Metaquartzite	Paleoproterozoic	Quartzite, siliceous schist, minor chert	
Metamorphosed Siltstone & Shale	Paleoproterozoic	Phyllite, slate, schist	
Metamorphosed Basalt	Paleoproterozoic	Amphibolite, schist, greenstone	
Metamorphosed Basalt	Paleoproterozoic	Alkalic basalt, greenstone, volcanoclastics, actinolite schists	

Field Data Collection

Proper data collection and samples preparation is vital to obtain accurate results during any analysis. Efficient data collection involves collecting large enough samples that there will not be any daughter product loss during sample preparation. Samples must be fresh and clean so that there is no influence of weathering or biological processes that may affect readings during the analysis. Documentation on samples is just as important (i.e., site location, surrounding environment influence). Proper sample collection and sample preparation promotes accurate results through various analytical methods performed during this study.

The sample collection focused on rocks, largely from road cuts and outcrops present on accessible public land, or with permission granted by private land owners (personal comm.) A critical factor in this radioactive analysis is obtaining non-weathered samples (not affected by rain, surrounding environment, or other natural deteriorating processes.) Hydrothermal alteration, faulting, and weathering can cause loss of the U and

Th from the rocks (Tilling, 1969); therefore, fresh samples were of high importance. The survey consists of 301 sites analyzed using a RS-230 γ-ray Spectrometer (GRS) in the field (Fig. 7; Appendices A and B). A total of 295, one-kg samples, were collected for laboratory analysis from the selected sites (see Chapter V, Methodology.) The GPS coordinates for each site visited and the samples collected were recorded in a field notebook, along with additional attributes as listed in Table 6.

Table 6. Noted Site and Sample Attributes of NBH

Site Name	GPS Coordinates	U (ppm), Th (ppm), K (pct)	Rock Type
Attributes	Weathering	Alterations	Other Info

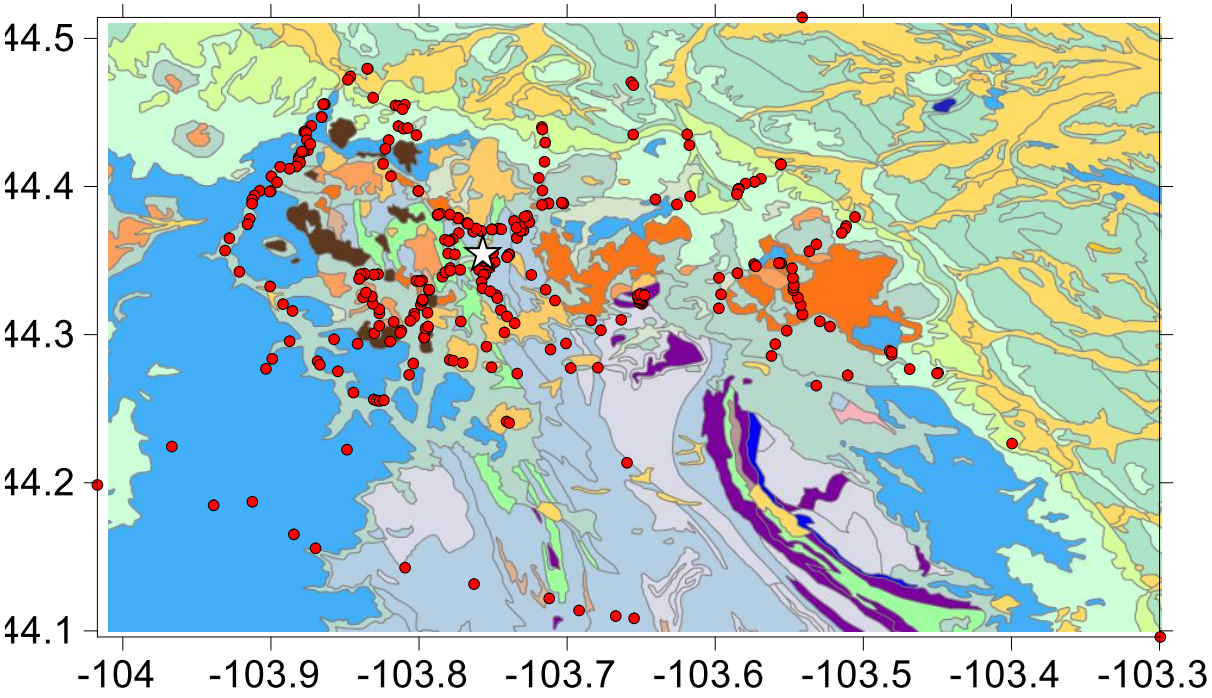

Figure 7. Geologic map of NBH area of study (Martin et al, 2004), modified in Surfer®. The white star is the location of the SURF and HGM. The red dots are sites surveyed during this study. Note: the geologic map is generalized; actual geology is highly variable by locality. See Fig. 6 for the lithology of the NBH.

Preparation

To prepare samples for GRS analysis, the rocks are cleaned and stripped of the weathered outer layer. Rock saws (Fig. 8 and Fig. 9) are used to strip the weathered material. Samples are further cut into rectangular strips that can be inserted inside a 4-cm by 4-cm opening inside a mechanical rock crusher. After crushing the samples into 2-cm by 2-cm fragments, the samples are then stored in 16 oz. paper containers to prevent cross contamination. All sample storage containers were stored for at least 45 days prior to the GRS analysis. The 45-day waiting period provides sufficient time for secular equilibrium to be restored in case of a loss of ^{222}Rn during sample preparation (based on the half-life of ^{222}Rn).

Figure 8. Rock saw in the sample preparation room used to cut large rocks into smaller segments that would fit inside of the rock crusher. The saw assisted in separating and removing the weathered sections of the samples.

Figure 9. Cut-off saw used for cutting specifically igneous rocks.

Figure 10. Rock crusher used to crush the fresh, clean section of rocks into 2-cm by 2-cm fragments. The paper storage container (Fig. 11) would be placed under the open section of the crusher to catch the small fragments.

Figure 11A and 11B. The pint-sized paper storage containers used to store the rock fragments after sample preparation.

Figure 12. Two hundred ninety-six samples were collected from the 2015 survey, located in the HHSGGE Geothermal Laboratory.

CHAPTER V
METHODOLOGY

This study incorporates Gamma-ray Spectrometry (GRS), mapping of the NBH, and calculating the antineutrino luminosity present in the NBH. GRS is used to determine the U, Th, and K content in each sample. Mapping consisted of the sample GPS coordinates and the distribution of the U, Th, and K content of each sample. Maps of the calculated heat production for each sample were also made. Lastly, calculations of the antineutrino luminosity are made for each rock sample to allow for the creation of luminosity contour maps of the NBH.

Gamma-ray Spectrometry

Two gamma-ray spectrometer detectors are used: a RS-230 Bismuth Germanate Oxide (BGO) Super-Spec Gamma-ray Spectrometry portable radiation detector for field analysis, and University of North Dakota's Canberra Germanium (Ge) Standard Electrode Detector (SED) Gamma-Ray Spectrometer for individual samples.

Figure 13. HHSGGE Geothermal Laboratory's Canberra Ge SED GRS

Figure 14. HHSGGE Geothermal Laboratory's RS-230 BGO GRS portable radiation detector

The gamma-ray windows about the centroids of the energy peaks were preset at 7 keV by Canberra, and the total counts within each window used in the analyses. The instrument is calibrated using two standards each of known K, U, and Th concentrations (Table 7) that are loaned to UND by the Geothermal Laboratory at Southern Methodist University (SMU). Table 8 lists the gamma-ray energy peaks and isotope sources for the gamma rays.

Table 7. Gamma-ray peaks and isotope sources of the γ rays

	U_1	**Th_1**	**Th_2**	**U_2**	**K**	**U_3**	**Th_3**
MeV	0.62	0.91	0.96	1.12	1.46	1.76	2.62
Parent	^{238}U	^{232}Th	^{232}Th	^{238}U	^{40}K	^{238}U	^{232}Th
Isotope	^{214}Bi	^{228}Ac	^{228}Ac	^{214}Bi	^{40}Ca & ^{40}Ar	^{214}Bi	^{208}Tl

Table 8. Standards with known concentrations of U, Th and K, present at the UND Geothermal Lab (samples loaned to UND from SMU)

Sample	U (ppm)	Th (ppm)	K (pct)	Mass (g)
SMU # 7	14.80	0.00	0.00	786.97
SMU # 8	27.80	0.00	0.00	786.80
SMU # 2	0.00	13.00	0.00	782.38
SMU # 4	0.00	26.30	0.00	783.81
SMU # 10	0.00	0.00	4.70	774.52
SMU # 11	0.00	0.00	10.10	688.18

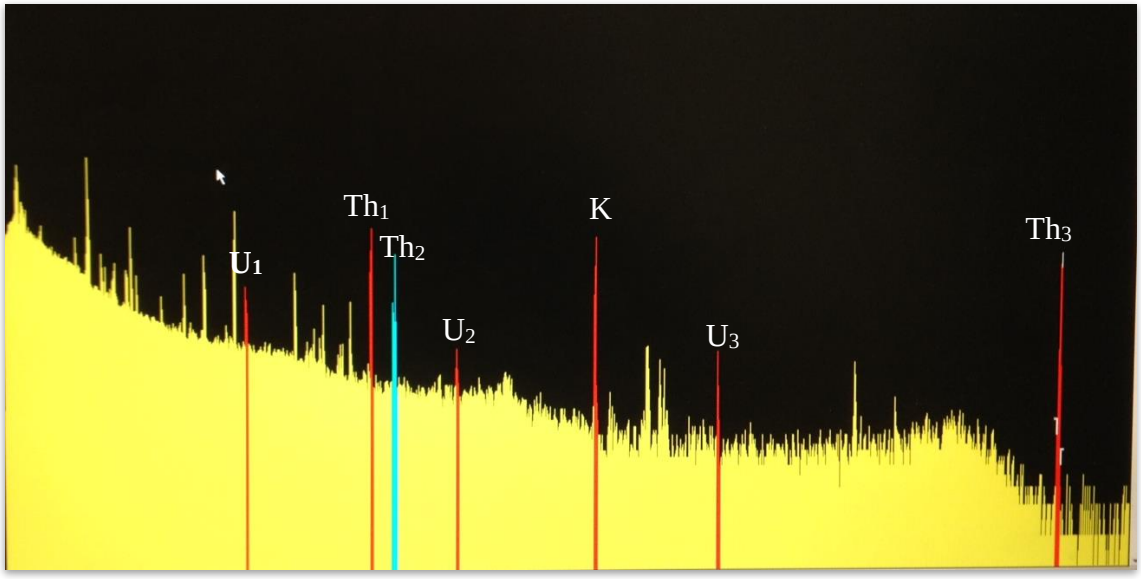

Figure 15. Gamma-ray emission spectrum determined by the SED of the Ge GRS. The peaks are of the daughter radioisotopes for calculating the abundance of ^{235,238}U, ^{232}Th and ^{40}K.

Recording the gamma-ray spectra of each standard sample for a 24-hour period, ten times, provides a calibration of counts per hour per ppm per unit mass in each of the seven windows. The total counts in each window correlate to the contributions of each

radioelement in a cascade of energy levels, due to Compton scattering of gamma rays after emission. The highest energy gamma-ray used in this analysis, 2.62 MeV from 208-thallium (^{208}Tl), adds some counts to each of the lower energy levels. Thus, the total count (C_t) in each energy window can be written as shown in Expression 1 below (Arya, 1966).

Expression 1: $$C_t = a_1U + a_2Th + a_3K$$

The counts in three selected windows, one for each radioelement, combine to form a set of simultaneous expressions as shown in Matrix 1 below (Arya, 1966). C_1, C_2, and C_3 represent the matrix constants in counts per ppm per element for the row matrix.

Matrix 1: $$C_1 = a_{11}U + a_{12}Th + a_{13}K$$

$$C_2 = a_{21}U + a_{22}Th + a_{23}K$$

$$C_3 = a_{31}U + a_{32}Th + a_{33}K$$

Solution of the three simultaneous expressions by inversion of the 3 x 3 matrices yields the concentrations of K, U, and Th. Measurements of the gamma-ray emissions fluctuated by ± 2% due to cosmic ray bombardment, setting the accuracy of this analysis to ± 2% as well.

Mapping of the Northern Black Hills

After the gamma-ray analysis, maps are created based on the populated data with Surfer®. Maps are formatted by gridding all the measured data and interpolations using the kriging method, a Gaussian process regression interpolation method in which the unmeasured data localities and values are estimated based on the previous covariance of the known data points. The kriging method is applied to promote smoother results when

compared to other interpolation methods (e.g., Inverse Distance Weighted [IDW], spline, and natural neighbor) for mapping, especially when dealing with data clusters.

Multiple maps of the concentrations of U, Th, and K were constructed based on the different rock types. Radiogenic heat production maps are also created for each rock type as determined from each of the two GRS instruments. Finally, statistical data is determined and plotted using Excel®. The statistical data is broken up into igneous, metamorphic, and sedimentary sections. Each of the three sections are total compilations of the U, Th, K, and heat production minimum, maximum, averages, median, standard deviation (SDev), variance, and count. The igneous, metamorphic and sedimentary sections are further broken up into individual rock types (i.e., rhyolite, phyllite, sandstone). The statistical data for individual rock types consists of the survey sample U, Th, K, and heat production averages, standard deviations and ratios.

Homestake Gold Mine Survey

A radioelement survey was conducted at SURF during September 2016 in addition to the initial GRS analysis. This survey took place at the surface and in the -1700, -4100 and -4850-ft levels of the HGM (equivalent to above sea level elevation of 3526, 1127, and 382 ft.) The survey analyzed 142 sites within the HGM property. This survey depended on the use of the RS-230 GRS since the radiation detector was small and handheld. Each survey location was documented by the calculated position coordinates, the GRS readings, rock type and/or formation. The survey consisted of the igneous rock rhyolite and the metamorphic rocks (i.e., Homestake Fm) scattered throughout the mine and property. The metamorphic formations and igneous rock types were the only rocks accessible at the HGM. The mapped position coordinates were later

converted to GPS coordinates at the Harold Hamm School of Geology and Geological Engineering (HHSGGE) Geothermal Laboratory.

The -1700 and -4100-ft levels of HGM were the largest contributions to this survey. A total of 60 samples were analyzed at the -1700-ft level of HGM. Another 44 samples were analyzed at the -4100-ft level. Twenty-four samples were analyzed in the -4850-ft level, and fourteen sample were analyzed at the surface of SURF. Although the research conducted by Zimney (2014) consisted of igneous samples within the same area in the NBH, Zimny did not include any rhyolite or metamorphic data from inside the HGM or within the SURF property. The near surface emplacement of young rocks and clear hydrothermal influence have been observed to correlate with higher radioactivity (Gosnold, 1987). By surveying the igneous and metamorphic rocks inside the HGM and SURF property, the data compilation in this study was complementary to the regional geoneutrino flux in NBH.

Calculations: Antineutrino Luminosity

The term antineutrino luminosity means the total antineutrinos per unit mass per unit time emitted by the radioactive decay of U, Th, and K. Antineutrino luminosity was determined using the expressions from Coltori et al., (2011) and is displayed in Table 9.

Expression 2:

$^{238}U \rightarrow {}^{206}Pb + 8{}^{4}He + 6e^{-} + 6_{e} + 51.7MeV$

$^{235}U \rightarrow {}^{207}Pb + 7{}^{4}He + 4e^{-} + 4_{e} + 46.0MeV$

$^{232}Th \rightarrow {}^{208}Pb + 6{}^{4}He + 4e^{-} + 4_{e} + 42.7MeV$

$^{40}K \rightarrow {}^{40}Ca + e^{-} + \nu_{e} + 1.31MeV$

$^{40}K + e^{-} \rightarrow {}^{40}Ar + \nu_{e} + 1.51MeV$

(Emonoto et al., 2007)

Table 9. The main properties of geoneutrinos: where Q represents the Q-value of the decay chains, $T_{1/2}$ is the half-life of the parent isotopes, E_{max} is the maximal geoneutrino energy, Q_{eff} is the Q-value - $<E_{(\upsilon,\bar{\upsilon})}>$, ε_H and ε_v are the heat and antineutrino production rate per unit mass and natural composition (Coltori et al., 2011).

	Q (MeV)	$T_{½}$ (10^9 year)	E_{max} (MeV)	Q_{eff} (MeV)	ε_H (W kg^{-1})	ε_v (kg^{-1} s^{-1})
^{238}U	51.7	4.47	3.26	47.7	0.95×10^{-4}	7.41×10^{7}
^{232}Th	42.7	14.0	2.25	40.4	0.27×10^{-4}	1.62×10^{7}
^{40}K	1.311	1.28	1.311	0.590	0.22×10^{-4}	2.71×10^{4}

^{238,235}U, ^{232}Th, and ^{40}K generate radiogenic heat through the standard decay chain, involving either alpha or beta decay, or electron capture. In Expression 2, the ^{235}U values (and their antineutrino production rate) at natural isotopic abundances, is a magnitude less than ^{238}U and ^{232}Th (Coltori et al., 2011). ^{235}U antineutrinos, therefore, are below the threshold of inverse beta decay (Coltori et al., 2011). ^{40}K antineutrinos, on the other hand, are below the detectable threshold of current antineutrino detectors. The previous expressions were converted (Expression 3) and were applied to the creation of antineutrino luminosity maps (Coltori et al., 2011).

Expression 3:

$$^{238}\text{U}\ [\varepsilon_v] = 7.41\text{x}10^{7}(\text{kg}^{-1}\text{s}^{-1}) \cdot \text{M[kg]}$$

$$^{232}\text{Th}\ [\varepsilon_v] = 1.62\text{x}10^{7}(\text{kg}^{-1}\text{s}^{-1}) \cdot \text{M[kg]}$$

$$^{40}\text{K}\ [\varepsilon_v] = 2.71\text{x}10^{4}(\text{kg}^{-1}\text{s}^{-1}) \cdot \text{M[kg]}$$

The antineutrino luminosity, ε_v, is the number of antineutrino particles emitted per mass (kg) per unit time (seconds). These expressions can be rewritten as in Expression 4, which individual samples are applied instead of the BSE estimates.

Expression 4:

$$^{238}U\ [\varepsilon_v\ (mg^{-1}\ s^{-1})] = 74.1 \cdot U[ppm]$$

$$^{232}Th\ [\varepsilon_v\ (mg^{-1}\ s^{-1})] = 16.2 \cdot Th[ppm]$$

$$^{40}K\ [\varepsilon_v\ (mg^{-1}\ s^{-1})] = 27.1 \cdot K[pct]$$

Expression 4 combines the ^{238}U and ^{235}U values to compensate for the low natural percentage of ^{235}U. The GRS in this study does not distinguish between the two U isotopes. Finally, to determine the total antineutrino luminosity of the NBH, each luminosity emitted by U, Th, and K is summed to provide the total antineutrino luminosity.

By performing GRS analyses, calculating the radioactive heat production and the antineutrino luminosity present in NBH, sample data is mapped and statistically analyzed with high accuracy, ensuring successful results. Accuracy in this study is especially important for the success of the future DUNE.

CHAPTER VI

RESULTS

Radioelement Analysis of Northern Black Hills

Overview

This study includes 736 samples analyzed for their U, Th, and K content. Three hundred and one analyses were obtained from outcrop samples across the NBH. Two hundred and ninety-two samples were analyzed in the Geothermal Laboratory at the UND HHSGGE. One hundred and forty-three samples were surveyed with the handheld GRS in tunnels and shafts inside the HGM. The U, Th, and K content, the calculated radioactive heat production ($\mu W\ m^{-3}$), and geoneutrino luminosity (ε_v; $mg^{-1}s^{-1}$) are presented in Table 26 – Table 31, in Appendix A. Results are presented by rock type (i.e., igneous, metamorphic, sedimentary), broken up by specific rock name. I identified all the rocks in this research by various geological maps of the NBH and rock identification methods. A total geoneutrino luminosity (ε_v) of $4.44x10^5$ ($mg^{-1}s^{-1}$) was calculated from all analyses conducted in the Northern Black Hills.

Northern Black Hills Radiogenic Heat Production and Radioelement Content

The highest rock type contributors of radiogenic heat production found within the igneous rocks were phonolites (5.63 ± 2.95 μW m^{-3}), granodiorites (6.41 ± 3.00 μW m^{-3}), unidentified alkali volcanics (8.97 ± 7.59 μW m^{-3}), and trachytes (3.57 ± 2.46 μW m^{-3}). Rhyolites do not have the highest heat production (3.23 ± 3.57 μW m^{-3}) as compared to the other igneous rocks, however, they are important due to the rock distribution present in the BH. Basalt samples also had high radiogenic heat production levels (6.14 ± 2.00 μW m^{-3}); however, few samples were analyzed. The highest contributors of radiogenic heat production found in metamorphic rock types were schists (2.48 ± 1.67 μW m^{-3}), metagraywacke (3.10 ± 1.15 μW m^{-3}), and metabasalt (5.74 ± 8.14 μW m^{-3}). Graywacke (3.24 ± 0.81 μW m^{-3}) has the highest radiogenic heat production in the sedimentary rocks. Radioactivity of sedimentary rocks is low and inconsistent for this study. Sedimentary rocks were only included in this survey for completeness. All data collected during the survey is displayed in Table 25 - Table 30, in Appendix A.

Table 10. Radioelement averages in the Northern Black Hills from the Initial Survey and Lab Analysis.

	U (ppm)	Th (ppm)	K (pct)	A (μWm^{-3})	Th:U Ratio
Igneous	6.61 ± 5.69	19.74 ± 20.92	2.90 ± 2.26	4.03 ± 3.80	3.37 ± 3.66
Metamorphic	3.87 ± 5.90	9.99 ± 8.16	2.32 ± 1.62	2.28 ± 2.24	3.86 ± 4.83
Sedimentary	2.20 ± 4.17	2.60 ± 4.61	0.64 ± 1.10	0.96 ± 1.45	1.28 ± 1.79

Table 39 - Table 41 in Appendix G shows statistical data on U, Th, and K for each specific rock type in this study.

Bismuth Germanate Oxide RS-230 GRS Survey Mapping

The RS-230 survey includes the analysis of 106 igneous samples, 62 metamorphic samples, and 117 sedimentary samples. The igneous rock surveys include 34 rhyolites, 19 trachytes, 14 latitic andesites, 12 phonolites, 11 latites, eight alkali volcanic rocks, five granodiorites, two basalts and one episodite. The phonolites, alkali volcanic rocks, granodiorites, rhyolites, and trachytes, all of which are early Cenozoic, were emplaced at or near the surface.

Table 11. Radioelement content with standard deviations averages for Cenozoic igneous rocks

U (ppm)	Th (ppm)	K (pct)	A (μWm^{-3})	Th:U Ratio
9.21 ± 7.49	25.71 ± 24.04	4.1 ± 2.37	5.43 ± 4.33	2.77 ± 1.11

Most of the igneous outcrops lay within the western part of the study area; a few igneous outcrops lay in the eastern part (Fig. 12 – Fig. 18). The samples in the eastern area have low radioactivity and consist of deeply emplaced Precambrian and Mesozoic rocks. Fig. 16 – Fig. 18 were created to show the distribution and levels of U, Th, and K in the igneous rocks. Ratios between the radioelements (U:Th, U:K, and Th:K) in the igneous rocks can be compared in Appendix C, Figure 48A - Figure 48C. All data collected with the RS-230 GRS Survey is displayed in Table 25 and Table 26, in Appendix A.

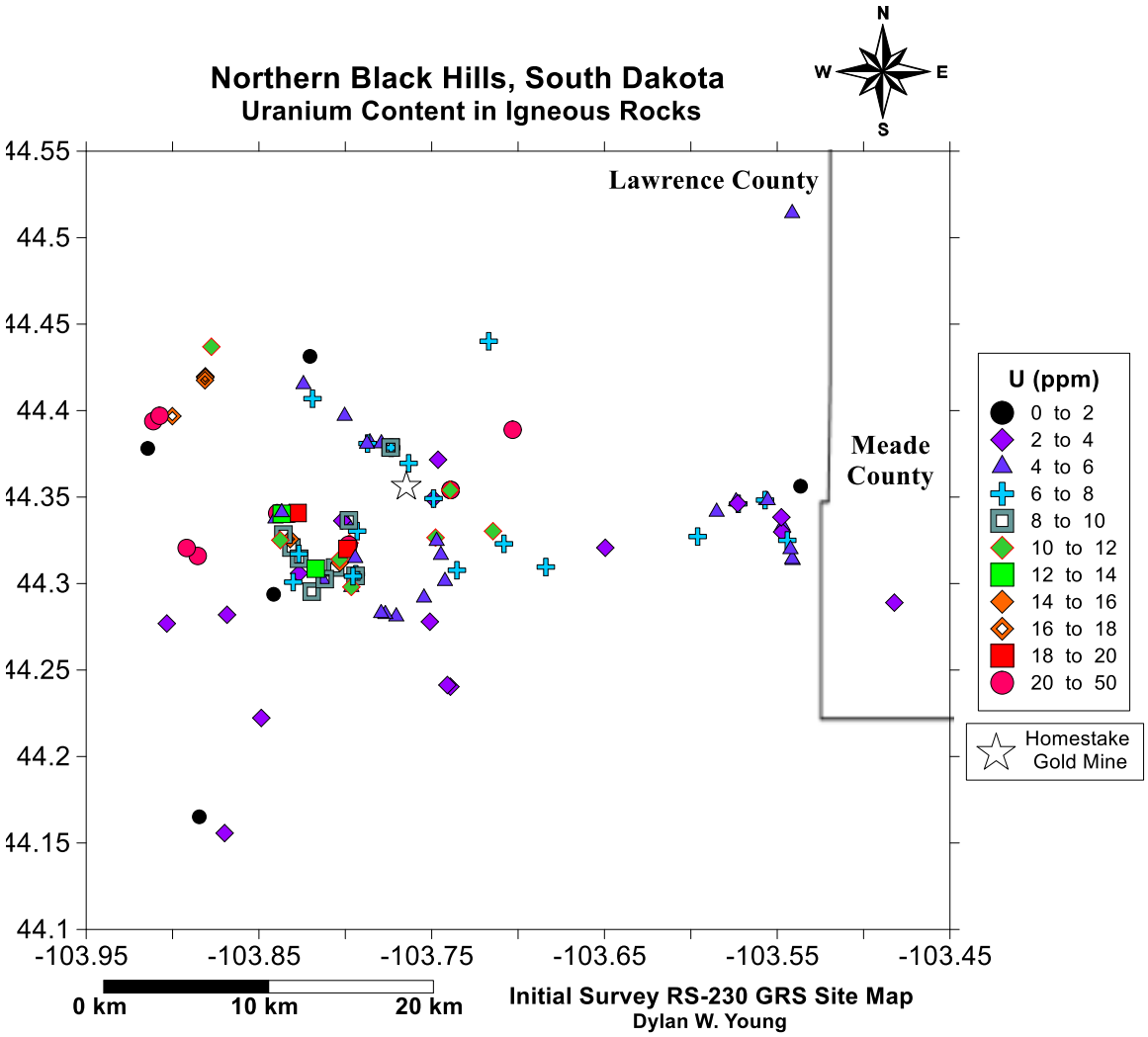

Figure 16. Uranium Content in Igneous Rocks

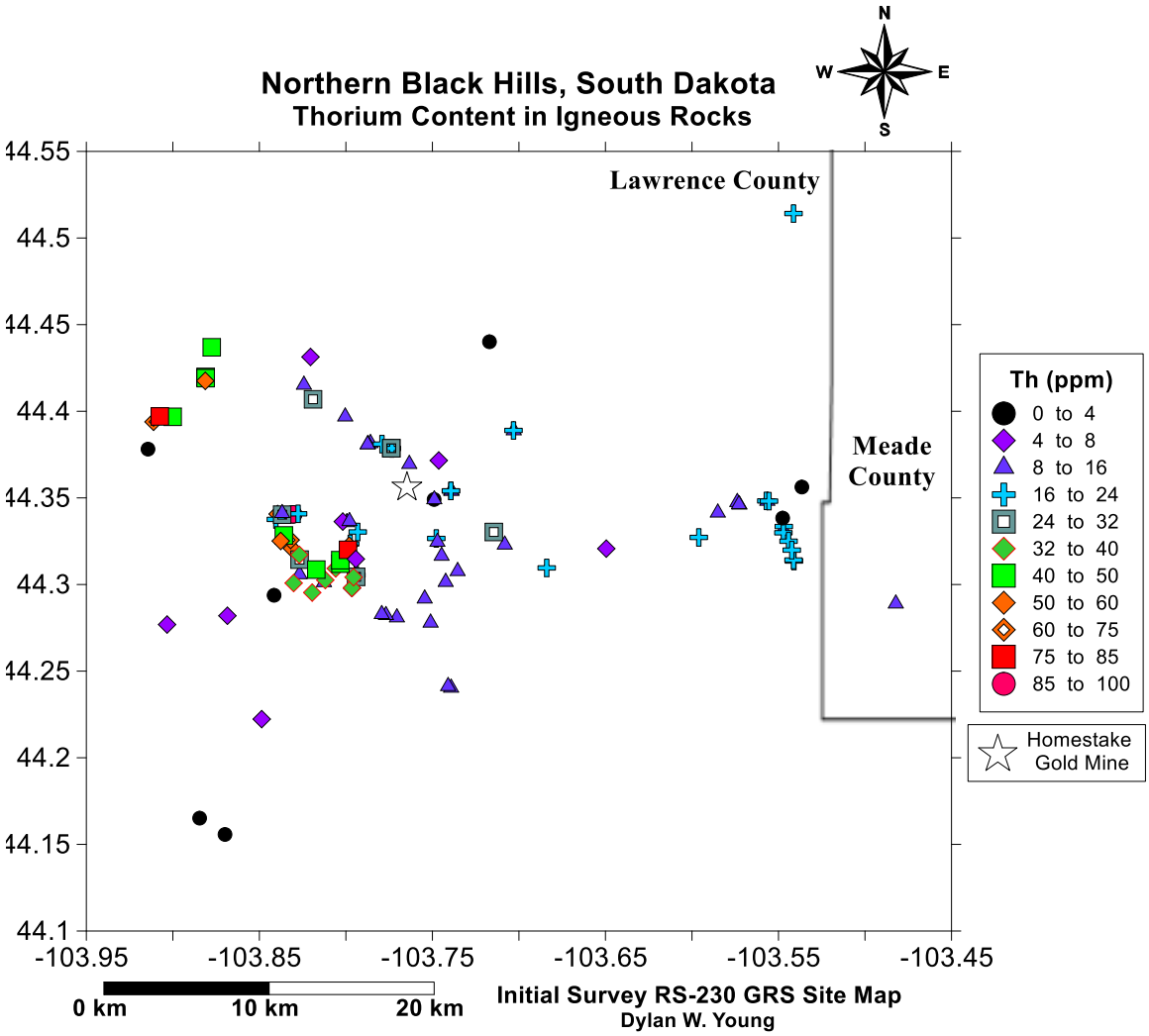

Figure 17. Thorium Content in Igneous Rocks

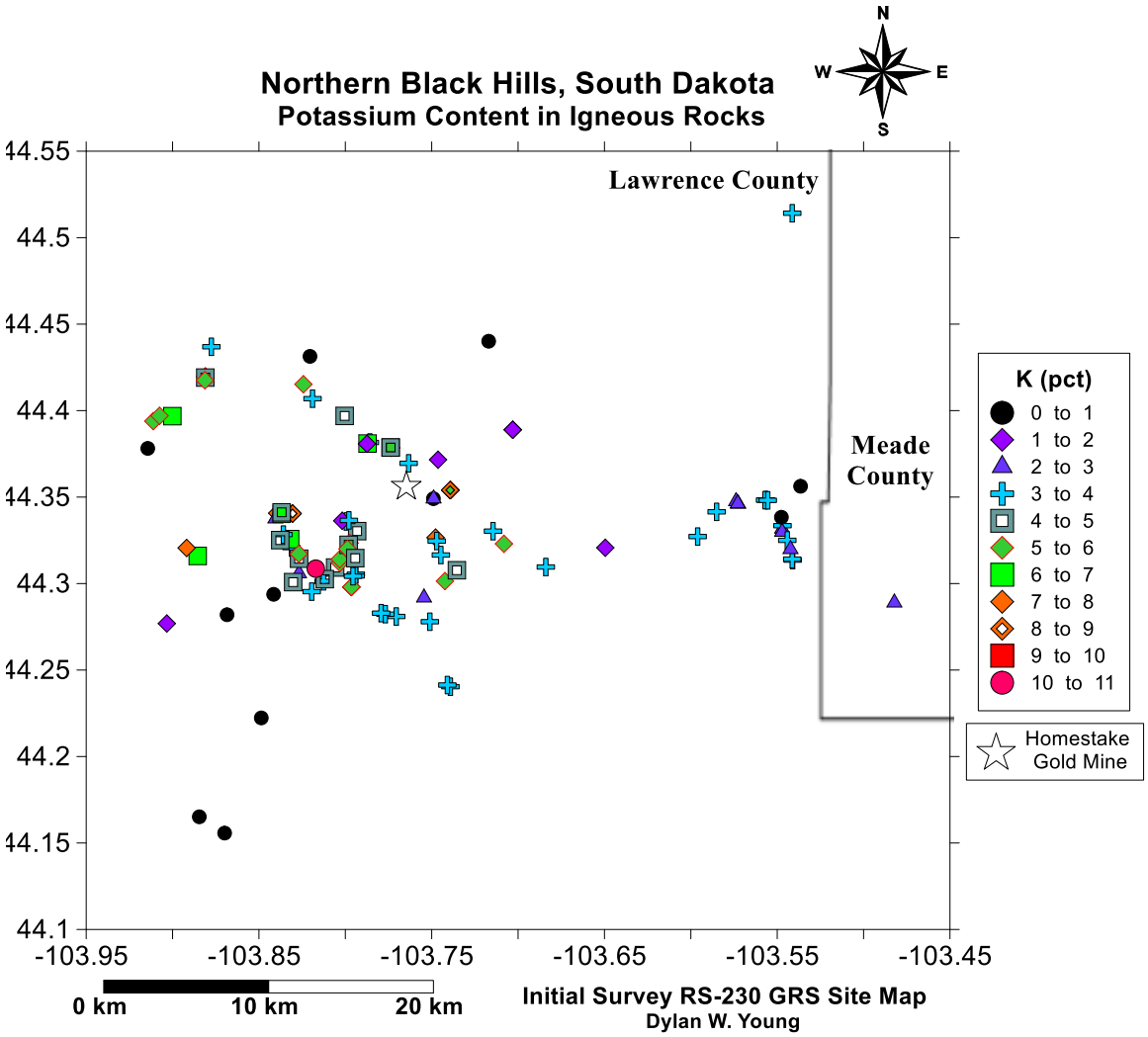

Figure 18. Potassium Content in Igneous Rocks

The metamorphic rocks surveyed included 31 schists, 18 phyllites, four quartzites, three metabasalts, three greenstones, two metagreywacke, and one metasandstone. The main contributors with high U, Th, and K content are in the north central region of the NBH.

Table 12. Radioelement content averages of metamorphic rocks

U (ppm)	**Th (ppm)**	**K (pct)**	**A (μWm^{-3})**	**Th:U Ratio**
6.25 ± 8.09	14.40 ± 7.05	3.04 ± 1.48	3.46 ± 1.48	2.84 ± 1.37

The central region of the study area has the largest abundance of metamorphic rocks. There is a higher U, Th, and K content in the younger rocks emplaced near the surface. Fig. 19 - Fig 21 shows the levels of U, Th, and K content in metamorphic rocks. Ratios between the radioelements (U:Th, U:K, and Th:K) in the metamorphic rocks analyzed can be compared in Appendix C, Fig. 49A - Fig. 49C.

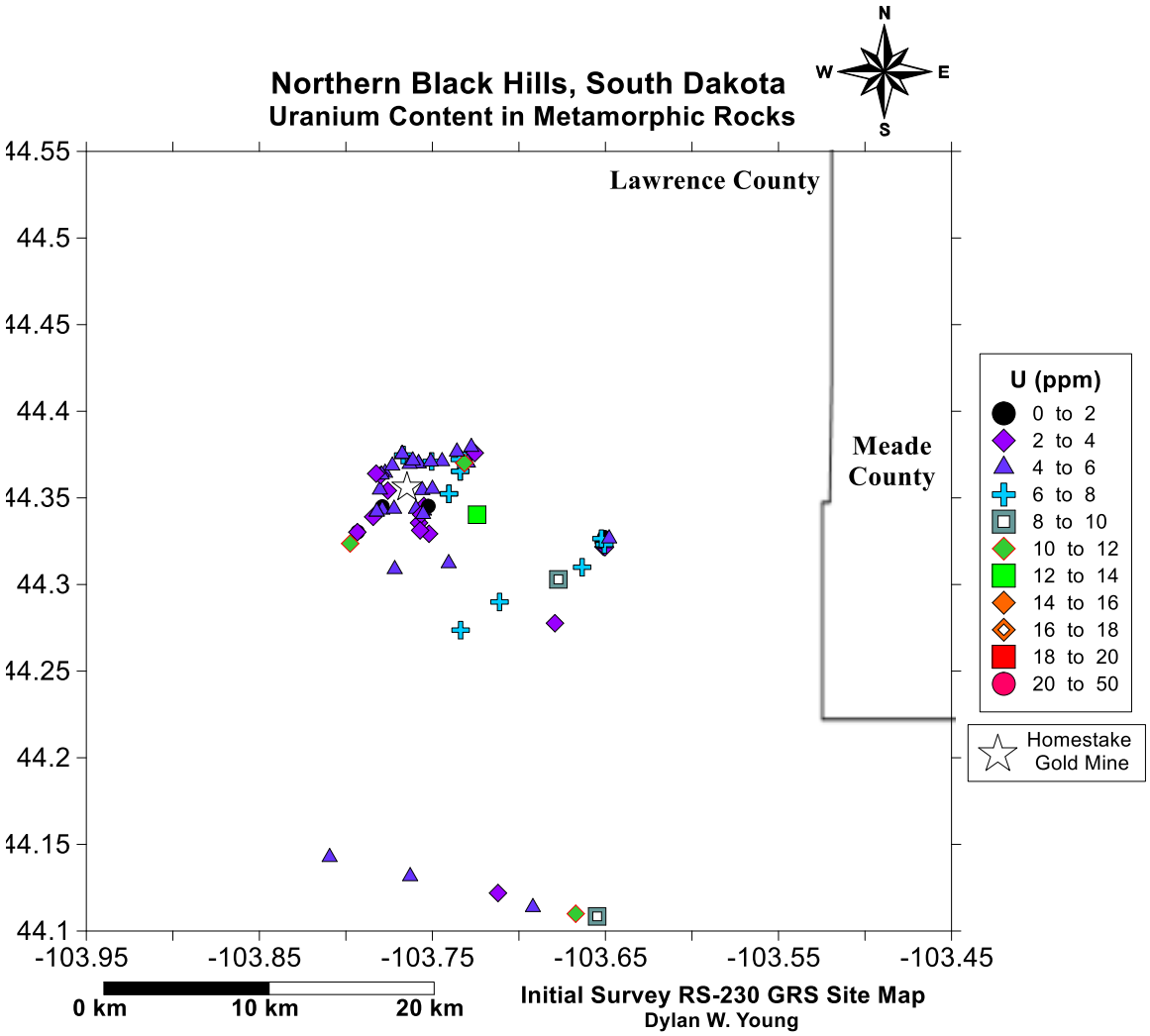

Figure 19. Uranium Content in Metamorphic Rocks

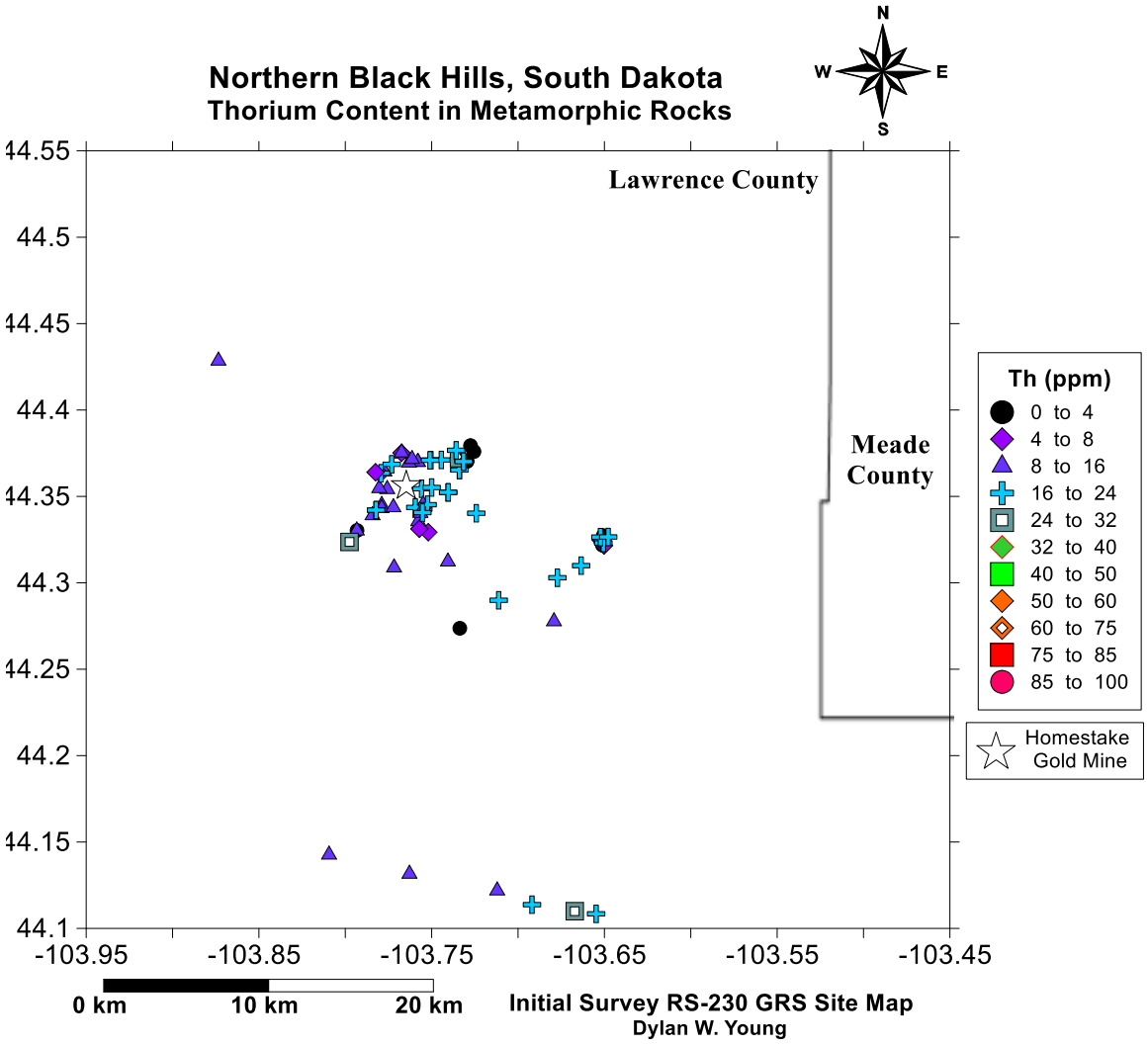

Figure 20. Thorium Content in Metamorphic Rocks

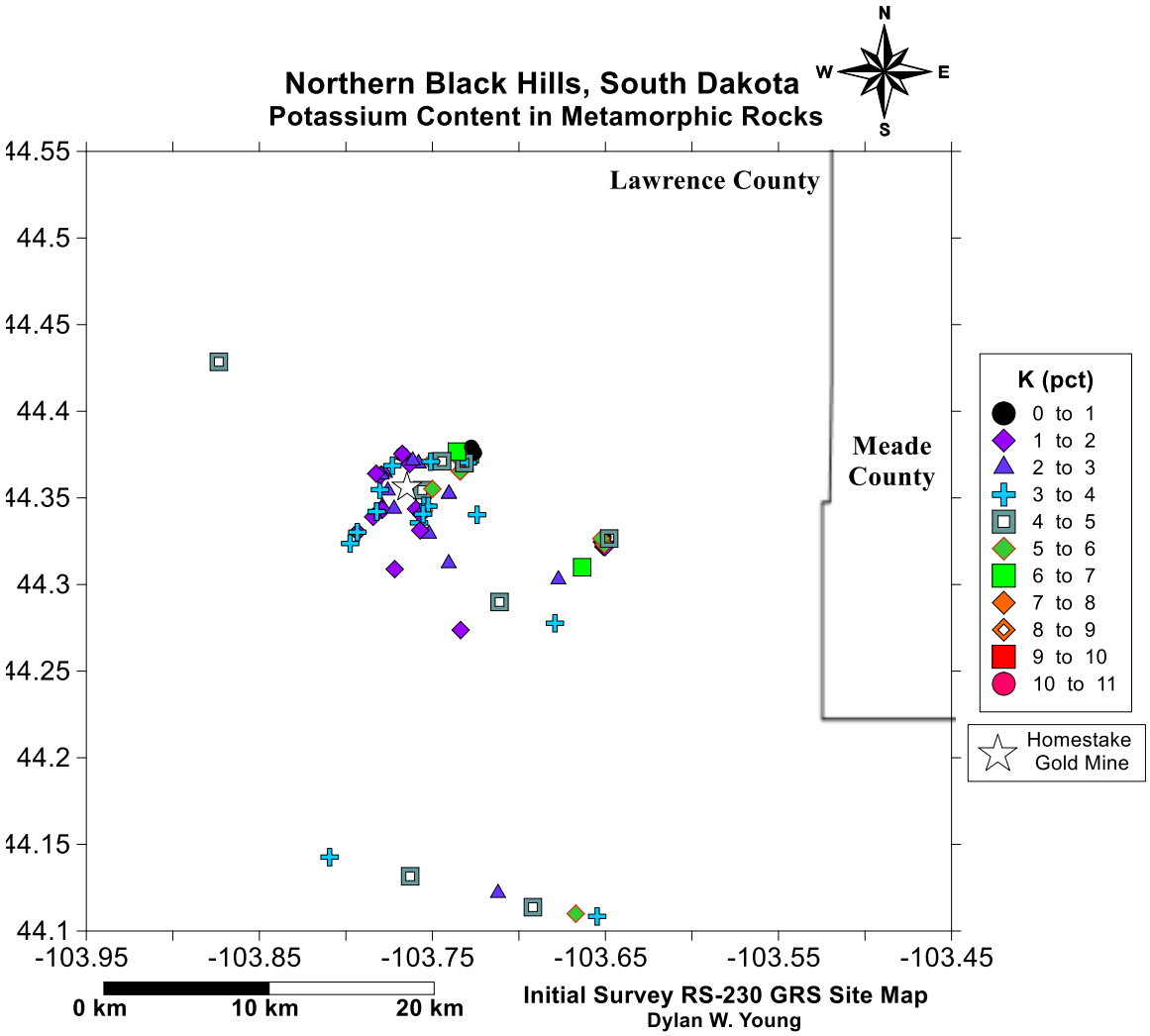

Figure 21. Potassium Content in Metamorphic Rocks

The sedimentary rocks surveyed with the RS-230 GRS include 43 sandstones, 64 limestones, seven shales, two gypsums, and one greywacke. Most of the sedimentary samples analyzed have relatively low U, Th, and K content.

Table 13. Radioelement content averages of sedimentary rocks

U (ppm)	Th (ppm)	K (pct)	A (μWm^{-3})	Th:U Ratio
3.08 ± 1.65	4.46 ± 3.93	1.13 ± 1.40	1.46 ± 0.75	1.67 ± 1.16

The Fig. 22 – Fig. 24 show the variation and distribution of the U, Th, and K from the survey of sedimentary rocks. Ratios between the radioelements (U:Th, U:K, and Th:K) in the sedimentary rocks can be compared in Appendix C, Fig. 50A – Fig. 50C.

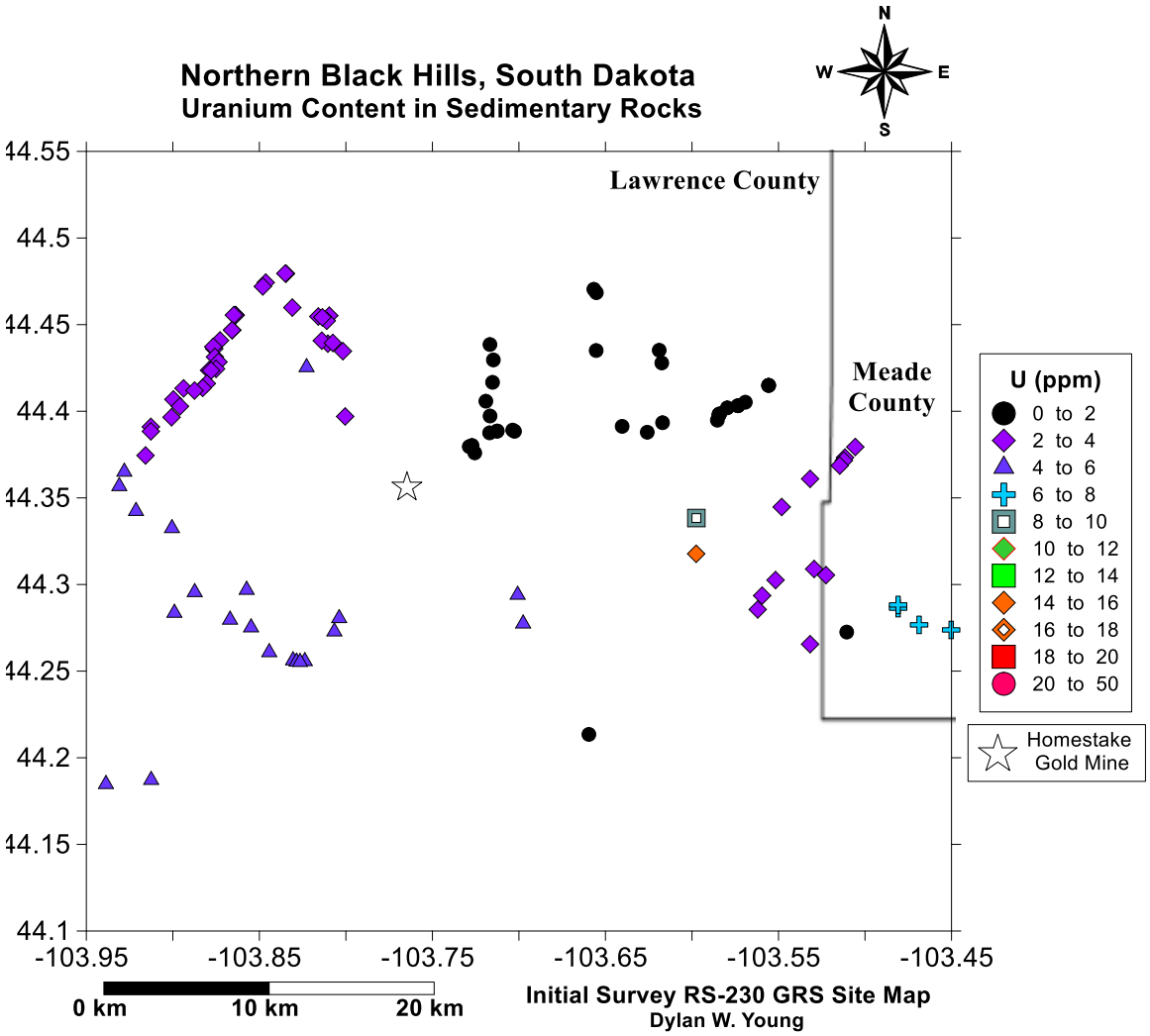

Figure 22. Uranium Content in Sedimentary Rocks

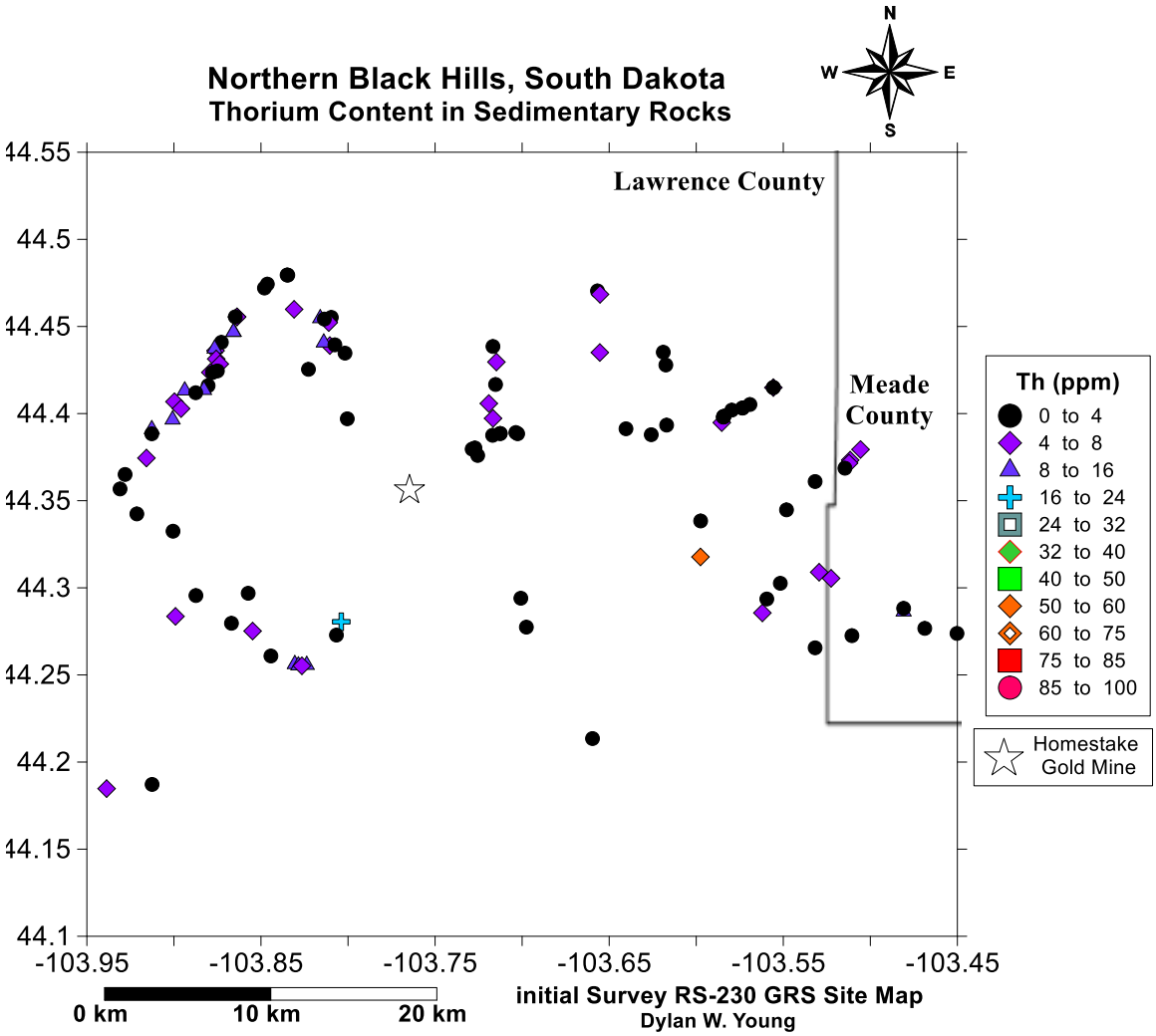

Figure 23. Thorium Content in Sedimentary Rocks

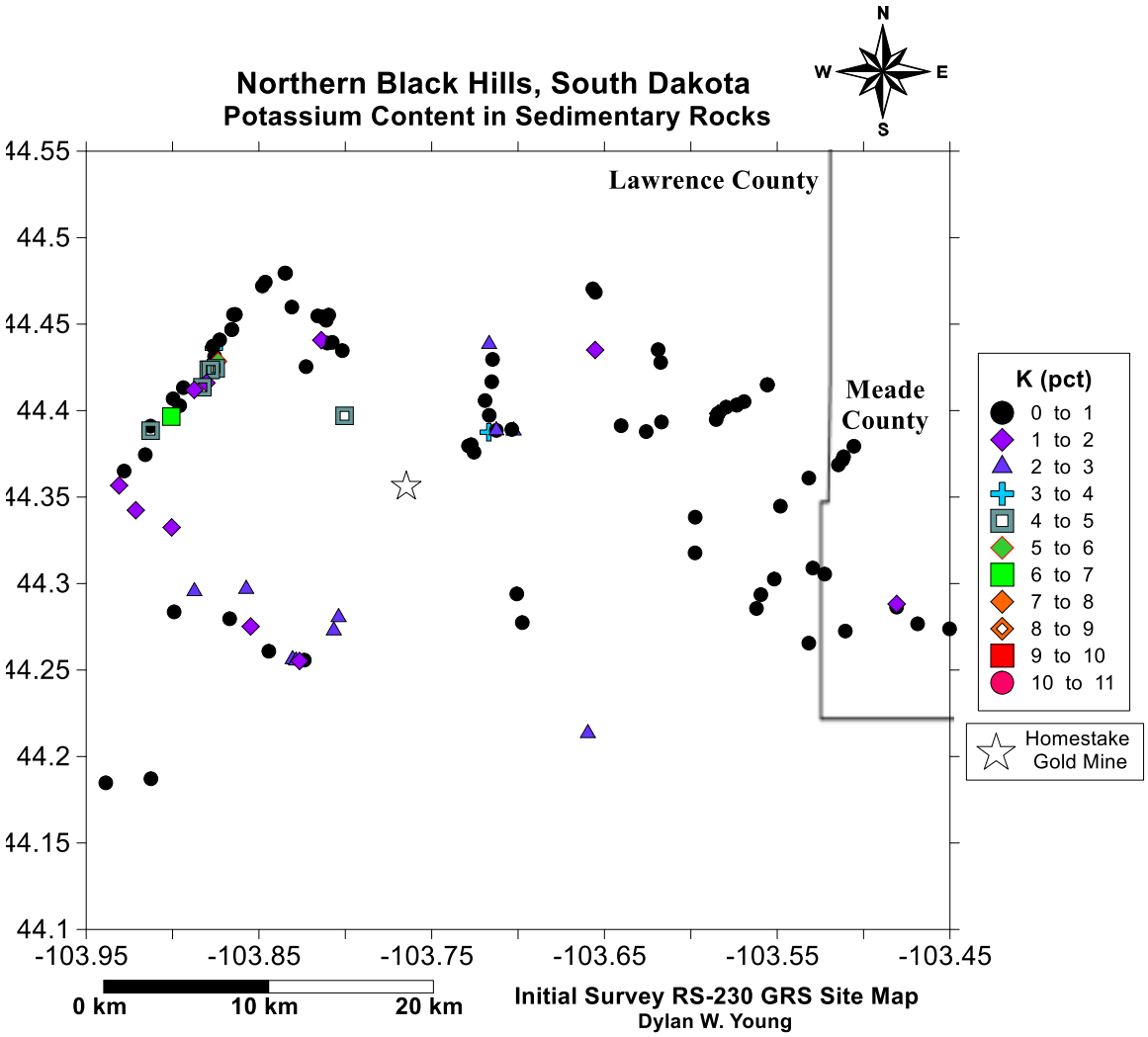

Figure 24-A. Potassium Content in Sedimentary Rocks

Germanium Standard Electron Detector GRS Analysis Mapping

The Ge SED GRS Analysis included 101 igneous rock samples, 68 metamorphic rock samples, and 115 sedimentary rock samples. All data is listed in Appendix A, Table 29 and 30. The igneous rock samples analyzed consisted of 32 rhyolites, 14 phonolites, 19 trachytes, 11 latitic andesites, ten latites, seven alkali volcanic rocks, four granodiorites, two basalts, one aplite, and lastly, one episodite.

Table 14. Radioelement content averages of Cenozoic igneous rocks

U (ppm)	**Th (ppm)**	**K (pct)**	**A (μWm^{-3})**	**Th:U Ratio**
4.15 ± 4.39	13.88 ± 15.24	2.24 ± 1.70	2.68 ± 2.58	3.96 ± 5.00

The igneous rocks are all early Cenozoic in age and are emplaced at or near the surface. The largest contributors to the high U, Th, and K content for the igneous rocks are present in the western region of the study area. Fig. 25 – Fig. 27 show the distribution and levels of U, Th, and K content in the igneous rocks. Ratios between the labeled radioelements (U:Th, U:K, and Th:K) present in the igneous rocks can be compared in Appendix C, Fig. 51A – Fig. 51C.

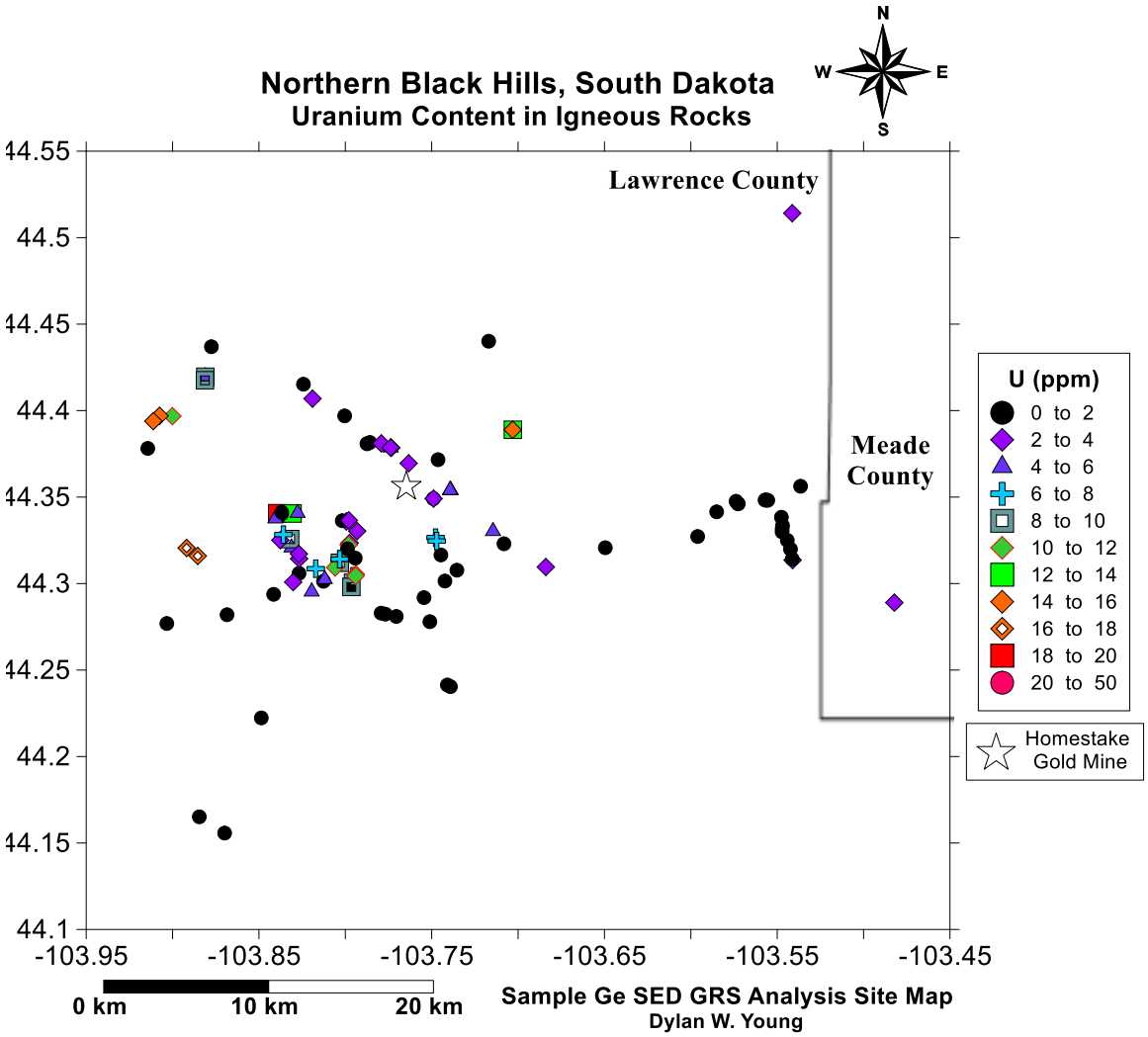

Figure 25. Uranium Content in Igneous Rocks

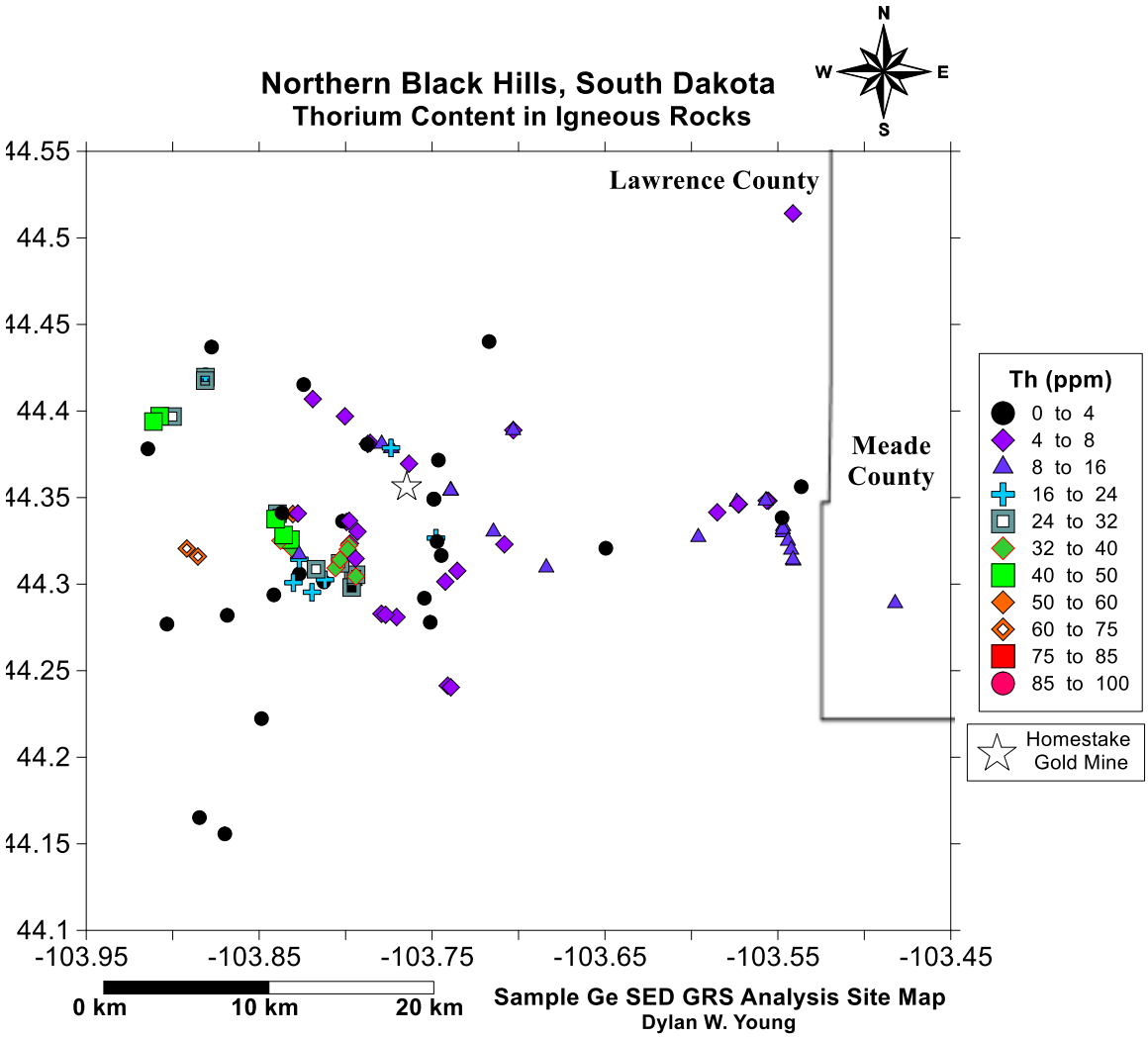

Figure 26. Thorium Content in Igneous Rocks

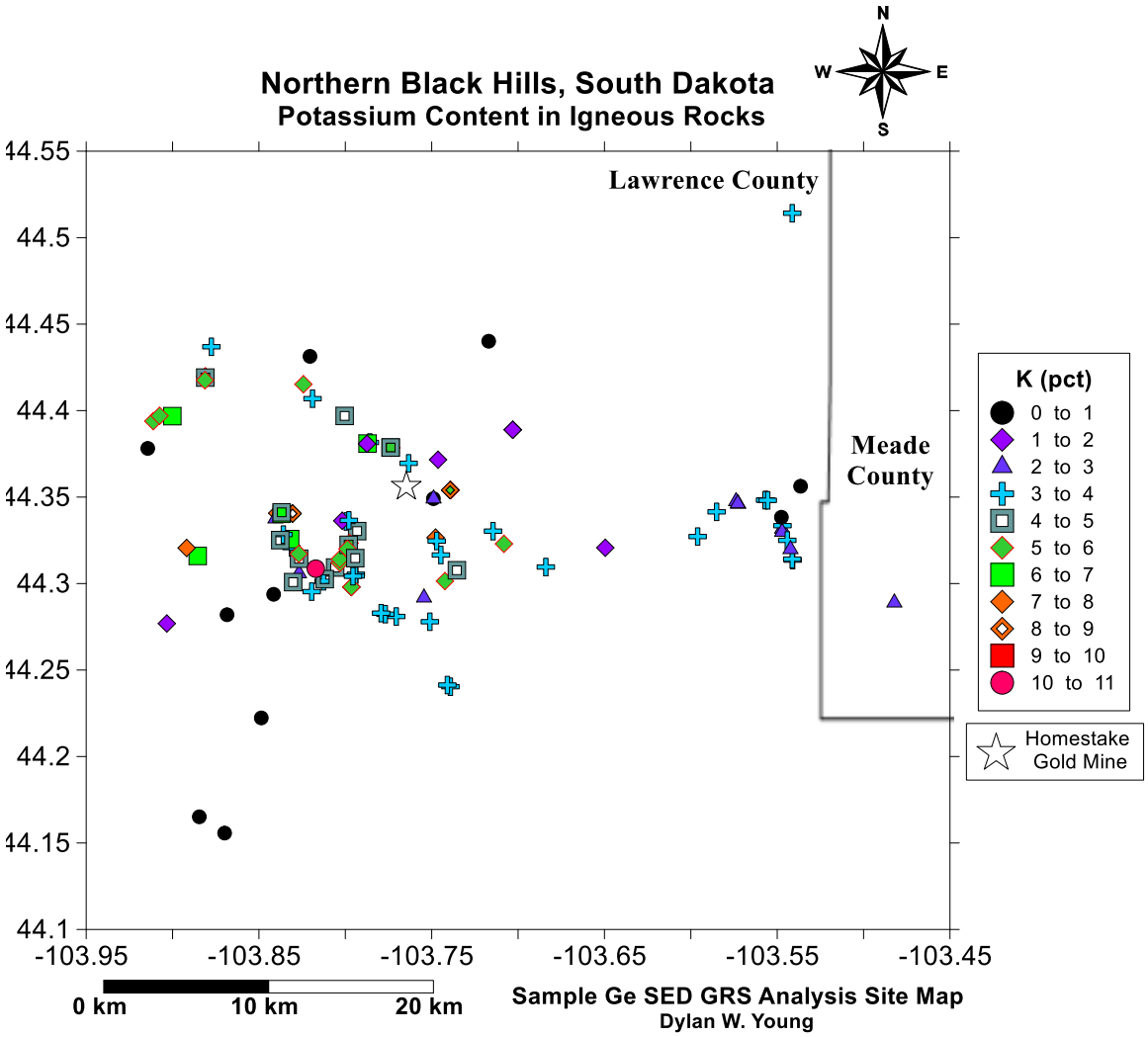

Figure 27. Potassium Content in Igneous Rocks

The metamorphic samples analyzed consisted of 31 schists, 20 phyllites, and six slates. The highest contributors to higher levels of U, Th, and K for the metamorphic rocks were present in the central region of the study area.

Table 15. Radioelement content averages of metamorphic rocks

U (ppm)	Th (ppm)	K (pct)	A (μWm^{-3})	Th:U Ratio
1.67 ± 1.79	5.62 ± 6.98	1.50 ± 1.35	1.15 ± 1.35	5.00 ± 6.68

Fig. 28 – Fig. 30 show the distribution and levels of U, Th, and K in the metamorphic rocks. Ratios between the radioelements (U:Th, U:K, and Th:K) present in the metamorphic rocks can be compared in Appendix C, Fig. 52A – Fig. 52C.

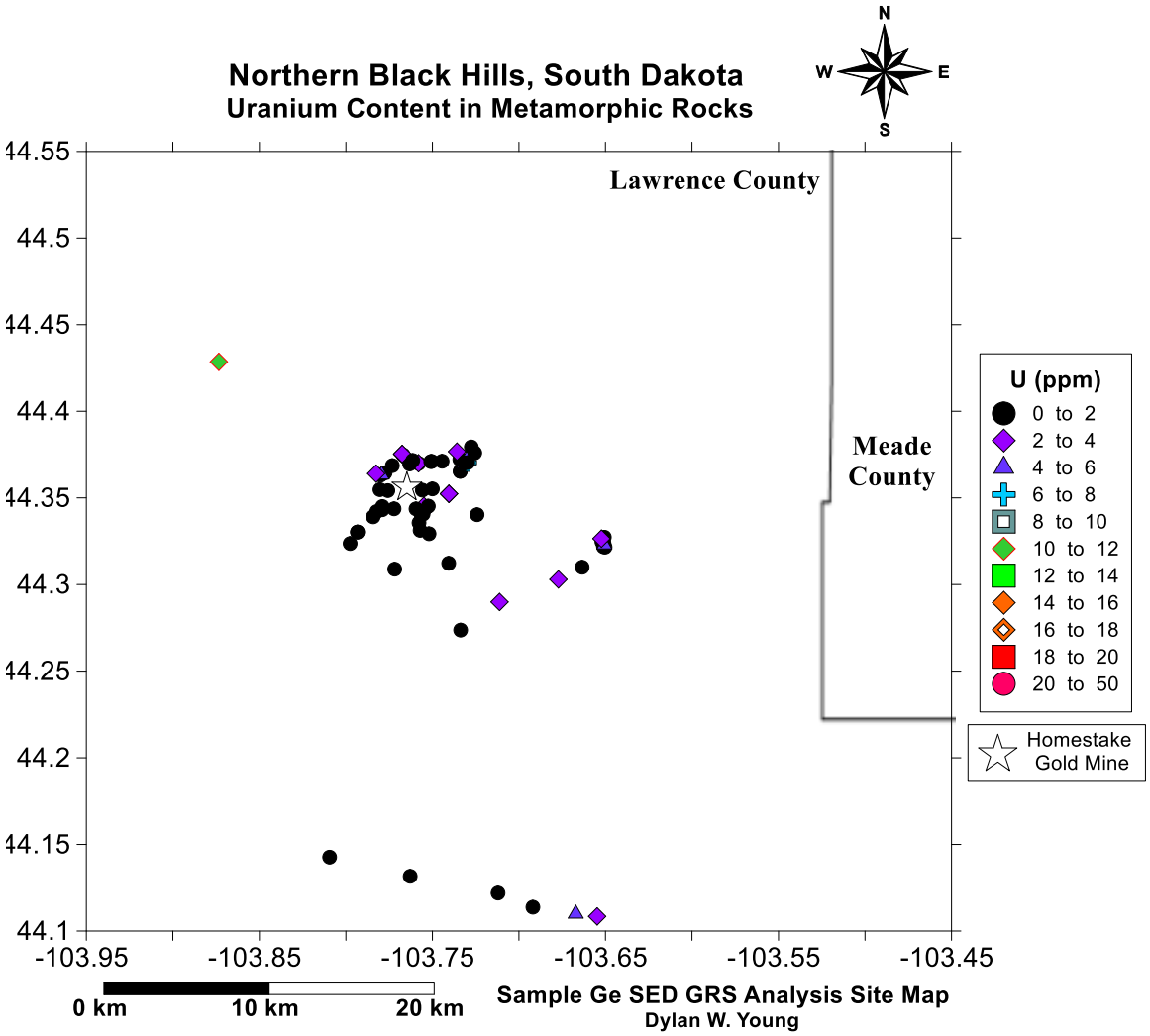

Figure 28. Uranium Content in Metamorphic Rocks

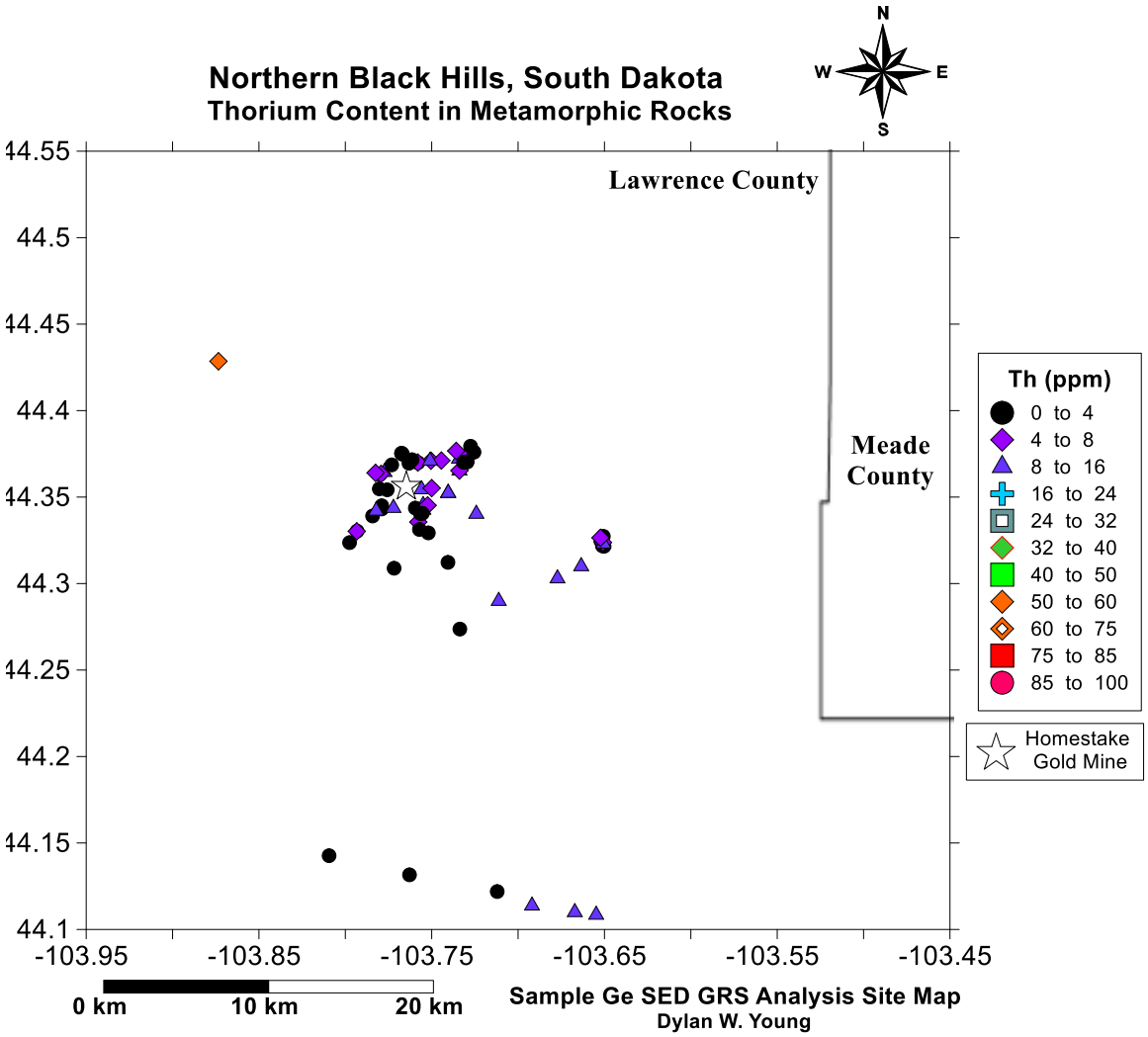

Figure 29. Thorium Content in Metamorphic Rocks

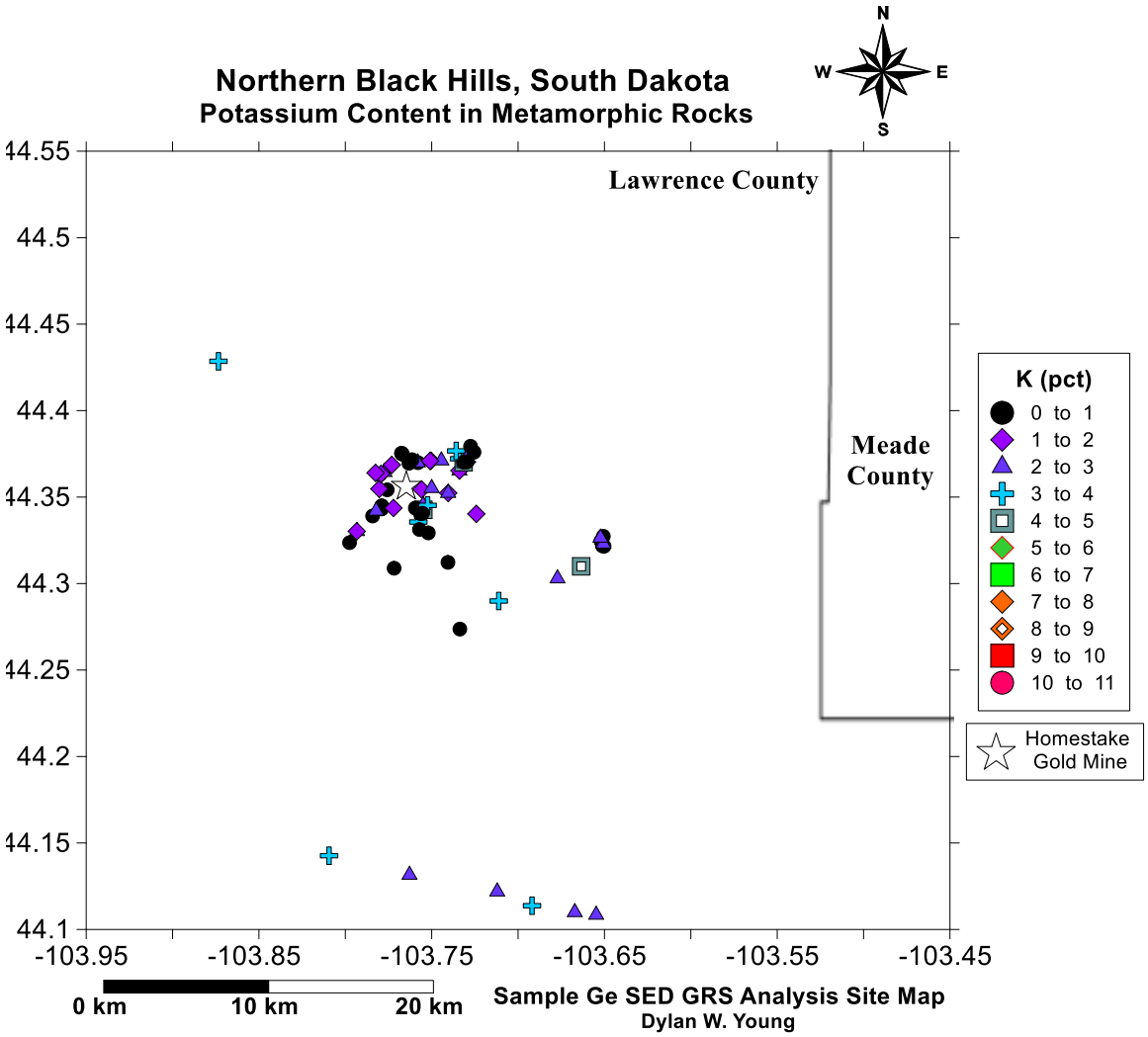

Figure 30. Potassium Content in Metamorphic Rocks

The sedimentary samples analyzed in this study consisted of 41 sandstones, 69 limestones, two gypsums, one shale, and one large calcite crystal, mostly located at the edges of the study area. Most sedimentary samples have low U, Th, and K content.

Table 16. Radioelement content averages of sedimentary rocks

U (ppm)	Th (ppm)	K (pct)	A (μWm^{-3})	Th:U Ratio
1.30 ± 5.50	0.59 ± 2.57	0.26 ± 1.72	0.47 ± 1.72	0.48 ± 1.74

Fig. 31 – Fig. 33 show the distribution and levels of U, Th, and K in the sedimentary samples. Ratios between the radioelements (U:Th, U:K, and Th:K) present in the sedimentary samples can be compared in Appendix C, Fig. 53A – Fig. 53C.

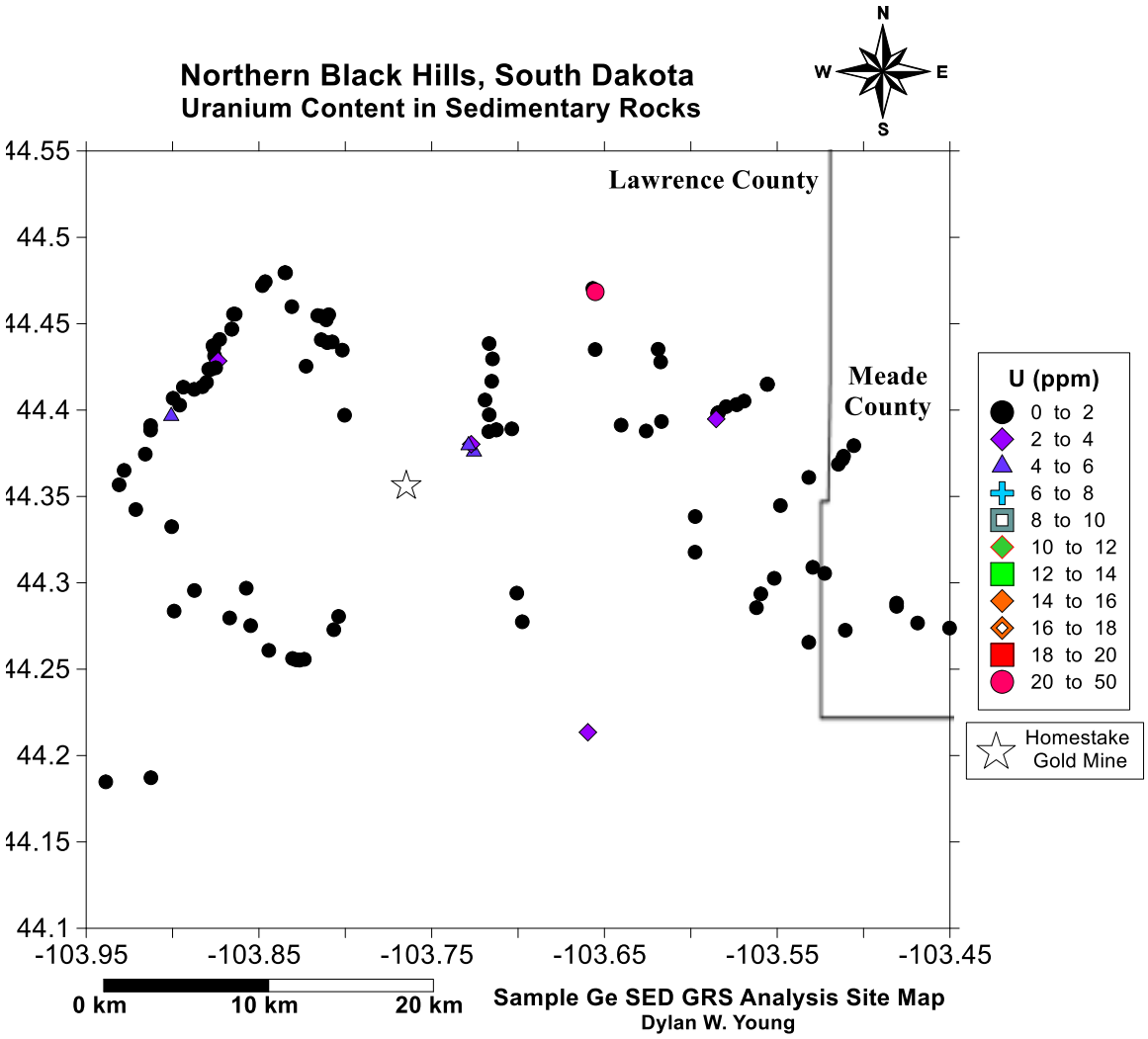

Figure 31. Uranium Content in Sedimentary Rocks

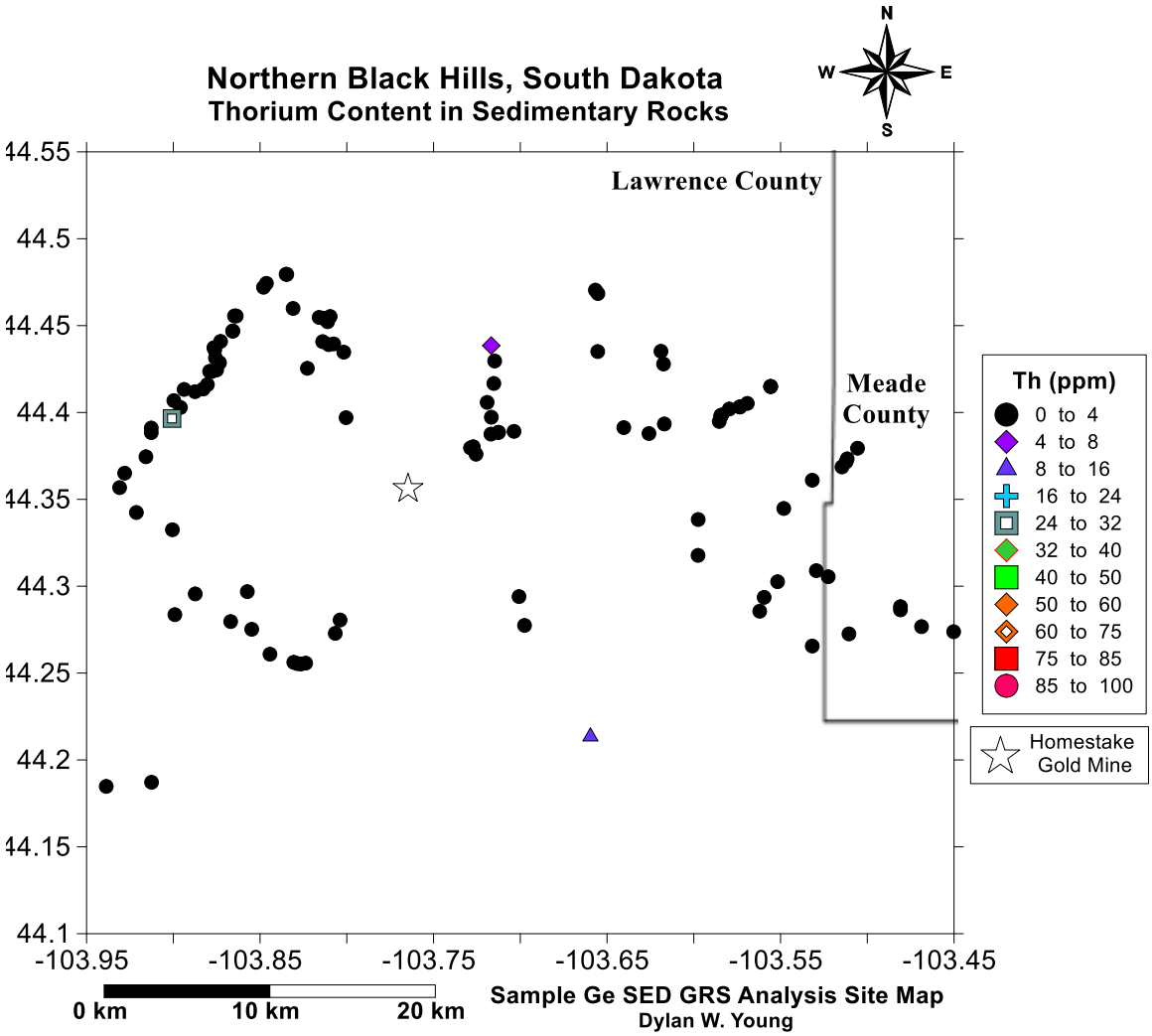

Figure 32. Thorium Content in Sedimentary Rocks

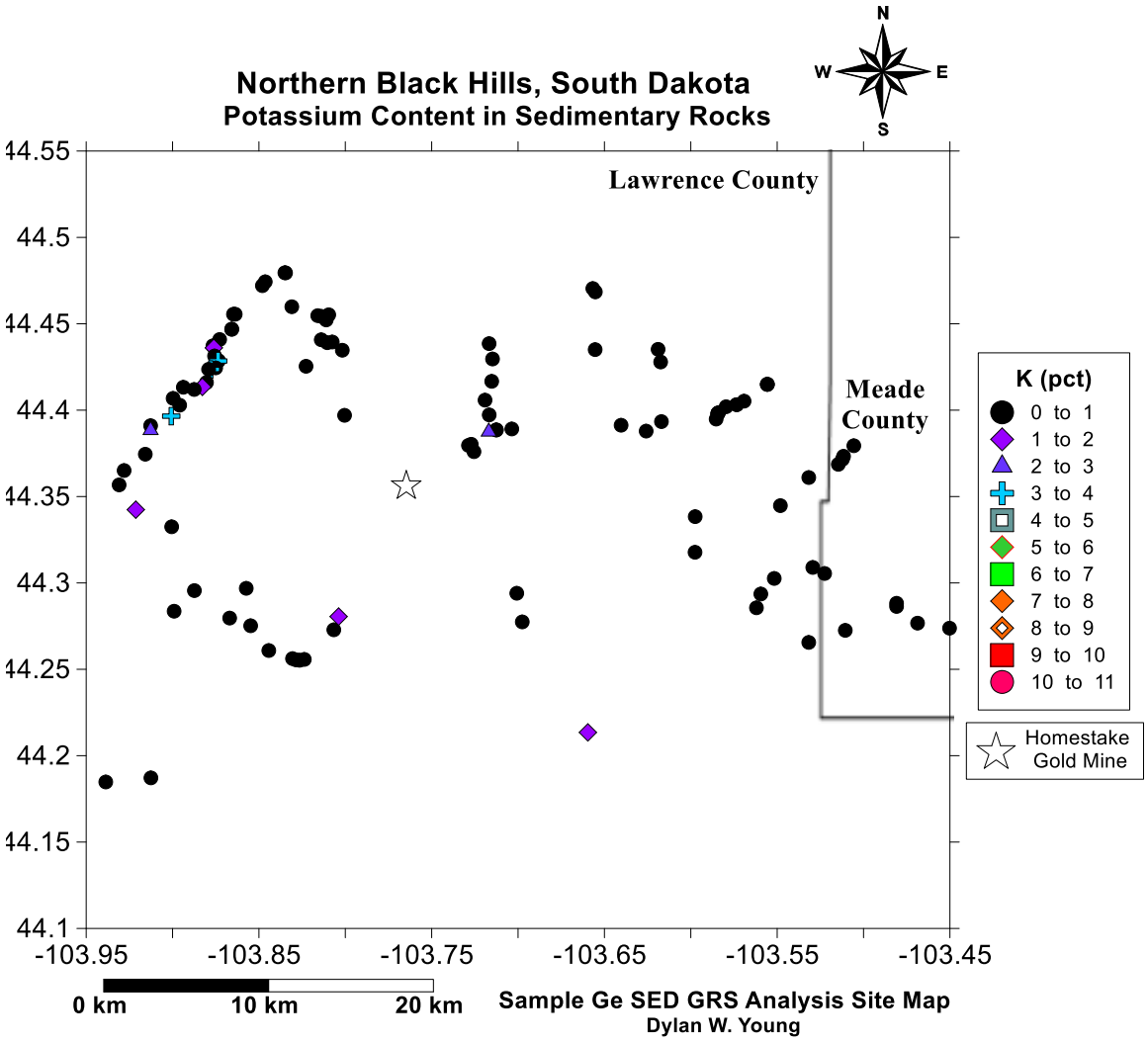

Figure 33. Potassium Content in Sedimentary Rocks

Radiogenic Heat Production Mapping

Figure 34 – Figure 39 demonstrate the calculated radiogenic heat production present in the NBH. Separate maps were created for the igneous, metamorphic, and sedimentary rocks present in both the field survey and the individual sample analysis. Contour mapping was not applied for the heat production distribution since it would not be representative of the entire geologic contributions in the region.

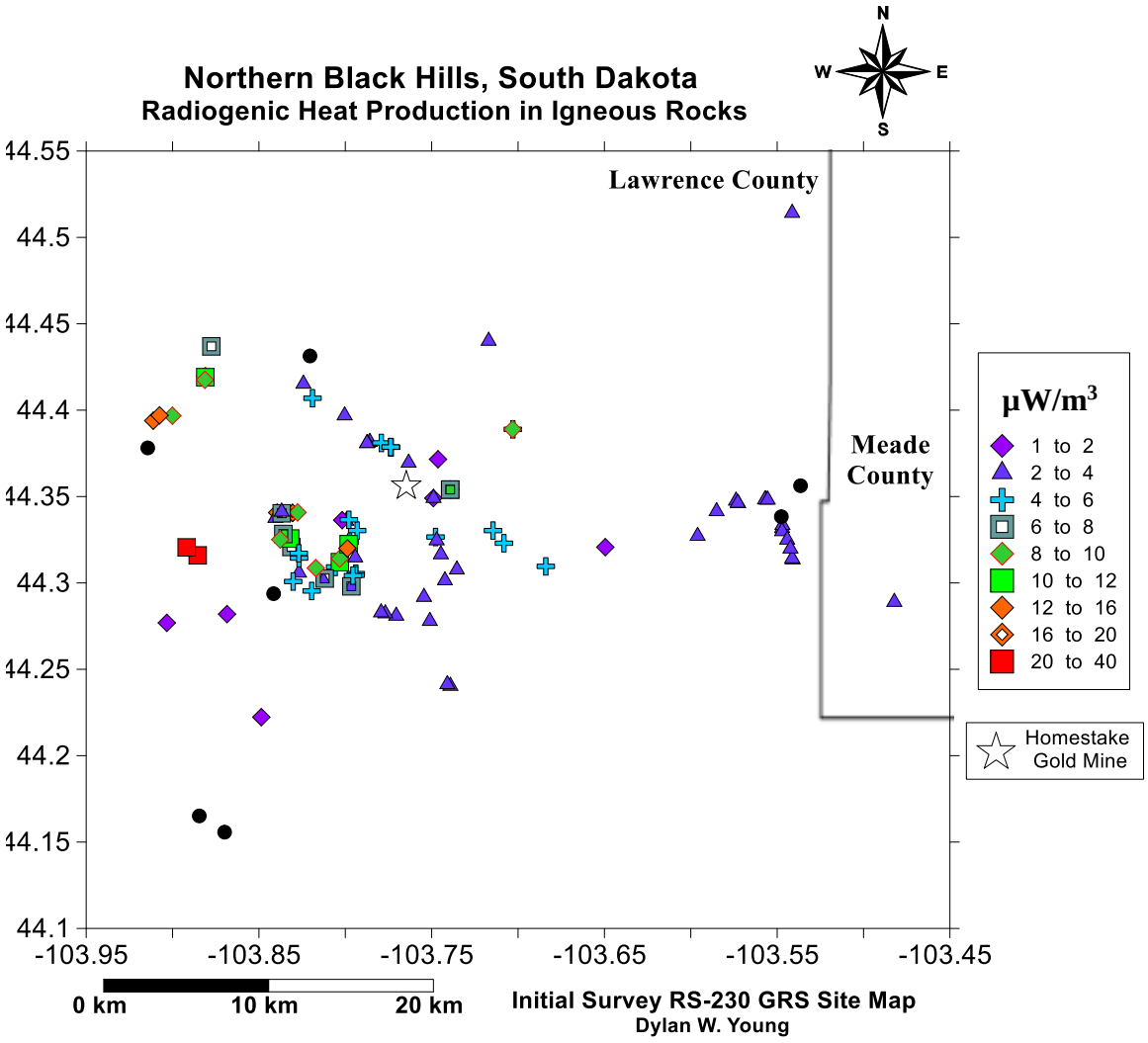

Figure 34. RS-230 GRS Survey of Igneous Radiogenic Heat Production

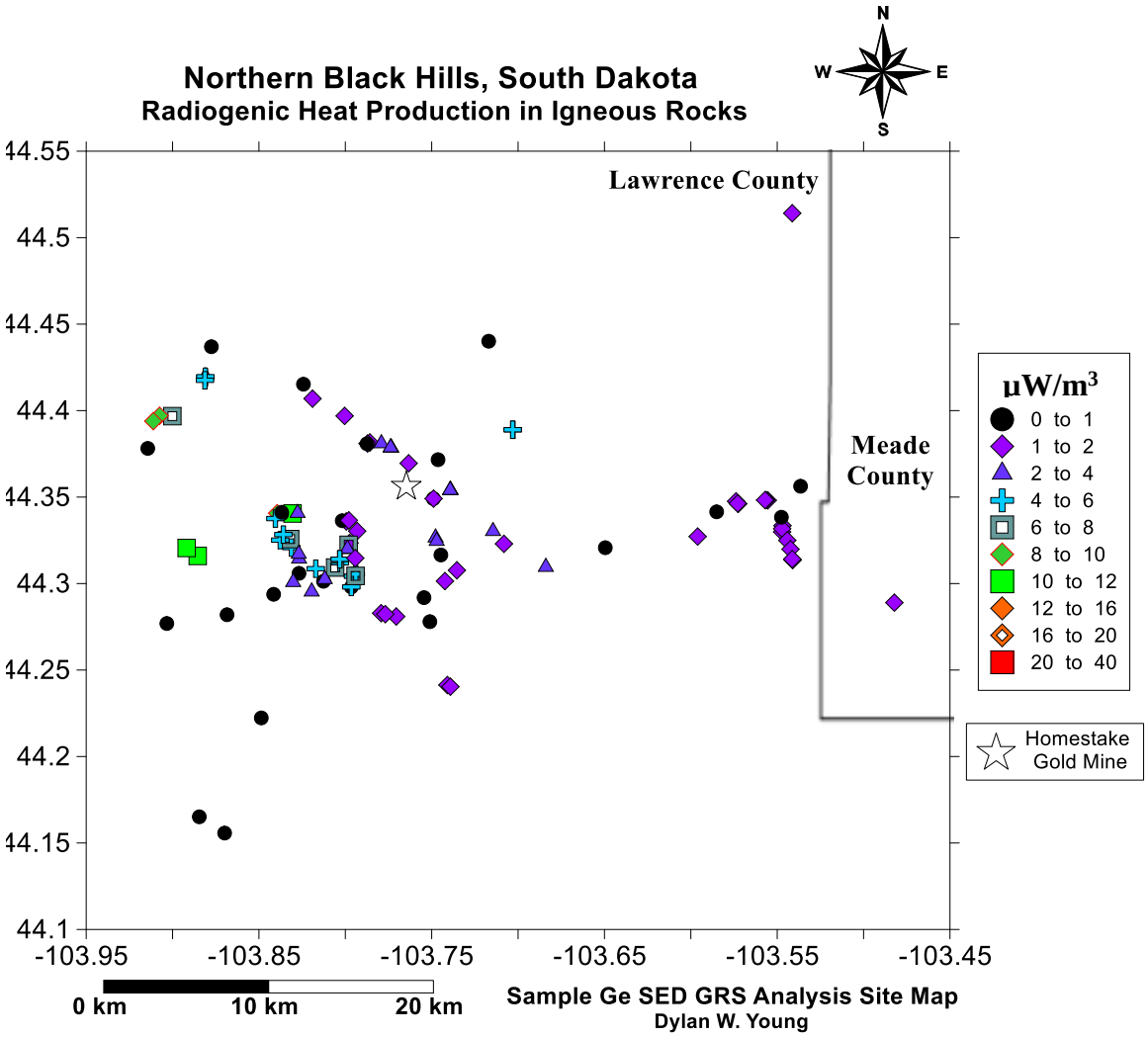

Figure 35. Ge SED GRS Analysis of Igneous Radiogenic Heat Production

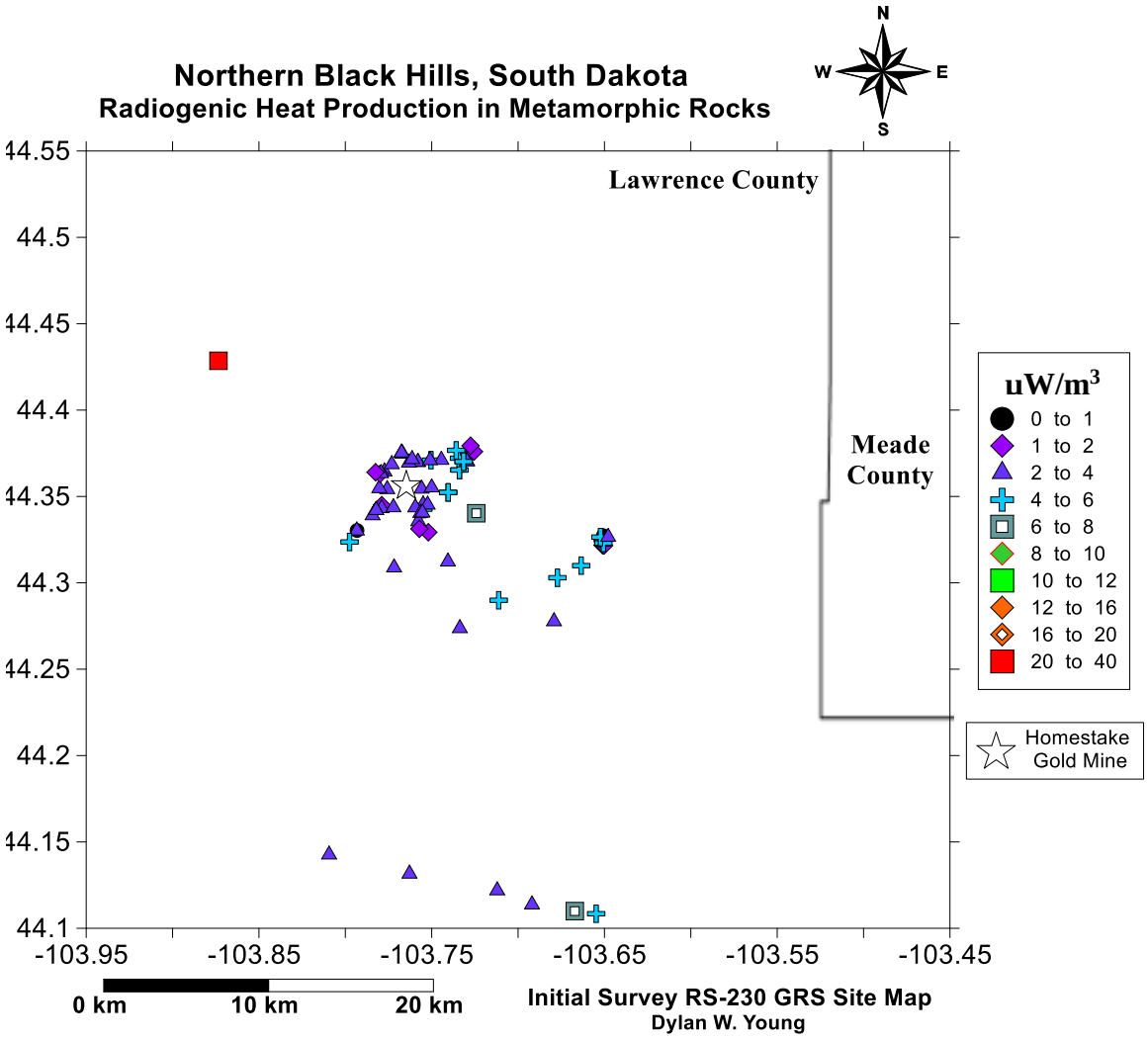

Figure 36. RS-230 GRS Survey of Metamorphic Radiogenic Heat Production

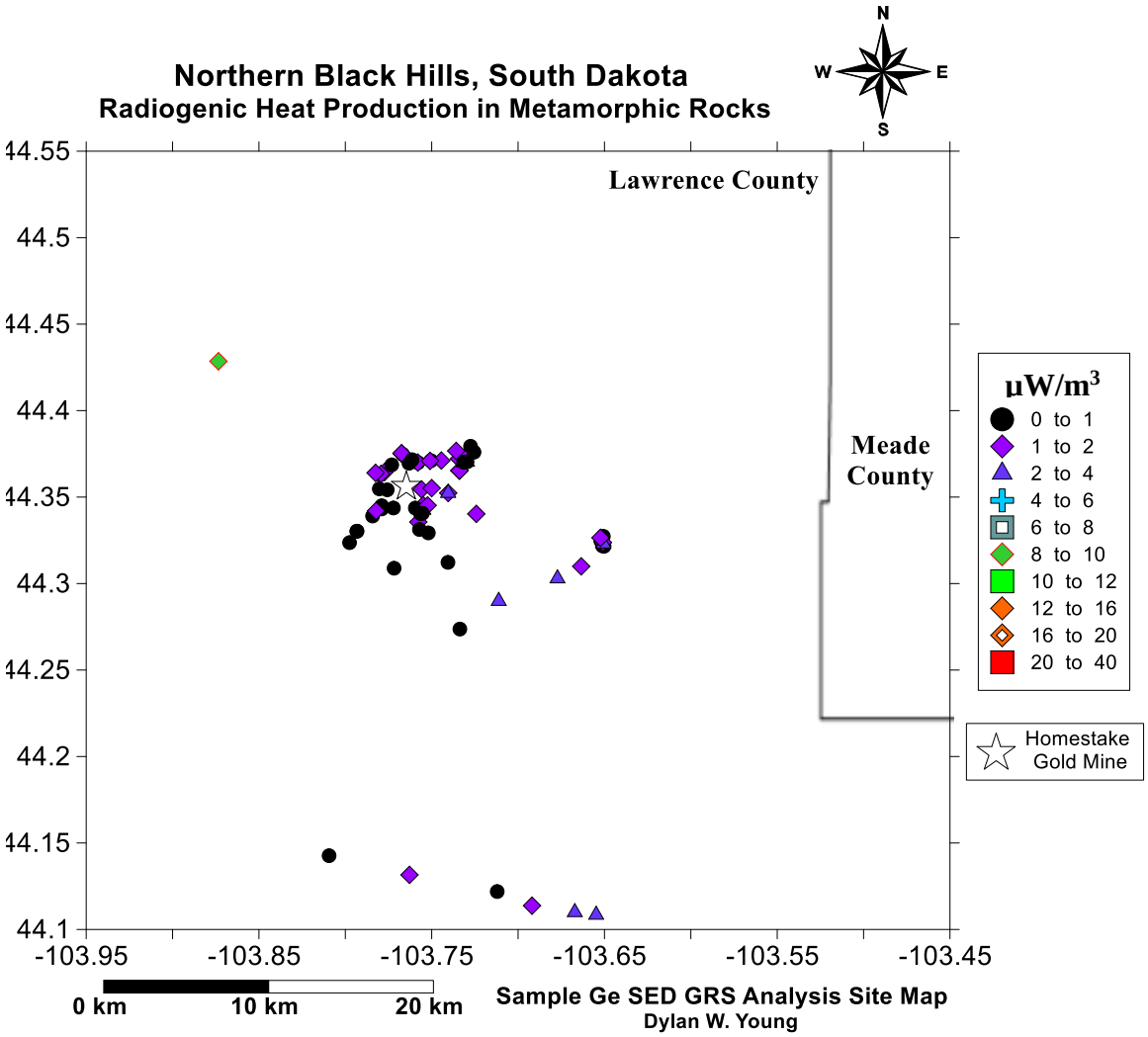

Figure 37. Ge SED GRS Analysis of Metamorphic Radiogenic Heat Production

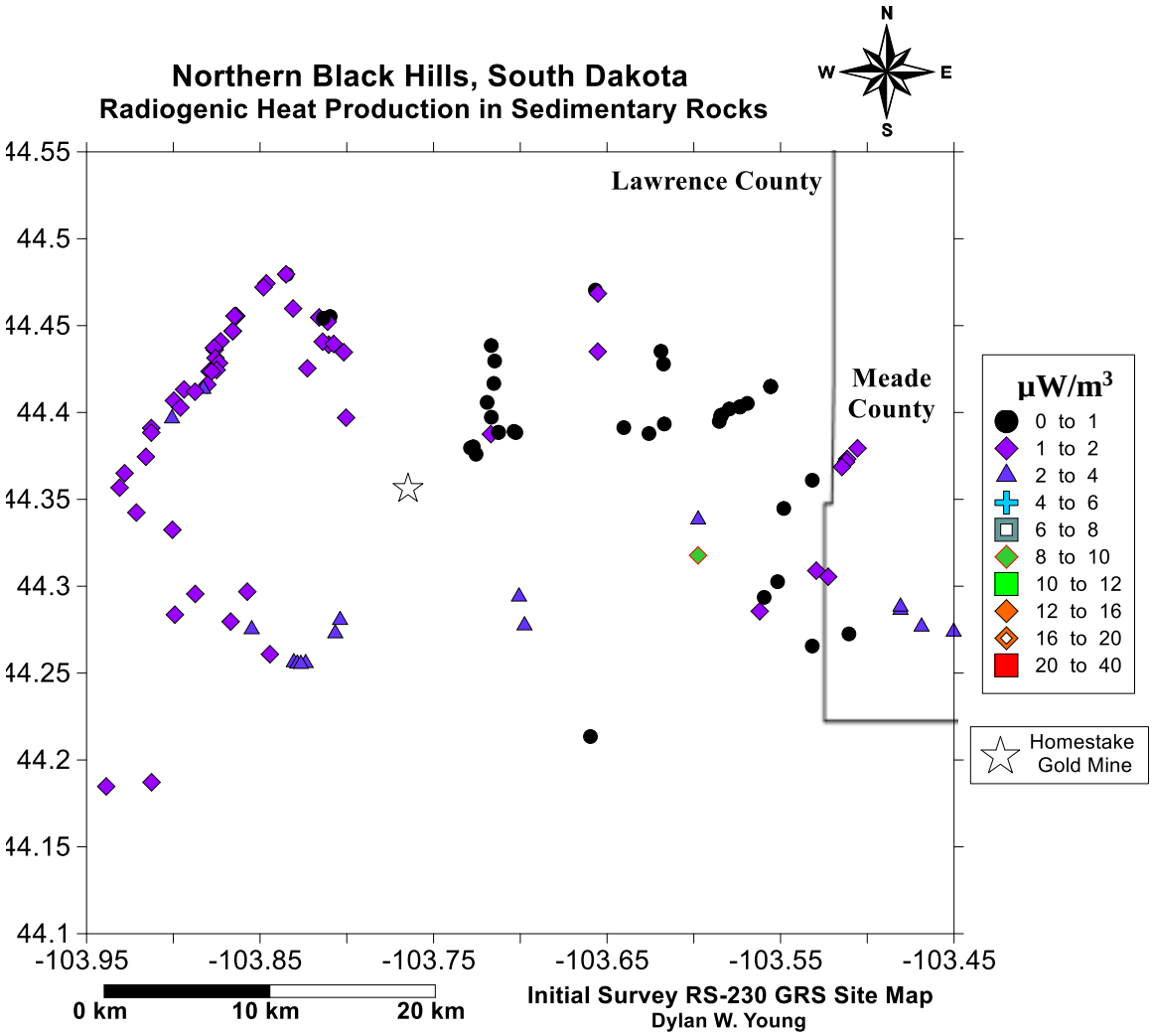

Figure 38. RS-230 GRS Survey of Sedimentary Radiogenic Heat Production

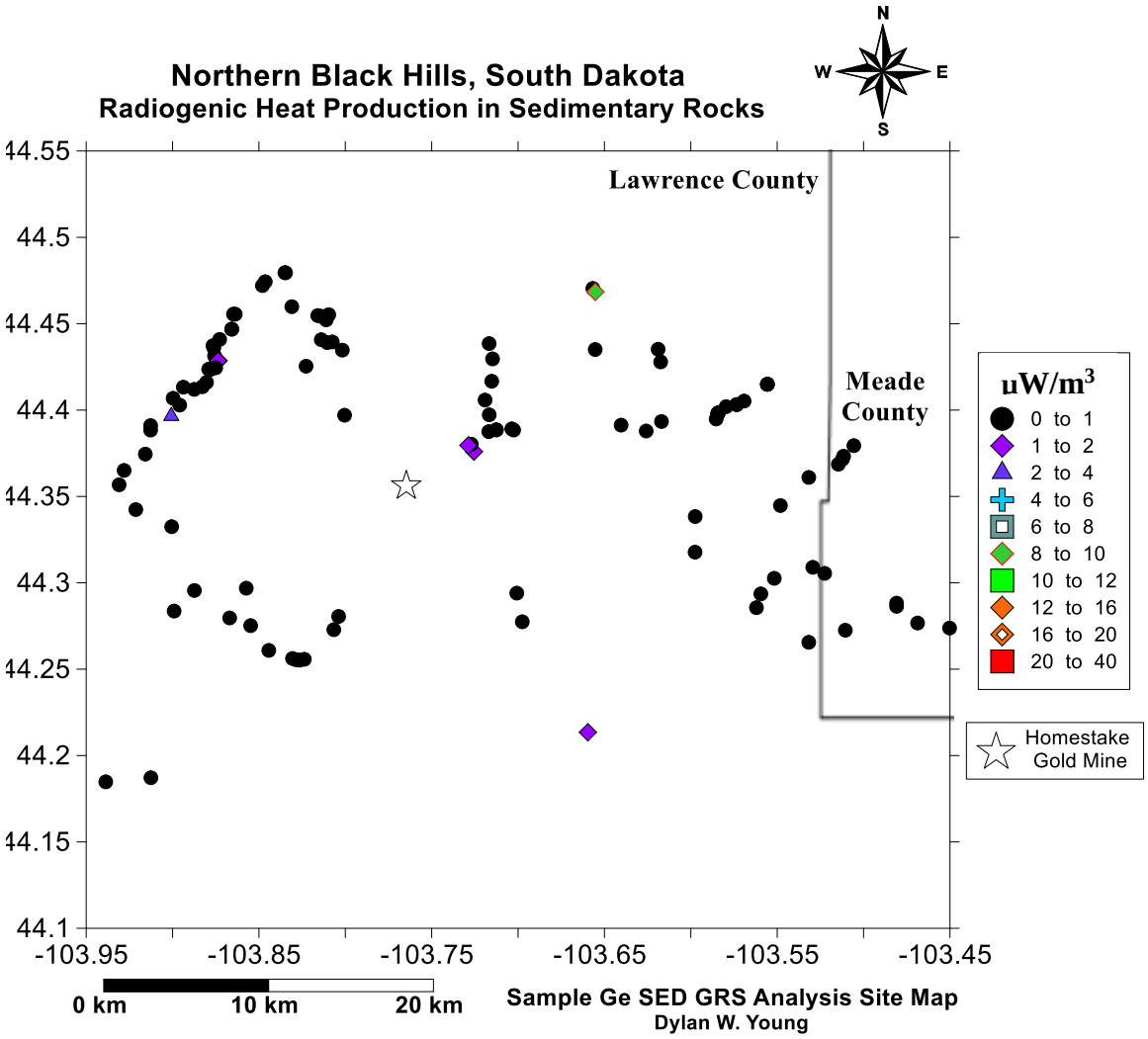

Figure 39. Ge SED GRS Analysis of Sedimentary Radiogenic Heat Production

Luminosity Mapping

The geoneutrino luminosity map presented in Figure 40 and Figure 41 represents where U, Th, and K in the NBH study area are potentially producing the highest number of antineutrinos that may affect the results of the future detector for DUNE. The map is derived from the numerical content of U, Th, and K in each sample, as well as the antineutrino production rate in Expression 4, modified from Table 9. Contour mapping was applied to accommodate this large dataset for the geoneutrino luminosity, since the luminosity is not dependent on individual data. A total geoneutrino luminosity (ε_v) of $2.24x10^5$ ($mg^{-1}s^{-1}$) was calculated from the RS-230 survey. A total geoneutrino luminosity (ε_v) of $9.40x10^4$ ($mg^{-1}s^{-1}$) was calculated from the Ge SED GRS analysis.

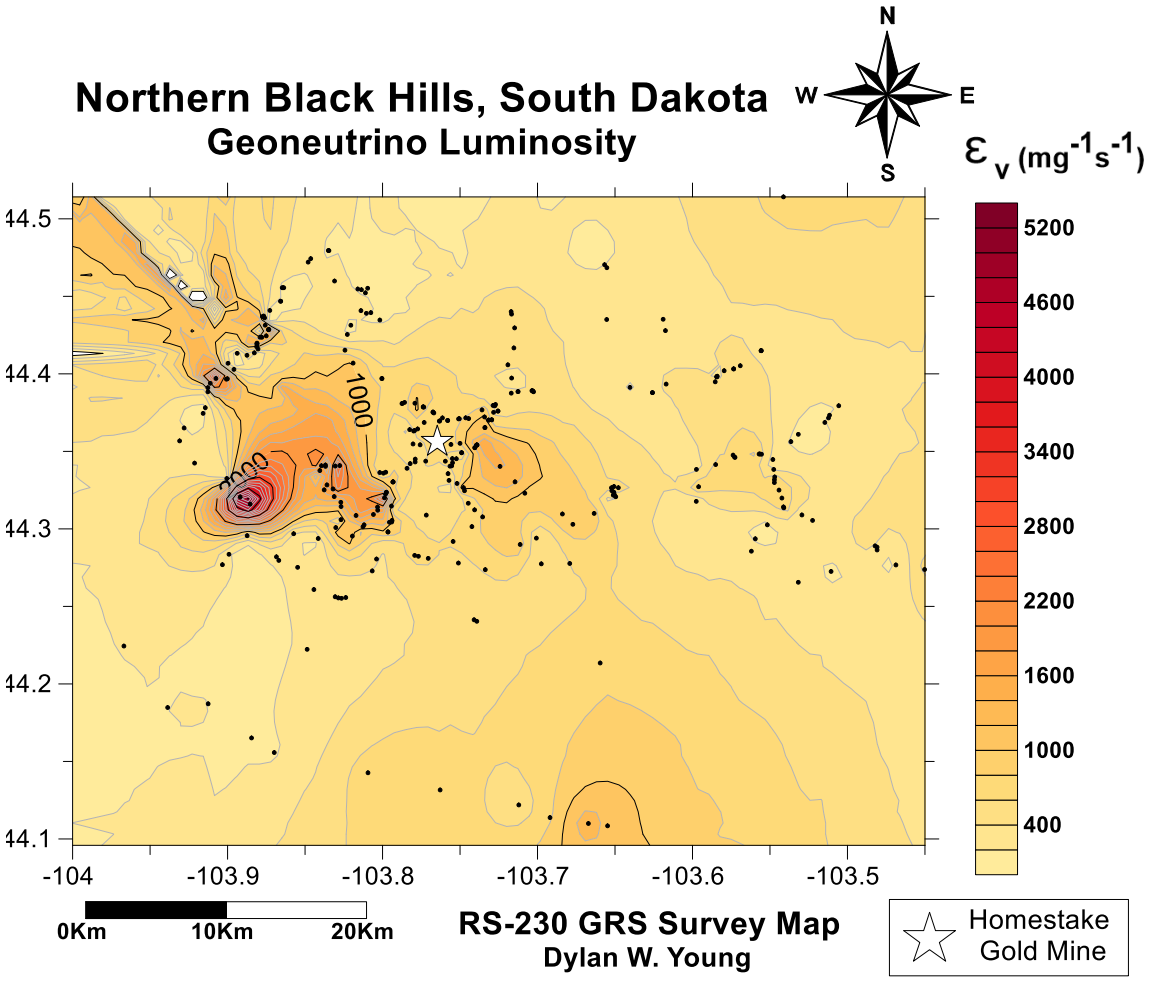

Figure 40. RS-230 GRS Survey
Geoneutrino Luminosity Map of the Northern Black Hills, SD

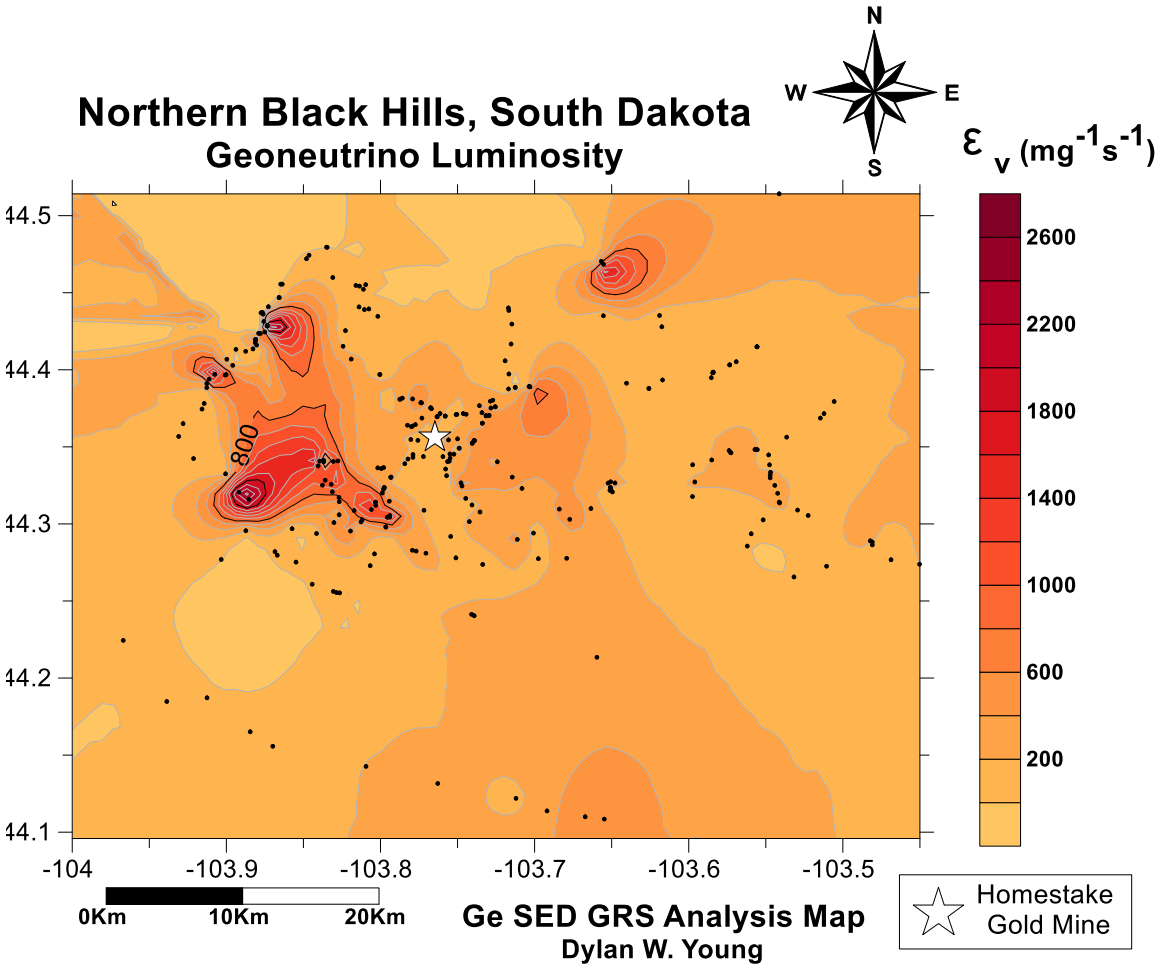

Figure 41. Ge SED GRS Analysis
Geoneutrino Luminosity Map of Northern Black Hills, SD

RS-230 GRS Homestake Gold Mine Survey

The HGM survey consisted of 143 analyzed samples. The survey took place at the -1700, -4100, and -4850-ft level of the HGM and at a few surface outcrops within the SURF property line. Only one phonolite sample (from the -2000 ft level) was collected from inside the HGM and analyzed at UND HHSGGE Geothermal Laboratory. The rest of the analyses were conducted by radiogenic survey using the RS-230 GRS. Of the 142 analyses directly surveyed by the RS-230 GRS, 61 were surveyed in the -1700-ft, 44 were surveyed in the -4100-ft, 24 were surveyed in the -4850-ft level, and 14 were

surveyed at surface outcrops. The metamorphic rocks have been described in several distinct units, while the rhyolites and phonolites are the only igneous rocks units in the HGM survey.

The radioelement survey consisted of 24 rhyolite analyses, 23 Yates Fm analyses (including 12 phyllites and 11 amphibolites), nine Northwestern Fm analyses (including four amphibolites and five phyllites), 30 Ellison Fm analyses (including seven amphibolites, 19 phyllites, and four schists), 37 Poorman Fm analyses (including 35 phyllites and 2 schists), five Flagrock Fm analyses (all phyllites), 14 Homestake Fm analyses (three phyllites and 11 schists) and lastly, the analysis of one phonolite sample. All the collected data is displayed in Table 29 – Table 30, in Appendix A. The U, Th, and K content, calculated heat production and luminosity are compared in Table 37 – Table 38, in Appendix B.

Figure 42. Overview of SURF, HGM and the town of Lead, South Dakota

Figure 43. Close-up view the Sanford Underground Research Facility

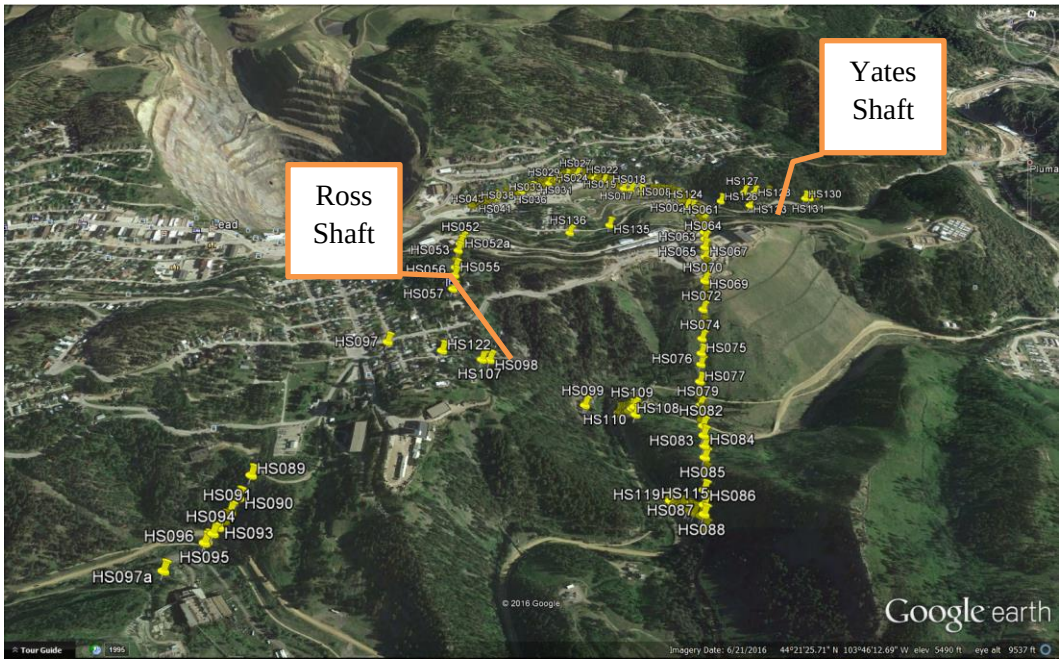

Figure 44. Overview of the distance surveyed underground in the HGM.

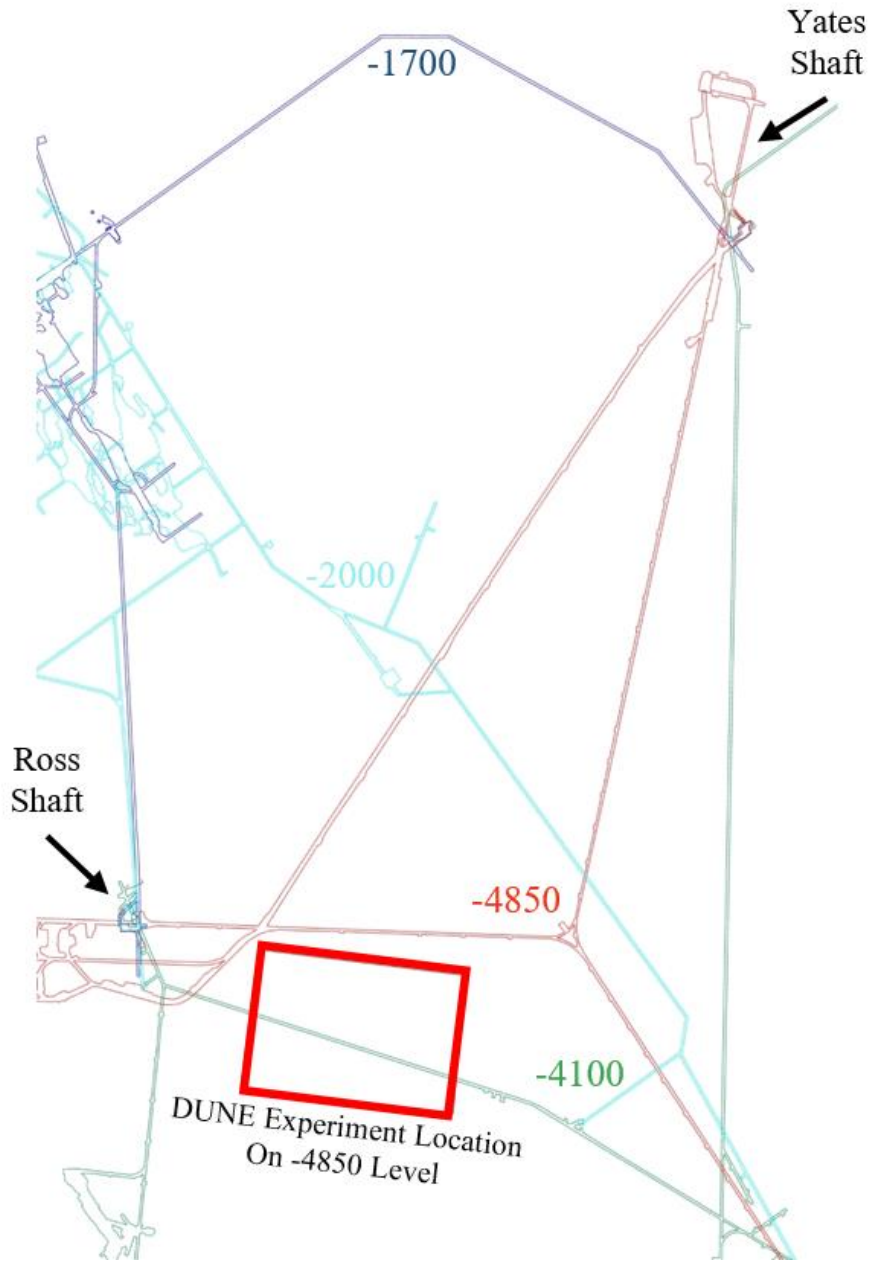

Figure 45. Diagram of the future DUNE facility inside the Homestake Gold mine, including the -1700 ft (dark blue), -2000 ft (light blue), 4100 ft (light green) and -4850 ft (red) levels, as well as the intersections of the Yates and Ross shafts. This map was originally created by Kathy Hart (SDSTA) at Sanford Underground Research Facility, which was modified for this thesis. Permission to include this diagram was granted by both Kathy Hart and Jaret Heise (SURF Science Liaison Director).

The -1700-ft level survey consisted of 24 Ellison Fm analyses, 13 Yates Fm analyses, 11 Poorman Fm analyses, four Northwestern Fm analyses, three Homestake Fm analyses, and five analyses of rhyolite rocks. The -4100-ft level survey consisted of 26 Poorman Fm analyses, seven Homestake Fm analyses, five Yates Fm analyses, and seven analyses of rhyolite rocks. The -4850-ft level of the HGM survey consisted of six Ellison Fm analyses, four Homestake Fm analyses, one Poorman Fm analysis, five Yates Fm analyses, and eight analyses of rhyolite rocks. The radioelement analyses of the surface outcrops consisted of five analyses of Northwestern Fm, five analyses of Flagrock Fm, and four analyses of rhyolite rocks.

Figures 54 – Figures 57 in Appendix D compare the radioelement ratios in the rocks surveyed inside the HGM and on within SURF property. Rhyolites are the most abundant and closest igneous rocks to the future detector, therefore, may directly affect the detector readings. In Appendix E, Fig. 58A – Fig. 58H compares the variation of the U:Th ratio of rhyolites at different levels of the HGM.

HGM U, Th, and K Content, Radiogenic Heat Production, and Luminosity

The average radiogenic heat production (*A*) and antineutrino luminosity (ε_v) of each formation and rhyolite intrusion are present in the table below. This is followed by the average U, Th, and K content, and the Th:U ratio of the different rock types in each formation and/or intrusion. A total geoneutrino luminosity (ε_v) of 1.26×10^5 ($mg^{-1}s^{-1}$) was calculated from the samples analyzed within the Homestake Gold Mine.

Table 17. Average radiogenic heat production and luminosity of formations and rhyolite intrusion at the Homestake Gold Mine

Formation/Intrusion	***A* (μWm^{-3})**	**ε_v ($mg^{-1}s^{-1}$)**
Ellison	3.8 ± 1.5	839 ± 291
Flagrock	3.3 ± 0.8	814 ±188
Homestake	2.9 ± 1.4	670 ± 327
Northwestern	3.5 ± 0.8	747 ± 127
Poorman	4.0 ± 1.3	940 ± 321
Yates	2.7 ± 1.3	577 ± 288
Rhyolite	5.8 ± 1.2	1340 ± 283

Table 18. Average radioelement content of rocks in the Ellison Formation

Rock	**U (ppm)**	**Th (ppm)**	**K (pct)**	**Th:U Ratio**
Amphibolite	5.29 ± 0.61	23.06 ± 2.76	4.66 ± 0.55	4.39 ± 0.51
Phyllite	6.16 ± 2.26	18.42 ± 10.03	3.91 ± 1.63	2.94 ± 0.79
Schist	5.88 ± 1.77	8.75 ± 2.56	2.65 ±0.90	1.55 ± 0.47

Table 19. Average radioelement content of rocks in the Flagrock Formation

Rock	**U (ppm)**	**Th (ppm)**	**K (pct)**	**Th:U Ratio**
Phyllite	8.68 ± 3.67	7.38 ± 6.56	1.90 ± 2.87	1.30 ± 1.76

Table 20. Average radioelement content of rocks in the Homestake Formation

Rock	U (ppm)	Th (ppm)	K (pct)	Th:U Ratio
Phyllite	7.50 ± 2.67	9.90 ± 3.27	2.77 ± 1.00	1.40 ± 0.28
Schist	6.01 ± 4.09	7.66 ± 1.91	2.39 ± 1.05	1.90 ± 1.15

Table 21. Average radioelement content of rocks in the Northwestern Formation

Rock	U (ppm)	Th (ppm)	K (pct)	Th:U Ratio
Amphibolite	4.43 ± 0.42	16.95 ± 2.15	4.05 ± 0.53	3.98 ± 0.85
Phyllite	5.68 ± 0.97	14.50 ± 3.60	4.42 ± 0.83	2.55 ± 0.49

Table 22. Average radioelement content of rocks in the Poorman Formation

Rock	U (ppm)	Th (ppm)	K (pct)	Th:U Ratio
Phyllite	8.49 ± 3.85	12.44 ± 6.05	3.71 ± 1.42	4.05 ± 1.40
Schist	9.35 ± 2.76	17.15 ± 8.85	4.60 ± 0.00	2.10 ± 1.55

Table 23. Average radioelement content of rocks in the Yates Formation

Rock	U (ppm)	Th (ppm)	K (pct)	Th:U Ratio
Amphibolite	4.74 ± 1.00	20.49 ± 5.25	4.31 ± 1.65	4.40 ± 1.02
Phyllite	3.07 ± 1.79	5.63 ± 4.34	2.08 ± 1.28	1.83 ± 1.31

Table 24. Average radioelement content of rocks of the igneous intrusions

Rock	U (ppm)	Th (ppm)	K (pct)	Th:U Ratio
Rhyolite	11.64 ± 2.91	16.89 ± 4.50	7.55 ± 2.64	1.55 ± 0.64

CHAPTER VII

DISCUSSION

Deep Underground Neutrino Experiment Location

The central United States underwent sedimentary deposition in epeiric seas on top of Precambrian era crystalline rocks throughout the Phanerozoic Era (Dewitt et al, 1986; Vickers, 1954). The GoogleEarth map (Figure 46) shows the general Midwest surface geology between the Fermilab in Batavia, IL, and SURF in Lead, SD. The various blue tone colors in Figure 56 show different sedimentary basement rocks (i.e., limestone, sandstone, shale) during the Mesozoic era, while the yellowish orange/tan colors represent clay, sand, and till from glaciation during the recent Quaternity Period (Burchett, 1986; Clayton, 1980; Diffendal, 1991; Hershey, 1969; Martin et al, 2004; Morey and Meints, 2000; Mudrey et al, 1982; William and others, 1967).

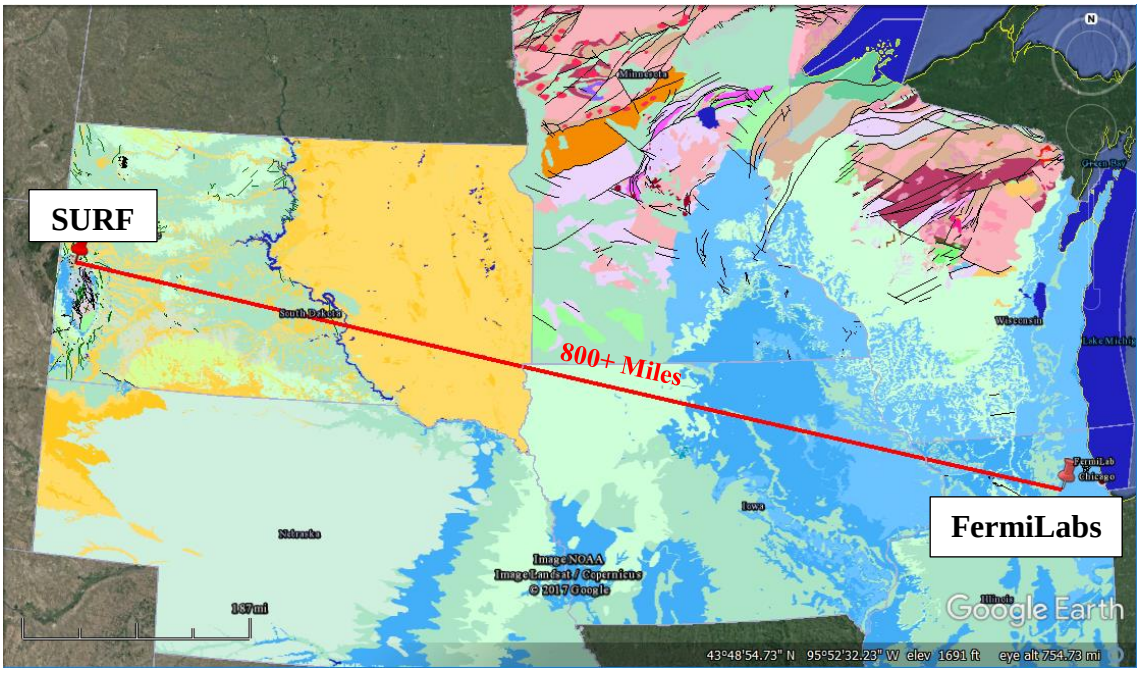

Figure 46. Overlying sedimentary influence between the Fermilab Accelerator Complex (Batavia, IL) and the Neutrino Detector at SURF, inside the HGM (Lead, SD). Sedimentary rocks contain little to no radioactivity and therefore could be discarded (Brenner, 1981; Burchett, 1966; Clayton, 1980; Diffendal, 1991; Hershey, 1969; Martin, 2004; Morrey & Meints, 2000; Mudray, 1992; William & Others, 1967; Yermolayev, 1973; Swinehart, 1985).

The Homestake Gold Mine was determined to be a qualified location to host the geoneutrino detector due to the mine's location and depth. The neutrino detector will be hosted at the -4850-ft level of HGM, in basement rock consisting of crystalline igneous and metamorphic rocks. The particle accelerator at Fermilab, Batavia, IL, will fire the particle beam through the deep basement rock (e.g., granite) underneath the overlying sedimentary deposits in central United States so that cosmic rays cannot affect the experiment. With the distance between the neutrino detector and the particle accelerator being more than 800 miles, geological influences must be minimal for the experiment to be successful. Sedimentary rocks lack notable levels of radioactivity (therefore, lack antineutrino production) that may interfere with particles that are emitted from the particle accelerator at Fermilab.

Igneous and metamorphic rocks, with assistance of hydrothermal events, can have interfering radiation, producing neutrinos and antineutrinos through beta decay. The midcontinent region of the North America basement rock is made up of various provinces of granitic/granitoids, metamorphosed Archean rocks, basaltic-rhyolitic volcanic suites and metasedimentary rocks (Atekwana, 1996). Figure 47 shows the generalized basement geology of the Midcontinent, United States (Sims, et al., 1987).

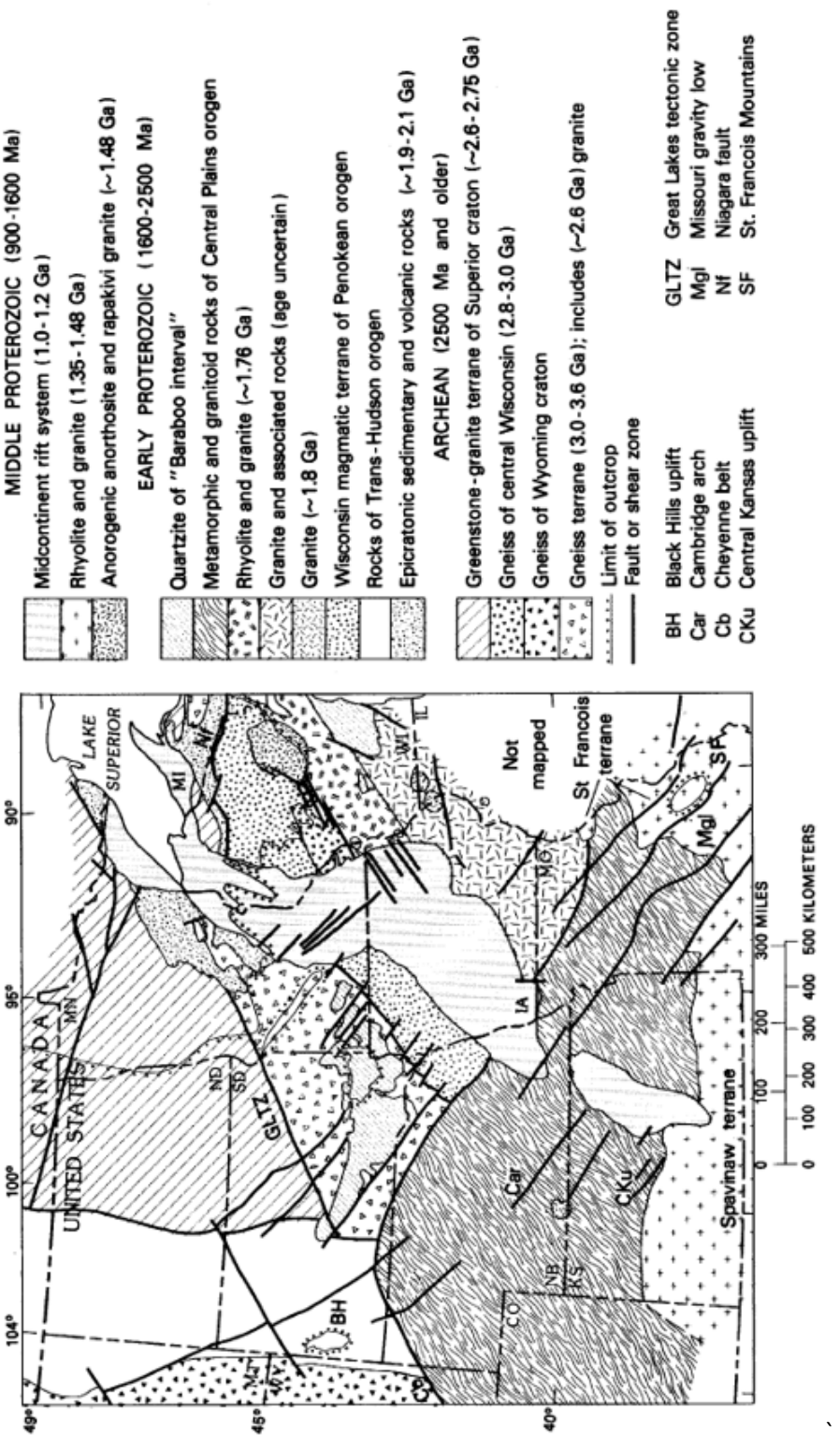

Figure 47. Generalized basement geology of the northern midcontinent (Midwest), U.S.A (Sims, et al., 1987)

For further basement rock descriptions and Precambrian tectonic provinces in the mid-continent region see Birchford et al. (1986), Klasner et al (1982), and Van Schmus (1992). For further study of the basement geology of North and South Dakota, see Bickford et al (1986), and Klasner and King (1986).

Thorium and Uranium Enrichment

Th:U content present in the rhyolite samples surveyed inside the HGM and within SURF property are highly variable, while the Th:U content in metamorphic samples analyzed are largely similar. Hydrothermal and magmatic interactions with different aqueous fluid phases can affect the content of U and Th in igneous rocks (Gosnold, 1976). Studies (Smithson and Decker, 1973; Wollenberg, 1974) have observed that U and Th content in hydrothermally altered plutons can be significantly higher than in non-hydrothermally altered ones (e.g., the Laramie Mountains in the Rockies.) After the Black Hills were uplifted during the Laramide orogeny (65-60 Ma), the west-northwestern belt of Tertiary alkalic rich igneous rocks (made up of stocks, laccoliths, dikes and sills) intruded the Precambrian, Paleozoic and Mesozoic rocks (Caddy et al., 1990), allowing for mobilization of U and Th with hydrous magmas and enrichment of the Quaternity rocks.

Metamorphism has also been reported to cause interference by the redistribution of U and Th content in continental crust through fluid phase rearrangement (Gosnold, 1976). U and Th may be mobilized with fluid phases of dehydration reactions during hydrothermal activity and magmatic events (Lambert and Heier, 1967). U is mobilized at low grade regional and contact metamorphism (Yermolayev, 1973). Thorium also can be mobilized, according to Yermolayev (1973), however it requires a higher grade of metamorphism when compared to U. Yermolayev

(1973) suggests three mechanisms during metamorphism that allows for the mobilization of the two radioelements:

1.) Desorption during early stages of metamorphism, when rocks are rich in H_2O and CO_2, allowing U to be more mobile (high Th:U ratio).
2.) Recrystallization throughout the progressive metamorphism, allowing for both Th and U to be mobilized (low Th:U ratio).
3.) Mineral dissolution and/or replacement in high grade metamorphic environments, mobilizing heavy elements (U and Th).

Within the HGM and Lead, SD, numerous hydrothermal alterations and corresponding events took place in the early Proterozoic rocks, during the early Cenozoic Eon, in response to high fluid fluxes (Caddy et al., 1991). These alterations were frequent in sheer zones with renewed thermal activity (Caddy et al., 1991). Zones of high fluid and corresponding alterations were confined to sections of shear zones inside and adjacent to the Homestake Fm and the Yates unit (lower Poorman Fm), which led to partial and complete mineral replacement that commonly entailed mass transfer, leaving significant rheologic contrast with the bounding phyllites (Caddy et al., 1991). Frequent hydrothermal alterations took place at separate stages throughout the Precambrian in the NBH and Lead, SD. The hydrothermal fluids and frequent metamorphism in HGM could have enabled for enrichment of U and Th, based on three mechanisms which Yermolayev (1973) outlined. Further information on the Proterozoic geology and hydrothermal alterations at of the Homestake Gold Mine, see Caddy et al. (1990).

High U and Th content has been correlated with larger silica content in rocks. Larsen et al. (1955) reported that there is frequent uranium enrichment in young igneous rocks (i.e., rhyolites, trachytes) with high SiO_2 and K_2O content and low CaO and MgO, in the Laramide orogeny and the Rocky Mountains, such as the California batholith and the San Juan mountains in western Colorado. The young SiO_2 rich igneous rocks with U and Th content are partially associated with fractional crystallization (Larsen et al., 1955).

Most of the rocks in the HGM are metamorphic bodies. The two igneous rock types in the mine are rhyolite and phonolite, which should have high SiO_2 content, however, do to limitations of funding for the study, a geochemical analysis of the samples was not included.

Phonolite Influence

An important section that must be examined further in the future is the phonolite rocks present in the -2000-ft level. Phonolites, after analyzing the number of samples present across the NBH, are critical contributors to higher levels of radiogenic heat production in the region. A single small phonolite sample (268.7g) was collected from the -2000-ft HGM, donated by Kathy Hart (SDSTA). The initial analysis determined a content of 5.57 ppm U, 18.74 ppm Th, and 4.14 pct K, producing a radiogenic heat production of 3.74 μWm^{-3}. Most of the samples analyzed weighed between 600 and 900 g. After correction for the size difference (750 g), contents of the sample were determined to be 10.04 ppm U, 23.61 ppm Th, and 4.54 pct K, producing a heat production of 5.56 $\mu W\ m^{-3}$. Two additional phonolite samples were gathered (thanks to Benjamin York [UND-MS] and Dr. Dexter Perkins) from the Devils Tower, a laccolithic butte present in the western edge of the NBH near Sundance, Wyoming. The Devils Tower also formed during the Laramide orogeny, which constructed the Rocky Mountains and the Black Hills outlier. The two phonolite samples collected have very high readings of U, Th, and K.

Sample 1 has 13.46 ppm U, 39.50 ppm Th, and 2.78 pct K. The radiogenic heat production in phonolite sample 1 was calculated to be 7.73 μWm^{-3}. Sample 2 has 9.66 ppm U, 26.45 ppm Th, and 3.65 pct K. The radiogenic heat production in phonolite sample 2 was calculated to be 5.58 $\mu W\ m^{-3}$.

The first phonolite sample was collected at the base of Devils Tower (44.589336° N, -104.716961° W). The second phonolite sample was collected near the top of the Warren Peak Lookout Tower (44.475905° N, -104.475905° W), 25-km to the southeast of the Devils Tower. The Devils Tower itself is approximately 81-km northwest of the HGM and Lead, SD. Warren Peak Lookout, on the other hand, is 56-km northwest of the HGM and Lead, SD. The higher radiogenic heat production from phonolites and similar alkali-volcanic igneous rocks consequently indicates that there is a much higher frequency of geoneutrino production throughout the NBH than what is present within the HGM and the 15-km study area.

The total U:Th ratios in the NBH do not follow standard estimations of BSE models or continental crust models, which were under consideration for detector calibrations. These models are largely based off cosmogenic abundances of elements through data gathered on a global scale. These models do not accommodate for small-scale distributions and variations, such as the hydrothermal metamorphic and igneous activity that took place in the Black Hills during the Precambrian and Phanerozoic eons.

A further, more complete analysis inside the HGM needs to be completed. This survey inside the HGM was a small-scale, short-term analysis and was not as thorough as needed for the complete calibration of the geoneutrino detector. The -4850-ft level of the HGM, specifically, only had a fewer sample analyses, as compared to the -1700 and the -4100-ft levels. The U, Th, K, and radiogenic heat production inside the HGM are higher than anticipated.

Radiogenic Heat Production/Heat Flow Relationship

There is a strong decrease in the levels of radioactivity and heat production going from upper crust to lower crust to the upper mantle, which is potentially influenced by accretion and differentiation of the incompatible elements in early stages of Earth (Anderson, 2007; Birch, et al., 1968; Lambert and Heier, 1966; Roy et al., 1968; Roy et al., 1972). The relationship between heat flow and heat production will be affected by large intrusive bodies, and the disturbances to the original distribution of U and Th content (Roy et al., 1972). Current estimates of the heat flow across the continental United States (Blackwell et al., 2011) show that the Black Hills have an anomalously low heat flow (20-35 mWm^{-2}) when compared to the surrounding Great Plains, the Nebraska Sand Hills, and the Laramide Belt (45-110 mWm^{-2}). South-central South Dakota, in comparison, has an anomalously high heat flow ($Q > 130$ mWm^{-2}) (Gosnold, 1999). Heat flow is dependent on radiogenic heat production, but the extent largely remains undetermined. The presented findings in this thesis argue with the accuracy of the U previously determined U, Th, and K content, as well as the radioactive heat production, present in the Northern Black Hills (Davies & Davies, 2010; Dewitt, 1986; McDonough, 1995; Paige, 1924; Tilling, 1969; Usman, 2015; Vickers, 1954; Wollenberg, 1968).

CHAPTER IIX

CONCLUSION

The Northern Black Hills underwent large-scale tectonism and hydrothermal metamorphism during the Laramide orogeny. Laramide tectonism, numerous metamorphism, and hydrothermal activities enriched the Northern Black Hills in economically valuable REE and mineral deposits deep beneath the surface. These events, in addition to more recent igneous intrusions, caused U, Th, and K enrichment higher than normal radioelement abundances in the rocks present in the BH, especially the NBH. This analysis conducted in the NBH illustrates the radioelement enrichment and potential hindrance to the DUNE experiment. The goal of this project was achieved and will improve the accuracy of the results of DUNE.

By conducting this radiogenic survey and analyzing numerous rock samples and outcrops present in the NBH, the radioelement content of U, Th, K, and heat production have been determined to be higher than previous interpretations. The higher radioelement distribution and content must be calibrated for, to ensure the future geoneutrino detector's readings are accurate and successful. The findings from this analysis concur with Zimney's (2014) conclusion that to address this issue, calibrations of the detector should not be based on the U, Th, and K content of the BSE model or continental crust models. BSE model estimates are based on cosmogenic, primordial Earth elemental abundances with global scale sampling, not on small-scale, localized geological contributions.

Results of my radiogenic analysis point out the necessity of further research toward the abundance and distribution of U, Th, and K inside the HGM, across the NBH, and the North American continent. Additional heat flow observations are also key to improved estimates of the United States heat production, heat flow, and potential geothermal resources.

Appendix A

Northern Black Hills and Homestake Gold Mine

Gamma-ray Spectrometer Results:

U, Th, And K Content, Calculated Heat Production (*A*) And Luminosity (ε_v)

Table 25: RS-230 GRS Survey results- listed with sample identification (ID), Latitude (N) and Longitude (W), Elevation (Elev.), Th:U ratio, U, Th, K content, calculated heat production (A) and anitneturino luminosity (ε_v)

Pre -	Name	ID	(N)	(W)	Elev. (ft)	Th:U	U (ppm)	Th (ppm)	K (pct)	A (μWm^{-3})	ε_v ($mg^{-1}s^{-1}$)
105	BHH385	S001	44.21347	-103.65958	5526	2.89	5.7	16.5	2.9	3.45	7.68E+02
105	BHH385	I002	44.30294	-103.67720	5262	2.26	8.2	18.5	2.9	4.38	9.86E+02
105	BHH385	S003	44.32299	-103.70818	5635	2.20	7.1	15.6	5.0	4.04	9.14E+02
105	BHH385	I003	44.30958	-103.68394	5358	2.32	7.9	18.3	3.3	4.32	9.71E+02
105	BHH385	I004	44.33031	-103.71451	5405	2.66	10.2	27.1	3.5	5.78	1.29E+03
105	BHH385	Ig005	44.34028	-103.72418	5119	1.70	13.4	22.8	3.7	6.42	1.46E+03
105	BHH385	M006	44.35235	-103.74046	4787	2.96	7.4	21.9	2.8	4.41	9.79E+02
105	BHH385	M007	44.35235	-103.74046	4787	2.96	7.4	21.9	2.8	4.41	9.79E+02
105	BHH385	M008	44.35409	-103.73906	4759	0.75	20.1	15.1	5.3	8.00	1.88E+03
108	BHH385	M008a	44.35409	-103.73906	4759	0.75	20.1	15.1	5.3	8.00	1.88E+03
105	BHH385	Ig009	44.35404	-103.73931	4770	1.85	11.9	22.0	8.6	6.45	1.47E+03
105	BHH85	Ig010	44.35404	-103.73931	4770	1.85	11.9	22.0	8.6	6.45	1.47E+03
105	BHH85	Sc011	44.36533	-103.73394	4678	3.37	6.3	21.2	5.0	4.26	9.46E+02
105	BHH85	Sc012	44.36533	-103.73394	4678	3.37	6.3	21.2	5.0	4.26	9.46E+02
105	BHH85	SS013	44.37596	-103.72552	4830	1.06	5.3	5.6	0.6	2.16	5.00E+02
105	BHH85	SS014	44.37596	-103.72552	4830	1.03	3.7	3.8	0.6	1.52	3.52E+02
105	BHDEAD	S015	44.37034	-103.72956	4635	0.42	5.7	2.4	3.2	2.30	5.48E+02
105	BHDEAD	S016	44.37034	-103.72956	4635	0.42	5.7	2.4	3.2	2.30	5.48E+02
105	BHDEAD	Sc017	44.37016	-103.73151	4618	1.81	11.1	20.1	4.3	5.56	1.26E+03
105	BHDEAD	Sc018	44.37016	-103.73151	4618	1.81	11.1	20.1	4.3	5.56	1.26E+03
105	BHDEAD	SS019	44.38025	-103.72711	4662	0.55	6.2	3.4	0.3	2.21	5.23E+02
105	BHDEAD	SS020	44.37959	-103.72871	4664	0.63	4.3	2.7	0.8	1.63	3.84E+02
105	BHDEAD	Sc021	44.37671	-103.73582	4660	3.64	5.8	21.1	6.2	4.24	9.40E+02
105	BHDEAD	Gc022	44.37217	-103.73418	4708	4.33	6.0	26.0	5.8	4.66	1.02E+03

Table 25: cont.

Pre -	Name	ID	(N)	(W)	Elev. (ft)	Th:U	U (ppm)	Th (ppm)	K (pct)	A (μWm^{-3})	ε_v ($mg^{-1}s^{-1}$)
105	BHDEAD	Sc023	44.37517	-103.72836	4548	2.53	7.3	18.5	4.4	4.27	9.60E+02
205	BHH14	RSS024	44.41493	-103.55570	3608	0.39	4.1	1.6	0.5	1.44	3.43E+02
205	BHH14	RSS025	44.41493	-103.55570	3608	0.53	5.7	3.0	0.5	2.05	4.85E+02
205	BHH14	SS026	44.41493	-103.55570	3608	0.46	5.7	2.6	0.6	2.03	4.81E+02
205	BHH14	LS027	44.40520	-103.56916	3666	0.43	6.0	2.6	0.8	2.14	5.08E+02
205	BHH14	LSS028	44.40317	-103.57343	3694	1.98	6.3	12.5	0.6	3.04	6.86E+02
205	BHH14	LSS029	44.40317	-103.57343	3694	1.39	4.9	6.8	0.3	2.10	4.81E+02
205	BHH14	LSS030	44.40198	-103.57956	3730	0.31	4.9	1.5	0.3	1.66	3.96E+02
205	BHH14	LS031	44.39848	-103.58404	3781	0.54	4.1	2.2	0.3	1.47	3.48E+02
205	BHH14	LS032	44.39827	-103.58423	3779	1.49	4.3	6.4	1.1	1.97	4.52E+02
205	BHH14	LS033	44.39811	-103.58434	3783	1.28	3.9	5.0	0.2	1.63	3.75E+02
205	BHH14	LS034	44.39801	-103.58435	3788	0.34	4.7	1.6	0.7	1.65	3.93E+02
205	BHH14	LSS034	44.39801	-103.58435	3788	0.33	5.7	1.9	0.3	1.93	4.61E+02
205	BHH14	LS035	44.39483	-103.58533	3833	0.33	5.7	1.9	0.3	1.93	4.61E+02
205	BHH14	LS036a	44.38787	-103.62584	4222	2.39	2.3	5.5	0.4	1.21	2.70E+02
205	BHH14	LS036b	44.39337	-103.61700	4198	1.00	2.0	2.0	0.4	0.82	1.91E+02
205	BHH14	LS037	44.39127	-103.64035	4323	1.28	1.8	2.3	0.5	0.80	1.84E+02
205	BHH14	LSS038	44.38842	-103.70256	4490	2.46	3.7	9.1	2.3	2.15	4.84E+02
205	BHH14	B039	44.38893	-103.70301	4455	0.68	15.8	10.7	1.2	5.86	1.38E+03
205	BHH14	B040	44.38893	-103.70313	4461	1.09	21.9	23.9	1.5	8.86	2.05E+03
205	BHH14	LSS041	44.38911	-103.70362	4456	0.67	4.2	2.8	0.5	1.57	3.70E+02
305	BHCCR	SS042	44.47039	-103.65672	3776	4.40	0.5	2.2	0.0	0.34	7.27E+01
305	BHCCR	SS043	44.46844	-103.65526	3832	1.05	4.4	4.6	0.4	1.77	4.11E+02
305	BHCCR	SS044	44.42787	-103.61745	3937	0.82	3.3	2.7	0.2	1.26	2.94E+02

Table 25: cont.

Pre -	Name	ID	(N)	(W)	Elev. (ft)	Th:U	U (ppm)	Th (ppm)	K (pct)	A (μWm^{-3})	ε_v ($mg^{-1}s^{-1}$)
305	BHCCR	SS045	44.43520	-103.61893	3909	0.59	3.2	1.9	0.1	1.15	2.71E+02
305	BHCCR	SS046	44.43504	-103.65537	4017	2.14	2.2	4.7	1.7	1.26	2.85E+02
305	BHUS85	SS047	44.44010	-103.71702	4067	0.25	6.4	1.6	0.3	2.12	5.08E+02
305	BHUS85	SS048	44.43850	-103.71676	4069	2.02	5.3	10.7	2.2	2.76	6.26E+02
305	BHUS85	RSS049	44.42961	-103.71478	4201	0.64	4.4	2.8	0.2	1.60	3.77E+02
305	BHUS85	RSS050	44.41668	-103.71525	4472	0.46	7.0	3.2	0.5	2.46	5.84E+02
305	BHUS85	SS051	44.40579	-103.71912	4786	0.50	5.4	2.7	0.5	1.93	4.57E+02
305	BHUS85	LS052	44.39725	-103.71670	4850	1.42	2.4	3.4	0.2	1.04	2.38E+02
305	BHDEAD	Ig053	44.38855	-103.71258	4555	1.07	4.3	4.6	0.9	1.80	4.18E+02
305	BHDEAD	SS054	44.38853	-103.71258	4553	1.73	4.9	8.5	2.1	2.45	5.58E+02
305	BHDEAD	MSS055	44.38752	-103.71695	4511	2.32	3.7	8.6	3.8	2.28	5.16E+02
305	BHDEAD	M056	44.37938	-103.72752	4549	0.80	4.0	3.2	0.7	1.57	3.67E+02
305	BHDEAD	MG057	44.37113	-103.74441	4682	3.22	5.8	18.7	4.5	3.84	8.55E+02
305	BHDEAD	MG058	44.37160	-103.74633	4701	1.19	3.7	4.4	1.0	1.61	3.73E+02
305	BHUS14a	MSc059	44.37104	-103.75043	4724	2.41	7.9	19.0	5.1	4.58	1.03E+03
305	BHUS14a	MSc060	44.37093	-103.75096	4727	4.24	5.0	21.2	3.3	3.67	8.03E+02
305	BHUS14a	MGn061	44.36989	-103.75794	4785	2.27	4.4	10.0	2.1	2.42	5.45E+02
305	BHUS14a	MSc062	44.36997	-103.75802	4795	2.48	5.8	14.4	2.6	3.27	7.34E+02
305	BHUS14a	M063	44.36956	-103.76316	4832	1.66	5.8	9.6	1.3	2.72	6.21E+02
305	BHUS14a	MLSS064	44.36953	-103.76335	4853	1.60	7.2	11.5	3.8	3.59	8.23E+02
305	BHUS14a	MSc065	44.36861	-103.77313	4980	4.02	5.0	20.1	3.5	3.60	7.91E+02
405	BHNM	LSS066	44.27253	-103.51057	5015	0.82	1.7	1.4	0.4	0.68	1.59E+02
405	BHNM	LSS067	44.26555	-103.53172	5107	0.74	3.8	2.8	0.2	1.42	3.32E+02
405	BHVCR	LSS068	44.28559	-103.56200	4856	0.32	4.4	1.4	0.0	1.46	3.49E+02

Table 25: cont.

Pre -	Name	ID	(N)	(W)	Elev. (ft)	Th:U	U (ppm)	Th (ppm)	K (pct)	A (μWm^{-3})	ε_v ($mg^{-1}s^{-1}$)
405	BHVCR	LS069	44.29358	-103.55946	4758	0.18	1.7	0.3	0.2	0.57	1.36E+02
405	BHVCR	LSS070	44.30258	-103.55170	4695	0.46	1.3	0.6	0.2	0.47	1.11E+02
405	BHVCR	I071	44.31414	-103.54130	4779	3.88	4.3	16.7	3.1	3.06	6.73E+02
405	BHVCR	I072	44.51414	-103.54131	3363	3.88	4.3	16.7	3.1	3.06	6.73E+02
405	BHVCR	LSS073	44.30895	-103.52939	4631	2.21	1.9	4.2	0.9	1.03	2.33E+02
405	BHVCR	I073	44.30545	-103.52252	4607	0.93	3.0	2.8	0.4	1.20	2.79E+02
405	BHVCR	I074	44.31356	-103.54106	4779	4.30	4.7	20.2	3.0	3.46	7.57E+02
405	BHVCR	I075	44.31985	-103.54231	4865	5.03	4.0	20.1	2.8	3.22	6.98E+02
405	BHVCR	I076	44.32499	-103.54417	4946	2.79	6.1	17.0	3.4	3.67	8.20E+02
405	BHVCR	I077	44.32987	-103.54716	5016	5.11	3.7	18.9	2.9	3.04	6.59E+02
405	BHVCR	I078	44.33170	-103.54714	4973	3.09	4.5	13.9	2.9	2.87	6.37E+02
405	BHVCR	I079	44.33348	-103.54694	4901	3.60	4.7	16.9	3.1	3.20	7.06E+02
405	BHVCR	I080	44.33833	-103.54758	4735	1.30	2.0	2.6	0.3	0.86	1.98E+02
405	BHVCR	I081	44.34473	-103.54814	4617	2.67	1.8	4.8	0.9	1.05	2.36E+02
405	BHVCR	I082	44.35625	-103.53648	4563	1.41	1.7	2.4	0.4	0.77	1.76E+02
405	BHVCR	I083	44.36099	-103.53171	4360	1.53	1.5	2.3	0.3	0.68	1.57E+02
405	BHVCR	SS084	44.37330	-103.51157	3858	3.00	1.0	3.0	0.3	0.59	1.31E+02
405	BHVCR	I085	44.37940	-103.50562	3732	1.54	2.6	4.0	0.3	1.16	2.66E+02
405	BHVCR	SSI086	44.37155	-103.51223	3896	0.53	4.3	2.3	0.5	1.56	3.69E+02
405	BHVCR	SSI087	44.36863	-103.51460	3967	1.21	1.4	1.7	0.5	0.63	1.45E+02
505	BHSCR	I088	44.47430	-103.84634	3769	4.88	2.5	12.2	0.2	1.81	3.88E+02
505	BHSPRF	SGyp089	44.47946	-103.83459	3824	3.47	1.5	5.2	0.7	0.97	2.14E+02
505	BHSPRF	SGyp090	44.47953	-103.83499	3824	5.29	0.7	3.7	0.3	0.56	1.20E+02
505	BHSPRF	I091	44.45985	-103.83097	4062	1.31	2.6	3.4	0.4	1.12	2.59E+02

Table 25: cont.

Pre -	Name	ID	(N)	(W)	Elev. (ft)	Th:U	U (ppm)	Th (ppm)	K (pct)	A (μWm^{-3})	ε_v ($mg^{-1}s^{-1}$)
505	BHSPRF	I092	44.45470	-103.81596	4307	0.40	2.5	1.0	0.0	0.85	2.01E+02
505	BHSPRF	I093	44.45424	-103.81362	4319	0.69	1.3	0.9	0.0	0.47	1.11E+02
505	BHSPRF	I094	44.45520	-103.80960	4302	0.91	1.1	1.0	0.1	0.43	1.00E+02
505	BHSPRF	SS095	44.45222	-103.81106	4183	0.40	2.5	1.0	0.3	0.88	2.10E+02
505	BHMLR	SS096	44.44074	-103.81394	4254	3.14	2.1	6.6	1.2	1.33	2.95E+02
505	BHMLR	SS097	44.43904	-103.81044	4366	1.36	1.4	1.9	0.2	0.61	1.40E+02
505	BHMLR	SS098	44.43944	-103.80755	4493	2.26	1.9	4.3	0.2	0.96	2.16E+02
505	BHMLR	I099	44.43135	-103.82046	4396	3.23	1.3	4.2	0.5	0.81	1.78E+02
505	BHMLR	SS099	44.43468	-103.80174	4601	1.67	1.5	2.5	0.2	0.69	1.57E+02
505	BHMLR	ISS099	44.39700	-103.80043	4936	2.55	4.4	11.2	4.3	2.77	6.24E+02
505	BHMLR	ISS100	44.38083	-103.78748	5293	1.64	5.8	9.5	1.0	2.68	6.11E+02
505	BHMLR	I101	44.37867	-103.77377	4995	3.33	8.0	26.6	4.6	5.19	1.15E+03
505	BHMLR	I102	44.37852	-103.77338	4994	2.87	7.1	20.4	5.0	4.44	9.92E+02
505	BHMLR	MSc103	44.37519	-103.76746	4907	1.80	4.4	7.9	0.6	2.07	4.70E+02
505	BHMLR	MSc104	44.37537	-103.76743	4918	2.53	4.0	10.1	1.1	2.19	4.90E+02
505	BHCC	MSc105	44.36444	-103.77734	5010	2.72	4.7	12.8	2.4	2.78	6.21E+02
505	BHCC	MGn106	44.36342	-103.77932	5073	2.78	5.9	16.4	2.0	3.40	7.57E+02
505	BHCC	MGn107	44.36401	-103.78250	5249	2.70	2.7	7.3	1.2	1.57	3.51E+02
505	BHCC	Qtz108	44.36309	-103.77992	5050	2.10	2.9	6.1	1.3	1.54	3.49E+02
705	BHH14a	I0111	44.47205	-103.84801	3777	0.92	2.4	2.2	0.4	0.96	2.24E+02
705	BHH14a	LSS112	44.45552	-103.86373	3846	0.68	1.9	1.3	0.1	0.70	1.65E+02
706	BHH14a	LSS112	44.45552	-103.86373	3844	0.68	1.9	1.3	0.1	0.70	1.65E+02
705	BHH14a	LSS113	44.45552	-103.86475	3862	0.88	1.6	1.4	0.2	0.63	1.47E+02
705	BHH14a	LS114	44.44684	-103.86570	3931	0.50	2.2	1.1	0.3	0.80	1.89E+02

Table 25: cont.

Pre -	Name	ID	(N)	(W)	Elev. (ft)	Th:U	U (ppm)	Th (ppm)	K (pct)	A (μWm^{-3})	ε_v ($mg^{-1}s^{-1}$)
705	BHH14a	LS115	44.44684	-103.86581	3930	0.68	2.2	1.5	0.3	0.83	1.95E+02
705	BHH14a	LS116	44.44089	-103.87274	4007	1.85	1.3	2.4	0.2	0.62	1.41E+02
705	BHH14a	IgS117	44.43692	-103.87753	4239	3.82	11.4	43.6	3.1	7.48	1.64E+03
705	BHH14a	LSS118	44.43724	-103.87663	4080	1.42	2.4	3.4	0.3	1.05	2.41E+02
705	BHH14a	MLSH119	44.43608	-103.87611	4107	2.60	2.5	6.5	3.1	1.66	3.75E+02
705	BHH14a	LSS120	44.43135	-103.87571	4110	1.63	1.9	3.1	0.4	0.88	2.02E+02
705	BHH14a	IgS121	44.42853	-103.87344	4120	0.13	65.9	8.5	4.1	21.30	5.13E+03
705	BHH14a	IgS122	44.42862	-103.87337	4121	3.00	3.1	9.3	3.1	2.08	4.64E+02
705	BHH14a	IgS123	44.42847	-103.87363	4147	1.92	5.1	9.8	5.4	2.99	6.83E+02
705	BHH14a	IgS124	44.42447	-103.87504	4150	3.24	2.9	9.4	4.1	2.14	4.78E+02
705	BHH14a	Ig125	44.42356	-103.87790	4159	2.89	2.7	7.8	4.6	2.00	4.51E+02
705	BHH14a	IgS126	44.42364	-103.87910	4171	3.27	3.0	9.8	4.5	2.24	5.03E+02
705	BHH14a	Ig127	44.41978	-103.88100	4214	2.69	15.3	41.2	5.0	8.69	1.94E+03
705	BHH14a	Ig127a	44.41960	-103.88103	4221	2.69	15.3	41.2	5.0	8.69	1.94E+03
705	BHH14a	Ig128	44.41910	-103.88106	4235	2.80	17.6	49.3	4.9	10.05	2.24E+03
705	BHH14a	Ig129	44.41754	-103.88126	4234	3.04	16.6	50.4	5.1	9.86	2.18E+03
705	BHH14a	IgS130	44.41601	-103.88036	4260	4.16	2.5	10.4	1.8	1.84	4.03E+02
705	BHH14a	IgS131	44.41351	-103.88274	4303	2.26	3.4	7.7	4.1	2.15	4.88E+02
705	BHH14a	IgS132	44.41196	-103.88748	4319	2.45	3.3	8.1	1.8	1.89	4.25E+02
705	BHH14a	LS133	44.41324	-103.89378	4410	1.29	0.7	0.9	0.2	0.31	7.19E+01
705	BHH14a	LS134	44.40682	-103.89970	4419	4.55	1.1	5.0	0.8	0.84	1.84E+02
705	BHH14a	LSS134	44.40286	-103.89589	4451	0.97	3.1	3.0	0.4	1.24	2.89E+02
705	BHH14a	Ig135	44.39680	-103.90012	4520	2.64	17.0	44.8	6.8	9.71	2.17E+03
705	BHH14a	IgS136	44.39654	-103.90076	4522	3.60	14.2	51.1	6.9	9.39	2.07E+03

Table 25: cont.

Pre -	Name	ID	(N)	(W)	Elev. (ft)	Th/U Ratio	U (ppm)	Th (ppm)	K (pct)	A (μWm^{-3})	ε_v ($mg^{-1}s^{-1}$)
705	BHH14a	Ig137	44.39701	-103.90753	4559	3.09	24.4	75.5	5.3	14.37	3.17E+03
705	BHH14a	Ig138	44.39391	-103.91116	4605	2.93	24.4	71.4	5.0	13.99	3.10E+03
705	BHH14a	LSS139	44.39101	-103.91271	5019	1.63	1.6	2.6	0.6	0.77	1.77E+02
705	BHH14a	LSS140	44.38840	-103.91271	4710	2.94	3.2	9.4	4.4	2.26	5.09E+02
705	BHH14a	LSS141	44.37449	-103.91579	4834	1.27	1.5	1.9	0.4	0.66	1.53E+02
705	BHH14a	LSS143	44.36505	-103.92805	4877	1.28	1.8	2.3	0.4	0.79	1.81E+02
705	BHH14a	LSS143	44.35673	-103.93095	4962	1.45	3.1	4.5	1.2	1.46	3.35E+02
705	BHH14a	LSS144	44.34240	-103.92129	5025	2.09	2.3	4.8	1.4	1.26	2.86E+02
705	BHH14a	LSS145	44.33248	-103.90052	5126	1.39	2.3	3.2	1.0	1.08	2.49E+02
705	BHH14a	Ig146	44.32058	-103.89185	5180	2.80	42.8	120.0	7.1	23.92	5.31E+03
705	BHH14a	Ig147	44.31596	-103.88544	5246	3.61	36.2	130.7	6.4	22.72	4.97E+03
806	BHRFR	IF148	44.10844	-103.65479	5023	2.99	8.0	23.9	3.7	4.86	1.08E+03
806	BHRFR	IF149	44.10996	-103.66717	5077	2.56	10.8	27.7	5.1	6.19	1.39E+03
806	BHRFR	IF150	44.11375	-103.69193	5171	4.93	4.1	20.2	4.8	3.48	7.61E+02
806	BHRFR	IF151	44.12191	-103.71208	5296	2.51	3.5	8.8	2.7	2.11	4.75E+02
806	BHRFR	IF152	44.13158	-103.76285	5521	3.06	5.2	15.9	4.8	3.46	7.73E+02
806	BHRFR	MGn153	44.14265	-103.80940	5715	1.96	5.7	11.2	3.7	3.10	7.04E+02
806	BHSRCR	Ig154	44.15572	-103.86987	6109	0.55	2.0	1.1	0.2	0.73	1.71E+02
806	BHSRCR	Ig155	44.16513	-103.88453	6302	1.11	1.9	2.1	0.3	0.79	1.83E+02
806	BHSRCR	Ig156	44.18714	-103.91254	6519	0.19	2.6	0.5	0.1	0.85	2.03E+02
806	BHSRCR	Ig157	44.18476	-103.93867	6397	2.28	1.8	4.1	0.3	0.93	2.08E+02
806	BHSRCR	Ig158	44.19852	-104.01717	6617	0.46	1.3	0.6	0.1	0.46	1.09E+02
806	BHUS85	Ig159	44.22440	-103.96689	6245	1.38	2.1	2.9	0.3	0.92	2.11E+02
806	BHUS85	Ig160	44.27689	-103.90333	5650	2.34	3.2	7.5	1.1	1.73	3.88E+02

Table 25: cont.

Pre -	Name	ID	(N)	(W)	Elev. (ft)	Th:U	U (ppm)	Th (ppm)	K (pct)	A (μWm^{-3})	ε_v ($mg^{-1}s^{-1}$)
806	BHUS85	Ig161	44.28361	-103.89910	5552	0.38	2.1	0.8	0.1	0.72	1.71E+02
806	BHUS85	IgS162	44.29555	-103.88737	5452	2.75	2.4	6.6	2.6	1.58	3.55E+02
806	BHUS85	M163	44.29686	-103.85735	5500	2.11	2.7	5.7	2.1	1.54	3.49E+02
806	BHUS85	Ig164	44.29377	-103.84151	5930	1.17	1.8	2.1	0.4	0.77	1.78E+02
806	BHUS85	Ig165	44.32004	-103.79877	5754	4.01	18.8	75.3	5.4	12.65	2.76E+03
806	BHUS85	Ig166	44.32242	-103.79807	5695	2.69	21.1	56.7	4.4	11.69	2.60E+03
806	BHUS85	MIg167	44.32347	-103.79752	5667	2.20	10.5	23.1	5.5	5.76	1.30E+03
806	BHUS85	MIg168	44.32365	-103.79755	5647	2.52	10.8	27.2	3.2	5.94	1.33E+03
806	BHUS85	Sh169	44.33023	-103.79337	5450	3.97	3.5	13.9	3.1	2.58	5.69E+02
806	BHUS85	Ig170	44.33033	-103.79315	5457	3.04	7.3	22.2	4.0	4.54	1.01E+03
806	BHUS85	MIg171	44.33029	-103.79322	5455	1.65	1.7	2.8	1.5	0.92	2.12E+02
806	BHUS85	Ig172	44.33905	-103.78423	5277	3.94	3.6	14.2	1.3	2.43	5.32E+02
806	BHUS85	MSc173	44.34207	-103.78217	5267	4.50	4.2	18.9	3.1	3.21	7.01E+02
806	BHUS85	MSc173	44.34207	-103.78217	5267	4.50	4.2	18.9	3.1	3.21	7.01E+02
806	BHUS85	M174	44.34498	-103.77891	5317	5.63	1.9	10.7	2.1	1.71	3.71E+02
806	BHLead	M175	44.35474	-103.78033	5334	2.88	4.1	11.8	3.2	2.60	5.82E+02
806	BHLead	M176	44.35419	-103.77575	5439	3.26	3.9	12.7	2.4	2.53	5.60E+02
806	BHLead	M177	44.35445	-103.75585	5049	4.37	4.1	17.9	4.1	3.21	7.05E+02
806	BHLead	M178	44.35517	-103.75001	4929	3.74	5.3	19.8	5.5	3.90	8.63E+02
906	BHHR	IgS179	44.09589	-103.29947	3489	0.42	1.2	0.5	0.2	0.43	1.02E+02
906	BHHR	IgSS180	44.28196	-103.86847	5469	2.17	2.3	5.0	0.9	1.22	2.76E+02
906	BHHR	LSS181	44.27964	-103.86695	5480	1.37	2.7	3.7	0.8	1.22	2.82E+02
906	BHHR	LSS182	44.27519	-103.85480	5565	3.59	1.7	6.1	1.3	1.18	2.60E+02
906	BHHR	LSS183	44.22230	-103.84865	6593	2.05	2.0	4.1	0.6	1.02	2.31E+02

Table 25: cont.

Pre -	Name	ID	(N)	(W)	Elev. (ft)	Th:U	U (ppm)	Th (ppm)	K (pct)	A (μWm^{-3})	ε_v ($mg^{-1}s^{-1}$)
906	BHHR	LSS184	44.26086	-103.84430	5689	2.13	3.0	6.4	0.6	1.52	3.42E+02
906	BHHR	RSS185	44.25618	-103.83057	5842	2.95	2.2	6.5	2.1	1.45	3.25E+02
906	BHHR	RSS186	44.25544	-103.82851	5876	3.11	2.8	8.7	2.2	1.83	4.08E+02
906	BHHR	RSS187	44.25522	-103.82649	5889	1.42	2.6	3.7	1.1	1.23	2.82E+02
906	BHHR	SS188	44.25571	-103.82373	5999	1.76	1.7	3.0	0.6	0.84	1.91E+02
906	BHRR	RSS189	44.27285	-103.80666	5857	1.50	3.6	5.4	2.4	1.82	4.19E+02
906	BHRR	RSS190	44.28053	-103.80388	5801	1.47	3.0	4.4	2.1	1.52	3.50E+02
906	BHBFR	GSc191	44.30442	-103.79408	5937	3.21	9.7	31.1	3.4	5.95	1.31E+03
906	BHBFR	GSc192	44.30425	-103.79557	5966	5.20	7.1	36.9	3.9	5.70	1.23E+03
906	BHBFR	GSc193	44.30541	-103.79393	5872	2.69	7.0	18.8	3.3	4.08	9.13E+02
906	BHBVR	GSc194	44.29804	-103.79651	5859	3.11	11.5	35.8	5.1	7.08	1.57E+03
906	BHEWR	IgS195	44.29797	-103.79651	5854	1.16	5.1	5.9	1.7	2.24	5.20E+02
906	BHEWR	IgS196	44.30885	-103.77178	5460	2.10	4.2	8.8	1.4	2.18	4.92E+02
906	BHBVR	IgG197	44.28289	-103.77928	5855	2.71	5.2	14.1	3.5	3.16	7.09E+02
906	BHBVR	IgS198	44.28232	-103.77685	5916	2.20	4.9	10.8	3.3	2.77	6.27E+02
906	BHBVR	Ig199	44.28097	-103.77052	6113	2.08	5.0	10.4	3.4	2.78	6.31E+02
906	BHBVR	Ig200	44.27794	-103.75106	5951	2.21	3.9	8.6	3.8	2.34	5.31E+02
906	BHBVR	Ig201	44.27368	-103.73370	5678	0.43	6.9	3.0	1.8	2.56	6.09E+02
906	BHBVR	SS202	44.27742	-103.69756	5530	0.80	4.1	3.3	0.8	1.62	3.79E+02
906	BHHWR	IgS203	44.29401	-103.70074	5577	1.87	3.0	5.6	0.9	1.49	3.37E+02
906	BHIOR	MGn204	44.28992	-103.71120	5533	2.61	7.5	19.6	4.6	4.45	9.98E+02
906	BHYCR	MGn205	44.34913	-103.74891	4865	1.71	6.8	11.6	2.9	3.38	7.70E+02
906	BHYCR	MGn206	44.34908	-103.74902	4861	1.56	2.5	3.9	0.8	1.18	2.70E+02
906	BHYCR	MB207	44.34534	-103.75494	4936	4.59	3.4	15.6	3.8	2.77	6.08E+02

Table 25: cont.

Pre -	Name	ID	(N)	(W)	Elev. (ft)	Th:U	U (ppm)	Th (ppm)	K (pct)	A (μWm^{-3})	ε_v ($mg^{-1}s^{-1}$)
1006	BHYCR	MSc208	44.34522	-103.75236	4913	8.84	1.9	16.8	3.2	2.35	5.00E+02
1006	BHYCR	M209	44.34264	-103.75484	4951	3.93	5.6	22.0	5.1	4.13	9.10E+02
1006	BHYCR	M210	44.34064	-103.75537	5005	4.90	4.2	20.6	3.0	3.35	7.26E+02
1006	BHYCR	M211	44.34364	-103.75948	5048	3.40	4.7	16.0	1.9	2.99	6.59E+02
1006	BHYCR	MSc212	44.34368	-103.77216	5190	2.78	4.9	13.6	2.4	2.91	6.48E+02
1006	BHYCR	MSc213	44.34315	-103.77896	5209	2.88	4.1	11.8	1.1	2.36	5.25E+02
1006	BHYCR	MSc214	44.34043	-103.75651	5010	3.62	3.4	12.3	1.2	2.20	4.84E+02
1006	BHYCR	MSc215	44.33559	-103.75774	5120	3.18	3.9	12.4	3.4	2.61	5.82E+02
1006	BHYCR	IF216	44.33126	-103.75711	5195	1.72	2.9	5.0	1.4	1.46	3.34E+02
1006	BHYCR	MSc217	44.32928	-103.75195	5279	3.35	2.3	7.7	2.3	1.61	3.58E+02
1006	BHYCR	IgS218	44.32658	-103.74776	5376	2.12	10.6	22.5	7.0	5.91	1.34E+03
1006	BHYCR	MIg219	44.32460	-103.74711	5410	1.88	5.1	9.6	3.4	2.75	6.26E+02
1006	BHYCR	MIF220	44.31652	-103.74469	5623	2.18	5.7	12.4	3.3	3.15	7.13E+02
1006	BHYCR	IgIF221	44.31225	-103.74060	5762	2.52	4.6	11.6	2.9	2.70	6.07E+02
1006	BHYCR	IgS222	44.30770	-103.73542	5903	2.62	6.0	15.7	4.8	3.69	8.29E+02
1006	BHYCR	Ig223	44.30144	-103.74234	5933	2.30	5.6	12.9	5.0	3.35	7.59E+02
1006	BHYCR	Ig224	44.29186	-103.75446	5951	1.80	5.4	9.7	2.3	2.72	6.20E+02
1006	BHVCR	MSc225	44.30996	-103.66346	5156	2.93	6.1	17.9	6.4	4.08	9.15E+02
1006	BHUR	Ig226	44.34081	-103.82763	6139	1.30	18.3	23.7	11.0	8.82	2.04E+03
1006	BHUR	MIg227	44.34050	-103.83054	6151	3.24	28.9	93.6	8.9	17.66	3.90E+03
1006	BHUR	Mig227a	44.34050	-103.83054	6151	3.24	28.9	93.6	8.9	17.66	3.90E+03
1006	BHUR	MIg228	44.34031	-103.83683	6316	2.33	12.3	28.6	6.5	6.88	1.55E+03
1006	BHUR	MIg229	44.34119	-103.83685	6348	2.08	5.9	12.3	4.0	3.28	7.45E+02
1006	BHUR	MIg230	44.34070	-103.83945	6417	3.50	21.4	74.8	8.8	13.79	3.04E+03

Table 25: cont.

Pre -	Name	ID	(N)	(W)	Elev. (ft)	Th:U	U (ppm)	Th (ppm)	K (pct)	A (μWm^{-3})	ε_v ($mg^{-1}s^{-1}$)
1006	BHUR	MIg231	44.33759	-103.84048	6487	4.21	4.7	19.8	2.9	3.42	7.48E+02
1006	BHTGR	Ig232	44.33654	-103.79794	5485	1.82	8.2	14.9	3.9	4.19	9.55E+02
1006	BHTGR	Ig233	44.33632	-103.80180	5559	2.19	3.1	6.8	1.0	1.63	3.67E+02
1006	BHTGR	Ig234	44.33591	-103.79943	5606	3.29	4.1	13.5	3.5	2.78	6.17E+02
1006	BHDM	Ig235	44.31406	-103.80324	5905	4.38	11.3	49.5	5.7	8.24	1.79E+03
1006	BHDM	GrSc236	44.31202	-103.80313	5911	2.66	17.9	47.6	5.8	10.11	2.25E+03
1006	BHDM	GrSc237	44.30928	-103.80589	5913	3.92	8.4	32.9	4.6	5.84	1.28E+03
1006	BHTSR	Ig238	44.30083	-103.83019	6373	4.89	7.0	34.2	4.7	5.53	1.20E+03
1006	BHTSR	Ig239	44.30589	-103.82681	6454	2.88	3.3	9.5	2.9	2.13	4.77E+02
1006	BHTSR	Ig240	44.31438	-103.82677	6457	2.99	9.0	26.9	4.9	5.55	1.24E+03
1006	BHTSR	Ig241	44.31716	-103.82693	6519	4.25	7.6	32.3	5.8	5.68	1.24E+03
1006	BHTSR	Ig242	44.32082	-103.83119	6625	6.21	8.5	52.8	3.8	7.44	1.59E+03
1006	BHTSR	Ig243	44.32571	-103.83194	6780	3.68	17.0	62.5	6.8	11.19	2.46E+03
1006	BHTSR	Ig244	44.32512	-103.83767	6918	5.29	10.1	53.4	4.5	8.06	1.74E+03
1006	BHTSR	Ig245	44.32833	-103.83587	7034	4.94	9.9	48.9	3.5	7.51	1.62E+03
1106	BHUS14a	LS246	44.37813	-103.91437	4772	1.19	1.6	1.9	0.4	0.69	1.60E+02
1106	BHUS14a	Ig247	44.29534	-103.81947	6120	3.59	9.0	32.3	3.8	5.88	1.29E+03
1106	BHUS14a	Ig248	44.30256	-103.81191	6135	3.43	9.6	32.9	4.5	6.19	1.37E+03
1106	BHUS14a	IgS249	44.30131	-103.81264	6132	2.02	4.5	9.1	3.3	2.51	5.70E+02
1106	BHUS14a	MIg250	44.30861	-103.81710	6043	3.36	13.4	45.0	10.7	9.07	2.01E+03
1106	BHUS14a	IF251	44.31471	-103.79426	5878	1.72	4.6	7.9	4.7	2.60	5.96E+02
1106	BHCC	GrSc252	44.37157	-103.76135	4818	1.62	5.0	8.1	2.0	2.43	5.56E+02
1106	BHCC	MIg253	44.37476	-103.76689	4916	2.24	6.7	15.0	2.0	3.53	7.94E+02
1106	BHCC	Ig254	44.37863	-103.77375	4994	2.80	9.3	26.0	4.6	5.54	1.23E+03

Table 25: cont.

Pre -	Name	ID	(N)	(W)	Elev. (ft)	Th:U	U (ppm)	Th (ppm)	K (pct)	A (μWm^{-3})	ε_v ($mg^{-1}s^{-1}$)
1106	BHCC	Ig255	44.38104	-103.77915	5076	3.76	5.4	20.3	13.8	4.91	1.10E+03
1106	BHCC	IgS256	44.38158	-103.78579	5237	2.31	4.8	11.1	3.5	2.79	6.30E+02
1106	BHCC	IgS267	44.38097	-103.78715	5282	2.39	6.4	15.3	6.3	3.95	8.93E+02
1106	BHBG	IgS258	44.39693	-103.80039	4933	2.71	5.5	14.9	4.5	3.44	7.71E+02
1106	BHBG	IgS259	44.40691	-103.81899	4700	3.35	7.4	24.8	3.8	4.76	1.05E+03
1106	BHBG	IgS260	44.41525	-103.82426	4603	2.02	5.2	10.5	5.2	3.05	6.96E+02
1106	BHBG	IgS261	44.42539	-103.82273	4505	1.79	1.4	2.5	0.2	0.66	1.50E+02
1206	BHBR	SS262	44.27422	-103.44952	3782	0.26	9.3	2.4	0.7	3.12	7.47E+02
1206	BHBR	SS263	44.27380	-103.45022	3782	0.28	7.9	2.2	0.5	2.65	6.35E+02
1206	BHBR	SS264	44.27671	-103.46873	3909	0.79	1.9	1.5	0.4	0.75	1.76E+02
1206	BHBR	SS265	44.28637	-103.48088	3995	1.04	2.6	2.7	0.5	1.08	2.50E+02
1206	BHBR	SS266	44.28821	-103.48088	4140	3.00	1.3	3.9	1.2	0.86	1.92E+02
1206	BHBR	Ig267	44.28897	-103.48219	4118	3.47	3.6	12.5	2.4	2.42	5.34E+02
1206	BHBR	IgS268	44.22646	-103.39957	3653	0.67	3.0	2.0	0.3	1.12	2.63E+02
1206	BHGR	Ig269	44.34814	-103.55547	4551	4.36	4.2	18.3	3.2	3.18	6.94E+02
1206	BHGR	Ig270	44.34827	-103.55646	4585	2.85	5.5	15.7	3.4	3.38	7.54E+02
1206	BHGR	Ig271	44.34826	-103.55704	4582	2.98	6.1	18.2	3.4	3.77	8.39E+02
1206	BHGR	Ig272	44.34756	-103.57381	4653	3.45	4.2	14.5	2.5	2.78	6.14E+02
1206	BHGR	Ig273	44.34630	-103.57285	4710	3.49	3.7	12.9	2.9	2.54	5.62E+02
1206	BHGR	Ig274	44.34610	-103.57256	4714	2.29	6.2	14.2	2.9	3.41	7.68E+02
1206	BHGR	Ig275	44.34147	-103.58506	4596	3.07	4.6	14.1	3.8	3.01	6.72E+02
1206	BHGR	Ig276	44.33836	-103.59746	4588	2.38	2.1	5.0	0.6	1.13	2.53E+02
1206	BHER	Ig277	44.32718	-103.59605	4693	2.92	6.1	17.8	3.7	3.77	8.41E+02
1206	BHER	IgLS278	44.31773	-103.59756	4793	1.67	1.8	3.0	0.7	0.88	2.01E+02

Table 25: cont.

Pre -	Name	ID	(N)	(W)	Elev. (ft)	Th:U	U (ppm)	Th (ppm)	K (pct)	A (μWm^{-3})	ε_v ($mg^{-1}s^{-1}$)
1206	BHGR	Ig279	44.32071	-103.64951	4989	1.55	2.9	4.5	1.5	1.43	3.28E+02
1206	BHGR	MIg280	44.32157	-103.65022	4979	2.05	2.0	4.1	1.6	1.13	2.58E+02
1206	BHGR	Ig281	44.32177	-103.65114	4962	1.00	2.2	2.2	1.7	1.05	2.45E+02
1206	BHGR	MGn282Sc	44.32307	-103.65062	4935	3.03	6.6	20.0	5.2	4.28	9.54E+02
1206	BHGR	MSc283	44.32377	-103.65085	4925	4.67	4.2	19.6	3.8	3.35	7.32E+02
1206	BHGR	MGn284	44.32461	-103.65205	4932	2.73	1.5	4.1	1.5	0.97	2.18E+02
1206	BHGR	MGn285	44.32648	-103.65231	4928	3.40	6.0	20.4	5.2	4.13	9.16E+02
1206	BHER	M286	44.32729	-103.65065	4929	2.23	1.3	2.9	0.9	0.74	1.68E+02
1206	BHGR	M287	44.32654	-103.64783	4890	3.87	4.6	17.8	4.5	3.40	7.51E+02
1206	BHNM	MIg288	44.27767	-103.67920	5468	3.74	3.9	14.6	3.4	2.80	6.18E+02
1206	BHCLP	IgS289	44.24133	-103.74093	6262	3.17	3.6	11.4	3.8	2.48	5.54E+02
1206	BHCLP	Ig290	44.24038	-103.73917	6178	2.86	3.5	10.0	3.3	2.28	5.11E+02

Note: Latitude and Longitude are set to DDD.DDDDD° (Decimal Degree) Format

Table 26: RS-230 GRS Survey- Sample Identification (ID), Rock type, Rock classification and Formation

Pre -	Name	ID	Rock Type	*Rock Classification*	Formation
105	BHH385	S001	Sedimentary	Sandstone	Undetermined
105	BHH385	I002	Metamorphic	Metagraywacke	–
105	BHH385	S003	Igneous	Episodite	–
105	BHH385	I003	Igneous	Latite	–
105	BHH385	Ig004	Igneous	Rhyolite	–
105	BHH385	Ig005	Metamorphic	Schist	–
105	BHH385	M005	Metamorphic	Schist	–
105	BHH385	M007	Metamorphic	Schist	–
105	BHH385	M008	Igneous	Latite	–
105	BHH385	M008a	Igneous	Latite	–
105	BHH385	Ig009	Igneous	Latite	–
105	BHH85	Ig010	Igneous	Rhyolite	–
105	BHH85	Sc011	Metamorphic	Mica Schist	–
105	BHH85	Sc012	Metamorphic	Mica Schist	–
105	BHH85	SS013	Sedimentary	Sandstone	Undetermined
105	BHH85	SS014	Metamorphic	Phyllite	–
105	BHDEAD	S015	Metamorphic	Mica Schist	–
105	BHDEAD	S016	Metamorphic	Quartzite	–
105	BHDEAD	Sc017	Metamorphic	Mica Schist	–
105	BHDEAD	Sc018	Metamorphic	Schist	–
105	BHDEAD	SS019	Sedimentary	Sandstone	Deadwood
105	BHDEAD	SS020	Sedimentary	Sandstone	Deadwood
105	BHDEAD	Sc021	Metamorphic	Schist	–
105	BHDEAD	Gc022	Metamorphic	Mica Schist	–
105	BHDEAD	Sc023	Metamorphic	Mica Schist	–
205	BHH14	RSS024	Sedimentary	Limestone	Spearfish
205	BHH14	RSS025	Sedimentary	Calcareous Sandstone	Spearfish
205	BHH14	SS026	Sedimentary	Sandstone	Spearfish
205	BHH14	LS027	Sedimentary	Sandstone	Minnelusa
205	BHH14	LSS028	Sedimentary	Sandstone	Minnelusa
205	BHH14	LSS029	Sedimentary	Limestone	Minnelusa
205	BHH14	LSS030	Sedimentary	Limestone	Minnelusa
205	BHH14	LS031	Sedimentary	Limestone	Minnelusa
205	BHH14	LS032	Sedimentary	Limestone	Minnelusa
205	BHH14	LS033	Sedimentary	Limestone	Minnelusa
205	BHH14	LS034	Sedimentary	Limestone	Minnelusa
205	BHH14	LSS034	Sedimentary	Limestone	Minnelusa

Table 26: cont.

Pre -	Name	ID	Rock Type	*Rock Classification*	Formation
205	BHH14	LS035	Sedimentary	Bedded Limestone	Minnelusa
205	BHH14	LS036a	Sedimentary	Sandstone	Minnelusa
205	BHH14	LS036b	Sedimentary	Limestone	Minnelusa
205	BHH14	LS037	Sedimentary	Calcareous Sandstone	Brule
205	BHH14	LSS038	Sedimentary	Limestone	Pahasapa
205	BHH14	B039	Igneous	Basalt	–
205	BHH14	B040	Igneous	Basalt	–
205	BHH14	LSS041	Sedimentary	Limestone	Englewood
305	BHCCR	SS042	Sedimentary	Sandstone	Inyan Kara
305	BHCCR	SS043	Sedimentary	Sandstone	Inyan Kara
305	BHCCR	SS044	Sedimentary	Limestone	Inyan Kara
305	BHCCR	SS045	Sedimentary	Limestone	Minnekahta
305	BHCCR	SS046	Sedimentary	Sandstone	Spearfish
305	BHUS85	SS047	Igneous	Rhyolite	–
305	BHUS85	SS048	Sedimentary	Sandstone	–
305	BHUS85	RSS049	Sedimentary	Limestone	Minnelusa
305	BHUS85	RSS050	Sedimentary	Sandy Limestone	Minnelusa
305	BHUS85	SS051	Sedimentary	Sandy Limestone	Minnelusa
305	BHUS85	LS052	Sedimentary	Limestone	Pahasapa
305	BHDEAD	Ig053	Sedimentary	Calcite deposite	Pahasapa
305	BHDEAD	SS054	Sedimentary	Limestone	Pahasapa
305	BHDEAD	MSS055	Sedimentary	Bedded Sandstone	Pahasapa
305	BHDEAD	M056	Metamorphic	Schist	–
305	BHDEAD	MG057	Metamorphic	Schist	–
305	BHDEAD	MG058	Igneous	Silicious Granodiorite	–
305	BHUS14a	MSc059	Metamorphic	Mica Schist	–
305	BHUS14a	MSc060	Metamorphic	Siliceous Schist	–
305	BHUS14a	MGn061	Metamorphic	Phyllite	–
305	BHUS14a	MSc062	Metamorphic	Phyllite	–
305	BHUS14a	M063	Metamorphic	Phyllite	–
305	BHUS14a	MLSS064	Igneous	Altered Rhyolite	–
305	BHUS14a	MSc065	Metamorphic	Phyllite	–
405	BHNM	LSS066	Sedimentary	Limestone	Pahasapa
405	BHNM	LSS067	Sedimentary	Sandstone	Deadwood
405	BHVCR	LSS068	Sedimentary	Limestone	Deadwood
405	BHVCR	LS069	Sedimentary	Limestone	Pahasapa
405	BHVCR	LSS070	Sedimentary	Limestone	Pahasapa

Table 26: cont.

Pre -	Name	ID	Rock Type	*Rock Classification*	Formation
405	BHVCR	I071	Igneous	Latitic Andesite	–
405	BHVCR	I072	Igneous	Latite	–
405	BHVCR	LSS073	Sedimentary	Limestone	Pahasapa
405	BHVCR	I073	Sedimentary	Limestone	Pahasapa
405	BHVCR	I074	Igneous	Latite	–
405	BHVCR	I075	Igneous	Latitic Andesite	–
405	BHVCR	I076	Igneous	Latitic Andesite	–
405	BHVCR	I077	Igneous	Latite	–
405	BHVCR	I078	Igneous	Latite	–
405	BHVCR	I079	Igneous	Latite	–
405	BHVCR	I080	Igneous	Trachyte	–
405	BHVCR	I081	Sedimentary	Calcareous Sandstone	Whitewood
405	BHVCR	I082	Igneous	Alkalic Rhyolite	–
405	BHVCR	I083	Sedimentary	Limestone	Englewood
405	BHVCR	SS084	Sedimentary	Sandstone	Minnelusa
405	BHVCR	I085	Sedimentary	Limestone	Minnekahta
405	BHVCR	SSI086	Sedimentary	Sandstone	Minnelusa
405	BHVCR	SSI087	Sedimentary	Sandstone	Minnelusa
505	BHSCR	I088	Sedimentary	Limestone	Minnekahta
505	BHSPRF	SGyp089	Sedimentary	Gypsum	Spearfish
505	BHSPRF	SGyp090	Sedimentary	Gypsum	Spearfish
505	BHSPRF	I091	Sedimentary	Limestone	Spearfish
505	BHSPRF	I092	Sedimentary	Limestone	Minnekahta
505	BHSPRF	I093	Sedimentary	Silty Limestone	Spearfish
505	BHSPRF	I094	Sedimentary	Limy Red Shale	Opeche
505	BHSPRF	SS095	Sedimentary	Sandstone	Minnelusa
505	BHMLR	SS096	Sedimentary	Sandstone	Minnelusa
505	BHMLR	SS097	Sedimentary	Calcareous Sandstone	Minnelusa
505	BHMLR	SS098	Sedimentary	Sandstone	Minnelusa
505	BHMLR	I099	Igneous	Rhyolite	–
505	BHMLR	SS099	Sedimentary	Sandstone	Minnelusa
505	BHMLR	ISS099	Sedimentary	Sandstone	Minnelusa
505	BHMLR	ISS100	Igneous	Trachyte	–
505	BHMLR	I101	Igneous	Trachyte	–
505	BHMLR	I102	Igneous	Trachyte	–
505	BHMLR	MSc103	Metamorphic	Phyllite	–
505	BHMLR	MSc104	Metamorphic	Schist	–

Table 26: Cont.

Pre -	Name	ID	Rock Type	*Rock Classification*	Formation
505	BHCC	MSc105	Metamorphic	Metabasalt	–
505	BHCC	MGn106	Metamorphic	Siliceous Phyllite	–
505	BHCC	MGn107	Metamorphic	Siliceous Phyllite	–
505	BHCC	Qtz108	Metamorphic	Quartzite	–
705	BHH14a	I0111	Sedimentary	Limestone	Minnekahta
705	BHH14a	LSS112	Sedimentary	Dolomitic Sandstone	Minnelusa
706	BHH14a	LSS112	Sedimentary	Dolomitic Sandstone	Minnelusa
705	BHH14a	LSS113	Sedimentary	Limestone	Minnelusa
705	BHH14a	LS114	Sedimentary	Limestone	Pahasapa
705	BHH14a	LS115	Sedimentary	Limestone	Pahasapa
705	BHH14a	LS116	Sedimentary	Limestone	Pahasapa
705	BHH14a	IgS117	Igneous	Igneous	–
705	BHH14a	LSS118	Sedimentary	Limestone	Pahasapa
705	BHH14a	MLSH119	Sedimentary	Dolomitic Siltstone	Englewood
705	BHH14a	LSS120	Sedimentary	Limestone	Pahasapa
705	BHH14a	IgS121	Metamorphic	Metabasalt	–
705	BHH14a	IgS122	Sedimentary	Limestone	Whitewood
705	BHH14a	IgS123	Sedimentary	Limestone	Whitewood
705	BHH14a	IgS124	Sedimentary	Limestone	Whitewood
705	BHH14a	Ig125	Sedimentary	Limestone	Whitewood
705	BHH14a	IgS126	Sedimentary	Dolomitic Sandstone	Whitewood
705	BHH14a	Ig127	Igneous	Granodiorite	–
705	BHH14a	Ig127a	Igneous	Granodiorite	–
705	BHH14a	Ig128	Igneous	Granodiorite	–
705	BHH14a	Ig129	Igneous	Granodiorite	–
705	BHH14a	IgS130	Sedimentary	Limestone	Whitewood
705	BHH14a	IgS131	Sedimentary	Limestone	Whitewood
705	BHH14a	IgS132	Sedimentary	Limestone	Whitewood
705	BHH14a	LS133	Sedimentary	Fossiliferous Limestone	Pahasapa
705	BHH14a	LS134	Sedimentary	Calcareous Sandstone	Whitewood
705	BHH14a	LSS134	Sedimentary	Limestone	Whitewood
705	BHH14a	Ig135	Igneous	Phonolite	–
705	BHH14a	IgS136	Sedimentary	Limy Graywacke	Deadwood
705	BHH14a	Ig137	Igneous	Volcanic	–
705	BHH14a	Ig138	Igneous	Volcanic	–
705	BHH14a	LSS139	Sedimentary	Limestone	Pahasapa
705	BHH14a	LSS140	Sedimentary	Sandstone	Deadwood

Table 26: cont.

Pre -	Name	ID	Rock Type	*Rock Classification*	Formation
705	BHH14a	LSS141	Sedimentary	Limestone	Whitewood
705	BHH14a	LSS142	Sedimentary	Limestone	Whitewood
705	BHH14a	LSS143	Sedimentary	Dolomitic Limestone	Whitewood
705	BHH14a	LSS144	Sedimentary	Limestone	Whitewood
705	BHH14a	LSS145	Sedimentary	Limestone	Whitewood
705	BHH14a	Ig146	Igneous	Volcanic	–
705	BHH14a	Ig147	Igneous	Alkalic Volcanic	–
806	BHRFR	IF148	Metamorphic	Phyllite	–
806	BHRFR	IF149	Metamorphic	Phyllitic Schist	–
806	BHRFR	IF150	Metamorphic	Phyllitic Slate	–
806	BHRFR	IF151	Metamorphic	Philitic Schist	–
806	BHRFR	IF152	Metamorphic	Phyllite	–
806	BHRFR	MGn153	Metamorphic	Phyllite	–
806	BHSRCR	Ig154	Igneous	Aplite	–
806	BHSRCR	Ig155	Igneous	Rhyolite	–
806	BHSRCR	Ig156	Sedimentary	Limestone	Pahasapa
806	BHSRCR	Ig157	Sedimentary	Limestone	Pahasapa
806	BHSRCR	Ig158	Sedimentary	Limestone	Pahasapa
806	BHUS85	Ig159	Sedimentary	Limestone	Pahasapa
806	BHUS85	Ig160	Igneous	Rhyolite	–
806	BHUS85	Ig161	Sedimentary	Limestone	Pahasapa
806	BHUS85	IgS162	Sedimentary	Limestone	Whitewood
806	BHUS85	M163	Sedimentary	Calcareous Limestone	Deadwood
806	BHUS85	Ig164	Igneous	Rhyolite	–
806	BHUS85	Ig165	Igneous	Phonolite	–
806	BHUS85	Ig166	Igneous	Phonolite	–
806	BHUS85	MIg167	Igneous	Phonolite	–
806	BHUS85	MIg168	Metamorphic	Schist	–
806	BHUS85	Sh169	Metamorphic	Phyllite	–
806	BHUS85	Ig170	Igneous	Weathered Trachyte	–
806	BHUS85	MIg171	Metamorphic	Metasandstone	–
806	BHUS85	Ig172	Metamorphic	Phyllite	–
806	BHUS85	MSc173	Metamorphic	Phyllite	–
806	BHUS85	M174	Metamorphic	Fe Rich Hemetitic Schist	–
806	BHLead	M175	Metamorphic	Metaquartzite	–
806	BHLead	M176	Metamorphic	Calcareous Phyllite	–
806	BHLead	M177	Metamorphic	Phyllite	–

Table 26: cont.

Pre -	Name	ID	Rock Type	*Rock Classification*	Formation
806	BHLead	M178	Metamorphic	Phyllite	–
906	BHHR	IgS179	Sedimentary	Limestone	Spearfish
906	BHHR	IgSS180	Igneous	Rhyolite	–
906	BHHR	LSS181	Sedimentary	Limestone	Madison Gp
906	BHHR	LSS182	Sedimentary	Limestone	Whitewood
906	BHHR	LSS183	Igneous	Volcanic	–
906	BHHR	LSS184	Sedimentary	Calcareous Sandstone	Madison Gp
906	BHHR	RSS185	Sedimentary	Calcareous Sandstone	Deadwood
906	BHHR	RSS186	Sedimentary	Calcareous Sandstone	Deadwood
906	BHHR	RSS187	Sedimentary	Sandy Limestone	Whitewood
906	BHHR	SS188	Sedimentary	Limestone	Whitewood
906	BHRR	RSS189	Sedimentary	Sandy Limestone	Whitewood
906	BHRR	RSS190	Sedimentary	Calcareous Sandstone	Whitewood
906	BHBFR	GSc191	Igneous	Phonolite	–
906	BHBFR	GSc192	Igneous	Phonolite	–
906	BHBFR	GSc193	Igneous	Phonolite	–
906	BHBVR	GSc194	Igneous	Phonolite	–
906	BHEWR	IgS195	Igneous	Phonolite	–
906	BHEWR	IgS196	Metamorphic	Metaquartzite	–
906	BHBVR	IgG197	Igneous	Rhyolite	–
906	BHBVR	IgS198	Igneous	Rhyolite	–
906	BHBVR	Ig199	Igneous	Rhyolite	–
906	BHBVR	Ig200	Igneous	Rhyolite	–
906	BHBVR	Ig201	Metamorphic	Marble like Limestone	–
906	BHBVR	SS202	Sedimentary	Sandstone	Deadwood
906	BHHWR	IgS203	Sedimentary	Limestone	Whitewood
906	BHIOR	MGn204	Metamorphic	Phyllitic Slate	–
906	BHYCR	MGn205	Igneous	Rhyolite	–
906	BHYCR	MGn206	Igneous	Fine grained igneous	–
906	BHYCR	MB207	Metamorphic	Phyllitic Slate	–
1006	BHYCR	MSc208	Metamorphic	Schisty Phyllite	–
1006	BHYCR	M209	Metamorphic	Schisty Phyllite	–
1006	BHYCR	M210	Metamorphic	Schisty Phyllite	–
1006	BHYCR	M211	Metamorphic	Schist	–

Table 26: cont.

Pre -	Name	ID	Rock Type	*Rock Classification*	Formation
1006	BHYCR	MSc212	Metamorphic	Schisty Slate	–
1006	BHYCR	MSc213	Metamorphic	Mica Schist	–
1006	BHYCR	MSc214	Metamorphic	Schist	–
1006	BHYCR	MSc215	Metamorphic	Metamorphic Schist	–
1006	BHYCR	IF216	Metamorphic	Schist	–
1006	BHYCR	MSc217	Metamorphic	Phyllitic Slate	–
1006	BHYCR	IgS218	Igneous	Rhyolite	–
1006	BHYCR	MIg219	Igneous	volcanic	–
1006	BHYCR	MIF220	Igneous	Volcanic	–
1006	BHYCR	IgIF221	Metamorphic	Siliceous Slate	–
1006	BHYCR	IgS222	Igneous	Rhyolite	–
1006	BHYCR	Ig223	Igneous	Rhyolite	–
1006	BHYCR	Ig224	Igneous	Rhyolite	–
1006	BHVCR	MSc225	Metamorphic	Siliceous Mica Schist	–
1006	BHUR	Ig226	Igneous	Trachyte	–
1006	BHUR	MIg227	Igneous	Rhyolite	–
1006	BHUR	MIg227a	Igneous	Rhyolite	–
1006	BHUR	MIg228	Igneous	Trachyte	–
1006	BHUR	MIg229	Igneous	Weathered Trachyte	–
1006	BHUR	MIg230	Igneous	Rhyolite	–
1006	BHUR	MIg231	Igneous	Trachyte	–
1006	BHTGR	Ig232	Igneous	Trachyte	–
1006	BHTGR	Ig233	Igneous	Rhyolite	–
1006	BHTGR	Ig234	Igneous	Latitic Andesite	–
1006	BHDM	Ig235a	Igneous	Phonolite	–
1006	BHDM	Ig235	Igneous	Phonolite	–
1006	BHDM	GrSc236	Igneous	Phonolite	–
1006	BHDM	GrSc237	Igneous	Phonolite	–
1006	BHTSR	Ig238	Igneous	Trachy Andesite	–
1006	BHTSR	Ig239	Igneous	Heavily Weathered Trachyte	–
1006	BHTSR	Ig240	Igneous	Trachy Rhyolite	–
1006	BHTSR	Ig241	Igneous	Trachyte	–
1006	BHTSR	Ig242	Igneous	Alkalic Rhyolite	–
1006	BHTSR	Ig243	Igneous	Trachy Andesite	–
1006	BHTSR	Ig244	Igneous	Trachyte	–
1006	BHTSR	Ig245	Igneous	Trachyte	–
1106	BHUS14a	LS246	Igneous	Trachyte	–

Table 26: cont.

Pre -	Name	ID	Rock Type	*Rock Classification*	Formation
1106	BHUS14a	Ig247	Igneous	Trachy Andesite	–
1106	BHUS14a	Ig248	Igneous	Trachy Rhyolite	–
1106	BHUS14a	IgS249	Igneous	Phonolite	–
1106	BHUS14a	MIg250	Igneous	Trachyte	–
1106	BHUS14a	IF251	Igneous	Rhyolite	–
1106	BHCC	GrSc252	Metamorphic	Schist	–
1106	BHCC	MIg253	Metamorphic	Carboniferous Schist	–
1106	BHCC	Ig254	Igneous	Trachyte	–
1106	BHCC	Ig255	Igneous	Trachyte	–
1106	BHCC	IgS256	Igneous	Latite	–
1106	BHCC	IgS257	Igneous	Rhyolite	–
1106	BHBG	IgS258	Igneous	Rhyolite	–
1106	BHBG	IgS259	Igneous	Rhyolite	–
1106	BHBG	IgS260	Igneous	Rhyolite	–
1106	BHBG	IgS261	Sedimentary	Limestone	Pahasapa
1206	BHBR	SS262	Sedimentary	Sandstone	Minnelusa
1206	BHBR	SS263	Sedimentary	Sandstone	Minnelusa
1206	BHBR	SS264	Sedimentary	Calcareous Sandstone	Minnelusa
1206	BHBR	SS265	Sedimentary	Sandstone	Minnelusa
1206	BHBR	SS266	Sedimentary	Sandstone	Minnelusa
1206	BHBR	Ig267	Igneous	Latite	–
1206	BHBR	IgS268	Sedimentary	Limestone	Minnekahta
1206	BHGR	Ig269	Igneous	Latitic Andesite	–
1206	BHGR	Ig270	Igneous	Latitic Andesite	–
1206	BHGR	Ig271	Igneous	Latitic Andesite	–
1206	BHGR	Ig272	Igneous	Latitic Andesite	–
1206	BHGR	Ig273	Igneous	Trachyte	–
1206	BHGR	Ig274	Igneous	Latitic Andesite	–
1206	BHGR	Ig275	Igneous	Latitic Andesite	–
1206	BHGR	Ig276	Sedimentary	Quartz Sandstone	Brule
1206	BHER	Ig277	Igneous	Latitic Andesite	–
1206	BHER	IgLS278	Sedimentary	Siltstone	Pahasapa
1206	BHGR	Ig279	Igneous	Rhyolite	–
1206	BHGR	MIg280	Metamorphic	Metabasalt	–
1206	BHGR	Ig281	Metamorphic	Greenstone w/ Calcite Vein	–
1206	BHGR	MGnSc282	Metamorphic	Schist	–
1206	BHGR	MSc283	Metamorphic	Phyllitic Schist	–

Table 26: cont.

Pre -	Name	ID	Rock Type	*Rock Classification*	Formation
1206	BHGR	MGn284	Metamorphic	Metagabbro/Greenstone	–
1206	BHGR	MGn285	Metamorphic	Schist	–
1206	BHER	M286	Metamorphic	Greenstone	–
1206	BHGR	M287	Metamorphic	Schist	–
1206	BHNM	MIg288	Metamorphic	Metagraywacke	–
1206	BHCLP	IgS289	Igneous	Rhyolite	–
1206	BHCLP	Ig290	Igneous	Rhyolite	–

Table 27: Ge SED GRS Analysis results - Sample identification, Latitude (N) and Longitude (W), Elevation (Elev.), Th:U ratio, U, Th, K content, calculated heat production (A) and anitneturino luminosity (ε_v)

Pre	Name	ID	(N)	(W)	Elev. (ft)	Th:U	U (ppm)	Th (ppm)	K (pct)	A (μWm^{-3})	ε_v ($mg^{-1}s^{-1}$)
105	BHH385	S001	44.21347	-103.65958	5526	3.76	2.37	8.92	1.44	1.63	3.59E+02
105	BHH385	I002	44.30294	-103.67720	5262	3.40	3.11	10.57	2.68	2.14	4.74E+02
105	BHH385	I003	44.30958	-103.68394	5358	3.19	3.16	10.07	2.23	2.06	4.58E+02
105	BHH385	S003	44.32299	-103.70818	5635	8.68	0.90	7.81	3.11	1.28	2.77E+02
105	BHH385	Ig004	44.33031	-103.71451	5403	2.81	4.43	12.43	1.91	2.61	5.81E+02
105	BHH385	Ig005	44.34028	-103.72418	5090	4.24	1.95	8.26	1.88	1.50	3.29E+02
105	BHH385	M006	44.35235	-103.74046	4787	3.89	2.87	11.15	1.14	1.94	4.24E+02
105	BHH385	M007	44.35235	-103.74046	4787	4.52	2.56	11.58	2.41	2.02	4.43E+02
105	BHH385	M008	44.35409	-103.73906	4759	2.00	5.10	10.22	6.77	3.18	7.27E+02
105	BHH385	Ig009	44.35404	-103.73931	4770	2.42	4.30	10.39	6.49	2.92	6.63E+02
105	BHH85	Ig010	44.35404	-103.73931	4770	1.76	4.83	8.52	2.56	2.48	5.65E+02
105	BHH85	Sc011	44.36533	-103.73394	4678	5.93	1.35	8.00	2.77	1.39	3.05E+02
105	BHH85	Sc012	44.36533	-103.73394	4678	4.09	1.80	7.36	1.79	1.37	3.01E+02
105	BHH85	SS013	44.37596	-103.72552	4830	0.00	4.47	0.00	0.00	1.37	3.31E+02
105	BHH85	SS014	44.37596	-103.72552	4830	0.00	1.91	0.00	0.00	0.58	1.42E+02
105	BHDEAD	S015	44.37034	-103.72956	4635	0.00	6.84	0.00	1.81	2.29	5.56E+02
105	BHDEAD	S016	44.37034	-103.72956	4635	0.00	0.01	0.00	0.00	0.00	7.41E-01
105	BHDEAD	Sc017	44.37016	-103.73151	4618	0.43	4.51	1.93	4.24	2.02	4.80E+02
105	BHDEAD	Sc018	44.37016	-103.73151	4618	0.00	0.25	0.00	0.00	0.08	1.85E+01
105	BHDEAD	SS019	44.38025	-103.72711	4662	0.04	3.13	0.12	0.00	0.97	2.34E+02
105	BHDEAD	SS020	44.37959	-103.72871	4664	0.00	4.52	0.02	0.00	1.38	3.35E+02
105	BHDEAD	Sc021	44.37671	-103.73582	4660	2.86	2.53	7.23	3.65	1.79	4.04E+02
105	BHDEAD	Gc022	44.37217	-103.73418	4708	5.45	1.76	9.59	3.08	1.69	3.69E+02
105	BHDEAD	Sc023	44.37517	-103.72836	4548	1.34	4.07	5.44	2.21	1.95	4.50E+02

Table 27: cont.

Pre	Name	ID	(N)	(W)	Elev. (ft)	Th:U	U (ppm)	Th (ppm)	K (pct)	A (μWm^{-3})	ε_v ($mg^{-1}s^{-1}$)
205	BHH14	RSS024	44.41493	-103.55570	3608	0.00	0.76	0.00	0.00	0.23	5.63E+01
205	BHH14	RSS025	44.41493	-103.55570	3608	0.00	0.12	0.00	0.00	0.04	8.89E+00
205	BHH14	SS026	44.41493	-103.55570	3608	0.00	1.60	0.00	0.04	0.49	1.20E+02
205	BHH14	LS027	44.40520	-103.56916	3665	0.00	0.45	0.00	0.00	0.14	3.33E+01
205	BHH14	LSS028	44.40317	-103.57343	3694	2.76	0.66	1.82	0.00	0.35	7.84E+01
205	BHH14	LSS029	44.40317	-103.57343	3694	3.65	0.71	2.59	0.00	0.43	9.46E+01
205	BHH14	LSS030	44.40198	-103.57956	3730	0.00	0.00	0.00	0.00	0.00	0.00E+00
205	BHH14	LS031	44.39848	-103.58404	3781	0.00	0.09	0.00	0.00	0.03	6.67E+00
205	BHH14	LS032	44.39827	-103.58423	3779	0.00	0.11	0.00	0.00	0.03	8.15E+00
205	BHH14	LS033	44.39811	-103.58434	3783	0.00	0.00	0.41	0.00	0.03	6.64E+00
205	BHH14	LSS034	44.39801	-103.58435	3787	6.86	0.21	1.44	0.72	0.27	5.84E+01
205	BHH14	LS034	44.39801	-103.58435	3788	0.00	0.20	0.00	0.00	0.06	1.48E+01
205	BHH14	LS035	44.39483	-103.58533	3833	0.00	2.41	0.00	0.00	0.74	1.79E+02
205	BHH14	LS36a	44.38787	-103.62584	4217	0.92	0.26	0.24	0.00	0.10	2.32E+01
205	BHH14	LS36b	44.39337	-103.61700	4198	0.00	0.27	0.00	0.00	0.08	2.00E+01
205	BHH14	LS037	44.39127	-103.64035	4321	0.00	0.70	0.00	0.00	0.21	5.19E+01
205	BHH14	LSS038	44.38842	-103.70256	4490	0.00	0.00	0.00	0.00	0.00	0.00E+00
205	BHH14	B039	44.38893	-103.70301	4455	0.36	12.06	4.32	0.02	4.05	9.64E+02
205	BHH14	B040	44.38893	-103.70313	4461	1.03	14.81	15.27	0.07	5.81	1.35E+03
205	BHH14	LSS041	44.38911	-103.70362	4456	0.00	0.34	0.00	0.00	0.10	2.52E+01
305	BHCCR	SS042	44.47039	-103.65672	3776	4.50	0.12	0.54	0.00	0.08	1.76E+01
305	BHCCR	SS043	44.46844	-103.65526	3832	0.12	26.56	3.06	0.00	8.37	2.02E+03
305	BHCCR	SS044	44.42787	-103.61745	3937	0.00	0.56	0.00	0.00	0.17	4.15E+01
305	BHCCR	SS045	44.43520	-103.61893	3909	0.00	0.98	0.00	0.00	0.30	7.26E+01

Table 27: cont.

Pre	Name	ID	(N)	(W)	Elev. (ft)	Th:U	U (ppm)	Th (ppm)	K (pct)	A (μWm^{-3})	ε_v ($mg^{-1}s^{-1}$)
305	BHCCR	SS046	44.43504	-103.65537	4017	0.00	0.30	0.00	0.48	0.15	3.52E+01
305	BHUS85	SS047	44.44010	-103.71702	4067	0.00	1.10	0.00	0.00	0.34	8.15E+01
305	BHUS85	SS048	44.43850	-103.71676	4069	4.86	0.93	4.52	0.98	0.77	1.69E+02
305	BHUS85	RSS049	44.42961	-103.71478	4201	0.00	0.12	0.00	0.00	0.04	8.89E+00
305	BHUS85	RSS050	44.41668	-103.71525	4472	2.86	0.14	0.40	0.04	0.08	1.79E+01
305	BHUS85	SS051	44.40579	-103.71912	4784	0.00	0.23	0.00	0.00	0.07	1.70E+01
305	BHUS85	LS052	44.39725	-103.71670	4850	0.00	0.24	0.00	0.00	0.07	1.78E+01
305	BHDEAD	Ig053	44.38855	-103.71258	4555	0.00	0.08	0.00	0.00	0.02	5.93E+00
305	BHDEAD	SS054	44.38853	-103.71258	4553	0.55	1.86	1.03	0.25	0.68	1.61E+02
305	BHDEAD	MSS055	44.38752	-103.71695	4511	11.43	0.21	2.40	2.41	0.54	1.20E+02
305	BHDEAD	M056	44.37938	-103.72752	4549	0.00	0.00	0.00	0.00	0.00	0.00E+00
305	BHDEAD	MG057	44.37113	-103.74441	4681	8.53	0.78	6.65	2.49	1.08	2.33E+02
305	BHDEAD	MG058	44.37160	-103.74633	4701	0.00	0.08	0.00	0.00	0.02	5.93E+00
305	BHUS14a	MSc059	44.37104	-103.75043	4724	9.06	0.62	5.62	1.51	0.83	1.78E+02
305	BHUS14a	MSc060	44.37093	-103.75096	4727	8.52	1.13	9.63	1.57	1.33	2.82E+02
305	BHUS14a	MGn061	44.36989	-103.75794	4785	9.50	0.06	0.57	0.00	0.07	1.37E+01
305	BHUS14a	MSc062	44.36997	-103.75802	4795	3.24	2.40	7.77	2.24	1.64	3.64E+02
305	BHUS14a	M063	44.36956	-103.76316	4795	2.05	1.55	3.17	0.43	0.79	1.78E+02
305	BHUS14a	MLSS064	44.36953	-103.76335	4853	1.39	3.07	4.26	3.17	1.65	3.82E+02
305	BHUS14a	MSc065	44.36861	-103.77313	4980	1.09	1.78	1.94	1.03	0.82	1.91E+02
405	BHNM	LSS066	44.27253	-103.51057	5015	0.00	0.65	0.00	0.00	0.20	4.82E+01
405	BHNM	LSS067	44.26555	-103.53172	5108	0.00	0.02	0.00	0.00	0.01	1.48E+00
405	BHVCR	LSS068	44.28559	-103.56200	4854	0.00	0.02	0.00	0.00	0.01	1.48E+00
405	BHVCR	LS069	44.29358	-103.55946	4758	0.00	0.29	0.00	0.00	0.09	2.15E+01

Table 27: cont.

Pre	Name	ID	(N)	(W)	Elev. (ft)	Th:U	U (ppm)	Th (ppm)	K (pct)	A (μWm^{-3})	ε_v ($mg^{-1}s^{-1}$)
405	BHVCR	LSS070	44.30258	-103.55170	4695	0.00	0.13	0.00	0.00	0.04	9.63E+00
405	BHVCR	I071	44.31414	-103.54130	4779	11.93	0.85	10.14	1.62	1.29	2.71E+02
405	BHVCR	I072	44.51414	-103.54131	3362	3.38	2.30	7.78	1.44	1.52	3.35E+02
405	BHVCR	I073	44.30545	-103.52252	4607	0.00	0.07	0.00	0.00	0.02	5.19E+00
405	BHVCR	LSS073	44.30895	-103.52939	4630	0.00	0.02	0.00	0.00	0.01	1.48E+00
405	BHVCR	I074	44.31356	-103.54106	4779	4.33	2.10	9.09	1.41	1.56	3.41E+02
405	BHVCR	I075	44.31985	-103.54231	4865	8.16	1.13	9.22	1.78	1.32	2.81E+02
405	BHVCR	I076	44.32499	-103.54417	4945	7.32	1.25	9.15	1.79	1.35	2.89E+02
405	BHVCR	I077	44.32987	-103.54716	5014	7.06	1.19	8.40	1.76	1.27	2.72E+02
405	BHVCR	I078	44.33170	-103.54714	4998	9.50	0.92	8.74	1.59	1.19	2.53E+02
405	BHVCR	I079	44.33348	-103.54694	4901	7.54	1.15	8.67	1.60	1.26	2.69E+02
405	BHVCR	I080	44.33833	-103.54758	4735	0.00	0.47	0.00	0.00	0.14	3.48E+01
405	BHVCR	I081	44.34473	-103.54814	4617	0.00	0.11	0.00	0.00	0.03	8.15E+00
405	BHVCR	I082	44.35625	-103.53648	4561	0.00	0.62	0.00	0.00	0.19	4.59E+01
405	BHVCR	I083	44.36099	-103.53171	4360	0.00	0.00	0.00	0.00	0.00	0.00E+00
405	BHVCR	SS084	44.37330	-103.51157	3865	0.00	0.00	0.00	0.00	0.00	0.00E+00
405	BHVCR	I085	44.37940	-103.50562	3732	0.00	1.66	0.00	0.00	0.51	1.23E+02
405	BHVCR	SSI086	44.37155	-103.51223	3896	0.30	1.32	0.40	0.03	0.44	1.05E+02
405	BHVCR	SSI087	44.36863	-103.51460	3967	0.00	0.02	0.00	0.00	0.01	1.48E+00
505	BHSCR	I088	44.47430	-103.84634	3769	0.00	0.38	0.00	0.00	0.12	2.82E+01
505	BHSPRF	SGyp089	44.47946	-103.83459	3824	0.00	0.01	0.00	0.00	0.00	7.41E-01
505	BHSPRF	SGyp090	44.47953	-103.83499	3820	0.00	0.01	0.00	0.00	0.00	7.41E-01
505	BHSPRF	I091	44.45985	-103.83097	4062	0.00	1.14	0.00	0.00	0.35	8.45E+01
505	BHSPRF	I092	44.45470	-103.81596	4308	0.00	0.60	0.00	0.00	0.18	4.45E+01

Table 27: cont.

Pre	Name	ID	(N)	(W)	Elev. (ft)	Th:U	U (ppm)	Th (ppm)	K (pct)	A (μWm^{-3})	ε_v ($mg^{-1}s^{-1}$)
505	BHSPRF	I093	44.45424	-103.81362	4319	0.00	0.92	0.00	0.00	0.28	6.82E+01
505	BHSPRF	I094	44.45520	-103.80960	4302	0.00	0.53	0.00	0.00	0.16	3.93E+01
505	BHSPRF	SS095	44.45222	-103.81106	4183	0.00	0.01	0.00	0.00	0.00	7.41E-01
505	BHMLR	SS096	44.44074	-103.81394	4254	0.00	0.04	0.00	0.00	0.01	2.96E+00
505	BHMLR	SS097	44.43904	-103.81044	4366	0.00	0.18	0.00	0.00	0.05	1.33E+01
505	BHMLR	SS098	44.43944	-103.80755	4494	8.50	0.02	0.17	0.00	0.02	4.24E+00
505	BHMLR	ISS099	44.39700	-103.80043	4934	0.00	0.49	0.00	0.11	0.16	3.93E+01
505	BHMLR	SS099	44.43468	-103.80174	4601	0.00	0.45	0.00	0.00	0.14	3.33E+01
505	BHMLR	ISS100	44.38083	-103.78748	5293	0.00	1.35	0.00	0.00	0.41	1.00E+02
505	BHMLR	I101	44.37867	-103.77377	4995	5.10	3.39	17.28	2.40	2.75	5.96E+02
505	BHMLR	I102	44.37852	-103.77338	4994	3.59	3.82	13.72	2.17	2.56	5.64E+02
505	BHMLR	MSc103	44.37519	-103.76746	4907	0.76	2.72	2.07	0.00	1.00	2.35E+02
505	BHMLR	MSc104	44.37537	-103.76743	4918	0.50	3.07	1.55	0.19	1.09	2.58E+02
505	BHCC	MSc105	44.36444	-103.77734	5010	18.27	0.49	8.95	2.38	1.17	2.46E+02
505	BHCC	MGn106	44.36342	-103.77932	5072	1.35	4.40	5.96	1.03	1.96	4.51E+02
505	BHCC	MGn107	44.36401	-103.78250	5249	2.43	2.05	4.98	1.12	1.17	2.63E+02
505	BHCC	Qtz108	44.36309	-103.77992	5050	0.00	0.00	0.00	0.00	0.00	0.00E+00
705	BHH14a	I111	44.47205	-103.84801	3777	0.00	0.91	0.00	0.00	0.28	6.74E+01
705	BHH14a	LSS112	44.45552	-103.86373	3844	0.00	0.12	0.00	0.00	0.04	8.89E+00
705	BHH14a	LSS113	44.45552	-103.86475	3862	0.00	0.16	0.00	0.00	0.05	1.19E+01
705	BHH14a	LS114	44.44684	-103.86570	3931	0.00	0.49	0.00	0.00	0.15	3.63E+01
705	BHH14a	LS115	44.44684	-103.86581	3930	0.00	0.04	0.00	0.00	0.01	2.96E+00
705	BHH14a	LS116	44.44089	-103.87274	4007	0.00	0.04	0.00	0.00	0.01	2.96E+00
705	BHH14a	IgS117	44.43692	-103.87753	4239	14.48	0.25	3.62	1.81	0.58	1.26E+02

Table 27: cont.

Pre	Name	ID	(N)	(W)	Elev. (ft)	Th:U	U (ppm)	Th (ppm)	K (pct)	A (μWm^{-3})	ε_v ($mg^{-1}s^{-1}$)
705	BHH14a	LSS118	44.43724	-103.87663	4080	0.00	0.56	0.00	0.00	0.17	4.15E+01
705	BHH14a	MLSH119	44.43608	-103.87611	4107	4.43	0.21	0.93	1.05	0.26	5.91E+01
705	BHH14a	LSS120	44.43135	-103.87571	4110	0.00	0.02	0.00	0.00	0.01	1.48E+00
705	BHH14a	IgS121	44.42853	-103.87344	4120	4.77	10.94	52.20	3.00	8.05	1.74E+03
705	BHH14a	IgS122	44.42862	-103.87337	4121	0.00	52.81	0.00	0.45	16.18	3.93E+03
705	BHH14a	IgS123	44.42847	-103.87363	4147	1.19	2.13	2.53	3.79	1.29	3.02E+02
705	BHH14a	IgS124	44.42447	-103.87504	4150	1.93	0.14	0.27	0.69	0.14	3.34E+01
705	BHH14a	Ig125	44.42356	-103.87790	4159	4.53	0.59	2.67	3.18	0.76	1.73E+02
705	BHH14a	IgS126	44.42364	-103.87910	4171	8.25	0.12	0.99	0.84	0.21	4.77E+01
705	BHH14a	Ig127a	44.41960	-103.88103	4221	2.84	9.06	25.77	2.49	5.20	1.16E+03
705	BHH14a	Ig127b	44.41978	-103.88100	4214	4.39	5.14	22.54	2.70	3.76	8.19E+02
705	BHH14a	Ig128	44.41910	-103.88106	4235	3.04	7.28	22.15	2.29	4.34	9.60E+02
705	BHH14a	Ig129	44.41754	-103.88126	4234	3.17	9.16	29.03	2.30	5.49	1.21E+03
705	BHH14a	IgS130	44.41601	-103.88036	4260	0.00	0.07	0.00	0.00	0.02	5.19E+00
705	BHH14a	IgS131	44.41351	-103.88274	4303	5.18	0.28	1.45	1.62	0.39	8.81E+01
705	BHH14a	IgS132	44.41196	-103.88748	4319	2.03	0.29	0.59	0.00	0.14	3.10E+01
705	BHH14a	LS133	44.41324	-103.89378	4410	0.00	0.06	0.00	0.00	0.02	4.45E+00
705	BHH14a	LSS134	44.40286	-103.89589	4451	0.00	0.46	0.00	0.00	0.14	3.41E+01
705	BHH14a	LS134	44.40682	-103.89970	4419	0.00	0.32	0.00	0.00	0.10	2.37E+01
705	BHH14a	Ig135	44.39680	-103.90012	4520	2.52	11.32	28.55	3.63	6.26	1.40E+03
705	BHH14a	IgS136	44.39654	-103.90076	4522	5.73	4.42	25.33	3.08	3.82	8.21E+02
705	BHH14a	Ig137	44.39701	-103.90753	4559	2.83	14.87	42.05	2.70	8.37	1.86E+03
705	BHH14a	Ig138	44.39391	-103.91116	4605	3.44	14.21	48.84	2.82	8.75	1.92E+03
705	BHH14a	LSS139	44.39101	-103.91271	5019	0.00	0.20	0.00	0.00	0.06	1.48E+01

Table 27: cont.

Pre	Name	ID	(N)	(W)	Elev. (ft)	Th:U	U (ppm)	Th (ppm)	K (pct)	A (μWm^{-3})	ε_v ($mg^{-1}s^{-1}$)
705	BHH14a	LSS140	44.38840	-103.91271	4710	3.75	0.32	1.20	2.18	0.44	1.02E+02
705	BHH14a	LSS141	44.37449	-103.91579	4832	0.00	0.20	0.00	0.00	0.06	1.48E+01
705	BHH14a	LSS142	44.36505	-103.92805	4877	0.00	0.50	0.00	0.00	0.15	3.71E+01
705	BHH14a	LSS143	44.35673	-103.93095	4961	0.32	0.78	0.25	0.33	0.30	7.08E+01
705	BHH14a	LSS144	44.34240	-103.92129	5025	4.10	0.42	1.72	1.41	0.43	9.72E+01
705	BHH14a	LSS145	44.33248	-103.90052	5118	0.00	0.16	0.00	0.00	0.05	1.19E+01
705	BHH14a	Ig146	44.32058	-103.89185	5178	3.61	17.87	64.46	3.29	11.22	2.46E+03
705	BHH14a	Ig147	44.31596	-103.88544	5244	3.83	17.72	67.78	2.84	11.40	2.49E+03
806	BHRFR	IF148	44.10844	-103.65479	5020	3.25	3.37	10.96	2.04	2.18	4.83E+02
806	BHRFR	IF149	44.10996	-103.66717	5074	2.43	4.85	11.77	2.89	2.79	6.28E+02
806	BHRFR	IF150	44.11375	-103.69193	5169	10.47	0.87	9.11	3.51	1.42	3.07E+02
806	BHRFR	IF151	44.12191	-103.71208	5291	6.69	0.54	3.61	2.16	0.71	1.57E+02
806	BHRFR	IF152	44.13158	-103.76285	5521	1.62	1.95	3.16	2.57	1.15	2.65E+02
806	BHRFR	MGn153	44.14265	-103.80940	5710	4.01	0.84	3.37	3.38	0.92	2.08E+02
806	BHSRCR	Ig154	44.15572	-103.86987	6106	0.00	0.51	0.00	0.00	0.16	3.78E+01
806	BHSRCR	Ig155	44.16513	-103.88453	6302	0.00	0.46	0.00	0.00	0.14	3.41E+01
806	BHSRCR	Ig156	44.18714	-103.91254	6512	0.00	0.20	0.00	0.00	0.06	1.48E+01
806	BHSRCR	Ig157	44.18476	-103.93867	6397	0.00	0.82	0.00	0.00	0.25	6.08E+01
806	BHSRCR	Ig158	44.19852	-104.01717	6593	0.00	0.17	0.00	0.00	0.05	1.26E+01
806	BHUS85	Ig159	44.22440	-103.96689	6236	0.00	0.56	0.00	0.00	0.17	4.15E+01
806	BHUS85	Ig160	44.27689	-103.90333	5603	0.00	0.16	0.00	0.00	0.05	1.19E+01
806	BHUS85	Ig161	44.28361	-103.89910	5552	0.00	0.00	0.00	0.00	0.00	0.00E+00
806	BHUS85	IgS162	44.29555	-103.88737	5452	9.00	0.08	0.72	0.64	0.16	3.49E+01
806	BHUS85	M163	44.29686	-103.85735	5500	2.22	0.18	0.40	0.55	0.15	3.47E+01

Table 27: cont.

Pre	Name	ID	(N)	(W)	Elev. (ft)	Th:U	U (ppm)	Th (ppm)	K (pct)	A (μWm^{-3})	ε_v ($mg^{-1}s^{-1}$)
806	BHUS85	Ig164	44.29377	-103.84151	5924	0.00	0.50	0.00	0.00	0.15	3.71E+01
806	BHUS85	Ig165	44.32004	-103.79877	5751	44.73	0.78	34.89	2.61	3.45	6.94E+02
806	BHUS85	Ig166	44.32242	-103.79807	5695	2.97	11.17	33.12	2.80	6.50	1.44E+03
806	BHUS85	MIg167	44.32347	-103.79752	5667	1.88	3.32	6.25	3.68	1.95	4.47E+02
806	BHUS85	MIg168	44.32365	-103.79755	5647	0.00	1.04	0.00	0.00	0.32	7.71E+01
806	BHUS85	Sh169	44.33023	-103.79337	5450	4.73	1.05	4.97	1.33	0.89	1.94E+02
806	BHUS85	Ig170	44.33033	-103.79315	5457	2.64	2.44	6.45	1.58	1.46	3.28E+02
806	BHUS85	MIg171	44.33029	-103.79322	5455	0.00	0.02	0.00	2.54	0.29	7.03E+01
806	BHUS85	Ig172	44.33905	-103.78423	5277	17.13	0.23	3.94	0.00	0.40	8.09E+01
806	BHUS85	MSc173	44.34207	-103.78217	5267	8.11	1.32	10.71	2.24	1.55	3.32E+02
806	BHUS85	M174	44.34498	-103.77891	5317	3.93	0.90	3.54	0.49	0.63	1.37E+02
806	BHLead	M175	44.35474	-103.78033	5333	2.34	1.49	3.49	1.51	0.92	2.08E+02
806	BHLead	M176	44.35419	-103.77575	5439	7.58	0.31	2.35	0.60	0.36	7.73E+01
806	BHLead	M177	44.35445	-103.75585	5049	18.26	0.46	8.40	1.90	1.06	2.22E+02
806	BHLead	M178	44.35517	-103.75001	4929	18.19	0.42	7.64	2.63	1.06	2.26E+02
906	BHHR	IgS179	44.09589	-103.29947	3489	0.00	0.31	0.00	0.00	0.09	2.30E+01
906	BHHR	IgSS180	44.28196	-103.86847	5465	12.57	0.07	0.88	0.00	0.10	1.94E+01
906	BHHR	LSS181	44.27964	-103.86695	5480	0.00	0.77	0.00	0.00	0.24	5.71E+01
906	BHHR	LSS182	44.27519	-103.85480	5565	0.00	0.40	0.00	0.00	0.12	2.96E+01
906	BHHR	LSS183	44.22230	-103.84865	6590	0.00	0.00	0.00	0.00	0.00	0.00E+00
906	BHHR	LSS184	44.26086	-103.84430	5687	0.00	0.10	0.00	0.00	0.03	7.41E+00
906	BHHR	RSS185	44.25618	-103.83057	5842	0.59	0.37	0.22	0.69	0.21	4.97E+01
906	BHHR	RSS186	44.25544	-103.82851	5876	1.19	0.32	0.38	0.38	0.17	4.02E+01
906	BHHR	RSS187	44.25522	-103.82649	5876	0.00	1.11	0.00	0.00	0.34	8.23E+01

Table 27: cont.

Pre	Name	ID	(N)	(W)	Elev. (ft)	Th:U	U (ppm)	Th (ppm)	K (pct)	A (μWm^{-3})	ε_v ($mg^{-1}s^{-1}$)
906	BHHR	SS188	44.25571	-103.82373	5999	0.00	0.00	0.00	0.00	0.00	0.00E+00
906	BHRR	RSS189	44.27285	-103.80666	5857	0.55	0.29	0.16	0.50	0.16	3.76E+01
906	BHRR	RSS190	44.28053	-103.80388	5800	0.19	0.95	0.18	1.39	0.46	1.11E+02
906	BHBFR	GSc191	44.30442	-103.79408	5924	2.90	11.18	32.44	3.93	6.57	1.46E+03
906	BHBFR	GSc192	44.30425	-103.79557	5966	4.36	6.32	27.57	3.54	4.64	1.01E+03
906	BHBFR	GSc193	44.30541	-103.79393	5872	2.94	10.09	29.63	3.55	5.96	1.32E+03
906	BHBVR	GSc194	44.29804	-103.79651	5859	2.95	9.44	27.84	3.56	5.62	1.25E+03
906	BHEWR	IgS195	44.29797	-103.79651	5854	0.04	1.46	0.06	0.00	0.45	1.09E+02
906	BHEWR	IgS196	44.30885	-103.77178	5460	0.00	1.35	0.00	0.00	0.41	1.00E+02
906	BHBVR	IgG197	44.28289	-103.77928	5843	4.16	1.40	5.82	2.12	1.15	2.55E+02
906	BHBVR	IgS198	44.28232	-103.77685	5916	3.30	1.90	6.27	2.23	1.36	3.03E+02
906	BHBVR	Ig199	44.28097	-103.77052	6113	3.11	1.72	5.35	2.08	1.21	2.70E+02
906	BHBVR	Ig200	44.27794	-103.75106	5944	0.95	1.10	1.04	2.51	0.71	1.66E+02
906	BHBVR	Ig201	44.27368	-103.73370	5678	0.00	0.75	0.00	0.00	0.23	5.56E+01
906	BHBVR	SS202	44.27742	-103.69756	5530	0.00	1.55	0.00	0.00	0.47	1.15E+02
906	BHHWR	IgS203	44.29401	-103.70074	5577	0.00	0.82	0.00	0.00	0.25	6.08E+01
906	BHIOR	MGn204	44.28992	-103.71120	5533	4.73	2.66	12.57	3.01	2.20	4.82E+02
906	BHYCR	MGn205	44.34913	-103.74891	4863	0.07	3.20	0.22	0.89	1.10	2.65E+02
906	BHYCR	MGn206	44.34908	-103.74902	4860	0.00	0.08	0.00	0.00	0.02	5.93E+00
906	BHYCR	MB207	44.34534	-103.75494	4936	4.58	2.04	9.34	2.24	1.66	3.63E+02
1006	BHYCR	MSc208	44.34522	-103.75236	4913	4.14	1.60	6.62	3.29	1.41	3.15E+02
1006	BHYCR	M209	44.34264	-103.75484	4951	5.00	2.30	11.49	4.45	2.17	4.77E+02
1006	BHYCR	M210	44.34064	-103.75537	5005	4.20	0.59	2.48	0.48	0.44	9.69E+01
1006	BHYCR	M211	44.34364	-103.75948	5048	4.27	0.73	3.12	0.08	0.49	1.07E+02

Table 27: cont.

Pre	Name	ID	(N)	(W)	Elev. (ft)	Th:U	U (ppm)	Th (ppm)	K (pct)	A (μWm^{-3})	ε_v ($mg^{-1}s^{-1}$)
1006	BHYCR	MSc212	44.34368	-103.77216	5190	32.76	0.25	8.19	1.76	0.96	1.99E+02
1006	BHYCR	MSc213	44.34315	-103.77896	5209	34.63	0.08	2.77	0.00	0.26	5.08E+01
1006	BHYCR	MSc214	44.34043	-103.75651	5010	2.86	0.50	1.43	0.00	0.27	6.02E+01
1006	BHYCR	MSc215	44.33559	-103.75774	5120	6.54	1.00	6.54	3.04	1.20	2.62E+02
1006	BHYCR	IF216	44.33126	-103.75711	5195	0.00	0.83	0.00	0.00	0.25	6.15E+01
1006	BHYCR	MSc217	44.32928	-103.75195	5279	0.00	0.00	0.00	0.00	0.00	0.00E+00
1006	BHYCR	IgS218	44.32658	-103.74776	5376	2.60	6.19	16.08	5.51	3.86	8.68E+02
1006	BHYCR	MIg219	44.32460	-103.74711	5410	0.54	6.93	3.75	2.76	2.74	6.49E+02
1006	BHYCR	MIF220	44.31652	-103.74469	5613	0.00	1.61	0.00	0.00	0.49	1.19E+02
1006	BHYCR	IgIF221	44.31225	-103.74060	5762	0.00	0.94	0.00	0.00	0.29	6.97E+01
1006	BHYCR	IgS222	44.30770	-103.73542	5903	3.14	1.45	4.55	2.58	1.12	2.51E+02
1006	BHYCR	Ig223	44.30144	-103.74234	5936	3.28	1.69	5.54	2.74	1.29	2.89E+02
1006	BHYCR	Ig224	44.29186	-103.75446	5951	0.62	0.81	0.50	0.42	0.34	7.95E+01
1006	BHVCR	MSc225	44.30996	-103.66346	5149	5.26	1.58	8.31	4.51	1.69	3.74E+02
1006	BHUR	Ig226	44.34081	-103.82763	6139	1.70	4.08	6.94	7.84	2.71	6.27E+02
1006	BHUR	MIg227	44.34050	-103.83054	6151	5.16	12.44	64.21	8.31	10.11	2.19E+03
1006	BHUR	MIg228	44.34031	-103.83683	6316	1.47	1.39	2.04	2.73	0.90	2.10E+02
1006	BHUR	MIg229	44.34119	-103.83685	6348	1.71	1.32	2.26	1.93	0.81	1.87E+02
1006	BHUR	MIg230	44.34070	-103.83945	6417	1.43	18.64	26.64	6.17	8.62	1.98E+03
1006	BHUR	MIg231	44.33759	-103.84048	6487	7.80	5.34	41.67	2.40	5.39	1.14E+03
1006	BHTGR	Ig232	44.33654	-103.79794	5485	1.66	3.81	6.32	1.64	1.88	4.29E+02
1006	BHTGR	Ig233	44.33632	-103.80180	5559	0.00	0.98	0.00	0.00	0.30	7.26E+01
1006	BHTGR	Ig234	44.33591	-103.79943	5606	1.66	3.39	5.64	1.58	1.69	3.85E+02
1006	BHDM	Ig235a	44.31406	-103.80324	5905	4.94	7.20	35.57	2.94	5.51	1.19E+03

Table 27: cont.

Pre	Name	ID	(N)	(W)	Elev. (ft)	Th:U	U (ppm)	Th (ppm)	K (pct)	A (μWm^{-3})	ε_v ($mg^{-1}s^{-1}$)
1006	BHDM	Ig235	44.31406	-103.80324	5905	5.52	6.43	35.50	2.99	5.27	1.13E+03
1006	BHDM	GrSc236	44.31202	-103.80313	5911	3.88	8.04	31.17	3.21	5.43	1.19E+03
1006	BHDM	GrSc237	44.30928	-103.80589	5913	2.80	11.65	32.60	3.65	6.70	1.49E+03
1006	BHTSR	Ig238	44.30083	-103.83019	6372	4.22	3.98	16.81	2.64	2.92	6.39E+02
1006	BHTSR	Ig239	44.30589	-103.82681	6454	0.03	1.64	0.05	0.17	0.52	1.27E+02
1006	BHTSR	Ig240	44.31438	-103.82677	6457	5.06	3.26	16.51	2.47	2.66	5.76E+02
1006	BHTSR	Ig241	44.31716	-103.82693	6519	4.37	3.61	15.77	3.99	2.87	6.31E+02
1006	BHTSR	Ig242	44.32082	-103.83119	6625	8.27	4.39	36.32	2.49	4.66	9.81E+02
1006	BHTSR	Ig243	44.32571	-103.83194	6780	4.92	8.44	41.50	3.23	6.42	1.39E+03
1006	BHTSR	Ig244	44.32512	-103.83767	6918	10.29	3.44	35.39	2.45	4.29	8.95E+02
1006	BHTSR	Ig245	44.32833	-103.83587	7034	6.64	6.04	40.09	2.32	5.46	1.16E+03
1106	BHUS14a	LS246	44.37813	-103.91437	4772	0.00	0.14	0.00	0.00	0.04	1.04E+01
1106	BHUS14a	Ig247	44.29534	-103.81947	6109	4.98	4.19	20.87	2.54	3.31	7.17E+02
1106	BHUS14a	Ig248	44.30256	-103.81191	6135	4.44	4.35	19.32	2.51	3.23	7.03E+02
1106	BHUS14a	IgS249	44.30131	-103.81264	6132	7.00	0.12	0.84	1.39	0.26	6.02E+01
1106	BHUS14a	MIg250	44.30861	-103.81710	6043	4.01	6.67	26.74	6.78	5.04	1.11E+03
1106	BHUS14a	IF251	44.31471	-103.79426	5878	4.02	1.35	5.43	2.25	1.12	2.49E+02
1106	BHCC	GrSc252	44.37157	-103.76135	4818	1.28	1.13	1.45	0.00	0.47	1.07E+02
1106	BHCC	MIg253	44.37476	-103.76689	4916	2.39	0.76	1.82	0.00	0.38	8.58E+01
1106	BHCC	Ig254	44.37863	-103.77375	4994	3.31	4.17	13.79	2.21	2.68	5.92E+02
1106	BHCC	Ig255	44.38104	-103.77915	5076	3.83	3.66	14.03	2.22	2.54	5.59E+02
1106	BHCC	IgS256	44.38158	-103.78579	5237	4.21	1.11	4.67	4.17	1.20	2.71E+02
1106	BHCC	IgS257	44.38097	-103.78715	5282	2.37	1.77	4.20	3.37	1.27	2.91E+02
1106	BHBG	IgS258	44.39693	-103.80039	4933	3.68	1.33	4.89	2.31	1.08	2.40E+02

Table 27: cont.

Pre	Name	ID	(N)	(W)	Elev. (ft)	Th:U	U (ppm)	Th (ppm)	K (pct)	A (μWm^{-3})	ε_v ($mg^{-1}s^{-1}$)
1106	BHBG	IgS259	44.40691	-103.81899	4699	1.62	3.08	4.99	1.73	1.55	3.56E+02
1106	BHBG	IgS260	44.41525	-103.82426	4603	12.59	0.27	3.40	1.00	0.48	1.02E+02
1106	BHBG	IgS261	44.42539	-103.82273	4849	0.00	0.28	0.00	0.00	0.09	2.07E+01
1206	BHBR	SS262	44.27422	-103.44952	3781	0.00	4.26	0.00	0.00	1.30	3.16E+02
1206	BHBR	SS263	44.27380	-103.45022	3782	0.00	1.67	0.00	0.00	0.51	1.24E+02
1206	BHBR	SS264	44.27671	-103.46873	3909	0.00	0.15	0.00	0.00	0.05	1.11E+01
1206	BHBR	SS265	44.28637	-103.48088	3994	0.00	0.22	0.00	0.00	0.07	1.63E+01
1206	BHBR	SS266	44.28821	-103.48088	4140	0.08	0.12	0.01	0.37	0.08	1.91E+01
1206	BHBR	Ig267	44.28897	-103.48219	4118	3.65	2.62	9.56	1.71	1.79	3.95E+02
1206	BHBR	IgS268	44.22646	-103.39957	3651	0.00	2.11	0.00	0.00	0.64	1.56E+02
1206	BHGR	Ig269	44.34814	-103.55547	4551	9.26	0.81	7.50	1.72	1.07	2.28E+02
1206	BHGR	Ig270	44.34827	-103.55646	4585	4.79	1.65	7.90	1.52	1.34	2.91E+02
1206	BHGR	Ig271	44.34826	-103.55704	4582	4.82	1.68	8.09	1.67	1.38	3.01E+02
1206	BHGR	Ig272	44.34756	-103.57381	4653	4.81	1.67	8.04	1.52	1.35	2.95E+02
1206	BHGR	Ig273	44.34630	-103.57285	4710	6.03	1.26	7.60	1.69	1.21	2.62E+02
1206	BHGR	Ig274	44.34610	-103.57256	4714	3.41	1.77	6.04	1.60	1.23	2.72E+02
1206	BHGR	Ig275	44.34147	-103.58506	4596	3.89	1.27	4.94	1.75	1.00	2.22E+02
1206	BHGR	Ig276	44.33836	-103.59746	4588	0.00	0.22	0.00	0.00	0.07	1.63E+01
1206	BHER	Ig277	44.32718	-103.59605	4692	4.45	1.91	8.49	1.62	1.48	3.23E+02
1206	BHER	IgLS278	44.31773	-103.59756	4793	0.00	0.19	0.00	0.00	0.06	1.41E+01
1206	BHGR	Ig279	44.32071	-103.64951	4988	0.00	0.08	0.00	0.00	0.02	5.93E+00
1206	BHGR	MIg280	44.32157	-103.65022	4979	0.00	0.00	0.00	0.01	0.00	2.71E-01
1206	BHGR	Ig281	44.32177	-103.65114	4962	2.27	0.26	0.59	0.00	0.13	2.88E+01
1206	BHGR	MGn2Sc282	44.32307	-103.65062	4935	2.83	4.11	11.65	2.88	2.56	5.71E+02

Table 27: cont.

Pre	Name	ID	(N)	(W)	Elev. (ft)	Th:U	U (ppm)	Th (ppm)	K (pct)	A (μWm^{-3})	ε_v ($mg^{-1}s^{-1}$)
1206	BHGR	MSc283	44.32377	-103.65085	4925	4.13	1.58	6.53	2.07	1.26	2.79E+02
1206	BHGR	MGn284	44.32461	-103.65205	4932	0.00	0.00	0.00	0.00	0.00	0.00E+00
1206	BHGR	MGn285	44.32648	-103.65231	4928	3.31	2.39	7.92	2.43	1.67	3.71E+02
1206	BHER	M286	44.32729	-103.65065	4923	0.00	0.03	0.00	0.00	0.01	2.22E+00
1206	BHGR	M287	44.32654	-103.64783	4890	5.79	1.37	7.93	2.23	1.33	2.90E+02
1206	BHNM	MIg288	44.27767	-103.67920	5468	6.30	1.52	9.58	2.88	1.59	3.46E+02
1206	BHCLP	IgS289	44.24133	-103.74093	6261	4.13	1.35	5.57	2.19	1.13	2.50E+02
1206	BHCLP	Ig290	44.24038	-103.73917	6178	3.70	1.59	5.89	2.12	1.22	2.71E+02

Note: Latitude and Longitude are set to DDD.DDDDD° (Decimal Degree) Format

Table 28: Ge-SED GRS Analysis- Sample Identification (ID), Weight (Wt.), Rock type, Rock Classification and Formation

Pre -	Name	ID	Wt.(g)	Rock Type	*Rock Classification*	Formation
105	BHH385	S001	836.76	Sedimentary	Sandstone	–
105	BHH385	I002	839.98	Metamorphic	Metagraywacke	–
105	BHH385	I003	819.16	Igneous	Latite	–
105	BHH385	S003	799.20	Igneous	Episodite	–
105	BHH385	Ig004	786.71	Igneous	Rhyolite	–
105	BHH385	Ig005	927.07	Metamorphic	Schist	–
105	BHH385	M006	823.96	Metamorphic	Schist	–
105	BHH385	M007	817.38	Metamorphic	Schist	–
105	BHH385	M008	799.20	Igneous	Latite	–
105	BHH385	Ig009	791.12	Igneous	Latite	–
105	BHH85	Ig010	736.48	Igneous	Rhyolite	–
105	BHH85	Sc011	856.31	Metamorphic	Mica Schist	–
105	BHH85	Sc012	782.70	Metamorphic	Mica Schist	–
105	BHH85	SS013	791.80	Sedimentary	Sandstone	–
105	BHH85	SS014	780.85	Metamorphic	Phyllite	–
105	BHDEAD	S015	619.19	Metamorphic	Mica Schist	–
105	BHDEAD	S016	802.39	Metamorphic	Quartzite	–
105	BHDEAD	Sc017	721.54	Metamorphic	Mica Schist	–
105	BHDEAD	Sc018	807.28	Metamorphic	Schist	–
105	BHDEAD	SS019	880.43	Sedimentary	Sandstone	Deadwood
105	BHDEAD	SS020	850.04	Sedimentary	Sandstone	Deadwood
105	BHDEAD	Sc021	759.44	Metamorphic	Schist	–
105	BHDEAD	Gc022	808.66	Metamorphic	Mica Schist	–
105	BHDEAD	Sc023	734.03	Metamorphic	Mica Schist	–
205	BHH14	RSS024	844.96	Sedimentary	Limestone	Spearfish
205	BHH14	RSS025	654.29	Sedimentary	Calcareous Sandstone	Spearfish
205	BHH14	SS026	783.63	Sedimentary	Sandstone	Spearfish
205	BHH14	LS027	802.60	Sedimentary	Sandstone	Minnelusa
205	BHH14	LSS028	922.87	Sedimentary	Sandstone	Minnelusa
205	BHH14	LSS029	768.41	Sedimentary	Limestone	Minnelusa
205	BHH14	LSS030	877.17	Sedimentary	Limestone	Minnelusa
205	BHH14	LS031	890.43	Sedimentary	Limestone	Minnelusa
205	BHH14	LS032	791.98	Sedimentary	Limestone	Minnelusa
205	BHH14	LS033	844.96	Sedimentary	Limestone	Minnelusa
205	BHH14	LSS034	675.29	Sedimentary	Limestone	Minnelusa
205	BHH14	LS034	778.39	Sedimentary	Limestone	Minnelusa
205	BHH14	LS035	804.09	Sedimentary	Bedded Limestone	Minnelusa

Table 28: cont.

Pre -	Name	ID	Wt.(g)	Rock Type	*Rock Classification*	Formation
205	BHH14	LS36a	740.42	Sedimentary	Limestone	Minnelusa
205	BHH14	LS36b	887.35	Sedimentary	Sandstone	Minnelusa
205	BHH14	LS037	716.55	Sedimentary	Calcareous Sandstone	Brule
205	BHH14	LSS038	877.17	Sedimentary	Limestone	Pahasapa
205	BHH14	B039	886.53	Igneous	Basalt	–
205	BHH14	B040	907.92	Igneous	Basalt	–
205	BHH14	LSS041	872.82	Sedimentary	Limestone	Englewood
305	BHCCR	SS042	600.66	Sedimentary	Sandstone	Inyan Kara
305	BHCCR	SS043	770.21	Sedimentary	Sandstone	Inyan Kara
305	BHCCR	SS044	860.55	Sedimentary	Limestone	Inyan Kara
305	BHCCR	SS045	868.09	Sedimentary	Limestone	Minnekahta
305	BHCCR	SS046	812.06	Sedimentary	Sandstone	Spearfish
305	BHUS85	SS047	751.29	Igneous	Rhyolite	–
305	BHUS85	SS048	814.25	Sedimentary	Sandstone	Minnelusa
305	BHUS85	RSS049	771.81	Sedimentary	Limestone	Minnelusa
305	BHUS85	RSS050	814.66	Sedimentary	Sandy Limestone	Minnelusa
305	BHUS85	SS051	771.37	Sedimentary	Sandy Limestone	Minnelusa
305	BHUS85	LS052	783.68	Sedimentary	Limestone	Pahasapa
305	BHDEAD	Ig053	694.86	Sedimentary	Calcite deposit	Pahasapa
305	BHDEAD	SS054	750.87	Sedimentary	Limestone	Pahasapa
305	BHDEAD	MSS055	808.52	Sedimentary	Bedded Sandstone	Pahasapa
305	BHDEAD	M056	997.83	Metamorphic	Schist	–
305	BHDEAD	MG057	814.11	Metamorphic	Schist	–
305	BHDEAD	MG058	757.54	Igneous	Siliceous Granodiorite	–
305	BHUS14a	MSc059	699.36	Metamorphic	Mica Schist	–
305	BHUS14a	MSc060	796.22	Metamorphic	Siliceous Schist	–
305	BHUS14a	MGn061	795.85	Metamorphic	Phyllite	–
305	BHUS14a	MSc062	832.29	Metamorphic	Phyllite	–
305	BHUS14a	M063	847.63	Metamorphic	Phyllite	–
305	BHUS14a	MLSS064	791.26	Igneous	Altered Rhyolite	–
305	BHUS14a	MSc065	823.84	Metamorphic	Phyllite	–
405	BHNM	LSS066	751.56	Sedimentary	Limestone	Pahasapa
405	BHNM	LSS067	728.43	Sedimentary	Sandstone	Deadwood
405	BHVCR	LSS068	800.54	Sedimentary	Limestone	Deadwood
405	BHVCR	LS069	771.29	Sedimentary	Limestone	Pahasapa
405	BHVCR	LSS070	743.14	Sedimentary	Limestone	Pahasapa
405	BHVCR	I071	760.90	Igneous	Latitic Andesite	–

Table 28: cont.

Pre -	Name	ID	Wt.(g)	Rock Type	*Rock Classification*	Formation
405	BHVCR	I072	776.36	Igneous	Latite	–
405	BHVCR	I073	868.56	Sedimentary	Limestone	Pahasapa
405	BHVCR	LSS073	847.74	Sedimentary	Limestone	Pahasapa
405	BHVCR	I074	778.70	Igneous	Latite	–
405	BHVCR	I075	811.89	Igneous	Latitic Andesite	–
405	BHVCR	I076	797.77	Igneous	Latitic Andesite	–
405	BHVCR	I077	779.20	Igneous	Latite	–
405	BHVCR	I078	787.48	Igneous	Latite	–
405	BHVCR	I079	771.28	Igneous	Latite	–
405	BHVCR	I080	861.88	Igneous	Trachyte	–
405	BHVCR	I081	762.88	Sedimentary	Calcareous Sandstone	Whitewood
405	BHVCR	I082	837.55	Igneous	Alkalic Rhyolite	–
405	BHVCR	I083	794.32	Sedimentary	Limestone	Englewood
405	BHVCR	SS084	594.66	Sedimentary	Sandstone	Minnelusa
405	BHVCR	I085	897.11	Sedimentary	Limestone	Minnekahta
405	BHVCR	SSI086	787.46	Sedimentary	Sandstone	Minnelusa
405	BHVCR	SSI087	726.13	Sedimentary	Sandstone	Minnelusa
505	BHSCR	I088	837.67	Sedimentary	Limestone	Minnekahta
505	BHSPRF	SGyp089	614.43	Sedimentary	Gypsum	Spearfish
505	BHSPRF	SGyp090	604.64	Sedimentary	Gypsum	Spearfish
505	BHSPRF	I091	829.16	Sedimentary	Limestone	Spearfish
505	BHSPRF	I092	842.89	Sedimentary	Limestone	Minnekahta
505	BHSPRF	I093	834.39	Sedimentary	Silty Limestone	Spearfish
505	BHSPRF	I094	868.44	Sedimentary	Limy Red Shale	Opeche
505	BHSPRF	SS095	578.22	Sedimentary	Sandstone	Minnelusa
505	BHMLR	SS096	702.80	Sedimentary	Sandstone	Minnelusa
505	BHMLR	SS097	720.00	Sedimentary	Calcareous Sandstone	Minnelusa
505	BHMLR	SS098	696.08	Sedimentary	Sandstone	Minnelusa
505	BHMLR	ISS099	854.66	Sedimentary	Sandstone	Minnelusa
505	BHMLR	SS099	801.53	Sedimentary	Sandstone	Minnelusa
505	BHMLR	ISS100	797.95	Igneous	Trachyte	–
505	BHMLR	I101	808.42	Igneous	Trachyte	–
505	BHMLR	I102	779.71	Igneous	Trachyte	–
505	BHMLR	MSc103	888.28	Metamorphic	Phyllite	–
505	BHMLR	MSc104	819.55	Metamorphic	Schist	–
505	BHCC	MSc105	895.38	Metamorphic	Metabasalt	–
505	BHCC	MGn106	804.07	Metamorphic	Siliceous Phyllite	–

Table 28: cont.

Pre -	Name	ID	Wt. (g)	Rock Type	*Rock Classification*	Formation
505	BHCC	MGn107	760.92	Metamorphic	Siliceous Phyllite	–
505	BHCC	Qtz108	846.79	Metamorphic	Quartzite	–
705	BHH14a	I111	819.99	Sedimentary	Limestone	Minnekahta
705	BHH14a	LSS112	753.94	Sedimentary	Dolomitic Sandstone	Minnelusa
705	BHH14a	LSS113	610.19	Sedimentary	Limestone	Minnelusa
705	BHH14a	LS114	733.03	Sedimentary	Limestone	Pahasapa
705	BHH14a	LS115	739.35	Sedimentary	Limestone	Pahasapa
705	BHH14a	LS116	753.21	Sedimentary	Limestone	Pahasapa
705	BHH14a	IgS117	772.78	Igneous	Igneous	–
705	BHH14a	LSS118	783.24	Sedimentary	Limestone	Pahasapa
705	BHH14a	MLSH119	783.90	Sedimentary	Dolomitic Siltstone	Englewood
705	BHH14a	LSS120	770.52	Sedimentary	Limestone	Pahasapa
705	BHH14a	IgS121	744.66	Metamorphic	Metabasalt	–
705	BHH14a	IgS122	–	Sedimentary	Limestone	Whitewood
705	BHH14a	IgS123	759.51	Sedimentary	Limestone	Whitewood
705	BHH14a	IgS124	737.13	Sedimentary	Limestone	Whitewood
705	BHH14a	Ig125	785.47	Sedimentary	Limestone	Whitewood
705	BHH14a	IgS126	794.02	Sedimentary	Dolomitic Sandstone	Whitewood
705	BHH14a	Ig127a	738.36	Igneous	Granodiorite	–
705	BHH14a	Ig127b	734.96	Igneous	Granodiorite	–
705	BHH14a	Ig128	758.41	Igneous	Granodiorite	–
705	BHH14a	Ig129	777.05	Igneous	Granodiorite	–
705	BHH14a	IgS130	792.34	Sedimentary	Limestone	Whitewood
705	BHH14a	IgS131	792.61	Sedimentary	Limestone	Whitewood
705	BHH14a	IgS132	764.04	Sedimentary	Limestone	Whitewood
705	BHH14a	LS133	664.12	Sedimentary	Fossiliferous Limestone	Pahasapa
705	BHH14a	LSS134	771.81	Sedimentary	Limestone	Whitewood
705	BHH14a	LS134	730.67	Sedimentary	Calcareous Sandstone	Whitewood
705	BHH14a	Ig135	704.98	Igneous	Phonolite	–
705	BHH14a	IgS136	686.98	Sedimentary	Limy Graywacke	Deadwood
705	BHH14a	Ig137	700.98	Igneous	Volcanic	–
705	BHH14a	Ig138	730.34	Igneous	Volcanic	–
705	BHH14a	LSS139	729.16	Sedimentary	Limestone	Pahasapa
705	BHH14a	LSS140	704.82	Sedimentary	Sandstone	Deadwood
705	BHH14a	LSS141	734.07	Sedimentary	Limestone	Whitewood

Table 28: cont.

Pre -	Name	ID	Wt.(g)	Rock Type	*Rock Classification*	Formation
705	BHH14a	LSS142	792.64	Sedimentary	Limestone	Whitewood
705	BHH14a	LSS143	861.05	Sedimentary	Dolomitic Limestone	Whitewood
705	BHH14a	LSS144	668.72	Sedimentary	Limestone	Whitewood
705	BHH14a	LSS145	726.12	Sedimentary	Limestone	Whitewood
705	BHH14a	Ig146	692.24	Igneous	Volcanic	–
705	BHH14a	Ig147	686.30	Igneous	Alkalic Volcanic	–
806	BHRFR	IF148	799.55	Metamorphic	Phyllite	–
806	BHRFR	IF149	791.08	Metamorphic	Phyllitic Schist	–
806	BHRFR	IF150	767.06	Metamorphic	Phyllitic Slate	–
806	BHRFR	IF151	833.90	Metamorphic	Phyllitic Schist	–
806	BHRFR	IF152	789.88	Metamorphic	Phyllite	–
806	BHRFR	MGn153	793.87	Metamorphic	Phyllite	–
806	BHSRCR	Ig154	798.74	Igneous	Aplite	–
806	BHSRCR	Ig155	821.88	Igneous	Rhyolite	–
806	BHSRCR	Ig156	760.87	Sedimentary	Limestone	Pahasapa
806	BHSRCR	Ig157	847.25	Sedimentary	Limestone	Pahasapa
806	BHSRCR	Ig158	826.89	Sedimentary	Limestone	Pahasapa
806	BHUS85	Ig159	804.70	Sedimentary	Limestone	Pahasapa
806	BHUS85	Ig160	816.92	Igneous	Rhyolite	–
806	BHUS85	Ig161	774.00	Sedimentary	Limestone	Pahasapa
806	BHUS85	IgS162	795.95	Sedimentary	Limestone	Whitewood
806	BHUS85	M163	819.53	Sedimentary	Calcareous Limestone Clast	Deadwood
806	BHUS85	Ig164	789.54	Igneous	Rhyolite	–
806	BHUS85	Ig165	716.06	Igneous	Phonolite	–
806	BHUS85	Ig166	758.54	Igneous	Phonolite	–
806	BHUS85	MIg167	683.90	Igneous	Phonolite	–
806	BHUS85	MIg168	767.20	Metamorphic	Schist	–
806	BHUS85	Sh169	821.59	Metamorphic	Phyllite	–
806	BHUS85	Ig170	716.45	Igneous	Heavily weathered Trachyte	–
806	BHUS85	MIg171	821.65	Metamorphic	Metasandstone	–
806	BHUS85	Ig172	786.62	Metamorphic	Phyllite	–
806	BHUS85	MSc173	763.17	Metamorphic	Phyllite	–
806	BHUS85	M174	814.51	Metamorphic	Fe Rich Hemetitic Schist	–
806	BHLead	M175	791.62	Metamorphic	Metaquartzite	–
806	BHLead	M176	762.51	Metamorphic	Calcareous Phyllite	–

Table 28: cont.

Pre -	Name	ID	Wt.(g)	Rock Type	*Rock Classification*	Formation
806	BHLead	M177	769.30	Metamorphic	Phyllite	–
806	BHLead	M178	742.27	Metamorphic	Phyllite	–
906	BHHR	IgS179	764.03	Sedimentary	Fine grained Limestone	Spearfish
906	BHHR	IgSS180	800.55	Igneous	Rhyolite	–
906	BHHR	LSS181	734.23	Sedimentary	Limestone	Madison Gp
906	BHHR	LSS182	731.06	Sedimentary	Limestone	Whitewood
906	BHHR	LSS183	736.14	Igneous	Volcanic	–
906	BHHR	LSS184	749.20	Sedimentary	Calcareous Sandstone	Madison Gp
906	BHHR	RSS185	726.21	Sedimentary	Calcareous Sandstone	Deadwood
906	BHHR	RSS186	748.24	Sedimentary	Calcareous Sandstone	Deadwood
906	BHHR	RSS187	762.26	Sedimentary	Sandy Limestone	Whitewood
906	BHHR	SS188	770.27	Sedimentary	Limestone	Whitewood
906	BHRR	RSS189	763.63	Sedimentary	Sandy Limestone	Whitewood
906	BHRR	RSS190	709.24	Sedimentary	Calcareous Sandstone	Whitewood
906	BHBFR	GSc191	709.65	Igneous	Phonolite	–
906	BHBFR	GSc192	655.09	Igneous	Phonolite	–
906	BHBFR	GSc193	712.04	Igneous	Phonolite	–
906	BHBVR	GSc194	685.84	Igneous	Phonolite	–
906	BHEWR	IgS195	802.40	Igneous	Phonolite	–
906	BHEWR	IgS196	779.32	Metamorphic	Metaquartzite	–
906	BHBVR	IgG197	704.32	Igneous	Rhyolite	–
906	BHBVR	IgS198	713.36	Igneous	Rhyolite	–
906	BHBVR	Ig199	695.01	Igneous	Rhyolite	–
906	BHBVR	Ig200	734.05	Igneous	Rhyolite	–
906	BHBVR	Ig201	737.06	Metamorphic	Marble like Limestone	–
906	BHBVR	SS202	783.35	Sedimentary	Sandstone	Deadwood
906	BHHWR	IgS203	792.25	Sedimentary	Limestone	–
906	BHIOR	MGn204	722.07	Metamorphic	Phyllitic Slate	–
906	BHYCR	MGn205	663.54	Igneous	Rhyolite	–
906	BHYCR	MGn206	750.31	Igneous	Fine grained igneous	–
906	BHYCR	MB207	832.13	Metamorphic	Phyllitic Slate	–
1006	BHYCR	MSc208	691.92	Metamorphic	Schisty Phyllite	–
1006	BHYCR	M209	770.94	Metamorphic	Schisty Phyllite	–
1006	BHYCR	M210	752.11	Metamorphic	Schisty Phyllite	–
1006	BHYCR	M211	710.35	Metamorphic	Schist	–

Table 28: cont.

Pre -	Name	ID	Wt.(g)	Rock Type	*Rock Classification*	Formation
1006	BHYCR	MSc212	–	Metamorphic	Schisty Slate	–
1006	BHYCR	MSc213	753.25	Metamorphic	Mica Schist	–
1006	BHYCR	MSc214	774.62	Metamorphic	Schist	–
1006	BHYCR	MSc215	746.13	Metamorphic	Metamorphic Schist	–
1006	BHYCR	IF216	768.17	Metamorphic	Schist	–
1006	BHYCR	MSc217	844.69	Metamorphic	Phyllitic Slate	–
1006	BHYCR	IgS218	672.89	Igneous	Rhyolite	–
1006	BHYCR	MIg219	751.40	Igneous	Volcanic	–
1006	BHYCR	MIF220	709.02	Igneous	Volcanic	–
1006	BHYCR	IgIF221	749.33	Metamorphic	Siliceous Slate	–
1006	BHYCR	IgS222	–	Igneous	Rhyolite	–
1006	BHYCR	Ig223	658.76	Igneous	Rhyolite	–
1006	BHYCR	Ig224	650.87	Igneous	Rhyolite	–
1006	BHVCR	MSc225	733.98	Metamorphic	Siliceous Mica Schist	–
1006	BHUR	Ig226	–	Igneous	Trachyte	–
1006	BHUR	MIg227	626.94	Igneous	Rhyolite	–
1006	BHUR	MIg228	681.32	Igneous	Trachyte	–
1006	BHUR	MIg229	628.43	Igneous	Weathered Trachyte	–
1006	BHUR	MIg230	655.98	Igneous	Rhyolite	–
1006	BHUR	MIg231	715.48	Igneous	Trachyte	–
1006	BHTGR	Ig232	671.55	Igneous	Trachyte	–
1006	BHTGR	Ig233	739.08	Igneous	Rhyolite	–
1006	BHTGR	Ig234	693.45	Igneous	Latitic Andesite	–
1006	BHDM	Ig235a	690.43	Igneous	Phonolite	–
1006	BHDM	Ig235	695.17	Igneous	Phonolite	–
1006	BHDM	GrSc236	672.02	Igneous	Phonolite	–
1006	BHDM	GrSc237	687.22	Igneous	Phonolite	–
1006	BHTSR	Ig238	712.29	Igneous	Trachy Andesite	–
1006	BHTSR	Ig239	679.86	Igneous	Heavily Weathered Trachyte	–
1006	BHTSR	Ig240	727.92	Igneous	Trachy Rhyolite	–
1006	BHTSR	Ig241	706.75	Igneous	Trachyte	–
1006	BHTSR	Ig242	694.20	Igneous	Alkalic Rhyolite	–
1006	BHTSR	Ig243	707.26	Igneous	Trachy Andesite	–
1006	BHTSR	Ig244	720.62	Igneous	Trachyte	–
1006	BHTSR	Ig245	695.51	Igneous	Trachyte	–

Table 28: cont.

Pre -	Name	ID	Wt.(g)	Rock Type	*Rock Classification*	Formation
1106	BHUS14a	LS246	763.46	Igneous	Trachyte	–
1106	BHUS14a	Ig247	711.83	Igneous	Trachy Andesite	–
1106	BHUS14a	Ig248	720.12	Igneous	Trachy Rhyolite	–
1106	BHUS14a	IgS249	696.31	Igneous	Phonolite	–
1106	BHUS14a	MIg250	661.98	Igneous	Trachyte	–
1106	BHUS14a	IF251	714.16	Igneous	Rhyolite	–
1106	BHCC	GrSc252	759.68	Metamorphic	Schist	–
1106	BHCC	MIg253	800.00	Metamorphic	Carboniferous Schist	–
1106	BHCC	Ig254	714.69	Igneous	Trachyte	–
1106	BHCC	Ig255	–	Igneous	Trachyte	–
1106	BHCC	IgS256	683.12	Igneous	Latite	–
1106	BHCC	IgS257	–	Igneous	Rhyolite	–
1106	BHBG	IgS258	643.67	Igneous	Rhyolite	–
1106	BHBG	IgS259	723.10	Igneous	Rhyolite	–
1106	BHBG	IgS260	678.05	Igneous	Rhyolite	–
1106	BHBG	IgS261	767.16	Sedimentary	Limestone	Pahasapa
1206	BHBR	SS262	724.43	Sedimentary	Sandstone	Minnelusa
1206	BHBR	SS263	586.32	Sedimentary	Sandstone	Minnelusa
1206	BHBR	SS264	783.84	Sedimentary	Calcareous Sandstone	Minnelusa
1206	BHBR	SS265	666.16	Sedimentary	Sandstone	Minnelusa
1206	BHBR	SS266	749.69	Sedimentary	Sandstone	Minnelusa
1206	BHBR	Ig267	734.26	Igneous	Latite	–
1206	BHBR	IgS268	789.41	Sedimentary	Limestone	Minnekahta
1206	BHGR	Ig269	719.66	Igneous	Latitic Andesite	–
1206	BHGR	Ig270	700.13	Igneous	Latitic Andesite	–
1206	BHGR	Ig271	716.69	Igneous	Latitic Andesite	–
1206	BHGR	Ig272	705.82	Igneous	Latitic Andesite	–
1206	BHGR	Ig273	–	Igneous	Trachyte	–
1206	BHGR	Ig274	729.99	Igneous	Latitic Andesite	–
1206	BHGR	Ig275	687.71	Igneous	Latitic Andesite	–
1206	BHGR	Ig276	797.22	Sedimentary	Calcareous Tuffaceous Quartz Sandstone	Brule
1206	BHER	Ig277	741.27	Igneous	Latitic Andesite	–
1206	BHER	IgLS278	755.00	Sedimentary	Siltstone/Limestone	Pahasapa
1206	BHGR	Ig279	830.46	Igneous	Rhyolite	–
1206	BHGR	MIg280	851.18	Metamorphic	Metabasalt	–

Table 28: cont.

Pre -	Name	ID	Wt.(g)	Rock Type	*Rock Classification*	Formation
1206	BHGR	Ig281	892.06	Metamorphic	Greenstone w/ Calcite Vein	–
1206	BHGR	MGn2Sc282	736.46	Metamorphic	Schist	–
1206	BHGR	MSc283	851.38	Metamorphic	Phyllitic Schist	–
1206	BHGR	MGn284	868.12	Metamorphic	Greenstone	–
1206	BHGR	MGn285	802.63	Metamorphic	Schist	–
1206	BHER	M286	908.28	Metamorphic	Greenstone	–
1206	BHGR	M287	826.68	Metamorphic	Schist	–
1206	BHNM	MIg288	794.10	Metamorphic	Metagraywacke	–
1206	BHCLP	IgS289	690.85	Igneous	Rhyolite	–
1206	BHCLP	Ig290	705.86	Igneous	Rhyolite	–

Table 29: Homestake Gold Mine RS-230 GRS Survey Results - Sample identification, Latitude (N) and Longitude (W), Elevation (Elev.), Th:U ratio, U, Th, K content, calculated heat production (A) and anitneturino luminosity ($\mathcal{E}_v$)

ID	(N)	(W)	Elev. (ft)	Th:U	U (ppm)	Th (ppm)	K (pct)	A (μWm^{-3})	$\mathcal{E}_v$ ($mg^{-1}s^{-1}$)
HS001	44.35383225	-103.75090	3526	3.12	3.4	10.6	1.5	2.09	4.64E+02
HS002	44.35394202	-103.75104	3526	5.82	2.8	16.3	2.4	2.49	5.37E+02
HS003	44.35398320	-103.75105	3526	3.70	5.6	20.7	5.2	4.03	8.91E+02
HS004	44.35403808	-103.75111	3526	3.79	4.3	16.3	2.3	2.94	6.45E+02
HS005	44.35416159	-103.75123	3526	3.45	5.8	20.0	4.3	3.93	8.70E+02
HS006	44.35418905	-103.75128	3526	6.16	5.0	30.8	6.4	4.83	1.04E+03
HS007	44.35427138	-103.75136	3526	4.02	4.9	19.7	3.9	3.59	7.88E+02
HS008	44.35434002	-103.75146	3526	4.25	5.7	24.2	5.8	4.42	9.72E+02
HS009	44.35440863	-103.75153	3526	4.00	3.3	13.2	3.4	2.50	5.51E+02
HS010	44.35451842	-103.75163	3526	3.77	5.6	21.1	4.2	3.95	8.71E+02
HS011	44.35460076	-103.75172	3526	5.11	2.8	14.3	3.0	2.39	5.20E+02
HS012	44.35464196	-103.75184	3526	5.00	2.5	12.5	3.4	2.19	4.80E+02
HS013	44.35468318	-103.75199	3526	4.00	4.5	18.0	4.8	3.42	7.55E+02
HS014	44.35473809	-103.75209	3526	5.15	4.0	20.6	5.9	3.61	7.90E+02
HS015	44.35477928	-103.75222	3526	2.61	7.0	18.3	5.4	4.28	9.62E+02
HS016	44.35483420	-103.75232	3526	5.23	4.8	25.1	5.5	4.19	9.11E+02
HS017	44.35495779	-103.75266	3526	4.08	5.1	20.8	4.5	3.81	8.37E+02
HS018	44.35508137	-103.75297	3526	3.85	5.4	20.8	4.9	3.94	8.70E+02
HS019	44.35517750	-103.75322	3526	3.81	5.4	20.6	4.4	3.87	8.53E+02
HS020	44.35527362	-103.75346	3526	5.14	4.4	22.6	4.6	3.75	8.17E+02
HS021	44.35538344	-103.75371	3526	3.75	5.3	19.9	3.8	3.71	8.18E+02
HS022	44.35545212	-103.75390	3526	4.60	6.0	27.6	3.9	4.58	9.97E+02
HS023	44.35552078	-103.75409	3526	4.33	6.0	26.0	5.7	4.65	1.02E+03
HS024	44.35552082	-103.75421	3526	1.01	14.0	14.2	13.3	6.97	1.63E+03

Table 29: cont.

ID	(N)	(W)	Elev. (ft)	Th:U	U (ppm)	Th (ppm)	K (pct)	A (μWm^{-3})	ε_v ($mg^{-1}s^{-1}$)
HS025	44.35552087	-103.75436	3526	1.54	10.8	16.6	11.2	5.95	1.37E+03
HS026	44.35552096	-103.75459	3526	4.89	4.7	23.0	4.6	3.88	8.46E+02
HS027	44.35552105	-103.75482	3526	4.77	5.2	24.8	5.8	4.32	9.44E+02
HS028	44.35542509	-103.75501	3526	4.22	3.2	13.5	2.6	2.40	5.26E+02
HS029	44.35535654	-103.75515	3526	3.17	4.6	14.6	4.1	3.09	6.88E+02
HS030	44.35527430	-103.75530	3526	2.80	5.6	15.7	3.3	3.40	7.59E+02
HS031	44.35520575	-103.75543	3526	4.25	6.7	28.5	5.3	5.03	1.10E+03
HS032	44.35513721	-103.75557	3526	3.62	6.1	22.1	3.3	4.09	8.99E+02
HS033	44.35505496	-103.75572	3526	1.35	9.2	12.4	2.8	4.16	9.58E+02
HS034	44.35498643	-103.75587	3526	1.59	12.2	19.4	10.2	6.50	1.49E+03
HS035	44.35489048	-103.75605	3526	3.16	7.4	23.4	4.6	4.74	1.05E+03
HS036	44.35478081	-103.75626	3526	2.65	10.0	26.5	6.4	5.99	1.34E+03
HS037	44.35471227	-103.75640	3526	4.51	5.9	26.6	5.9	4.69	1.03E+03
HS038	44.35461630	-103.75658	3526	2.12	5.8	12.3	3.8	3.23	7.32E+02
HS039	44.35452037	-103.75677	3526	4.17	12.4	51.7	6.0	8.79	1.92E+03
HS040	44.35442440	-103.75696	3526	3.05	8.2	25.0	4.1	5.06	1.12E+03
HS040a	44.35435586	-103.75710	3526	6.62	2.1	13.9	1.3	1.95	4.16E+02
HS041	44.35423248	-103.75733	3526	4.20	1.5	6.3	1.7	1.18	2.59E+02
HS042	44.35416393	-103.75746	3526	3.17	2.3	7.3	1.0	1.43	3.16E+02
HS043	44.35416396	-103.75750	3526	2.79	2.9	8.1	3.1	1.91	4.30E+02
HS044	44.35410912	-103.75758	3526	2.60	4.3	11.2	2.0	2.48	5.54E+02
HS045	44.35405428	-103.75769	3526	2.44	3.4	8.3	1.2	1.87	4.19E+02
HS046	44.35399945	-103.75779	3526	2.10	7.1	14.9	2.4	3.69	8.33E+02
HS047	44.35395832	-103.75786	3526	1.72	3.6	6.2	1.6	1.80	4.11E+02

Table 29: cont.

ID	(N)	(W)	Elev. (ft)	Th:U	U (ppm)	Th (ppm)	K (pct)	A (μWm^{-3})	$\mathcal{E}_v$ ($mg^{-1}s^{-1}$)
HS048	44.35394464	-103.75794	3526	1.94	6.5	12.6	2.8	3.36	7.62E+02
HS049	44.35388979	-103.75803	3526	3.26	11.2	36.5	3.4	6.86	1.51E+03
HS050	44.35382121	-103.75807	3526	2.98	4.1	12.2	3.4	2.66	5.94E+02
HS051	44.35172233	-103.75784	3526	2.47	4.3	10.6	2.0	2.43	5.45E+02
HS052	44.35158515	-103.75784	3526	2.60	4.7	12.2	3.3	2.83	6.35E+02
HS052a	44.35122847	-103.75781	3526	2.51	4.5	11.3	3.5	2.72	6.11E+02
HS053	44.35092668	-103.75779	3526	1.05	7.9	8.3	2.6	3.40	7.90E+02
HS054	44.35062487	-103.75777	3526	1.32	6.2	8.2	2.6	2.87	6.63E+02
HS055	44.35039166	-103.75775	3526	2.12	8.9	18.9	5.4	4.91	1.11E+03
HS056	44.35019962	-103.75773	3526	1.43	10.7	15.3	6.4	5.27	1.21E+03
HS057	44.34987039	-103.75771	3526	1.52	11.6	17.6	3.5	5.41	1.24E+03
HS058	–	–	3526	1.14	13.3	15.2	6.3	6.05	1.40E+03
HS058a	44.35379107	-103.75088	1127	0.92	1.2	1.1	1.1	0.58	1.37E+02
HS059	44.35353041	-103.75083	1127	1.19	1.6	1.9	0.7	0.73	1.68E+02
HS060	44.35325607	-103.75081	1127	0.50	2.2	1.1	0.5	0.82	1.94E+02
HS061	44.35298171	-103.75081	1127	1.50	1.4	2.1	1.0	0.72	1.65E+02
HS062	44.35270735	-103.75083	1127	1.56	1.8	2.8	0.7	0.86	1.98E+02
HS063	44.35241927	-103.75083	1127	1.23	8.4	10.3	3.0	3.77	8.71E+02
HS063a	–	–	1127	–	–	–	–	–	–
HS064	44.35213121	-103.75083	1127	1.92	6.2	11.9	3.3	3.26	7.42E+02
HS065	44.35184314	-103.75085	1127	1.08	15.7	17.0	8.9	7.22	1.68E+03
HS066	44.35169227	-103.75085	1127	1.39	6.6	9.2	3.7	3.20	7.38E+02
HS067	44.35155509	-103.75085	1127	1.02	8.5	8.7	3.3	3.70	8.60E+02
HS068	44.35128073	-103.75086	1127	1.48	6.6	9.8	3.0	3.17	7.29E+02

Table 29: cont.

ID	(N)	(W)	Elev. (ft)	Th:U	U (ppm)	Th (ppm)	K (pct)	A (μWm^{-3})	ε_v ($mg^{-1}s^{-1}$)
HS069	44.35100637	-103.75086	1127	0.81	10.2	8.3	2.8	4.13	9.66E+02
HS070	44.35097893	-103.75086	1127	1.05	8.7	9.1	2.4	3.69	8.57E+02
HS071	44.35071829	-103.75086	1127	1.11	8.0	8.9	3.8	3.62	8.40E+02
HS072	44.35044396	-103.75088	1127	0.91	9.0	8.2	4.1	3.90	9.11E+02
HS073	44.35016960	-103.75088	1127	1.06	8.6	9.1	3.6	3.79	8.82E+02
HS074	44.34989525	-103.75089	1127	1.33	7.0	9.3	3.0	3.26	7.51E+02
HS075	44.34962090	-103.75090	1127	2.05	6.4	13.1	3.3	3.42	7.76E+02
HS076	44.34942885	-103.75090	1127	1.23	9.0	11.1	3.7	4.10	9.47E+02
HS077	44.34914080	-103.75091	1127	1.10	4.8	5.3	2.1	2.15	4.98E+02
HS078	44.34885271	-103.75092	1127	1.35	5.2	7.0	1.9	2.39	5.50E+02
HS079	44.34857835	-103.75092	1127	0.93	11.1	10.3	3.6	4.66	1.09E+03
HS080	44.34829029	-103.75094	1127	1.68	4.0	6.7	2.2	2.03	4.65E+02
HS081	44.34800222	-103.75094	1127	1.93	4.1	7.9	2.2	2.16	4.91E+02
HS082	44.34772788	-103.75095	1127	1.00	8.6	8.6	3.1	3.70	8.61E+02
HS083	44.34745352	-103.75096	1127	0.72	9.6	6.9	2.4	3.78	8.88E+02
HS084	44.34717917	-103.75096	1127	0.90	9.3	8.4	3.2	3.90	9.12E+02
HS085a	44.34690483	-103.75097	1127	0.85	9.8	8.3	2.8	4.00	9.37E+02
HS085b	44.34663048	-103.75098	1127	0.46	21.7	9.9	3.2	7.82	1.86E+03
HS086	44.34635612	-103.75098	1127	3.17	6.9	21.9	4.4	4.44	9.85E+02
HS087	44.34610919	-103.75098	1127	0.83	8.8	7.3	2.5	3.58	8.38E+02
HS088	44.34591715	-103.75099	1127	1.00	8.1	8.1	3.2	3.51	8.18E+02
HS089	44.34537214	-103.76132	382	2.03	3.1	6.3	1.4	1.63	3.70E+02
HS090	44.34507043	-103.76153	382	0.94	17.1	16.1	5.1	7.15	1.67E+03
HS091	44.34486470	-103.76167	382	2.84	3.7	10.5	1.7	2.20	4.90E+02

Table 29: cont.

ID	(N)	(W)	Elev. (ft)	Th:U	U (ppm)	Th (ppm)	K (pct)	A (μWm^{-3})	ε_v ($mg^{-1}s^{-1}$)
HS092	44.34472757	-103.76176	382	2.47	7.4	18.3	4.7	4.32	9.72E+02
HS093	44.34461784	-103.76184	382	3.79	5.8	22.0	5.4	4.22	9.33E+02
HS094	44.34450811	-103.76192	382	2.69	7.8	21.0	5.8	4.79	1.08E+03
HS095	44.34437096	-103.76199	382	3.41	6.4	21.8	5.3	4.38	9.71E+02
HS096	44.34432984	-103.76202	382	4.05	6.0	24.3	5.6	4.50	9.90E+02
HS097a	44.34365780	-103.76249	382	2.33	2.4	5.6	1.3	1.35	3.04E+02
HS097	44.34832072	-103.75903	382	1.45	9.3	13.5	3.9	4.41	1.01E+03
HS098	44.34825124	-103.75641	382	1.67	4.9	8.2	3.3	2.56	5.85E+02
HS099	44.34816802	-103.75394	382	1.36	6.7	9.1	2.3	3.07	7.06E+02
HS100	44.34816769	-103.75306	382	1.43	12.7	18.1	6.8	6.16	1.42E+03
HS101	44.34817039	-103.75299	382	1.31	10.1	13.2	5.3	4.79	1.11E+03
HS102	44.34816764	-103.75295	382	1.17	16.0	18.7	8.6	7.42	1.72E+03
HS103	44.34817036	-103.75291	382	1.26	13.5	17.0	6.7	6.30	1.46E+03
HS104	44.34816761	-103.75287	382	1.42	11.0	15.6	7.2	5.48	1.26E+03
HS104a	44.34817582	-103.75285	382	1.41	5.6	7.9	2.1	2.61	6.00E+02
HS105	44.34818131	-103.75282	382	1.14	13.5	15.4	6.4	6.13	1.42E+03
HS106	44.34819501	-103.75280	382	1.48	10.4	15.4	6.0	5.14	1.18E+03
HS107	44.34821015	-103.75660	382	1.80	3.0	5.4	4.3	1.85	4.26E+02
HS108	44.34824986	-103.75272	382	1.31	3.9	5.1	2.4	1.89	4.37E+02
HS109	44.34829100	-103.75266	382	1.40	7.2	10.1	3.1	3.39	7.81E+02
HS110	44.34809892	-103.75262	382	1.42	3.1	4.4	2.2	1.56	3.61E+02
HS111	44.34590347	-103.75106	1127	0.96	11.3	10.9	4.6	4.88	1.14E+03
HS112	44.34597212	-103.75121	1127	1.12	12.6	14.1	9.4	6.09	1.42E+03
HS113	44.34599958	-103.75129	1127	1.18	13.9	16.4	11.5	6.92	1.61E+03

Table 29: cont.

ID	(N)	(W)	Elev. (ft)	Th:U	U (ppm)	Th (ppm)	K (pct)	A (μWm^{-3})	ε_v ($mg^{-1}s^{-1}$)
HS114	44.34602702	-103.75132	1127	1.13	14.7	16.6	11.1	7.13	1.66E+03
HS115	44.34604075	-103.75136	1127	1.35	13.2	17.8	8.3	6.46	1.49E+03
HS116	44.34609568	-103.75148	1127	0.73	8.9	6.5	2.9	3.59	8.43E+02
HS117	44.34610942	-103.75154	1127	1.17	13.9	16.2	7.1	6.40	1.48E+03
HS118	44.34615061	-103.75163	1127	0.81	10.6	8.6	3.6	4.36	1.02E+03
HS119	44.34620552	-103.75175	1127	0.72	13.3	9.6	3.7	5.28	1.24E+03
HS120	44.34623298	-103.75180	1127	1.20	10.0	12.0	4.0	4.51	1.04E+03
HS121	44.34560165	-103.75100	1127	1.11	8.7	9.7	4.9	4.02	9.35E+02
HS122	44.34819677	-103.75760	1127	1.58	4.5	7.1	2.0	2.19	5.03E+02
HS123	44.35273392	-103.75096	4861	3.06	5.1	15.6	4.6	3.38	7.55E+02
HS124	44.35395087	-103.75121	5121	2.04	5.3	10.8	4.9	3.08	7.00E+02
HS125	44.35413393	-103.75138	5121	2.19	4.8	10.5	4.4	2.84	6.45E+02
HS126	44.35500090	-103.74998	5142	3.36	3.3	11.1	4.3	2.42	5.41E+02
HS127	44.35538394	-103.74918	4913	2.68	6.5	17.4	5.4	4.05	9.10E+02
HS128	44.35541791	-103.74884	4914	3.93	4.3	16.9	6.2	3.43	7.60E+02
HS129	44.35550086	-103.74838	4921	2.40	13.9	33.4	5.9	7.71	1.73E+03
HS130	44.35560095	-103.74708	4914	0.52	12.4	6.5	0.5	4.39	1.04E+03
HS131	44.35566790	-103.74689	4929	3.50	6.2	21.7	6.5	4.44	9.87E+02
HS132	44.35576789	-103.74666	4916	2.83	6.9	19.5	8.2	4.67	1.05E+03
HS133	44.35491794	-103.74904	5142	0.41	7.1	2.9	0.6	2.48	5.89E+02
HS134	44.35501785	-103.74899	4911	0.29	10.9	3.2	0.3	3.63	8.68E+02
HS135	44.35306787	-103.75361	5124	2.63	6.4	16.8	4.2	3.84	8.60E+02
HS136	44.35250090	-103.75479	5324	3.29	4.9	16.1	3.2	3.21	7.11E+02

Note: Latitude and Longitude are set to DDD.DDDDD° (Decimal Degree) Format

Table 30: Homestake Gold Mine RS-230 GRS Survey: Sample Identification (ID), Rock type, Rock Classification and Formation

ID	Rock Type	*Rock Classification*	Formation
HS001	Metamorphic	Amphibolite	Yates
HS002	Metamorphic	Amphibolite	Yates
HS003	Metamorphic	Amphibolite	Yates
HS004	Metamorphic	Amphibolite	Yates
HS005	Metamorphic	Amphibolite	Yates
HS006	Metamorphic	Amphibolite	Yates
HS007	Metamorphic	Amphibolite	Yates
HS008	Metamorphic	Amphibolite	Yates
HS009	Metamorphic	Phyllite	Yates
HS010	Metamorphic	Amphibolite	Yates
HS011	Metamorphic	Amphibolite	Northwestern
HS012	Metamorphic	Phyllite	Yates
HS013	Metamorphic	Amphibolite	Northwestern
HS014	Metamorphic	Amphibolite	Yates
HS015	Metamorphic	Phyllite	Northwestern
HS016	Metamorphic	Amphibolite	Yates
HS017	Metamorphic	Amphibolite	Ellison
HS018	Metamorphic	Amphibolite	Ellison
HS019	Metamorphic	Amphibolite	Ellison
HS020	Metamorphic	Amphibolite	Ellison
HS021	Metamorphic	Amphibolite	Northwestern
HS022	Metamorphic	Amphibolite	Ellison
HS023	Metamorphic	Amphibolite	Ellison
HS024	Igneous	Rhyolite	–
HS025	Igneous	Rhyolite	–
HS026	Metamorphic	Amphibolite	Ellison
HS027	Metamorphic	Phyllite	Ellison
HS028	Metamorphic	Phyllite	Poorman
HS029	Metamorphic	Phyllite	Poorman
HS030	Metamorphic	Phyllite	Poorman
HS031	Metamorphic	Phyllite	Poorman
HS032	Metamorphic	Pyrrhotitic Phyllite	Poorman
HS033	Metamorphic	Pyrrhotitic Phyllite	Poorman
HS034	Igneous	Rhyolite	–
HS035	Metamorphic	Schist	Poorman
HS036	Metamorphic	Phyllite	Poorman(Dschmidt)
HS037	Metamorphic	Phyllite	Poorman(Dschmidt)

Table 30: cont.

ID	Rock Type	*Rock Classification*	Formation
HS038	Metamorphic	Schist	Ellison
HS039	Metamorphic	Pyrotitic Phyllite	Ellison
HS040	Metamorphic	Pyrotitic Phyllite	Ellison
HS040a	Metamorphic	Granulite Schist	Homestake
HS041	Metamorphic	Granulite Schist	Homestake
HS042	Metamorphic	Granulite Schist	Homestake
HS043	Metamorphic	Phyllite	Poorman
HS044	Metamorphic	Phyllite	Ellison
HS045	Metamorphic	Phyllite	Ellison
HS046	Metamorphic	Quartzite rich Phyllite	Ellison
HS047	Metamorphic	Quartzite rich Schist	Ellison
HS048	Metamorphic	Phyllite	Ellison (Ross)
HS049	Metamorphic	Phyllite	Ellison (Ross)
HS050	Metamorphic	Phyllite	Ellison (Ross)
HS051	Metamorphic	Phyllite	Ellison
HS052	Metamorphic	Phyllite	Ellison
HS052a	Metamorphic	Phyllite	Ellison
HS053	Metamorphic	Schist	Ellison
HS054	Metamorphic	Schist	Ellison
HS055	Metamorphic	Phyllite	Ellison
HS056	Igneous	Rhyolite	–
HS057	Igneous	Rhyolite	–
HS058	Metamorphic	Phyllite	Poorman
HS058a	Metamorphic	Phyllite	Yates
HS059	Metamorphic	Phyllite	Yates
HS060	Metamorphic	Phyllite	Yates
HS061	Metamorphic	Phyllite	Yates
HS062	Metamorphic	Phyllite	Yates
HS063	Metamorphic	Phyllite	Poorman
HS063a	Metamorphic	Phyllite	Poorman
HS064	Metamorphic	Phyllite	Poorman
HS065	Igneous	Rhyolite	–
HS066	Metamorphic	Phyllite	Poorman
HS067	Metamorphic	Phyllite	Poorman
HS068	Metamorphic	Phyllite	Poorman
HS069	Metamorphic	Phyllite	Homestake
HS070	Metamorphic	Phyllite	Poorman

Table 30: cont.

ID	Rock Type	*Rock Classification*	Formation
HS071	Metamorphic	Phyllite	Poorman
HS072	Metamorphic	Phyllite	Poorman
HS073	Metamorphic	Phyllite	Poorman
HS074	Metamorphic	Phyllite	Poorman
HS075	Metamorphic	Phyllite	Poorman
HS076	Metamorphic	Phyllite	Poorman
HS077	Metamorphic	Phyllite	Poorman
HS078	Metamorphic	Phyllite	Poorman
HS079	Metamorphic	Phyllite	Poorman
HS080	Metamorphic	Schist	Homestake
HS081	Metamorphic	Phyllite	Poorman
HS082	Metamorphic	Schist	Homestake
HS083	Metamorphic	Phyllite	Poorman
HS084	Metamorphic	Phyllite	Poorman
HS085a	Metamorphic	Phyllite	Poorman
HS085b	Metamorphic	Phyllite	Poorman
HS086	Metamorphic	Phyllite	Poorman
HS087	Metamorphic	Phyllite	Poorman
HS088	Metamorphic	Phyllite	Poorman
HS089	Metamorphic	Schist	Homestake
HS090	Metamorphic	Phyllite	Poorman
HS091	Metamorphic	Phyllite	Ellison
HS092	Metamorphic	Phyllite	Ellison
HS093	Metamorphic	Phyllite	Ellison
HS094	Metamorphic	Phyllite	Ellison
HS095	Metamorphic	Phyllite	Ellison
HS096	Metamorphic	Phyllite	Ellison
HS097a	Metamorphic	Schist	Homestake
HS097	Metamorphic	Phyllite	Homestake
HS098	Metamorphic	Schist	Homestake
HS099	Igneous	Rhyolite	–
HS100	Igneous	Rhyolite	–
HS101	Igneous	Rhyolite	–
HS102	Igneous	Rhyolite	–
HS103	Igneous	Rhyolite	–
HS104	Igneous	Rhyolite	–

Table 30: cont.

ID	Rock Type	*Rock Classification*	Formation
HS105	Igneous	Rhyolite	–
HS106	Igneous	Rhyolite	–
HS107	Metamorphic	Phyllite	Yates
HS108	Metamorphic	Phyllite	Yates
HS109	Metamorphic	Phyllite	Yates
HS110	Metamorphic	Phyllite	Yates
HS111	Metamorphic	Mica Schist	Poorman
HS112	Igneous	Rhyolite	–
HS113	Igneous	Rhyolite	–
HS114	Igneous	Rhyolite	–
HS115	Igneous	Rhyolite	–
HS116	Metamorphic	Schist	Homestake
HS117	Igneous	Rhyolite	–
HS118	Metamorphic	Phyllite	Poorman
HS119	Metamorphic	Schist	Homestake
HS120	Metamorphic	Schist	Homestake
HS121	Igneous	Rhyolite	–
HS122	Metamorphic	Phyllite	Homestake
HS123	Metamorphic	Amphibolite	Northwestern
HS124	Metamorphic	Phyllite	Northwestern
HS125	Metamorphic	Phyllite	Northwestern
HS126	Metamorphic	Phyllite	Flagrock
HS127	Igneous	Rhyolite	–
HS128	Metamorphic	Phyllite	Flagrock
HS129	Igneous	Rhyolite	–
HS130	Metamorphic	Phyllite	Flagrock
HS131	Igneous	Rhyolite	–
HS132	Igneous	Rhyolite	–
HS133	Metamorphic	Phyllite	Flagrock
HS134	Metamorphic	Phyllite	Flagrock
HS135	Metamorphic	Phyllite	Northwestern
HS136	Metamorphic	Phyllite	Northwestern

Appendix B

Northern Black Hills and Homestake Gold Mine

Igneous, Metamorphic, and Sedimentary Sample Data Comparison

Table 31A: RS-230 GRS Survey Igneous Comparison – Rhyolite ID, Radioelement Content, Th:U Ratio, Heat Production (A) and Antineutrino Luminosity ($\varepsilon_{v)}$

Name	ID #	U (ppm)	Th (ppm)	K (pct)	Th/U	A (μWm^{-3})	ε_v ($mg^{-1}s^{-1}$)
BHUR	MIg227	28.9	93.6	8.9	3.24	17.66	3.90E+03
BHUR	MIg227a	28.9	93.6	8.9	3.24	17.66	3.90E+03
BHUR	MIg230	21.4	74.8	8.8	3.50	13.79	3.04E+03
BHTSR	Ig242	8.5	52.8	3.8	6.21	7.44	1.59E+03
BHH85	Ig010	11.9	22.0	8.6	1.85	6.45	1.47E+03
BHUS14a	Ig248	9.6	32.9	4.5	3.43	6.19	1.37E+03
BHH385	Ig004	10.2	27.1	3.5	2.66	5.78	1.29E+03
BHYCR	IgS218	10.6	22.5	7.0	2.12	5.91	1.34E+03
BHTSR	Ig240	9.0	26.9	4.9	2.99	5.55	1.24E+03
BHBG	IgS259	7.4	24.8	3.8	3.35	4.76	1.05E+03
BHCC	IgS257	6.4	15.3	6.3	2.39	3.95	8.93E+02
BHUS14a	MLSS064	7.2	11.5	3.8	1.60	3.59	8.23E+02
BHYCR	IgS222	6.0	15.7	4.8	2.62	3.69	8.29E+02
BHYCR	MGn205	6.8	11.6	2.9	1.71	3.38	7.70E+02
BHBG	IgS258	5.5	14.9	4.5	2.71	3.44	7.71E+02
BHYCR	Ig223	5.6	12.9	5.0	2.30	3.35	7.59E+02
BHBVR	IgG197	5.2	14.1	3.5	2.71	3.16	7.09E+02
BHBG	IgS260	5.2	10.5	5.2	2.02	3.05	6.96E+02
BHYCR	Ig224	5.4	9.7	2.3	1.80	2.72	6.20E+02
BHBVR	Ig199	5.0	10.4	3.4	2.08	2.78	6.31E+02
BHBVR	IgS198	4.9	10.8	3.3	2.20	2.77	6.27E+02
BHUS14a	IF251	4.6	7.9	4.7	1.72	2.60	5.96E+02
BHCLP	IgS289	3.6	11.4	3.8	3.17	2.48	5.54E+02
BHUS85	SS047	6.4	1.6	0.3	0.25	2.12	5.08E+02
BHBVR	Ig200	3.9	8.6	3.8	2.21	2.34	5.31E+02
BHCLP	Ig290	3.5	10.0	3.3	2.86	2.28	5.11E+02
BHUS85	Ig160	3.2	7.5	1.1	2.34	1.73	3.88E+02
BHTGR	Ig233	3.1	6.8	1.0	2.19	1.63	3.67E+02
BHGR	Ig279	2.9	4.5	1.5	1.55	1.43	3.28E+02
BHHR	IgSS180	2.3	5.0	0.9	2.17	1.22	2.76E+02
BHSRCR	Ig155	1.9	2.1	0.3	1.11	0.79	1.83E+02
BHMLR	I099	1.3	4.2	0.5	3.23	0.81	1.78E+02
BHUS85	Ig164	1.8	2.1	0.4	1.17	0.77	1.78E+02
BHVCR	I082	1.7	2.4	0.4	1.41	0.77	1.76E+02

Table 31B: RS-230 GRS Survey Igneous Comparison – Phonolite ID, Radioelement Content, Th:U Ratio, Heat Production (A) and Antineutrino Luminosity (ε_v)

Name	ID #	U (ppm)	Th (ppm)	K (pct)	Th/U	A (μWm^{-3})	ε_v ($mg^{-1}s^{-1}$)
BHUS85	Ig165	18.8	75.3	5.4	4.01	12.65	2.76E+03
BHUS85	Ig166	21.1	56.7	4.4	2.69	11.69	2.60E+03
BHDM	GrSc236	17.9	47.6	5.8	2.66	10.11	2.25E+03
BHDM	Ig235	11.3	49.5	5.7	4.38	8.24	1.79E+03
BHBVR	GSc194	11.5	35.8	5.1	3.11	7.08	1.57E+03
BHBFR	GSc191	9.7	31.1	3.4	3.21	5.95	1.31E+03
BHDM	GrSc237	8.4	32.9	4.6	3.92	5.84	1.28E+03
BHUS85	MIg167	10.5	23.1	5.5	2.20	5.76	1.30E+03
BHBFR	GSc192	7.1	36.9	3.9	5.20	5.70	1.23E+03
BHBFR	GSc193	7.0	18.8	3.3	2.69	4.08	9.13E+02
BHUS14a	IgS249	4.5	9.1	3.3	2.02	2.51	5.70E+02

Table 31C: RS-230 GRS Survey Igneous Comparison – Trachyte ID, Radioelement Content, Th:U Ratio, Heat Production (A) and Antineutrino Luminosity (ε_v)

Name	ID #	U (ppm)	Th (ppm)	K (pct)	Th/U	A (μWm^{-3})	ε_v ($mg^{-1}s^{-1}$)
BHUS14a	MIg250	13.4	45.0	10.7	3.36	9.07	2.01E+03
BHUR	Ig226	18.3	23.7	11.0	1.30	8.82	2.04E+03
BHTSR	Ig244	10.1	53.4	4.5	5.29	8.06	1.74E+03
BHTSR	Ig245	9.9	48.9	3.5	4.94	7.51	1.62E+03
BHUR	MIg228	12.3	28.6	6.5	2.33	6.88	1.55E+03
BHTSR	Ig241	7.6	32.3	5.8	4.25	5.68	1.24E+03
BHCC	Ig254	9.3	26.0	4.6	2.80	5.54	1.23E+03
BHMLR	I101	8.0	26.6	4.6	3.33	5.19	1.15E+03
BHUS85	Ig170	7.3	22.2	4.0	3.04	4.54	1.01E+03
BHMLR	I102	7.1	20.4	5.0	2.87	4.44	9.92E+02
BHCC	Ig255	5.4	20.3	13.8	3.76	4.91	1.10E+03
BHTGR	Ig232	8.2	14.9	3.9	1.82	4.19	9.55E+02
BHUR	MIg231	4.7	19.8	2.9	4.21	3.42	7.48E+02
BHUR	MIg229	5.9	12.3	4.0	2.08	3.28	7.45E+02
BHMLR	ISS100	5.8	9.5	1.0	1.64	2.68	6.11E+02
BHGR	Ig273	3.7	12.9	2.9	3.49	2.54	5.62E+02

Table 31C: Cont.

Name	ID #	U (ppm)	Th (ppm)	K (pct)	Th/U	A (μWm^{-3})	ε_v ($mg^{-1}s^{-1}$)
BHTSR	Ig239	3.3	9.5	2.9	2.88	2.13	4.77E+02
BHVCR	I080	2.0	2.6	0.3	1.30	0.86	1.98E+02
BHUS14a	LS246	1.6	1.9	0.4	1.19	0.69	1.60E+02

Table 31D: RS-230 GRS Survey Igneous Comparison – Basalt ID, Radioelement Content, Th:U Ratio, Heat Production (A) and Antineutrino Luminosity (ε_v)

Name	ID #	U (ppm)	Th (ppm)	K (pct)	Th/U	A (μWm^{-3})	ε_v ($mg^{-1}s^{-1}$)
BHH14	B040	21.9	23.9	1.5	1.09	8.86	2.05E+03
BHH14	B039	15.8	10.7	1.2	0.68	5.86	1.38E+03

Table 31E: RS-230 GRS Survey Igneous Comparison – Latite ID, Radioelement Content, Th:U Ratio, Heat Production (A) and Antineutrino Luminosity (ε_v)

Name	ID #	U (ppm)	Th (ppm)	K (pct)	Th/U	A (μWm^{-3})	ε_v ($mg^{-1}s^{-1}$)
BHH385	M008	20.1	15.1	5.3	0.75	8.00	1.88E+03
BHH385	M008a	20.1	15.1	5.3	0.75	8.00	1.88E+03
BHH385	Ig009	11.9	22.0	8.6	1.85	6.45	1.47E+03
BHH385	I003	7.9	18.3	3.3	2.32	4.32	9.71E+02
BHVCR	I074	4.7	20.2	3.0	4.30	3.46	7.57E+02
BHVCR	I079	4.7	16.9	3.1	3.60	3.20	7.06E+02
BHVCR	I072	4.3	16.7	3.1	3.88	3.06	6.73E+02
BHVCR	I077	3.7	18.9	2.9	5.11	3.04	6.59E+02
BHVCR	I078	4.5	13.9	2.9	3.09	2.87	6.37E+02
BHCC	IgS256	4.8	11.1	3.5	2.31	2.79	6.30E+02
BHBR	Ig267	3.6	12.5	2.4	3.47	2.42	5.34E+02

Table 31F: RS-230 GRS Survey Igneous Comparison – Latitic Andesite ID, Radioelement Content, Th:U Ratio, Heat Production (A) and Antineutrino Luminosity (ε_v)

Name	ID #	U (ppm)	Th (ppm)	K (pct)	Th/U	A (μWm^{-3})	ε_v ($mg^{-1}s^{-1}$)
BHTSR	Ig243	17.0	62.5	6.8	3.68	11.19	2.46E+03
BHUS14a	Ig247	9.0	32.3	3.8	3.59	5.88	1.29E+03
BHTSR	Ig238	7.0	34.2	4.7	4.89	5.53	1.20E+03
BHGR	Ig271	6.1	18.2	3.4	2.98	3.77	8.39E+02

Table 31F: Cont.

Name	ID #	U (ppm)	Th (ppm)	K (pct)	Th/U	A (μWm^{-3})	ε_v ($mg^{-1}s^{-1}$)
BHER	Ig277	6.1	17.8	3.7	2.92	3.77	8.41E+02
BHVCR	I076	6.1	17.0	3.4	2.79	3.67	8.20E+02
BHGR	Ig274	6.2	14.2	2.9	2.29	3.41	7.68E+02
BHGR	Ig270	5.5	15.7	3.4	2.85	3.38	7.54E+02
BHVCR	I075	4.0	20.1	2.8	5.03	3.22	6.98E+02
BHGR	Ig269	4.2	18.3	3.2	4.36	3.18	6.94E+02
BHVCR	I071	4.3	16.7	3.1	3.88	3.06	6.73E+02
BHGR	Ig275	4.6	14.1	3.8	3.07	3.01	6.72E+02
BHGR	Ig272	4.2	14.5	2.5	3.45	2.78	6.14E+02
BHTGR	Ig234	4.1	13.5	3.5	3.29	2.78	6.17E+02

Table 31G: RS-230 GRS Survey Igneous Comparison – Episodite ID, Radioelement Content, Th:U Ratio, Heat Production (A) and Antineutrino Luminosity (ε_v)

Name	ID #	U (ppm)	Th (ppm)	K (pct)	Th/U	A (μWm^{-3})	ε_v ($mg^{-1}s^{-1}$)
BHH385	S002	7.1	15.6	5.0	2.20	4.04	9.14E+02

Table 31H: RS-230 GRS Survey Igneous Comparison – Granodiorite ID, Radioelement Content, Th:U Ratio, Heat Production (A) and Antineutrino Luminosity (ε_v)

Name	ID #	U (ppm)	Th (ppm)	K (pct)	Th/U	A (μWm^{-3})	ε_v ($mg^{-1}s^{-1}$)
BHH14a	Ig128	17.6	49.3	4.9	2.80	10.05	2.24E+03
BHH14a	Ig129	16.6	50.4	5.1	3.04	9.86	2.18E+03
BHH14a	Ig127	15.3	41.2	5.0	2.69	8.69	1.94E+03
BHH14a	Ig127a	15.3	41.2	5.0	2.69	8.69	1.94E+03
BHDEAD	MG058	3.7	4.4	1.0	1.19	1.61	3.73E+02

Table 31I: RS-230 GRS Survey Igneous Comparison – Volcanic Alkalic ID, Radioelement Content, Th:U Ratio, Heat Production (A) and Antineutrino Luminosity (ε_v)

Name	ID #	U (ppm)	Th (ppm)	K (pct)	Th/U	A (μWm^{-3})	ε_v ($mg^{-1}s^{-1}$)
BHH14a	Ig146	42.8	120.0	7.1	2.80	23.92	5.31E+03
BHH14a	Ig147	36.2	130.7	6.4	3.61	22.72	4.97E+03
BHH14a	Ig137	24.4	75.5	5.3	3.09	14.37	3.17E+03
BHH14a	Ig138	24.4	71.4	5.0	2.93	13.99	3.10E+03
BHH14a	Ig135	17.0	44.8	6.8	2.64	9.71	2.17E+03

Table 31I: Cont.

Name	ID #	U (ppm)	Th (ppm)	K (pct)	Th/U	A (μWm^{-3})	ε_v ($mg^{-1}s^{-1}$)
BHYCR	MIF220	5.7	12.4	3.3	2.18	3.15	7.13E+02
BHYCR	MIg219	5.1	9.6	3.4	1.88	2.75	6.26E+02
BHHR	LSS183	2.0	4.1	0.6	2.05	1.02	2.31E+02

Table 32A: RS-230 GRS Survey Metamorphic Comparison – Schist ID, Radioelement Content, Th:U Ratio, Heat Production (A) and Antineutrino Luminosity (ε_v)

Name	ID #	U (ppm)	Th (ppm)	K (pct)	Th/U	A (μWm^{-3})	ε_v ($mg^{-1}s^{-1}$)
BHH385	Ig005	13.4	22.8	3.7	1.70	6.42	1.46E+03
BHRFR	IF149	10.8	27.7	5.1	2.56	6.19	1.39E+03
BHUS85	MIg168	10.8	27.2	3.2	2.52	5.94	1.33E+03
BHDEAD	Sc017	11.1	20.1	4.3	1.81	5.56	1.26E+03
BHDEAD	Sc018	11.1	20.1	4.3	1.81	5.56	1.26E+03
BHUS14a	MSc059	7.9	19.0	5.1	2.41	4.58	1.03E+03
BHDEAD	Gc022	6.0	26.0	5.8	4.33	4.66	1.02E+03
BHH385	M006	7.4	21.9	2.8	2.96	4.41	9.79E+02
BHH385	M007	7.4	21.9	2.8	2.96	4.41	9.79E+02
BHDEAD	Sc023	7.3	18.5	4.4	2.53	4.27	9.60E+02
BHGR	MGnSc282	6.6	20.0	5.2	3.03	4.28	9.54E+02
BHH85	Sc011	6.3	21.2	5.0	3.37	4.26	9.46E+02
BHH85	Sc012	6.3	21.2	5.0	3.37	4.26	9.46E+02
BHDEAD	Sc021	5.8	21.1	6.2	3.64	4.24	9.40E+02
BHGR	MGn285	6.0	20.4	5.2	3.40	4.13	9.16E+02
BHDEAD	MG057	5.8	18.7	4.5	3.22	3.84	8.55E+02
BHUS14a	MSc060	5.0	21.2	3.3	4.24	3.67	8.03E+02
BHCC	MIg253	6.7	15.0	2.0	2.24	3.53	7.94E+02
BHGR	M287	4.6	17.8	4.5	3.87	3.40	7.51E+02
BHGR	MSc283	4.2	19.6	3.8	4.67	3.35	7.32E+02
BHUS85	MSc173	4.2	18.9	3.1	4.50	3.21	7.01E+02
BHYCR	M211	4.7	16.0	1.9	3.40	2.99	6.59E+02
BHCC	GrSc252	5.0	8.1	2.0	1.62	2.43	5.56E+02
BHYCR	MSc213	4.1	11.8	1.1	2.88	2.36	5.25E+02
BHDEAD	S015	5.7	2.4	3.2	0.42	2.30	5.48E+02
BHMLR	MSc104	4.0	10.1	1.1	2.53	2.19	4.90E+02
BHYCR	MSc214	3.4	12.3	1.2	3.62	2.20	4.84E+02
BHRFR	IF151	3.5	8.8	2.7	2.51	2.11	4.75E+02

Table 32A: Cont.

Name	ID #	U (ppm)	Th (ppm)	K (pct)	Th/U	A (μWm^{-3})	ε_v ($mg^{-1}s^{-1}$)
BHDEAD	M056	4.0	3.2	0.7	0.80	1.57	3.67E+02
BHUS85	M174	1.9	10.7	2.1	5.63	1.71	3.71E+02
BHYCR	IF216	2.9	5.0	1.4	1.72	1.46	3.34E+02

Table 32B: RS-230 GRS Survey Metamorphic Comparison – Phyllite ID, Radioelement Content, Th:U Ratio, Heat Production (A) and Antineutrino Luminosity (ε_v)

Name	ID #	U (ppm)	Th (ppm)	K (pct)	Th/U	A (μWm^{-3})	ε_v ($mg^{-1}s^{-1}$)
BHRFR	IF148	8.0	23.9	3.7	2.99	4.86	1.08E+03
BHYCR	M209	5.6	22.0	5.1	3.93	4.13	9.10E+02
BHLead	M178	5.3	19.8	5.5	3.74	3.90	8.63E+02
BHUS14a	MSc065	5.0	20.1	3.5	4.02	3.60	7.91E+02
BHCC	MGn106	5.9	16.4	2.0	2.78	3.40	7.57E+02
BHRFR	IF152	5.2	15.9	4.8	3.06	3.46	7.73E+02
BHUS14a	MSc062	5.8	14.4	2.6	2.48	3.27	7.34E+02
BHYCR	M210	4.2	20.6	3.0	4.90	3.35	7.26E+02
BHLead	M177	4.1	17.9	4.1	4.37	3.21	7.05E+02
BHRFR	MGn153	5.7	11.2	3.7	1.96	3.10	7.04E+02
BHUS14a	M063	5.8	9.6	1.3	1.66	2.72	6.21E+02
BHUS85	Sh169	3.5	13.9	3.1	3.97	2.58	5.69E+02
BHLead	M176	3.9	12.7	2.4	3.26	2.53	5.60E+02
BHUS14a	MGn061	4.4	10.0	2.1	2.27	2.42	5.45E+02
BHYCR	MSc208	1.9	16.8	3.2	8.84	2.35	5.00E+02
BHMLR	MSc103	4.4	7.9	0.6	1.80	2.07	4.70E+02
BHH85	SS014	3.7	3.8	0.6	1.03	1.52	3.52E+02
BHCC	MGn107	2.7	7.3	1.2	2.70	1.57	3.51E+02

Table 32C: RS-230 GRS Survey Metamorphic Comparison – Metagraywacke ID, Radioelement Content, Th:U Ratio, Heat Production (A) and Luminosity (ε_v)

Name	ID #	U (ppm)	Th (ppm)	K (pct)	Th/U	A (μWm^{-3})	ε_v ($mg^{-1}s^{-1}$)
BHH385	I002	8.2	18.5	2.9	2.26	4.38	9.86E+02
BHNM	MIg288	3.9	14.6	3.4	3.74	2.80	6.18E+02

Table 32D: RS-230 GRS Survey Metamorphic Comparison – Metabasalt ID, Radioelement Content, Th:U Ratio, Heat Production (A) and Luminosity (ε_v)

Name	ID #	U (ppm)	Th (ppm)	K (pct)	Th/U	A (μWm^{-3})	ε_v ($mg^{-1}s^{-1}$)
BHH14a	IgS121	65.9	8.5	4.1	0.13	21.30	5.13E+03
BHCC	MSc105	4.7	12.8	2.4	2.72	2.78	6.21E+02
BHGR	MIg280	2.0	4.1	1.6	2.05	1.13	2.58E+02

Table 32E: RS-230 GRS Survey Metamorphic Comparison – Quartzite ID, Radioelement Content, Th:U Ratio, Heat Production (A) and Luminosity (ε_v)

Name	ID #	U (ppm)	Th (ppm)	K (pct)	Th/U	A (μWm^{-3})	ε_v ($mg^{-1}s^{-1}$)
BHLead	M175	4.1	11.8	3.2	2.88	2.60	5.82E+02
BHDEAD	S016	5.7	2.4	3.2	0.42	2.30	5.48E+02
BHEWR	IgS196	4.2	8.8	1.4	2.10	2.18	4.92E+02
BHCC	Qtz108	2.9	6.1	1.3	2.10	1.54	3.49E+02

Table 32F: RS-230 GRS Survey Metamorphic Comparison – Metasandstone ID, Radioelement Content, Th:U Ratio, Heat Production (A) and Luminosity (ε_v)

Name	ID #	U (ppm)	Th (ppm)	K (pct)	Th/U	A (μWm^{-3})	ε_v ($mg^{-1}s^{-1}$)
BHUS85	MIg171	1.7	2.8	1.5	1.65	0.92	2.12E+02

Table 32G: RS-230 GRS Survey Metamorphic Comparison – Greenstone ID, Radioelement Content, Th:U Ratio, Heat Production (A) and Luminosity (ε_v)

Name	ID #	U (ppm)	Th (ppm)	K (pct)	Th/U	A (μWm^{-3})	ε_v ($mg^{-1}s^{-1}$)
BHGR	Ig281	2.2	2.2	1.7	1.00	1.05	2.45E+02
BHGR	MGn284	1.5	4.1	1.5	2.73	0.97	2.18E+02
BHER	M286	1.3	2.9	0.9	2.23	0.74	1.68E+02

Table 33A: RS-230 GRS Survey Sedimentary Comparison – Sandstone ID, Radioelement Content, Th:U Ratio, Heat Production (A) and Luminosity (ε_v)

Name	ID #	U (ppm)	Th (ppm)	K (pct)	Th/U	A (μWm^{-3})	ε_v ($mg^{-1}s^{-1}$)
BHRR	RSS190	5.7	16.5	2.1	2.9	3.36	7.47E+02
BHGR	Ig276	9.3	2.4	0.6	0.3	3.11	7.44E+02

Table 33A: Cont.

Name	ID #	U (ppm)	Th (ppm)	K (pct)	Th/U	A (μWm^{-3})	ε_v ($mg^{-1}s^{-1}$)
BHBR	SS265	6.3	12.5	0.5	2.0	3.03	6.83E+02
BHBR	SS266	7.0	3.2	1.2	0.5	2.54	6.03E+02
BHHR	RSS186	5.1	9.8	2.2	1.9	2.63	5.96E+02
BHHR	RSS185	4.9	8.5	2.1	1.7	2.45	5.58E+02
BHBR	SS264	6.2	3.4	0.4	0.5	2.22	5.25E+02
BHBR	SS263	6.0	2.6	0.5	0.4	2.11	5.00E+02
BHBVR	SS202	5.7	3.0	0.8	0.5	2.08	4.93E+02
BHBR	SS262	5.7	1.9	0.7	0.3	1.98	4.72E+02
BHH14a	LS134	3.4	7.7	0.8	2.3	1.77	3.98E+02
BHHR	LSS184	4.9	1.5	0.6	0.3	1.69	4.04E+02
BHMLR	SS096	2.5	10.4	1.2	4.2	1.77	3.86E+02
BHH14a	LSS140	3.8	2.8	4.4	0.7	1.89	4.46E+02
BHH14a	MLSH119	3.0	6.4	3.1	2.1	1.80	4.10E+02
BHH14a	IgS126	3.1	4.5	4.5	1.5	1.83	4.25E+02
BHH14a	LSS112	2.7	7.8	0.1	2.9	1.49	3.29E+02
BHSPRF	SS095	2.5	6.5	0.3	2.6	1.34	2.99E+02
BHH14a	LSS112a	2.7	5.7	0.1	2.1	1.31	2.95E+02
BHVCR	SS084	2.2	6.5	0.3	3.0	1.25	2.76E+02
BHMLR	SS097	2.6	4.0	0.2	1.5	1.15	2.63E+02
BHVCR	SSI086	2.3	4.8	0.5	2.1	1.16	2.62E+02
BHMLR	SS099	2.6	3.7	0.2	1.4	1.13	2.58E+02
BHMLR	SS098	2.6	3.4	0.2	1.3	1.10	2.53E+02
BHMLR	ISS099	2.6	0.5	4.3	0.2	1.32	3.17E+02
BHDEAD	MSS055	1.9	3.1	3.8	1.6	1.27	2.94E+02
BHCCR	SS046	1.8	4.8	1.7	2.7	1.14	2.57E+02
BHCCR	SS043	1.7	6.1	0.4	3.6	1.07	2.36E+02
BHVCR	SSI087	2.3	3.2	0.5	1.4	1.03	2.36E+02
BHUS85	SS048	1.8	2.3	2.2	1.3	0.99	2.30E+02
BHVCR	I081	2.2	1.1	0.9	0.5	0.87	2.05E+02
BHNM	LSS067	2.0	2.0	0.2	1.0	0.80	1.86E+02
BHH14	RSS025	1.1	5.0	0.5	4.5	0.81	1.76E+02
BHH14	LS036b	1.5	1.9	0.4	1.3	0.66	1.53E+02
BHH14	LS037	1.6	1.4	0.5	0.9	0.66	1.55E+02
BHDEAD	SS020	1.0	3.0	0.8	3.0	0.65	1.44E+02
BHCCR	SS042	1.7	0.3	0.0	0.2	0.54	1.31E+02

Table 33A: Cont.

Name	ID #	U (ppm)	Th (ppm)	K (pct)	Th/U	A (μWm^{-3})	ε_v ($mg^{-1}s^{-1}$)
BHH85	SS013	0.7	3.7	0.6	5.3	0.59	1.28E+02
BHH14	LSS028	1.3	0.9	0.6	0.7	0.54	1.27E+02
BHH14	LS027	1.3	0.6	0.8	0.5	0.54	1.28E+02
BHH385	S001	0.5	2.2	2.9	4.4	0.66	1.51E+02
BHH14	SS026	1.2	0.5	0.6	0.4	0.48	1.13E+02
BHDEAD	SS019	0.7	0.9	0.3	1.3	0.32	7.46E+01

Table 33B: RS-230 GRS Survey Sedimentary Comparison – Limestone ID, Radioelement Content, Th:U Ratio, Heat Production (A) and Luminosity (ε_v)

Name	ID #	U (ppm)	Th (ppm)	K (pct)	Th/U	A (μWm^{-3})	ε_v ($mg^{-1}s^{-1}$)
BHBR	IgS168	7.9	2.2	0.3	0.3	2.63	6.29E+02
BHHR	SS188	5.3	10.7	0.6	2.0	2.58	5.82E+02
BHHR	IgS179	4.4	11.2	0.2	2.5	2.30	5.13E+02
BHHR	LSS182	4.9	6.8	1.3	1.4	2.21	5.08E+02
BHHWR	IgS203	5.7	2.6	0.9	0.5	2.06	4.89E+02
BHBG	IgS261	5.7	1.9	0.2	0.3	1.92	4.59E+02
BHH14a	IgS131	3.2	9.4	4.1	2.9	2.23	5.01E+02
BHSRCR	Ig157	4.3	6.4	0.3	1.5	1.88	4.30E+02
BHH14a	LSS139	3.7	8.6	0.6	2.3	1.92	4.30E+02
BHUS85	Ig161	4.4	4.6	0.1	1.0	1.74	4.03E+02
BHUS85	IgS162	4.4	2.8	2.6	0.6	1.87	4.42E+02
BHSPRF	I092	2.5	12.2	0.0	4.9	1.78	3.83E+02
BHSRCR	Ig158	4.3	4.6	0.1	1.1	1.71	3.96E+02
BHH14a	LSS118	3.0	9.8	0.3	3.3	1.77	3.89E+02
BHH14a	LS133	3.3	8.1	0.2	2.5	1.71	3.81E+02
BHHR	LSS181	4.7	1.6	0.8	0.3	1.66	3.96E+02
BHH14a	IgS123	3.0	5.6	5.4	1.9	1.99	4.59E+02
BHH14a	LS115	2.9	9.4	0.3	3.2	1.71	3.75E+02
BHH14a	LSS141	3.9	5.0	0.4	1.3	1.65	3.81E+02
BHH14a	LSS144	4.1	3.3	1.4	0.8	1.69	3.95E+02
BHUS85	M163	4.4	1.4	2.1	0.3	1.70	4.06E+02
BHH14a	LSS145	4.2	2.8	1.0	0.7	1.63	3.84E+02
BHH14a	LSS134	3.6	5.4	0.4	1.5	1.60	3.65E+02
BHSRCR	Ig156	4.3	2.7	0.1	0.6	1.55	3.65E+02

Table 33B: Cont.

Name	ID #	U (ppm)	Th (ppm)	K (pct)	Th/U	A (μWm^{-3})	ε_v ($mg^{-1}s^{-1}$)
BHH14a	LS114	2.8	8.7	0.3	3.1	1.62	3.57E+02
BHUS85	Ig159	4.3	2.3	0.3	0.5	1.54	3.64E+02
BHH14a	LSS143	4.1	2.2	1.2	0.5	1.57	3.72E+02
BHH14a	Ig125	3.1	3.0	4.6	1.0	1.72	4.03E+02
BHH14a	LSS142	4.1	1.6	0.4	0.4	1.43	3.41E+02
BHH14a	IgS132	3.3	2.7	1.8	0.8	1.44	3.37E+02
BHH14a	IgS124	3.0	2.0	4.1	0.7	1.55	3.66E+02
BHH14a	LSS120	3.0	4.4	0.4	1.5	1.33	3.04E+02
BHSPRF	I091	2.4	6.6	0.4	2.8	1.33	2.96E+02
BHH14a	IgS130	3.2	1.9	1.8	0.6	1.34	3.17E+02
BHH14a	LS116	3.0	2.8	0.2	0.9	1.17	2.73E+02
BHVCR	LSS068	2.1	6.6	0.0	3.1	1.19	2.63E+02
BHVCR	I085	2.3	5.5	0.3	2.4	1.20	2.68E+02
BHH14a	LSS113	2.7	3.7	0.2	1.4	1.16	2.65E+02
BHVCR	LSS073	2.1	5.0	0.9	2.4	1.16	2.61E+02
BHVCR	I073	2.2	4.7	0.4	2.1	1.11	2.50E+02
BHH14a	I111	2.6	2.7	0.4	1.0	1.07	2.47E+02
BHSCR	I088	2.4	3.4	0.2	1.4	1.04	2.38E+02
BHUS85	LS052	1.9	4.3	0.2	2.3	0.96	2.16E+02
BHVCR	LS069	2.1	2.9	0.2	1.4	0.91	2.08E+02
BHUS85	RSS049	1.8	4.1	0.2	2.3	0.92	2.05E+02
BHH14	LS035	1.5	5.2	0.3	3.5	0.93	2.04E+02
BHVCR	I083	2.2	1.5	0.3	0.7	0.83	1.95E+02
BHH14	LSS038	1.6	2.6	2.3	1.6	0.97	2.23E+02
BHDEAD	SS054	1.9	1.3	2.1	0.7	0.93	2.19E+02
BHCCR	SS044	1.7	3.0	0.2	1.8	0.79	1.80E+02
BHCCR	SS045	1.8	2.3	0.1	1.3	0.75	1.73E+02
BHDEAD	Ig053	1.9	1.3	0.9	0.7	0.79	1.86E+02
BHNM	LSS066	1.9	1.5	0.4	0.8	0.75	1.76E+02
BHVCR	LSS070	2.1	0.8	0.2	0.4	0.73	1.74E+02
BHH14	LS031	1.3	3.9	0.3	3.0	0.76	1.68E+02
BHH14	LS036a	1.5	2.5	0.4	1.7	0.71	1.62E+02
BHH14	LSS041	1.7	1.4	0.5	0.8	0.69	1.62E+02
BHH14	LS034	1.4	2.5	0.7	1.8	0.72	1.63E+02
BHH14	LSS034	1.5	2.3	0.3	1.5	0.68	1.57E+02

Table 33B: Cont.

Name	ID #	U (ppm)	Th (ppm)	K (pct)	Th/U	A (μWm^{-3})	ε_v ($mg^{-1}s^{-1}$)
BHH14	LS032	1.4	1.7	1.1	1.2	0.69	1.61E+02
BHH14	LSS029	1.3	2.4	0.3	1.8	0.63	1.43E+02
BHH14	LS033	1.4	1.9	0.2	1.4	0.61	1.40E+02
BHH14	LSS030	1.3	0.6	0.3	0.5	0.48	1.14E+02
BHH14	RSS024	1.1	1.0	0.5	0.9	0.48	1.11E+02

Table 33C: RS-230 GRS Survey Sedimentary Comparison – Gypsum ID, Radioelement Content, Th:U Ratio, Heat Production (A) and Antineutrino Luminosity (ε_v)

Name	ID #	U (ppm)	Th (ppm)	K (pct)	Th/U	A (μWm^{-3})	ε_v ($mg^{-1}s^{-1}$)
BHSPRF	SGyp090	2.4	3.4	0.3	1.4	1.05	2.41E+02
BHSPRF	SGyp089	2.4	2.2	0.7	0.9	1.00	2.32E+02

Table 33D: RS-230 GRS Survey Sedimentary Comparison – Shale ID, Radioelement Content, Th:U Ratio, Heat Production (A) and Antineutrino Luminosity (ε_v)

Name	ID #	U (ppm)	Th (ppm)	K (pct)	Th/U	A (μWm^{-3})	ε_v ($mg^{-1}s^{-1}$)
BHIOR	MGn204	7.5	19.6	4.6	2.6	4.45	9.98E+02
BHRFR	IF150	4.1	20.2	4.8	4.9	3.48	7.61E+02
BHYCR	MSc212	4.9	13.6	2.4	2.8	2.91	6.48E+02
BHYCR	MB207	3.4	15.6	3.8	4.6	2.77	6.08E+02
BHYCR	IgIF221	4.6	11.6	2.9	2.5	2.70	6.07E+02
BHYCR	MSc217	2.3	7.7	2.3	3.3	1.61	3.58E+02
BHSPRF	I094	2.5	1.0	0.1	0.4	0.86	2.04E+02

Table 33E: RS-230 GRS Survey Sedimentary Comparison – Graywacke ID, Radioelement Content, Th:U Ratio, Heat Production (A) and Luminosity (ε_v)

Name	ID #	U (ppm)	Th (ppm)	K (pct)	Th/U	A (μWm^{-3})	ε_v ($mg^{-1}s^{-1}$)
BHH14a	IgS136	3.7	9.1	6.9	2.5	2.67	6.09E+02

Table 34A: Ge SED GRS Analysis Igneous Comparison – Rhyolite ID, Radioelement Content, Th:U Ratio, Heat Production (A) and Antineutrino Luminosity (ε_{v})

Name	ID #	U (ppm)	Th (ppm)	K (pct)	Th/U	A (μWm^{-3})	ε_v ($mg^{-1}s^{-1}$)
BHUR	MIg227	12.44	64.21	8.31	5.16	10.11	2.19E+03
BHUR	MIg230	18.64	26.64	6.17	1.43	8.62	1.98E+03
BHTSR	Ig242	4.39	36.32	2.49	8.27	4.66	9.81E+02
BHYCR	IgS218	6.19	16.08	5.51	2.60	3.86	8.68E+02
BHUS14a	Ig248	4.35	19.32	2.51	4.44	3.23	7.03E+02
BHH385	Ig004	4.43	12.43	1.91	2.81	2.61	5.81E+02
BHTSR	Ig240	3.26	16.51	2.47	5.06	2.66	5.76E+02
BHH85	Ig010	4.83	8.52	2.56	1.76	2.48	5.65E+02
BHUS14a	MLSS064	3.07	4.26	3.17	1.39	1.65	3.82E+02
BHBG	IgS259	3.08	4.99	1.73	1.62	1.55	3.56E+02
BHBVR	IgS198	1.90	6.27	2.23	3.30	1.36	3.03E+02
BHYCR	Ig223	1.69	5.54	2.74	3.28	1.29	2.89E+02
BHYCR	MGn205	3.20	0.22	0.89	0.07	1.10	2.65E+02
BHCLP	Ig290	1.59	5.89	2.12	3.70	1.22	2.71E+02
BHBVR	Ig199	1.72	5.35	2.08	3.11	1.21	2.70E+02
BHCC	IgS257	1.77	4.20	3.37	2.37	1.27	2.91E+02
BHBVR	IgG197	1.40	5.82	2.12	4.16	1.15	2.55E+02
BHCLP	IgS289	1.35	5.57	2.19	4.13	1.13	2.50E+02
BHUS14a	IF251	1.35	5.43	2.25	4.02	1.12	2.49E+02
BHYCR	IgS222	1.45	4.55	2.58	3.14	1.12	2.51E+02
BHBG	IgS258	1.33	4.89	2.31	3.68	1.08	2.40E+02
BHBVR	Ig200	1.10	1.04	2.51	0.95	0.71	1.66E+02
BHBG	IgS260	0.27	3.40	1.00	12.59	0.48	1.02E+02
BHUS85	SS047	1.10	0.00	0.00	0.00	0.34	8.15E+01
BHYCR	Ig224	0.81	0.50	0.42	0.62	0.34	7.95E+01
BHTGR	Ig233	0.98	0.00	0.00	0.00	0.30	7.26E+01
BHVCR	I082	0.62	0.00	0.00	0.00	0.19	4.59E+01
BHUS85	Ig164	0.50	0.00	0.00	0.00	0.15	3.71E+01
BHSRCR	Ig155	0.46	0.00	0.00	0.00	0.14	3.41E+01
BHHR	IgSS180	0.07	0.88	0.00	12.57	0.10	1.94E+01
BHUS85	Ig160	0.16	0.00	0.00	0.00	0.05	1.19E+01
BHGR	Ig279	0.08	0.00	0.00	0.00	0.02	5.93E+00

Table 34B: Ge SED GRS Analysis Igneous Comparison – Phonolite ID, Radioelement Content, Th:U Ratio, Heat Production (A) and Antineutrino Luminosity (ε_v)

Name	ID #	U (ppm)	Th (ppm)	K (pct)	Th/U	A (μWm^{-3})	ε_v ($mg^{-1}s^{-1}$)
BHDM	GrSc237	11.65	32.60	3.65	2.80	6.70	1.46E+03
BHBFR	GSc191	11.18	32.44	3.93	2.90	6.57	1.44E+03
BHUS85	Ig166	11.17	33.12	2.80	2.97	6.50	1.40E+03
BHH14a	Ig135	11.32	28.55	3.63	2.52	6.26	1.32E+03
BHBFR	GSc193	10.09	29.63	3.55	2.94	5.96	1.25E+03
BHBVR	GSc194	9.44	27.84	3.56	2.95	5.62	1.19E+03
BHDM	Ig235a	7.20	35.57	2.94	4.94	5.51	1.19E+03
BHDM	GrSc236	8.04	31.17	3.21	3.88	5.43	1.13E+03
BHDM	Ig235	6.43	35.50	2.99	5.52	5.27	1.01E+03
BHBFR	GSc192	6.32	27.57	3.54	4.36	4.64	6.94E+02
BHUS85	Ig165	0.78	34.89	2.61	44.86	3.45	4.47E+02
BHUS85	MIg167	3.32	6.25	3.68	1.88	1.95	1.09E+02
BHEWR	IgS195	1.46	0.06	0.00	0.04	0.45	6.02E+01
BHUS14a	IgS249	0.12	0.84	1.39	7.00	0.26	1.46E+03

Table 34C: Ge SED GRS Analysis Igneous Comparison – Trachyte ID, Radioelement Content, Th:U Ratio, Heat Production (A) and Antineutrino Luminosity (ε_v)

Name	ID #	U (ppm)	Th (ppm)	K (pct)	Th/U	A (μWm^{-3})	ε_v ($mg^{-1}s^{-1}$)
BHTSR	Ig245	6.04	40.09	2.32	6.64	5.46	1.16E+03
BHUR	MIg231	5.34	41.67	2.40	7.80	5.39	1.14E+03
BHUS14a	MIg250	6.67	26.74	6.78	4.01	5.04	1.11E+03
BHTSR	Ig244	3.44	35.39	2.45	10.29	4.29	8.95E+02
BHTSR	Ig241	3.61	15.77	3.99	4.37	2.87	6.31E+02
BHMLR	I101	3.39	17.28	2.40	5.10	2.75	5.96E+02
BHCC	Ig254	4.17	13.79	2.21	3.31	2.68	5.92E+02
BHMLR	I102	3.82	13.72	2.17	3.59	2.56	5.64E+02
BHCC	Ig255	3.66	14.03	2.22	3.83	2.54	5.59E+02
BHUR	Ig226	4.08	6.94	7.84	1.70	2.71	6.27E+02
BHTGR	Ig232	3.81	6.32	1.64	1.66	1.88	4.29E+02
BHUS85	Ig170	2.44	6.45	1.58	2.64	1.46	3.28E+02
BHGR	Ig273	1.26	7.60	1.69	6.03	1.21	2.62E+02
BHUR	MIg228	1.39	2.04	2.73	1.47	0.90	2.10E+02
BHUR	MIg229	1.32	2.26	1.93	1.71	0.81	1.87E+02
BHTSR	Ig239	1.64	0.05	0.17	0.03	0.52	1.27E+02

Table 34C: Cont.

Name	ID #	U (ppm)	Th (ppm)	K (pct)	Th/U	A (μWm^{-3})	ε_v ($mg^{-1}s^{-1}$)
BHMLR	ISS100	1.35	0.00	0.00	0.00	0.41	1.00E+02
BHVCR	I080	0.47	0.00	0.00	0.00	0.14	3.48E+01
BHUS14a	LS246	0.14	0.00	0.00	0.00	0.04	1.04E+01

Table 34D: Ge SED GRS Analysis Igneous Comparison – Latite ID, Radioelement Content, Th:U Ratio, Heat Production (A) and Antineutrino Luminosity (ε_v)

Name	ID #	U (ppm)	Th (ppm)	K (pct)	Th/U	A (μWm^{-3})	ε_v ($mg^{-1}s^{-1}$)
BHH385	M008	5.10	10.22	6.77	2.00	3.18	7.27E+02
BHH385	Ig009	4.30	10.39	6.49	2.42	2.92	6.63E+02
BHH385	I003	3.16	10.07	2.23	3.19	2.06	4.58E+02
BHBR	Ig267	2.62	9.56	1.71	3.65	1.79	3.95E+02
BHVCR	I074	2.10	9.09	1.41	4.33	1.56	3.41E+02
BHVCR	I072	2.30	7.78	1.44	3.38	1.52	3.35E+02
BHVCR	I077	1.19	8.40	1.76	7.06	1.27	2.72E+02
BHVCR	I079	1.15	8.67	1.60	7.54	1.26	2.69E+02
BHVCR	I078	0.92	8.74	1.59	9.50	1.19	2.53E+02
BHCC	IgS256	1.11	4.67	4.17	4.21	1.20	2.71E+02

Table 34E: Ge SED GRS Analysis Igneous Comparison – Latitic Andesite ID, Radioelement Content, Th:U Ratio, Heat Production (A) and Luminosity (ε_v)

Name	ID #	U (ppm)	Th (ppm)	K (pct)	Th/U	A (μWm^{-3})	ε_v ($mg^{-1}s^{-1}$)
BHTGR	Ig234	3.39	5.64	1.58	1.66	1.69	3.85E+02
BHER	Ig277	1.91	8.49	1.62	4.45	1.48	3.23E+02
BHGR	Ig271	1.68	8.09	1.67	4.82	1.38	3.01E+02
BHGR	Ig272	1.67	8.04	1.52	4.81	1.35	2.95E+02
BHGR	Ig270	1.65	7.90	1.52	4.79	1.34	2.91E+02
BHVCR	I076	1.25	9.15	1.79	7.32	1.35	2.89E+02
BHVCR	I075	1.13	9.22	1.78	8.16	1.32	2.81E+02
BHVCR	I071	0.85	10.14	1.62	11.93	1.29	2.71E+02
BHGR	Ig274	1.77	6.04	1.60	3.41	1.23	2.72E+02
BHGR	Ig269	0.81	7.50	1.72	9.26	1.07	2.28E+02
BHGR	Ig275	1.27	4.94	1.75	3.89	1.00	2.22E+02

Table 34F: Ge SED GRS Analysis Igneous Comparison – Granodiorite ID, Radioelement Content, Th:U Ratio, Heat Production (A) and Luminosity (ε_v)

Name	ID #	U (ppm)	Th (ppm)	K (pct)	Th/U	A (μWm^{-3})	ε_v ($mg^{-1}s^{-1}$)
BHH14a	Ig129	9.16	29.03	2.30	3.17	5.49	1.21E+03
BHH14a	Ig127a	9.06	25.77	2.49	2.84	5.20	1.16E+03
BHH14a	Ig128	7.28	22.15	2.29	3.04	4.34	9.60E+02
BHH14a	Ig127b	5.14	22.54	2.70	4.39	3.76	8.19E+02

Table 34G: Ge SED GRS Analysis Igneous Comparison – Volcanic Alkalic ID, Radioelement Content, Th:U Ratio, Heat Production (A) and Luminosity (ε_v)

Name	ID #	U (ppm)	Th (ppm)	K (pct)	Th/U	A (μWm^{-3})	ε_v ($mg^{-1}s^{-1}$)
BHH14a	Ig147	17.72	67.78	2.84	3.83	11.40	2.49E+03
BHH14a	Ig146	17.87	64.46	3.29	3.61	11.22	2.46E+03
BHH14a	Ig138	14.21	48.84	2.82	3.44	8.75	1.92E+03
BHH14a	Ig137	14.87	42.05	2.70	2.83	8.37	1.86E+03
BHYCR	MIg219	6.93	3.75	2.76	0.54	2.74	6.49E+02
BHYCR	MIF220	1.61	0.00	0.00	0.00	0.49	1.19E+02
BHHR	LSS183	0.00	0.00	0.00	0.00	0.00	0.00E+00

Table 34H: Ge SED GRS Analysis Igneous Comparison –Aplite ID, Radioelement Content, Th:U Ratio, Heat Production (A) and Antineutrino Luminosity (ε_v)

Name	ID #	U (ppm)	Th (ppm)	K (pct)	Th/U	A (μWm^{-3})	ε_v ($mg^{-1}s^{-1}$)
BHSRCR	Ig154	0.51	0.00	0.00	0.00	0.16	3.78E+01

Table 34I: Ge SED GRS Analysis Igneous Comparison –Basalt ID, Radioelement Content, Th:U Ratio, Heat Production (A) and Antineutrino Luminosity (ε_v)

Name	ID #	U (ppm)	Th (ppm)	K (pct)	Th/U	A (μWm^{-3})	ε_v ($mg^{-1}s^{-1}$)
BHH14	B40	14.81	15.27	0.07	1.03	5.81	1.35E+03
BHH14	B39	12.06	4.32	0.02	0.36	4.05	9.64E+02

Table 34J: Ge SED GRS Analysis Igneous Comparison –Episodite ID, Radioelement Content, Th:U Ratio, Heat Production (A) and Antineutrino Luminosity (ε_v)

Name	ID #	U (ppm)	Th (ppm)	K (pct)	Th/U	A (μWm^{-3})	ε_v ($mg^{-1}s^{-1}$)
BHH385	S003	0.90	7.81	3.11	8.68	1.28	2.77E+02

Table 35A: Ge SED GRS Analysis Metamorphic Comparison – Schist ID, Radioelement Content, Th:U Ratio, Heat Production (A) and Luminosity (ε_v)

Name	ID #	U (ppm)	Th (ppm)	K (pct)	Th/U	A (μWm^{-3})	ε_v ($mg^{-1}s^{-1}$)
BHRFR	IF149	4.85	11.77	2.89	2.43	2.79	6.28E+02
BHGR	MGnSc285	4.11	11.65	2.88	2.83	2.56	5.71E+02
BHDEAD	S015	6.84	0.00	1.81	0.00	2.29	5.56E+02
BHDEAD	Sc023	4.07	5.44	2.21	1.34	1.95	4.50E+02
BHH385	M007	2.56	11.58	2.41	4.52	2.02	4.43E+02
BHH385	M006	2.87	11.15	1.14	3.89	1.94	4.24E+02
BHDEAD	Sc017	4.51	1.93	4.24	0.43	2.02	4.80E+02
BHDEAD	Sc021	2.53	7.23	3.65	2.86	1.79	4.04E+02
BHGR	MGn285	2.39	7.92	2.43	3.31	1.67	3.71E+02
BHDEAD	Gc022	1.76	9.59	3.08	5.45	1.69	3.69E+02
BHVCR	MSc225	1.58	8.31	4.51	5.26	1.69	3.74E+02
BHH385	Ig005	1.95	8.26	1.88	4.24	1.50	3.29E+02
BHH85	Sc012	1.80	7.36	1.79	4.09	1.37	3.01E+02
BHH85	Sc011	1.35	8.00	2.77	5.93	1.39	3.05E+02
BHUS14a	MSc060	1.13	9.63	1.57	8.52	1.33	2.82E+02
BHGR	MSc283	1.58	6.53	2.07	4.13	1.26	2.79E+02
BHMLR	MSc104	3.07	1.55	0.19	0.50	1.09	2.58E+02
BHYCR	MSc215	1.00	6.54	3.04	6.54	1.20	2.62E+02
BHDEAD	MG057	0.78	6.65	2.49	8.53	1.08	2.33E+02
BHUS14a	MSc059	0.62	5.62	1.51	9.06	0.83	1.78E+02
BHUS85	M174	0.90	3.54	0.49	3.93	0.63	1.37E+02
BHRFR	IF151	0.54	3.61	2.16	6.69	0.71	1.57E+02
BHYCR	M211	0.73	3.12	0.08	4.27	0.49	1.07E+02
BHCC	GrSc252	1.13	1.45	0.00	1.28	0.47	1.07E+02
BHCC	MIg253	0.76	1.82	0.00	2.39	0.38	8.58E+01
BHUS85	MIg168	1.04	0.00	0.00	0.00	0.32	7.71E+01
BHYCR	MSc214	0.50	1.43	0.00	2.86	0.27	6.02E+01
BHYCR	IF216	0.83	0.00	0.00	0.00	0.25	6.15E+01
BHYCR	MSc213	0.08	2.77	0.00	34.63	0.26	5.08E+01
BHDEAD	Sc018	0.25	0.00	0.00	0.00	0.08	1.85E+01
BHDEAD	M056	0.00	0.00	0.00	0.00	0.00	0.00E+00

Table 35B: Ge SED GRS Analysis Metamorphic Comparison – Phyllite ID, Radioelement Content, Th:U Ratio, Heat Production (A) and Luminosity ($\mathcal{E}_v$)

Name	ID #	U (ppm)	Th (ppm)	K (pct)	Th/U	A (μWm^{-3})	$\mathcal{E}_v$ ($mg^{-1}s^{-1}$)
BHRFR	IF148	3.37	10.96	2.04	3.25	2.18	4.83E+02
BHCC	MGn106	4.40	5.96	1.03	1.35	1.96	4.51E+02
BHYCR	M209	2.30	11.49	4.45	5.00	2.17	4.77E+02
BHUS14a	MSc062	2.40	7.77	2.24	3.24	1.64	3.64E+02
BHUS85	MSc173	1.32	10.71	2.24	8.11	1.55	3.32E+02
BHYCR	MSc208	1.60	6.62	3.29	4.14	1.41	3.15E+02
BHCC	MGn107	2.05	4.98	1.12	2.43	1.17	2.63E+02
BHMLR	MSc103	2.72	2.07	0.00	0.76	1.00	2.35E+02
BHRFR	IF152	1.95	3.16	2.57	1.62	1.15	2.65E+02
BHLead	M177	0.46	8.40	1.90	18.26	1.06	2.22E+02
BHLead	M178	0.42	7.64	2.63	18.19	1.06	2.26E+02
BHUS85	Sh169	1.05	4.97	1.33	4.73	0.89	1.94E+02
BHUS14a	MSc065	1.78	1.94	1.03	1.09	0.82	1.91E+02
BHUS14a	M063	1.55	3.17	0.43	2.05	0.79	1.78E+02
BHRFR	MGn153	0.84	3.37	3.38	4.01	0.92	2.08E+02
BHH85	SS014	1.91	0.00	0.00	0.00	0.58	1.42E+02
BHYCR	M210	0.59	2.48	0.48	4.20	0.44	9.69E+01
BHUS85	Ig172	0.23	3.94	0.00	17.13	0.40	8.09E+01
BHLead	M176	0.31	2.35	0.60	7.58	0.36	7.73E+01
BHUS14a	MGn061	0.06	0.57	0.00	9.50	0.07	1.37E+01

Table 35C: Ge SED GRS Analysis Metamorphic Comparison –Slate ID, Radioelement Content, Th:U Ratio, Heat Production (A) and Antineutrino Luminosity ($\mathcal{E}_v$)

Name	ID #	U (ppm)	Th (ppm)	K (pct)	Th/U	A (μWm^{-3})	$\mathcal{E}_v$ ($mg^{-1}s^{-1}$)
BHIOR	MGn204	2.66	12.57	3.01	4.73	2.20	4.82E+02
BHYCR	MB207	2.04	9.34	2.24	4.58	1.66	3.63E+02
BHRFR	IF150	0.87	9.11	3.51	10.47	1.42	3.07E+02
BHYCR	MSc212	0.25	8.19	1.76	32.76	0.96	1.99E+02
BHYCR	IgIF221	0.94	0.00	0.00	0.00	0.29	6.97E+01
BHYCR	MSc217	0.00	0.00	0.00	0.00	0.00	0.00E+00

Table 35D: Ge SED GRS Analysis Metamorphic Comparison –Metabasalt ID, Radioelement Content, Th:U Ratio, Heat Production (A) and Luminosity (ε_v)

Name	ID #	U (ppm)	Th (ppm)	K (pct)	Th/U	A (μWm^{-3})	ε_v ($mg^{-1}s^{-1}$)
BHYCR	MSc212	0.25	8.19	1.76	32.76	0.96	1.99E+02
BHYCR	IgIF221	0.94	0.00	0.00	0.00	0.29	6.97E+01
BHYCR	MSc217	0.00	0.00	0.00	0.00	0.00	0.00E+00

Table 35E: Ge SED GRS Analysis Metamorphic Comparison –Quartzite ID, Radioelement Content, Th:U Ratio, Heat Production (A) and Luminosity (ε_v)

Name	ID #	U (ppm)	Th (ppm)	K (pct)	Th/U	A (μWm^{-3})	ε_v ($mg^{-1}s^{-1}$)
BHDEAD	S016	0.01	0.00	0.00	0.00	0.00	7.41E-01
BHCC	Qtz108	0.00	0.00	0.00	0.00	0.00	0.00E+00

Table 35F: Ge SED GRS Analysis Metamorphic Comparison –Metaquartzite ID, Radioelement Content, Th:U Ratio, Heat Production (A) and Luminosity (ε_v)

Name	ID #	U (ppm)	Th (ppm)	K (pct)	Th/U	A (μWm^{-3})	ε_v ($mg^{-1}s^{-1}$)
BHLead	M175	1.49	3.49	1.51	2.34	0.92	2.08E+02
BHEWR	IgS196	1.35	0.00	0.00	0.00	0.41	1.00E+02

Table 35G: Ge SED GRS Analysis Metamorphic Comparison –Metagraywacke ID, Radioelement Content, Th:U Ratio, Heat Production (A) and Luminosity (ε_v)

Name	ID #	U (ppm)	Th (ppm)	K (pct)	Th/U	A (μWm^{-3})	ε_v ($mg^{-1}s^{-1}$)
BHH385	I002	3.11	10.57	2.68	3.40	2.14	4.74E+02

Table 35H: Ge SED GRS Analysis Metamorphic Comparison –Greenstone ID, Radioelement Content, Th:U Ratio, Heat Production (A) and Luminosity (ε_v)

Name	ID #	U (ppm)	Th (ppm)	K (pct)	Th/U	A (μWm^{-3})	ε_v ($mg^{-1}s^{-1}$)
BHGR	Ig281	0.26	0.59	0.00	2.27	0.13	2.88E+01
BHER	M286	0.03	0.00	0.00	0.00	0.01	2.22E+00
BHGR	MGn284	0.00	0.00	0.00	0.00	0.00	0.00E+00

Table 36A: Ge SED GRS Analysis Sedimentary Comparison – Sandstone ID, Radioelement Content, Th:U Ratio, Heat Production (A) and Luminosity (ε_v)

Name	ID #	U (ppm)	Th (ppm)	K (pct)	Th/U	A (μWm^{-3})	ε_v ($mg^{-1}s^{-1}$)
BHCCR	SS043	26.56	3.06	0.00	0.12	8.37	2.02E+03
BHH385	S001	2.37	8.92	1.44	3.76	1.63	3.59E+02
BHDEAD	SS020	4.52	0.02	0.00	0.00	1.38	3.35E+02
BHH85	SS013	4.47	0.00	0.00	0.00	1.37	3.31E+02
BHBR	SS262	4.26	0.00	0.00	0.00	1.30	3.16E+02
BHDEAD	SS019	3.13	0.12	0.00	0.04	0.97	2.34E+02
BHUS85	SS048	0.93	4.52	0.98	4.86	0.77	1.69E+02
BHBR	SS263	1.67	0.00	0.00	0.00	0.51	1.24E+02
BHH14	SS026	1.60	0.00	0.04	0.00	0.49	1.20E+02
BHBVR	SS202	1.55	0.00	0.00	0.00	0.47	1.15E+02
BHVCR	SSI086	1.32	0.40	0.03	0.30	0.44	1.05E+02
BHRR	RSS190	0.95	0.18	1.39	0.19	0.46	1.11E+02
BHDEAD	MSS055	0.21	2.40	2.41	11.43	0.54	1.20E+02
BHH14	LSS028	0.66	1.82	0.00	2.76	0.35	7.84E+01
BHH14a	LSS140	0.32	1.20	2.18	3.75	0.44	1.02E+02
BHH14a	MLSH119	0.21	0.93	1.05	4.43	0.26	5.91E+01
BHHR	RSS185	0.37	0.22	0.69	0.59	0.21	4.97E+01
BHMLR	ISS099	0.49	0.00	0.11	0.00	0.16	3.93E+01
BHH14a	IgS126	0.12	0.99	0.84	8.25	0.21	4.77E+01
BHHR	RSS186	0.32	0.38	0.38	1.19	0.17	4.02E+01
BHH14	LS027	0.45	0.00	0.00	0.00	0.14	3.33E+01
BHMLR	SS099	0.45	0.00	0.00	0.00	0.14	3.33E+01
BHCCR	SS046	0.30	0.00	0.48	0.00	0.15	3.52E+01
BHH14a	LS134	0.32	0.00	0.00	0.00	0.10	2.37E+01
BHH14	LS036b	0.27	0.00	0.00	0.00	0.08	2.00E+01
BHCCR	SS042	0.12	0.54	0.00	4.50	0.08	1.76E+01
BHBR	SS265	0.22	0.00	0.00	0.00	0.07	1.63E+01
BHGR	Ig276	0.22	0.00	0.00	0.00	0.07	1.63E+01
BHMLR	SS097	0.18	0.00	0.00	0.00	0.05	1.33E+01
BHBR	SS266	0.12	0.01	0.37	0.08	0.08	1.91E+01
BHBR	SS264	0.15	0.00	0.00	0.00	0.05	1.11E+01
BHH14	RSS025	0.12	0.00	0.00	0.00	0.04	8.89E+00

Table 36A: Cont.

Name	ID #	U (ppm)	Th (ppm)	K (pct)	Th/U	A (μWm^{-3})	ε_v ($mg^{-1}s^{-1}$)
BHH14a	LSS112	0.12	0.00	0.00	0.00	0.04	8.89E+00
BHVCR	I081	0.11	0.00	0.00	0.00	0.03	8.15E+00
BHHR	LSS184	0.10	0.00	0.00	0.00	0.03	7.41E+00
BHMLR	SS098	0.02	0.17	0.00	8.50	0.02	4.24E+00
BHMLR	SS096	0.04	0.00	0.00	0.00	0.01	2.96E+00
BHNM	LSS067	0.02	0.00	0.00	0.00	0.01	1.48E+00
BHVCR	SSI087	0.02	0.00	0.00	0.00	0.01	1.48E+00
BHSPRF	SS095	0.01	0.00	0.00	0.00	0.00	7.41E-01
BHVCR	SS084	0.00	0.00	0.00	0.00	0.00	0.00E+00

Table 36B: Ge SED GRS Analysis Sedimentary Comparison – Limestone ID, Radioelement Content, Th:U Ratio, Heat Production (A) and Luminosity (ε_v)

Name	ID #	U (ppm)	Th (ppm)	K (pct)	Th/U	A (μWm^{-3})	ε_v ($mg^{-1}s^{-1}$)
BHH14a	IgS122	52.81	0.00	0.45	0.00	16.18	3.93E+03
BHH14a	IgS123	2.13	2.53	3.79	1.19	1.29	3.02E+02
BHH14	LS035	2.41	0.00	0.00	0.00	0.74	1.79E+02
BHDEAD	SS054	1.86	1.03	0.25	0.55	0.68	1.61E+02
BHBR	IgS268	2.11	0.00	0.00	0.00	0.64	1.56E+02
BHH14a	Ig125	0.59	2.67	3.18	4.53	0.76	1.73E+02
BHVCR	I085	1.66	0.00	0.00	0.00	0.51	1.23E+02
BHH14	LSS029	0.71	2.59	0.00	3.65	0.43	9.46E+01
BHSPRF	I091	1.14	0.00	0.00	0.00	0.35	8.45E+01
BHHR	RSS187	1.11	0.00	0.00	0.00	0.34	8.23E+01
BHH14a	LSS144	0.42	1.72	1.41	4.10	0.43	9.72E+01
BHCCR	SS045	0.98	0.00	0.00	0.00	0.30	7.26E+01
BHSPRF	I093	0.92	0.00	0.00	0.00	0.28	6.82E+01
BHH14a	I111	0.91	0.00	0.00	0.00	0.28	6.74E+01
BHH14a	LSS143	0.78	0.25	0.33	0.32	0.30	7.08E+01
BHH14a	IgS131	0.28	1.45	1.62	5.18	0.39	8.81E+01
BHSRCR	Ig157	0.82	0.00	0.00	0.00	0.25	6.08E+01
BHHWR	IgS203	0.82	0.00	0.00	0.00	0.25	6.08E+01
BHHR	LSS181	0.77	0.00	0.00	0.00	0.24	5.71E+01
BHH14	RSS024	0.76	0.00	0.00	0.00	0.23	5.63E+01

Table 36B: Cont.

Name	ID #	U (ppm)	Th (ppm)	K (pct)	Th/U	A (μWm^{-3})	ε_v ($mg^{-1}s^{-1}$)
BHH14	LSS034	0.21	1.44	0.72	6.86	0.27	5.84E+01
BHNM	LSS066	0.65	0.00	0.00	0.00	0.20	4.82E+01
BHSPRF	I092	0.60	0.00	0.00	0.00	0.18	4.45E+01
BHCCR	SS044	0.56	0.00	0.00	0.00	0.17	4.15E+01
BHH14a	LSS118	0.56	0.00	0.00	0.00	0.17	4.15E+01
BHUS85	Ig159	0.56	0.00	0.00	0.00	0.17	4.15E+01
BHH14a	LSS142	0.50	0.00	0.00	0.00	0.15	3.71E+01
BHH14a	LS114	0.49	0.00	0.00	0.00	0.15	3.63E+01
BHH14a	LSS134	0.46	0.00	0.00	0.00	0.14	3.41E+01
BHH14a	IgS132	0.29	0.59	0.00	2.03	0.14	3.10E+01
BHRR	RSS189	0.29	0.16	0.50	0.55	0.16	3.76E+01
BHHR	LSS182	0.40	0.00	0.00	0.00	0.12	2.96E+01
BHSCR	I088	0.38	0.00	0.00	0.00	0.12	2.82E+01
BHUS85	M163	0.18	0.40	0.55	2.22	0.15	3.47E+01
BHUS85	IgS162	0.08	0.72	0.64	9.00	0.16	3.49E+01
BHH14	LSS041	0.34	0.00	0.00	0.00	0.10	2.52E+01
BHH14	LS036a	0.26	0.24	0.00	0.92	0.10	2.32E+01
BHHR	IgS179	0.31	0.00	0.00	0.00	0.09	2.30E+01
BHH14a	IgS124	0.14	0.27	0.69	1.93	0.14	3.34E+01
BHVCR	LS069	0.29	0.00	0.00	0.00	0.09	2.15E+01
BHBG	IgS261	0.28	0.00	0.00	0.00	0.09	2.07E+01
BHUS85	RSS050	0.14	0.40	0.04	2.86	0.08	1.79E+01
BHUS85	LS052	0.24	0.00	0.00	0.00	0.07	1.78E+01
BHUS85	SS051	0.23	0.00	0.00	0.00	0.07	1.70E+01
BHH14	LS034	0.20	0.00	0.00	0.00	0.06	1.48E+01
BHH14a	LSS139	0.20	0.00	0.00	0.00	0.06	1.48E+01
BHH14a	LSS141	0.20	0.00	0.00	0.00	0.06	1.48E+01
BHSRCR	Ig156	0.20	0.00	0.00	0.00	0.06	1.48E+01
BHER	IgLS278	0.19	0.00	0.00	0.00	0.06	1.41E+01
BHSRCR	Ig158	0.17	0.00	0.00	0.00	0.05	1.26E+01
BHH14a	LSS113	0.16	0.00	0.00	0.00	0.05	1.19E+01
BHH14a	LSS145	0.16	0.00	0.00	0.00	0.05	1.19E+01
BHVCR	LSS070	0.13	0.00	0.00	0.00	0.04	9.63E+00

Table 36B: Cont.

Name	ID #	U (ppm)	Th (ppm)	K (pct)	Th/U	A (μWm^{-3})	ε_v ($mg^{-1}s^{-1}$)
BHUS85	RSS049	0.12	0.00	0.00	0.00	0.04	8.89E+00
BHH14	LS032	0.11	0.00	0.00	0.00	0.03	8.15E+00
BHH14	LS033	0.00	0.41	0.00	0.00	0.03	6.64E+00
BHH14	LS031	0.09	0.00	0.00	0.00	0.03	6.67E+00
BHVCR	I073	0.07	0.00	0.00	0.00	0.02	5.19E+00
BHH14a	IgS130	0.07	0.00	0.00	0.00	0.02	5.19E+00
BHH14a	LS133	0.06	0.00	0.00	0.00	0.02	4.45E+00
BHH14a	LS115	0.04	0.00	0.00	0.00	0.01	2.96E+00
BHH14a	LS116	0.04	0.00	0.00	0.00	0.01	2.96E+00
BHVCR	LSS068	0.02	0.00	0.00	0.00	0.01	1.48E+00
BHVCR	LSS073	0.02	0.00	0.00	0.00	0.01	1.48E+00
BHH14a	LSS120	0.02	0.00	0.00	0.00	0.01	1.48E+00
BHH14	LSS030	0.00	0.00	0.00	0.00	0.00	0.00E+00
BHVCR	I083	0.00	0.00	0.00	0.00	0.00	0.00E+00
BHUS85	Ig161	0.00	0.00	0.00	0.00	0.00	0.00E+00

Table 36C: Ge SED GRS Analysis Sedimentary Comparison –Graywacke ID, Radioelement Content, Th:U Ratio, Heat Production (A) and Luminosity (ε_v)

Name	ID #	U (ppm)	Th (ppm)	K (pct)	Th/U	A (μWm^{-3})	ε_v ($mg^{-1}s^{-1}$)
BHH14a	IgS136	4.42	25.33	3.08	5.73	3.82	8.21E+02

Table 36D: Ge SED GRS Analysis Sedimentary Comparison –Shale ID, Radioelement Content, Th:U Ratio, Heat Production (A) and Antineutrino Luminosity (ε_v)

Name	ID #	U (ppm)	Th (ppm)	K (pct)	Th/U	A (μWm^{-3})	ε_v ($mg^{-1}s^{-1}$)
BHSPRF	I094	0.53	0.00	0.00	0.00	0.16	3.93E+01

Table 36E: Ge SED GRS Analysis Sedimentary Comparison –Gypsum ID, Radioelement Content, Th:U Ratio, Heat Production (A) and Luminosity (ε_v)

Name	ID #	U (ppm)	Th (ppm)	K (pct)	Th/U	A (μWm^{-3})	ε_v ($mg^{-1}s^{-1}$)
BHSPRF	SGyp089	0.01	0.00	0.00	0.00	0.00	7.41E-01
BHSPRF	SGyp090	0.01	0.00	0.00	0.00	0.00	7.41E-01

Table 36F: Ge SED GRS Analysis Sedimentary Comparison –Calcite ID, Radioelement Content, Th:U Ratio, Heat Production (A) and Antineutrino Luminosity ($\varepsilon_{v)}$

Name	ID #	U (ppm)	Th (ppm)	K (pct)	Th/U	A (μWm^{-3})	ε_v ($mg^{-1}s^{-1}$)
BHDEAD	Ig053	0.08	0.00	0.00	0.00	0.02	5.93E+00

Table 37A: SURF RS-230 GRS Survey Igneous Comparison – Rhyolite ID, Elevation Radioelement Content, Th:U Ratio, Heat Production (A) and Luminosity (ε_v)

ID #	Elev. (ft)	U (ppm)	Th (ppm)	K (pct)	Th/U	A (μWm^{-3})	ε_v ($mg^{-1}s^{-1}$)
HS129	4921	13.9	33.4	5.9	2.40	7.71	1.73E+03
HS102	382	16.0	18.7	8.6	1.17	7.42	1.72E+03
HS065	1127	15.7	17.0	8.9	1.08	7.22	1.68E+03
HS114	1127	14.7	16.6	11.1	1.13	7.13	1.66E+03
HS024	3526	14.0	14.2	13.3	1.01	6.97	1.63E+03
HS113	1127	13.9	16.4	11.5	1.18	6.92	1.61E+03
HS034	3526	12.2	19.4	10.2	1.59	6.50	1.49E+03
HS115	1127	13.2	17.8	8.3	1.35	6.46	1.49E+03
HS117	1127	13.9	16.2	7.1	1.17	6.40	1.48E+03
HS103	382	13.5	17.0	6.7	1.26	6.30	1.46E+03
HS100	382	12.7	18.1	6.8	1.43	6.16	1.42E+03
HS105	382	13.5	15.4	6.4	1.14	6.13	1.42E+03
HS112	1127	12.6	14.1	9.4	1.12	6.09	1.42E+03
HS025	3526	10.8	16.6	11.2	1.54	5.95	1.37E+03
HS104	382	11.0	15.6	7.2	1.42	5.48	1.26E+03
HS057	3526	11.6	17.6	3.5	1.52	5.41	1.24E+03
HS056	3526	10.7	15.3	6.4	1.43	5.27	1.21E+03
HS106	382	10.4	15.4	6.0	1.48	5.14	1.18E+03
HS101	382	10.1	13.2	5.3	1.31	4.79	1.11E+03
HS132	4916	6.9	19.5	8.2	2.83	4.67	1.05E+03
HS131	4929	6.2	21.7	6.5	3.50	4.44	9.87E+02
HS127	4913	6.5	17.4	5.4	2.68	4.05	9.10E+02
HS121	1127	8.7	9.7	4.9	1.11	4.02	9.35E+02
HS099	382	6.7	9.1	2.3	1.36	3.07	7.06E+02

Table 37B: SURF RS-230 GRS Survey Igneous Comparison –Phonolite ID, Radioelement Content, Th:U Ratio, Heat Production and Antineutrino Luminosity

ID #	Elev. (ft)	U (ppm)	Th (ppm)	K (pct)	Th/U	A (μWm^{-3})	ε_v ($mg^{-1}s^{-1}$)
Phonolite	3232	10.04	23.61	4.54	2.35	5.56	1.25E+03

*After Corrections

Table 38A: SURF RS-230 GRS Survey - Ellison Formation Comparison – ID, Elevation, Radioelement Content, Th:U Ratio, Heat Production (A), Antineutrino Luminosity ($\mathcal{E}_v$), Rock Classification

ID #	Elev. (ft)	U (ppm)	Th (ppm)	K (pct)	Th/U	A (μWm^{-3})	$\mathcal{E}_v$ ($mg^{-1}s^{-1}$)	Rock Classification
HS023	3526	6	26	5.7	4.3	4.65	1.02E+03	Amphibolite
HS022	3526	6	27.6	3.9	4.6	4.58	9.97E+02	Amphibolite
HS018	3526	5.4	20.8	4.9	3.9	3.94	8.70E+02	Amphibolite
HS026	3526	4.7	23	4.6	4.9	3.88	8.46E+02	Amphibolite
HS019	3526	5.4	20.6	4.4	3.8	3.87	8.53E+02	Amphibolite
HS017	3526	5.1	20.8	4.5	4.1	3.81	8.37E+02	Amphibolite
HS020	3526	4.4	22.6	4.6	5.1	3.75	8.17E+02	Amphibolite
HS039	3526	12.4	51.7	6	4.2	8.79	1.92E+03	Pyrotitic Phyllite
HS040	3526	8.2	25	4.1	3.0	5.06	1.12E+03	Pyrotitic Phyllite
HS055	3526	8.9	18.9	5.4	2.1	4.91	1.11E+03	Phyllite
HS094	382	7.8	21	5.8	2.7	4.79	1.08E+03	Phyllite
HS096	382	6	24.3	5.6	4.1	4.50	9.90E+02	Phyllite
HS095	382	6.4	21.8	5.3	3.4	4.38	9.71E+02	Phyllite
HS092	382	7.4	18.3	4.7	2.5	4.32	9.72E+02	Phyllite
HS027	3526	5.2	24.8	5.8	4.8	4.32	9.44E+02	Phyllite
HS093	382	5.8	22	5.4	3.8	4.22	9.33E+02	Phyllite
HS046	3526	7.1	14.9	2.4	2.1	3.69	8.33E+02	Quartzite rich Phyllite
HS048	3526	6.5	12.6	2.8	1.9	3.36	7.62E+02	Phyllite
HS052	3526	4.7	12.2	3.3	2.6	2.83	6.35E+02	Phyllite
HS052a	3526	4.5	11.3	3.5	2.5	2.72	6.11E+02	Phyllite
HS050	3526	4.1	12.2	3.4	3.0	2.66	5.94E+02	Phyllite
HS044	3526	4.3	11.2	2	2.6	2.48	5.54E+02	Phyllite
HS051	3526	4.3	10.6	2	2.5	2.43	5.45E+02	Phyllite
HS091	382	3.7	10.5	1.7	2.8	2.20	4.90E+02	Phyllite
HS045	3526	3.4	8.3	1.2	2.4	1.87	4.19E+02	Phyllite
HS053	3526	7.9	8.3	2.6	1.1	3.40	7.90E+02	Schist
HS038	3526	5.8	12.3	3.8	2.1	3.23	7.32E+02	Schist
HS054	3526	6.2	8.2	2.6	1.3	2.87	6.63E+02	Schist
HS047	3526	3.6	6.2	1.6	1.7	1.80	4.11E+02	Quartzite rich Schist

Table 38B: SURF RS-230 GRS Survey - Yates Formation Comparison – ID, Elevation, Radioelement Content, Th:U Ratio, Heat Production (A), Antineutrino Luminosity ($\mathcal{E}_v$), Rock Classification

ID #	Elev. (ft)	U (ppm)	Th (ppm)	K (pct)	Th/U	A (μWm^{-3})	$\mathcal{E}_v$ ($mg^{-1}s^{-1}$)	Rock Classification
HS006	3526	5	30.8	6.4	6.2	4.83	1.04E+03	Amphibolite
HS008	3526	5.7	24.2	5.8	4.2	4.42	9.72E+02	Amphibolite
HS016	3526	4.8	25.1	5.5	5.2	4.19	9.11E+02	Amphibolite
HS003	3526	5.6	20.7	5.2	3.7	4.03	8.91E+02	Amphibolite
HS010	3526	5.6	21.1	4.2	3.8	3.95	8.71E+02	Amphibolite
HS005	3526	5.8	20	4.3	3.4	3.93	8.70E+02	Amphibolite
HS014	3526	4	20.6	5.9	5.2	3.61	7.90E+02	Amphibolite
HS007	3526	4.9	19.7	3.9	4.0	3.59	7.88E+02	Amphibolite
HS004	3526	4.3	16.3	2.3	3.8	2.94	6.45E+02	Amphibolite
HS002	3526	2.8	16.3	2.4	5.8	2.49	5.37E+02	Amphibolite
HS001	3526	3.4	10.6	1.5	3.1	2.09	4.64E+02	Amphibolite
HS109	382	7.2	10.1	3.1	1.4	3.39	7.81E+02	Phyllite
HS104a	382	5.6	7.9	2.1	1.4	2.61	6.00E+02	Phyllite
HS009	3526	3.3	13.2	3.4	4.0	2.50	5.51E+02	Phyllite
HS012	3526	2.5	12.5	3.4	5.0	2.19	4.80E+02	Phyllite
HS108	382	3.9	5.1	2.4	1.3	1.89	4.37E+02	Phyllite
HS107	382	3	5.4	4.3	1.8	1.85	4.26E+02	Phyllite
HS110	382	3.1	4.4	2.2	1.4	1.56	3.61E+02	Phyllite
HS062	1127	1.8	2.8	0.7	1.6	0.86	1.98E+02	Phyllite
HS060	1127	2.2	1.1	0.5	0.5	0.82	1.94E+02	Phyllite
HS059	1127	1.6	1.9	0.7	1.2	0.73	1.68E+02	Phyllite
HS061	1127	1.4	2.1	1	1.5	0.72	1.65E+02	Phyllite
HS058a	1127	1.2	1.1	1.1	0.9	0.58	1.37E+02	Phyllite

Table 38C: SURF RS-230 GRS Survey - Poorman Formation Comparison – ID, Elevation, Radioelement Content, Th:U Ratio, Heat Production (A), Antineutrino Luminosity ($\mathcal{E}_v$), Rock Classification

ID #	Elev. (ft)	U (ppm)	Th (ppm)	K (pct)	Th/U	A (μWm^{-3})	$\mathcal{E}_v$ ($mg^{-1}s^{-1}$)	Rock Classification
HS085	1127	21.7	9.9	3.2	0.5	7.82	1.86E+03	Phyllite
HS064	1127	15.7	17	8.9	1.1	7.22	1.68E+03	Phyllite
HS090	382	17.1	16.1	5.1	0.9	7.15	1.67E+03	Phyllite
HS058	3526	13.3	15.2	6.3	1.1	6.05	1.40E+03	Phyllite

Table 38C: Poorman Cont.

ID #	Elev. (ft)	U (ppm)	Th (ppm)	K (pct)	Th/U	A (μWm^{-3})	ε_v ($mg^{-1}s^{-1}$)	Rock Classification
HS036	3526	10	26.5	6.4	2.7	5.99	1.34E+03	Phyllite
HS031	3526	6.7	28.5	5.3	4.3	5.03	1.10E+03	Phyllite
HS037	3526	5.9	26.6	5.9	4.5	4.69	1.03E+03	Phyllite
HS078	1127	11.1	10.3	3.6	0.9	4.66	1.09E+03	Phyllite
HS086	1127	6.9	21.9	4.4	3.2	4.44	9.85E+02	Phyllite
HS118	1127	10.6	8.6	3.6	0.8	4.36	1.02E+03	Phyllite Pyrrhotitic
HS033	3526	9.2	12.4	2.8	1.3	4.16	9.58E+02	Phyllite
HS068	1127	10.2	8.3	2.8	0.8	4.13	9.66E+02	Phyllite
HS075	1127	9	11.1	3.7	1.2	4.10	9.47E+02	Phyllite Pyrrhotitic
HS032	3526	6.1	22.1	3.3	3.6	4.09	8.99E+02	Phyllite
HS084	1127	9.8	8.3	2.8	0.8	4.00	9.37E+02	Phyllite
HS083	1127	9.3	8.4	3.2	0.9	3.90	9.12E+02	Phyllite
HS071	1127	9	8.2	4.1	0.9	3.90	9.11E+02	Phyllite
HS072	1127	8.6	9.1	3.6	1.1	3.79	8.82E+02	Phyllite
HS063	1127	8.4	10.3	3	1.2	3.77	8.71E+02	Phyllite
HS066	1127	8.5	8.7	3.3	1.0	3.70	8.60E+02	Phyllite
HS081	1127	8.6	8.6	3.1	1.0	3.70	8.61E+02	Phyllite
HS070	1127	8	8.9	3.8	1.1	3.62	8.40E+02	Phyllite
HS087	1127	8.8	7.3	2.5	0.8	3.58	8.38E+02	Phyllite
HS088	1127	8.1	8.1	3.2	1.0	3.51	8.18E+02	Phyllite
HS074	1127	6.4	13.1	3.3	2.0	3.42	7.76E+02	Phyllite
HS030	3526	5.6	15.7	3.3	2.8	3.40	7.59E+02	Phyllite
HS063a	1127	6.2	11.9	3.3	1.9	3.26	7.42E+02	Phyllite
HS073	1127	7	9.3	3	1.3	3.26	7.51E+02	Phyllite
HS067	1127	6.6	9.8	3	1.5	3.17	7.29E+02	Phyllite
HS029	3526	4.6	14.6	4.1	3.2	3.09	6.88E+02	Phyllite
HS028	3526	3.2	13.5	2.6	4.2	2.40	5.26E+02	Phyllite
HS077	1127	5.2	7	1.9	1.3	2.39	5.50E+02	Phyllite
HS076	1127	4.8	5.3	2.1	1.1	2.15	4.98E+02	Phyllite
HS079	1127	4	6.7	2.2	1.7	2.03	4.65E+02	Phyllite
HS043	3526	2.9	8.1	3.1	2.8	1.91	4.30E+02	Phyllite
HS111	1127	11.3	10.9	4.6	1.0	4.88	1.14E+03	Mica Schist
HS035	3526	7.4	23.4	4.6	3.2	4.74	1.05E+03	Schist

Table 38D: SURF RS-230 GRS Survey - Northwestern Formation Comparison – ID, Elevation, Radioelement Content, Th:U Ratio, Heat Production (A), Antineutrino Luminosity ($\mathcal{E}_v$), Rock Classification

ID #	Elev. (ft)	U (ppm)	Th (ppm)	K (pct)	Th/U	A (μWm^{-3})	$\mathcal{E}_v$ ($mg^{-1}s^{-1}$)	Rock Classification
HS021	3526	5.3	19.9	3.8	3.8	3.71	8.18E+02	Amphibolite
HS013	3526	4.5	18	4.8	4.0	3.42	7.55E+02	Amphibolite
HS123	4861	5.1	15.6	4.6	3.1	3.38	7.55E+02	Amphibolite
HS011	3526	2.8	14.3	3	5.1	2.39	5.20E+02	Amphibolite
HS015	3526	7	18.3	5.4	2.6	4.28	9.62E+02	Phyllite
HS135	5124	6.4	16.8	4.2	2.6	3.84	8.60E+02	Phyllite
HS136	5324	4.9	16.1	3.2	3.3	3.21	7.11E+02	Phyllite
HS124	5121	5.3	10.8	4.9	2.0	3.08	7.00E+02	Phyllite
HS125	5121	4.8	10.5	4.4	2.2	2.84	6.45E+02	Phyllite

Table 38E: SURF RS-230 GRS Survey - Homestake Formation Comparison – ID, Elevation, Radioelement Content, Th:U Ratio, Heat Production (A), Antineutrino Luminosity ($\mathcal{E}_v$), Rock Classification

ID #	Elev. (ft)	U (ppm)	Th (ppm)	K (pct)	Th/U	A (μWm^{-3})	$\mathcal{E}_v$ ($mg^{-1}s^{-1}$)	Rock Classification
HS097	382	9.3	13.5	3.9	1.5	4.41	1.01E+03	Phyllite
HS069	1127	8.7	9.1	2.4	1.0	3.69	8.57E+02	Phyllite
HS122	1127	4.5	7.1	2.0	1.6	2.19	5.03E+02	Phyllite
HS119	1127	13.3	9.6	3.7	0.7	5.28	1.24E+03	Schist
HS120	1127	10.0	12.0	4.0	1.2	4.51	1.04E+03	Schist
HS082	1127	9.6	6.9	2.4	0.7	3.78	8.88E+02	Schist
HS116	1127	8.9	6.5	2.9	0.7	3.59	8.43E+02	Schist
HS098	382	4.9	8.2	3.3	1.7	2.56	5.85E+02	Schist
HS080	1127	4.1	7.9	2.2	1.9	2.16	4.91E+02	Schist
HS089	382	3.1	6.3	1.4	2.0	1.63	3.70E+02	Schist
HS042	3526	2.3	7.3	1.0	3.2	1.43	3.16E+02	Granulite Schist
HS097a	382	2.4	5.6	1.3	2.3	1.35	3.04E+02	Schist
HS041	3526	1.5	6.3	1.7	4.2	1.18	2.59E+02	Granulite Schist

Table 38F: SURF RS-230 GRS Survey - Flagrock Formation Comparison – ID, Elevation, Radioelement Content, Th:U Ratio, Heat Production (A), Antineutrino Luminosity ($\mathcal{E}_v$), Rock Classification

ID #	Elev. (ft)	U (ppm)	Th (ppm)	K (pct)	Th/U	A (μWm^{-3})	$\mathcal{E}_v$ ($mg^{-1}s^{-1}$)	Rock Classification
HS130	4914	12.4	6.5	0.5	0.5	4.39	1.04E+03	Phyllite
HS134	4911	10.9	3.2	0.3	0.3	3.63	8.68E+02	Phyllite
HS128	4914	4.3	16.9	6.2	3.9	3.43	7.60E+02	Phyllite
HS133	5142	7.1	2.9	0.6	0.4	2.48	5.89E+02	Phyllite

Appendix C

Plotted Th:U, Th:K, and U:K ratios for

Igneous, Metamorphic and Sedimentary samples in the Black Hills

Figure 48A: RS-230 GRS Survey Igneous Rocks Ratios Th Vs. U

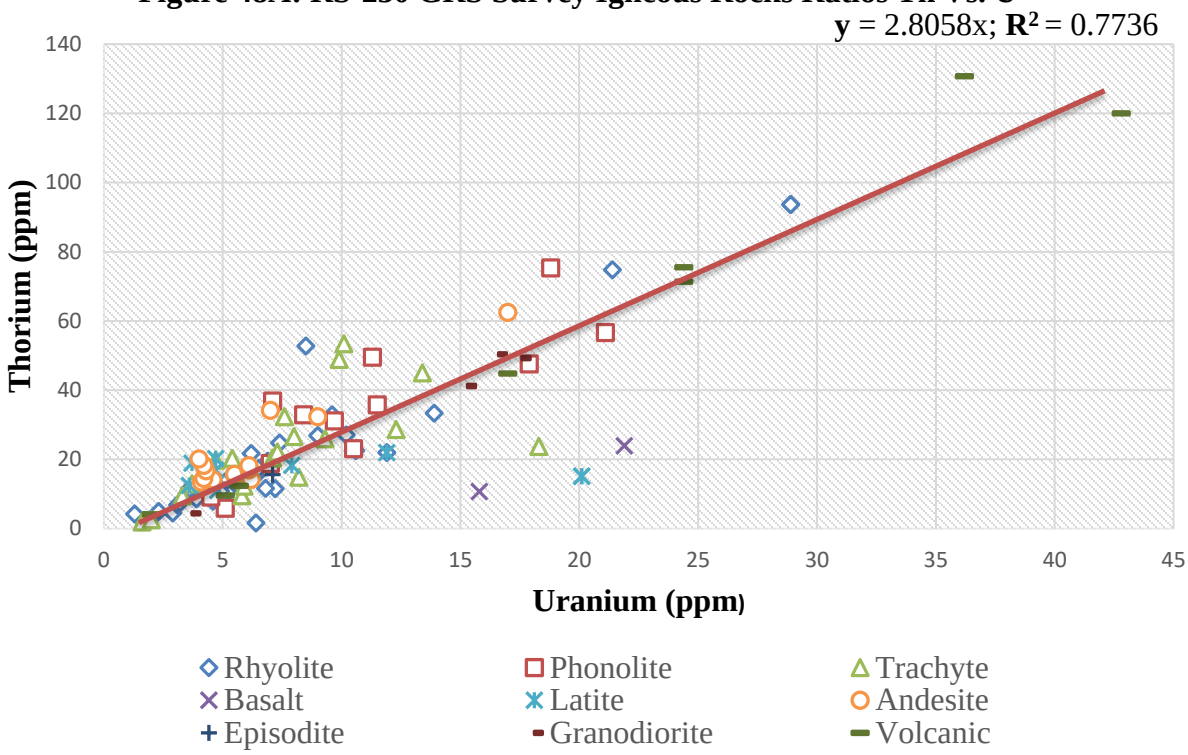

Figure 48B: RS-230 GRS Survey Igneous Rocks Ratios U Vs. K_2O

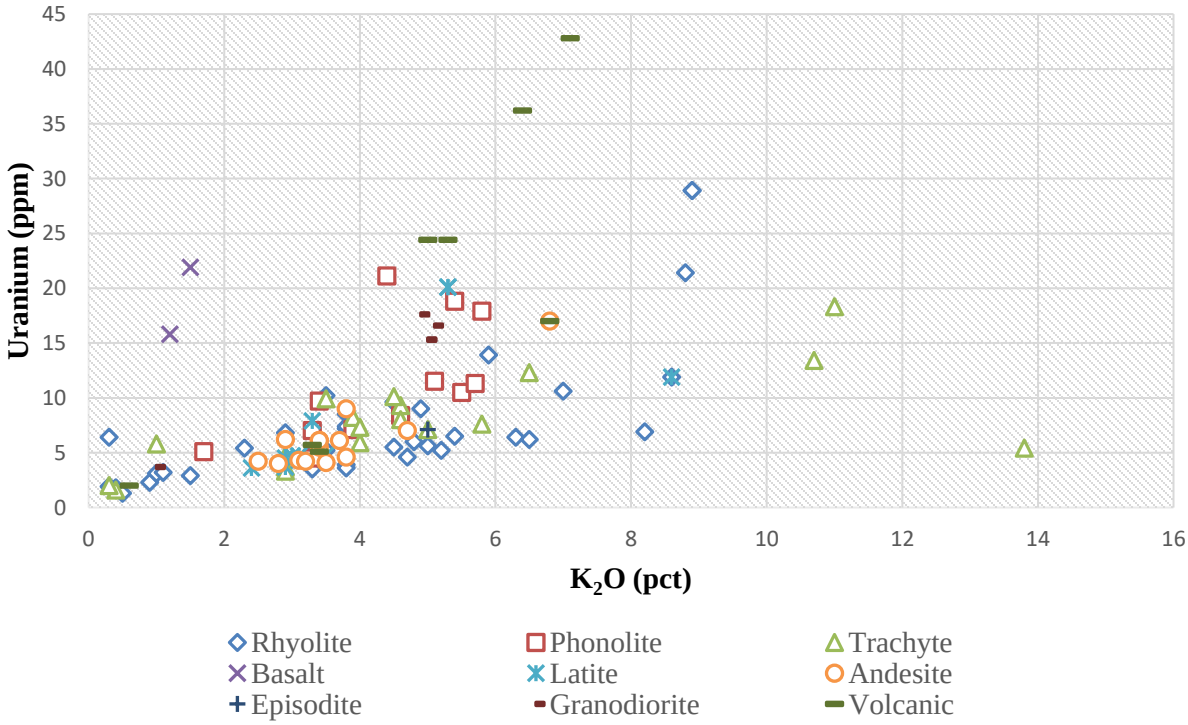

Figure 48C: RS-230 GRS Survey Igneous Rocks Ratios Th Vs. K_2O

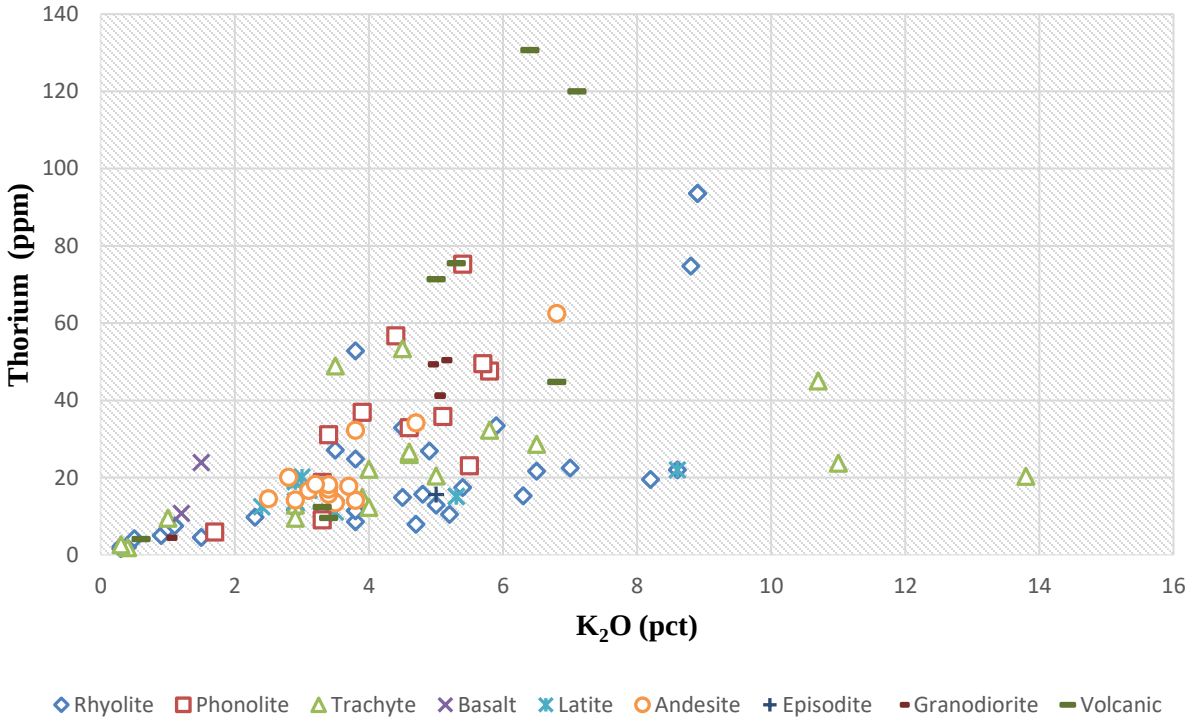

Figure 49A: RS-230 GRS Survey Metamorphic Rocks Ratios Th Vs. U

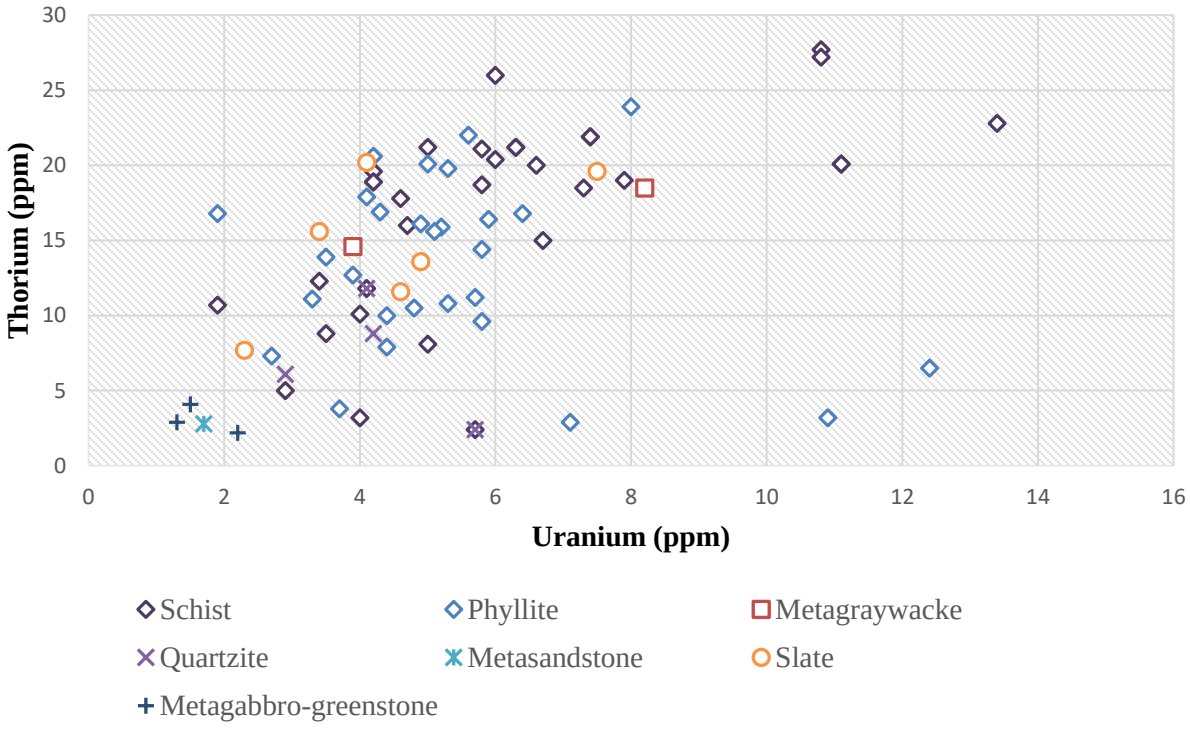

Figure 49A: RS-230 GRS Survey Metamorphic Rocks Ratios U Vs. K_2O

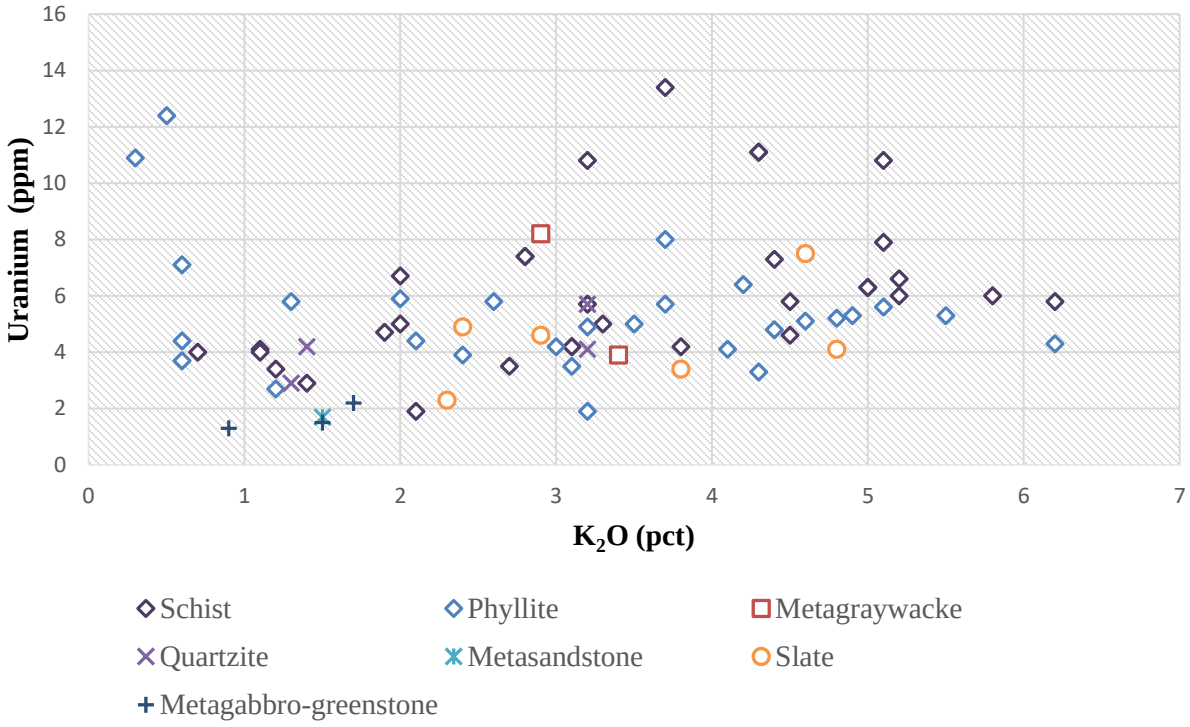

Figure 49C: RS-230 GRS Survey Metamorphic Rocks Ratios Th Vs. K_2O

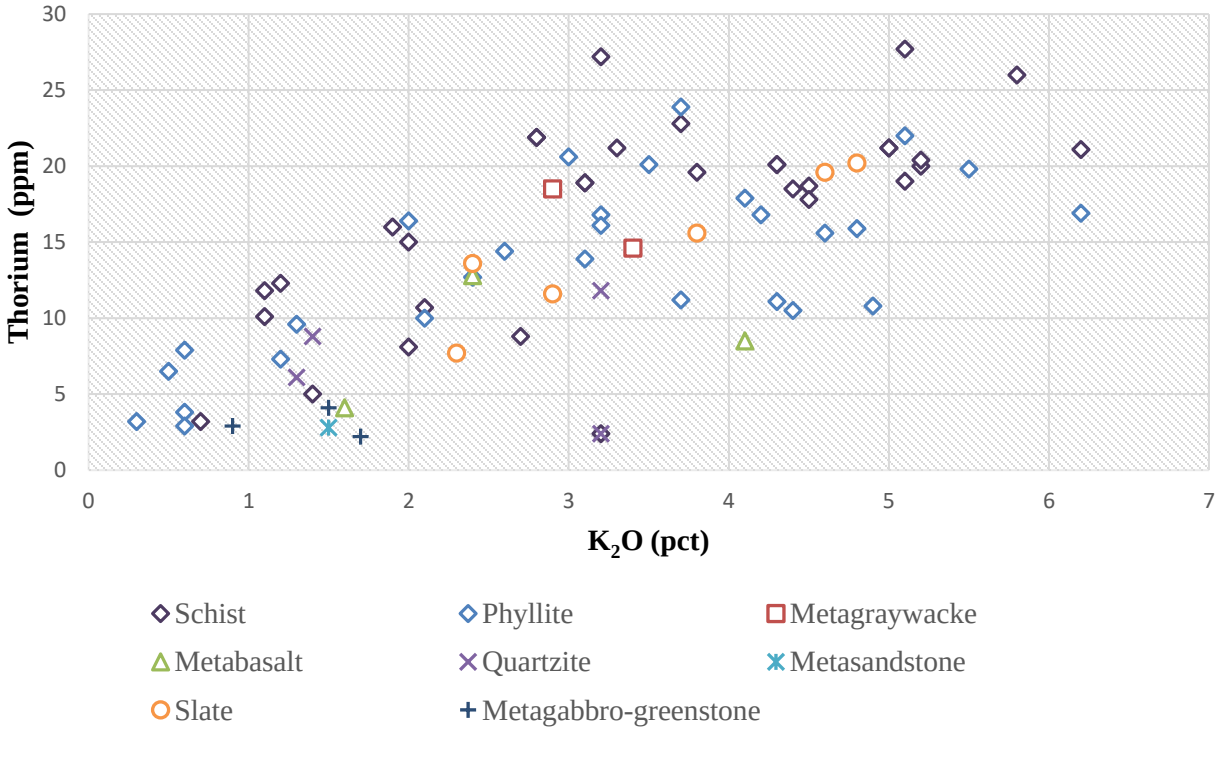

Figure 50A: RS-230 GRS Survey Sedimentary Rocks Ratios U Vs. Th

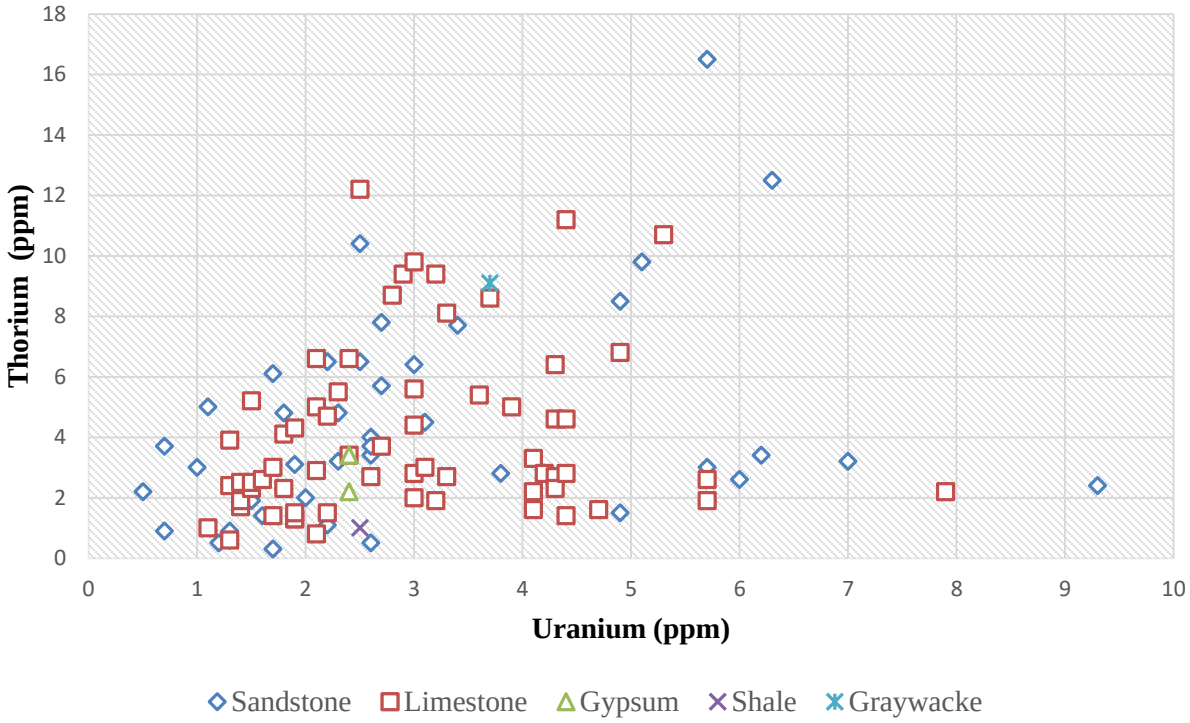

Figure 50B: RS-230 GRS Survey Sedimentary Rocks Ratios U Vs. K_2O

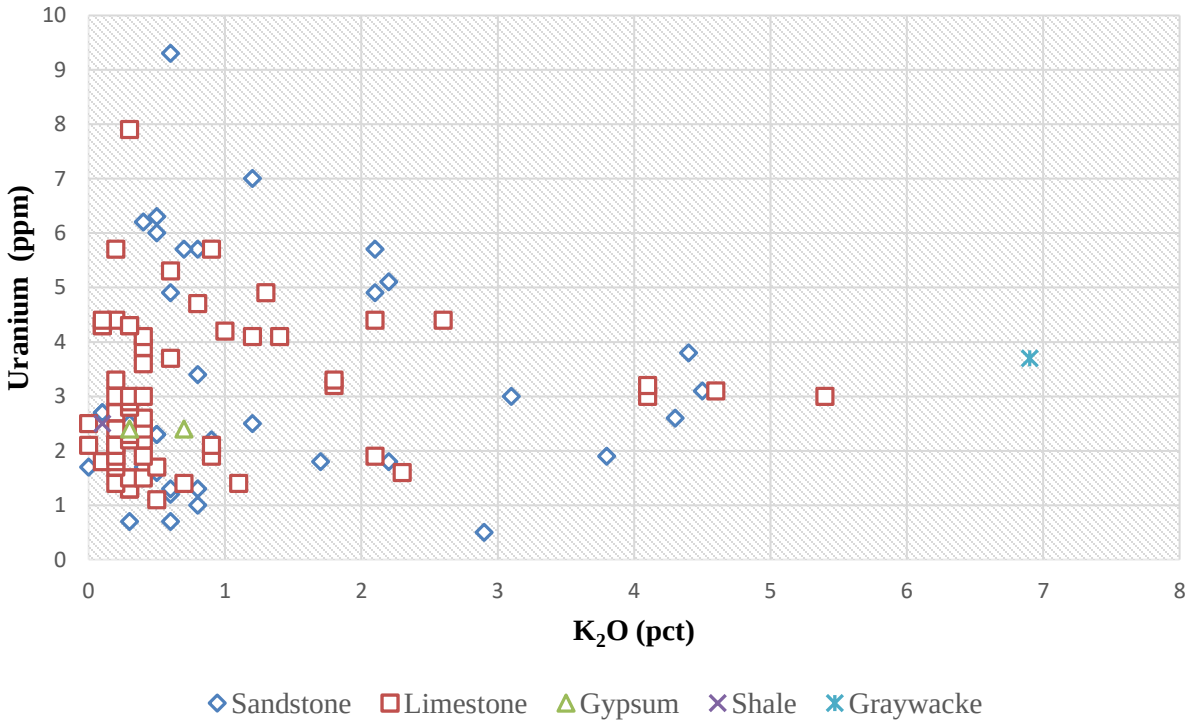

Figure 50C: RS-230 GRS Survey Sedimentary Rocks Ratios Th Vs. K_2O

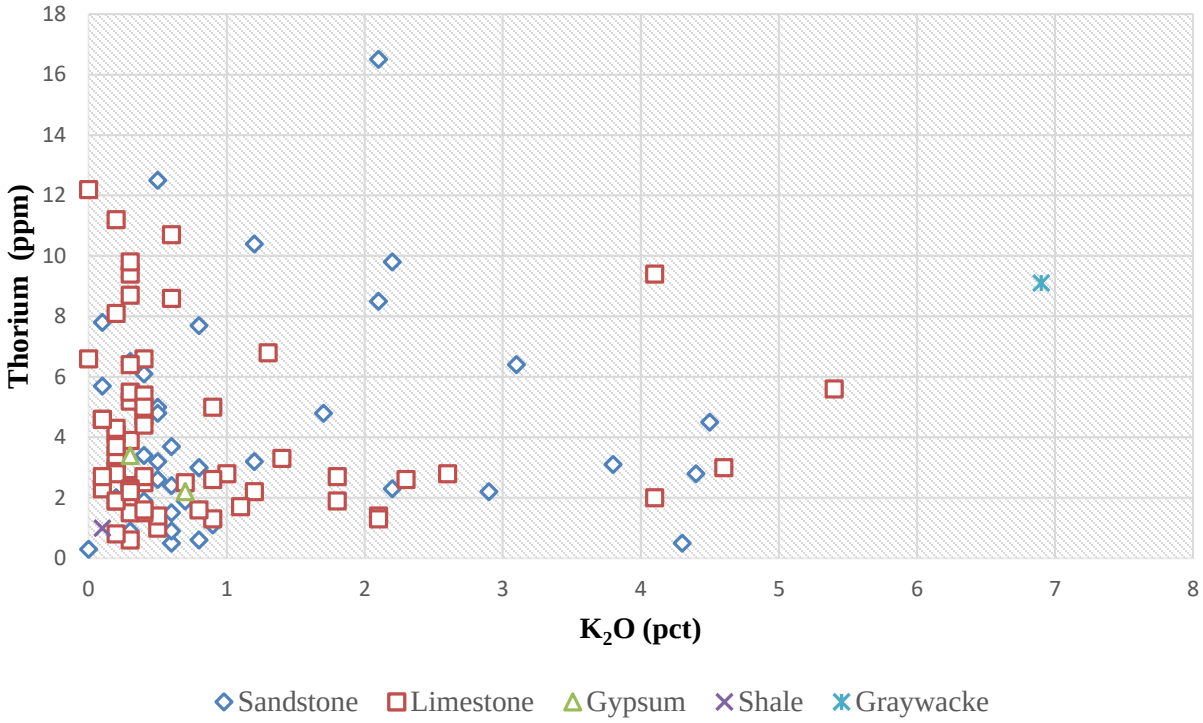

Figure 51A: Ge SED GRS Analysis Igneous Rocks Ratios Th Vs. U

y = 3.0491x; $\mathbf{R^2}$ = 0.7017

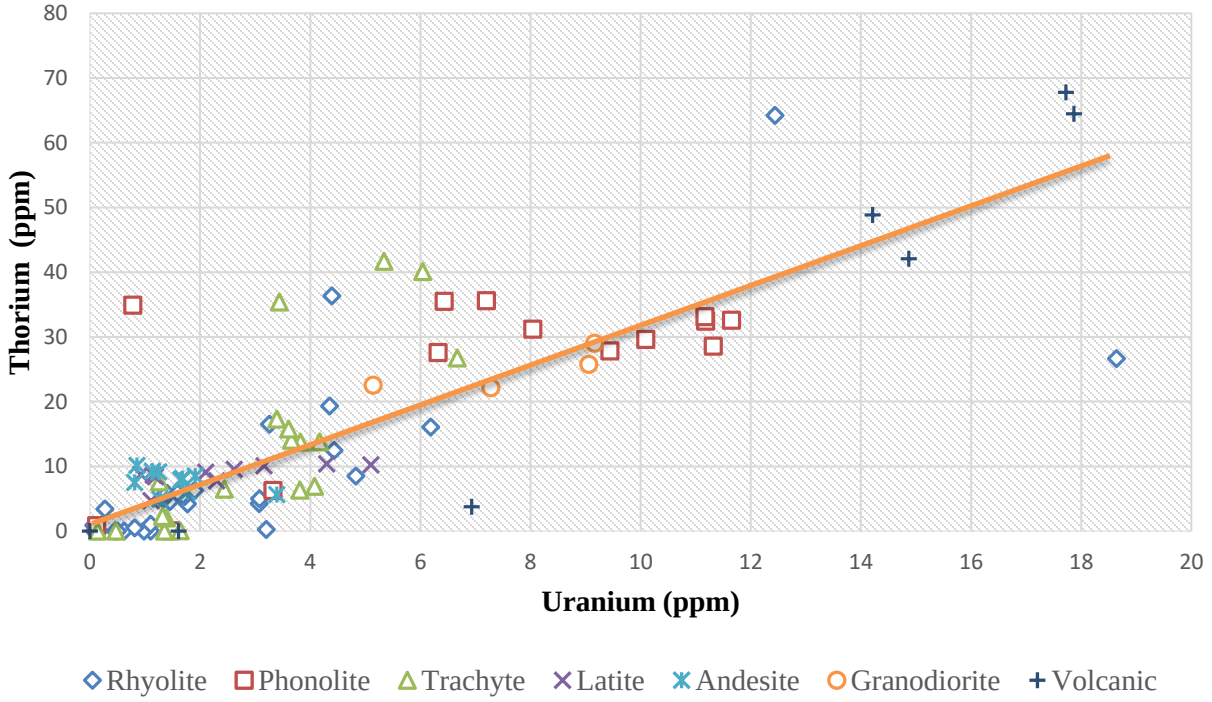

Figure 51B: Ge SED GRS Analysis Igneous Rocks Ratios U Vs. K_2O

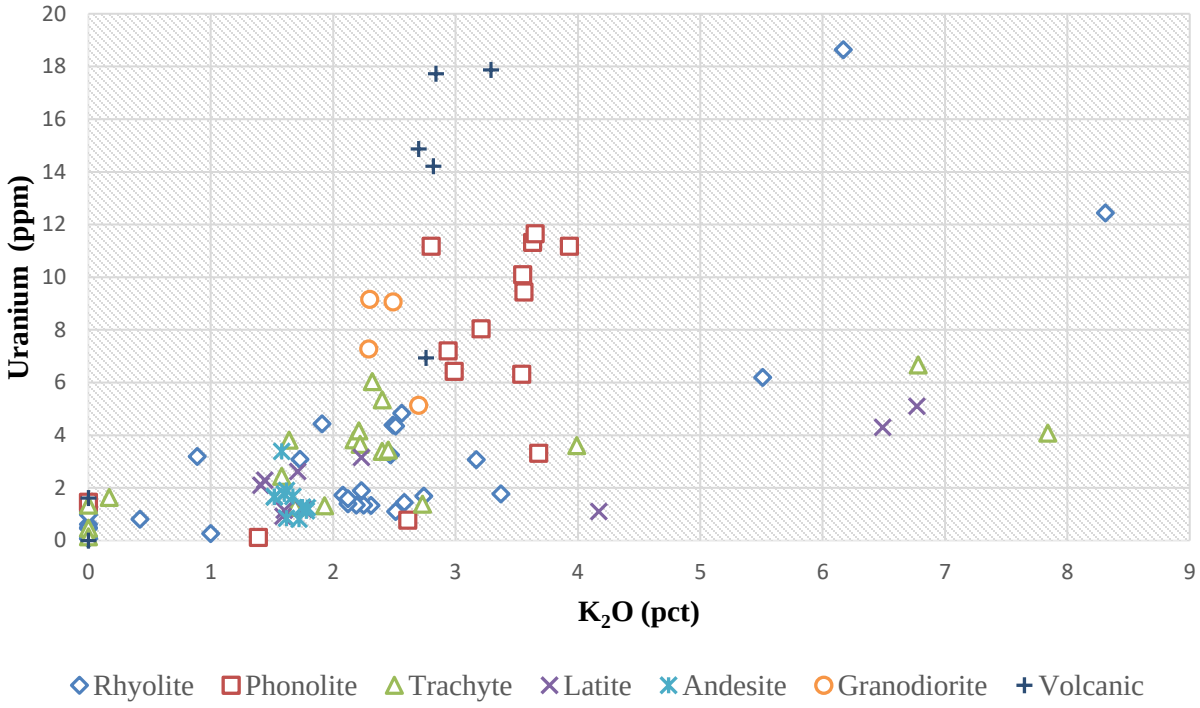

Figure 51C: Ge SED GRS Analysis Igneous Rocks Ratios Th Vs. K_2O

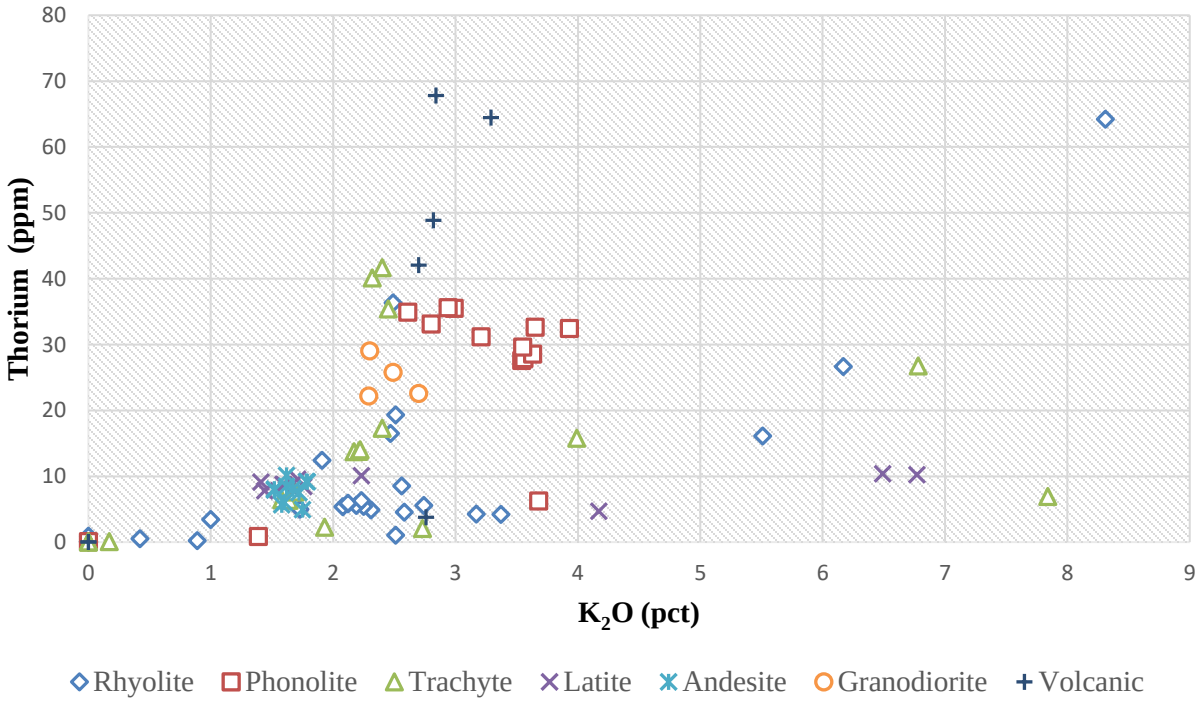

Figure 52A: Ge SED GRS Analysis Metamorphic Rocks Ratios Th Vs. U

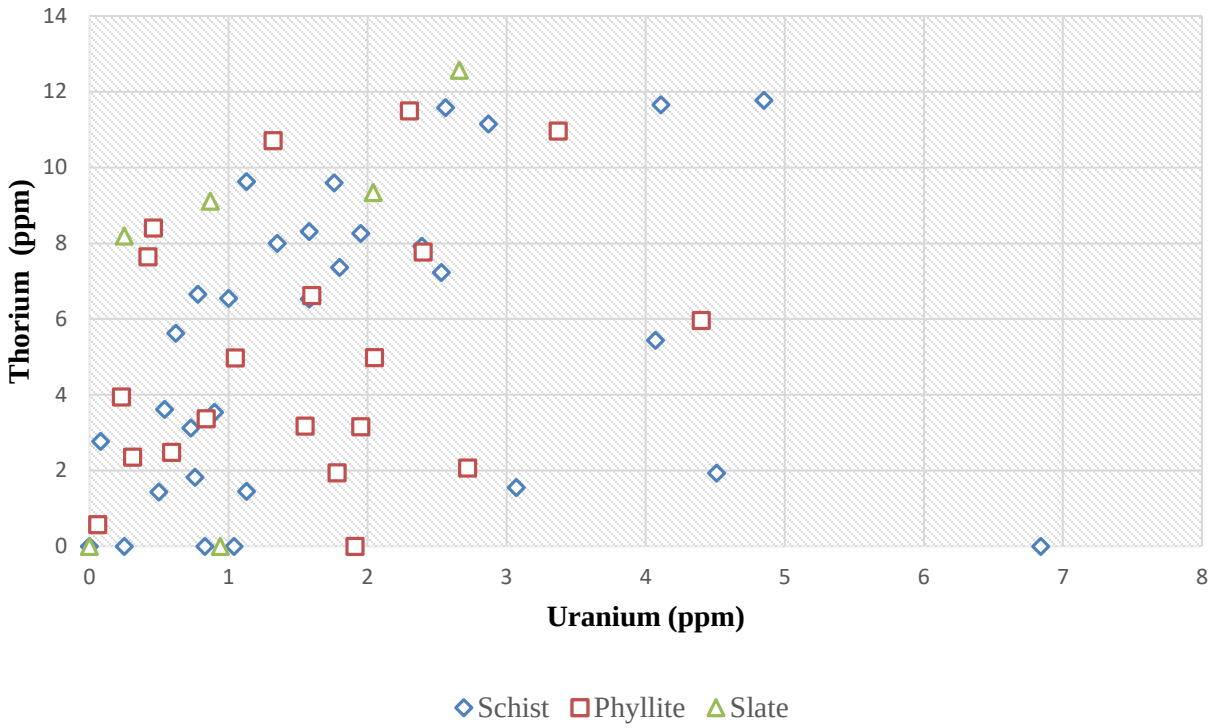

Figure 52B: Ge SED GRS Analysis Metamorphic Rocks Ratios U Vs. K_2O

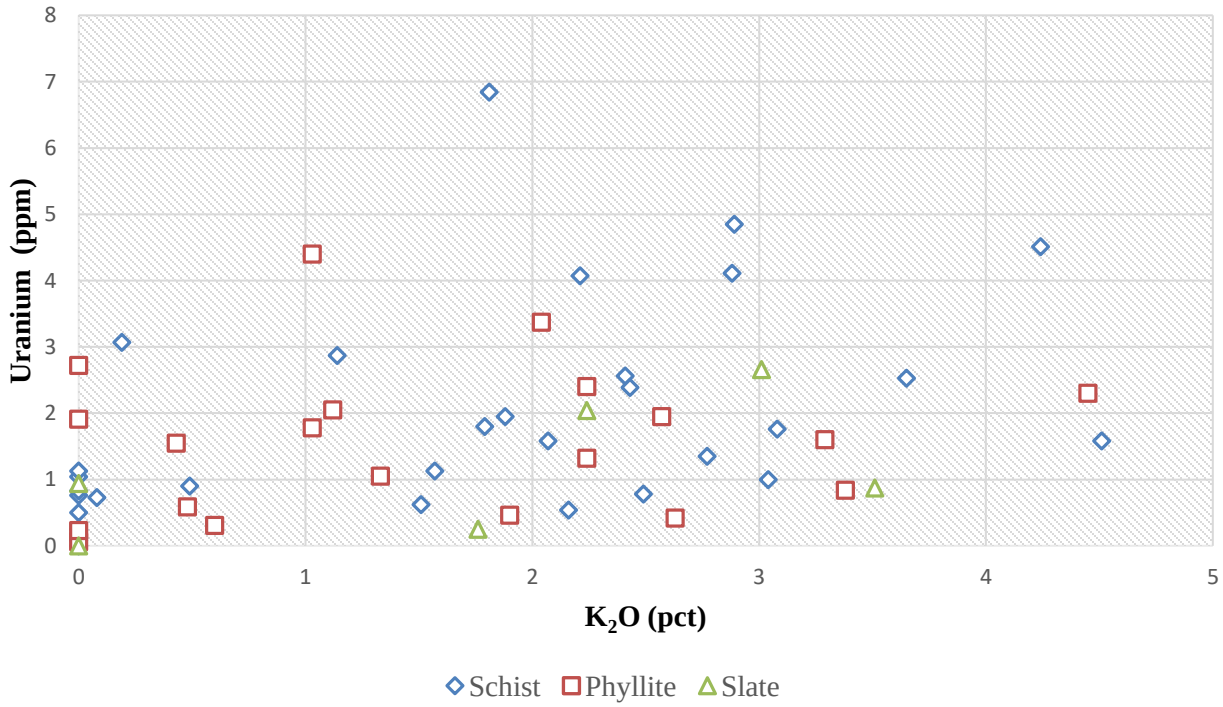

Figure 52C: Ge SED GRS Analysis Metamorphic Rocks Ratios Th Vs. K_2O

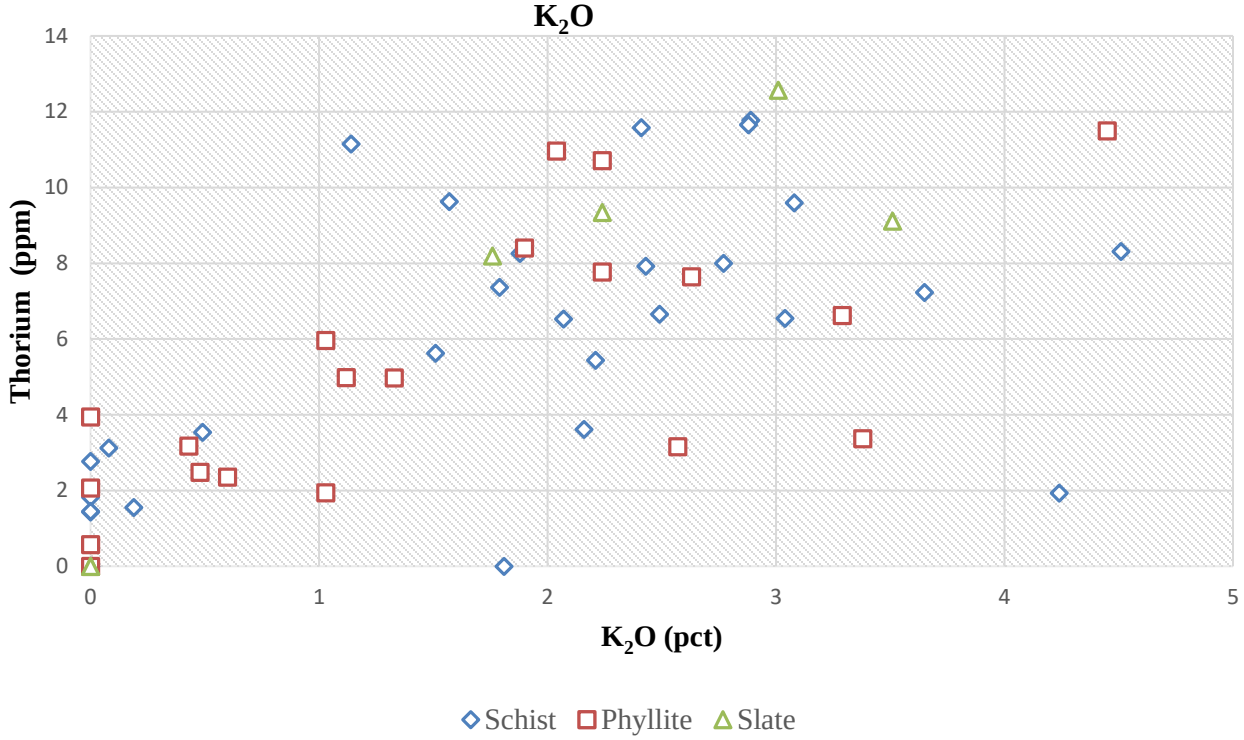

Figure 53A: Ge SED GRS Analysis Sedimentary Rocks Ratios Th Vs. U

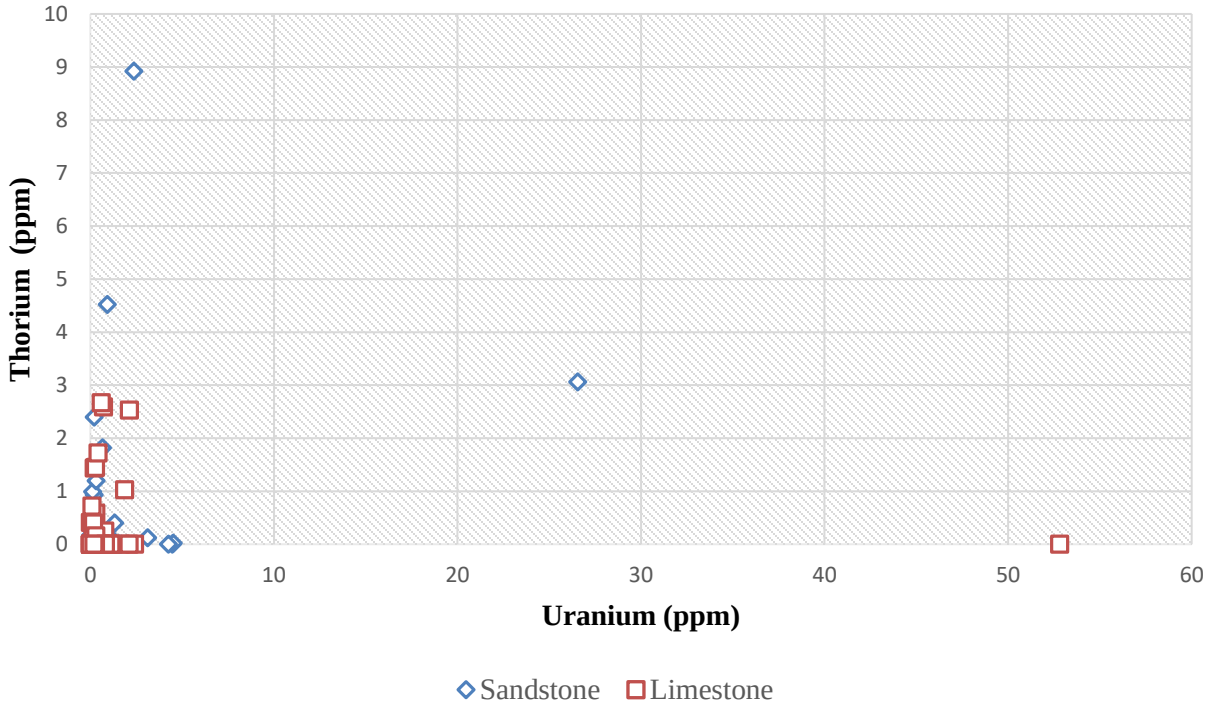

Figure 53B: Ge SED GRS Analysis Sedimentary Rocks Ratios U Vs. K_2O

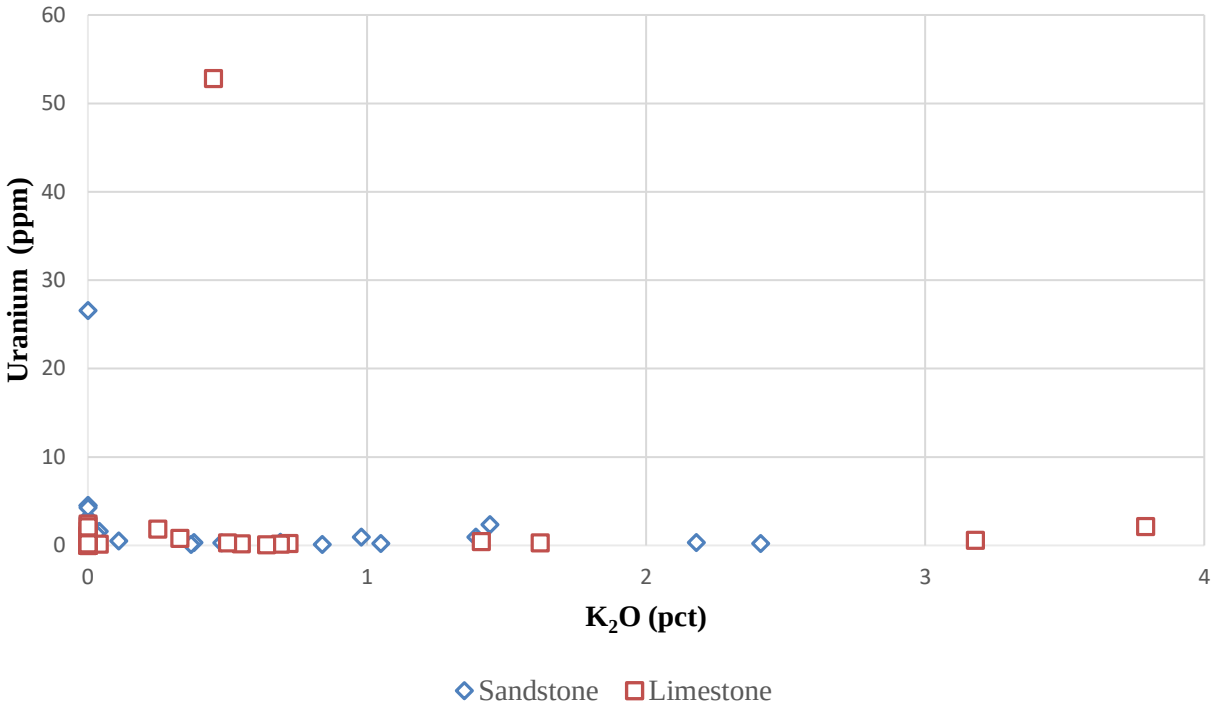

Figure 53C: Ge SED GRS Analysis Sedimentary Rocks Ratios Th Vs. K_2O

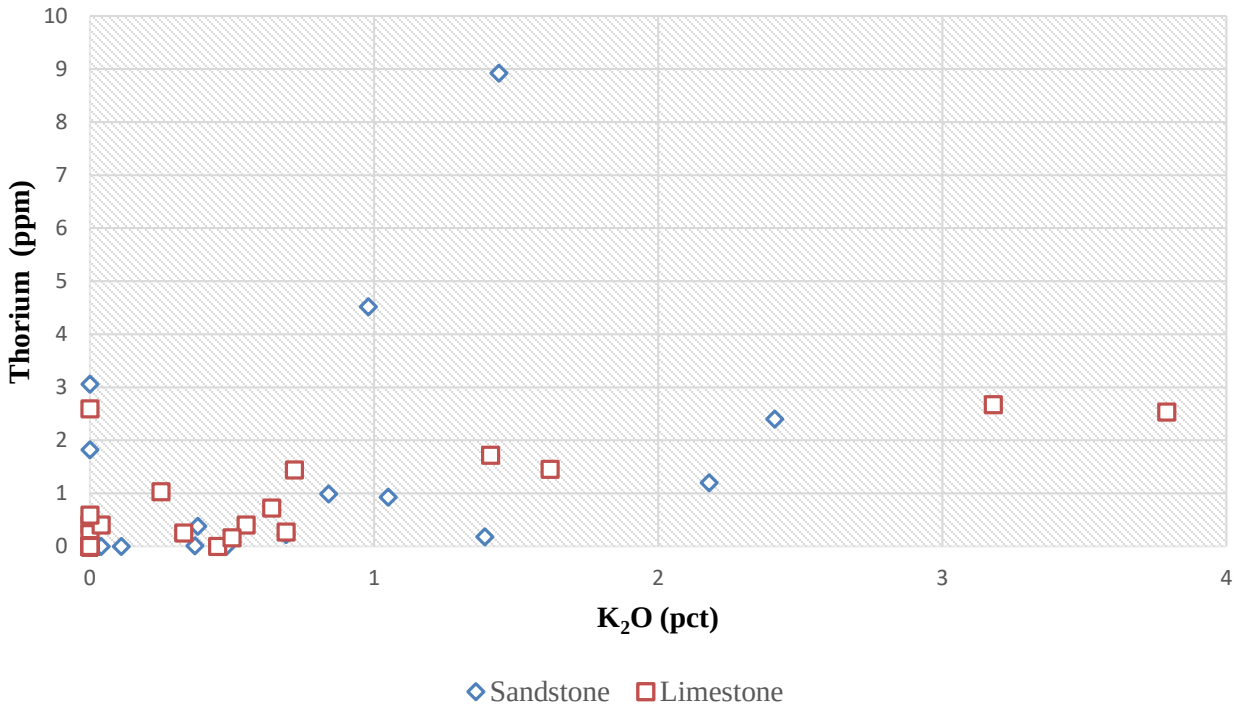

Appendix D

Uranium, Thorium, and Potassium Ratios present in the Homestake Gold Mine

Figure 54A: Homestake Survey 1700 Level Th Vs. U

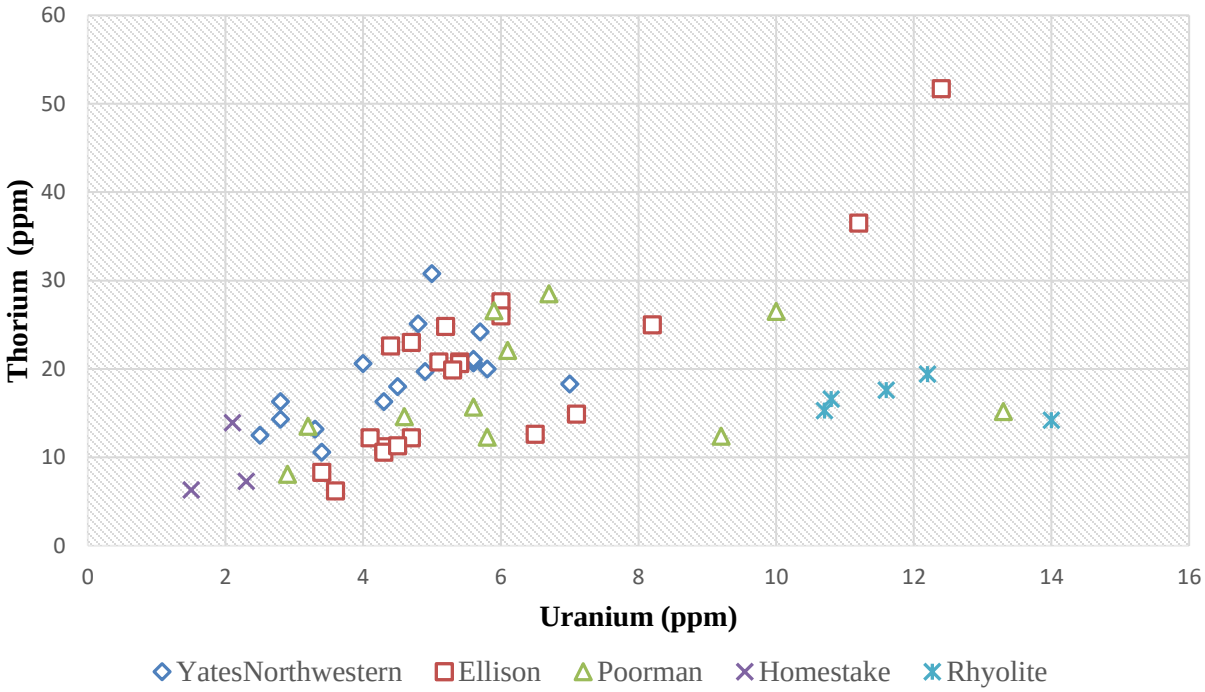

Figure 54B: Homestake Survey 1700 Level U Vs. K_2O

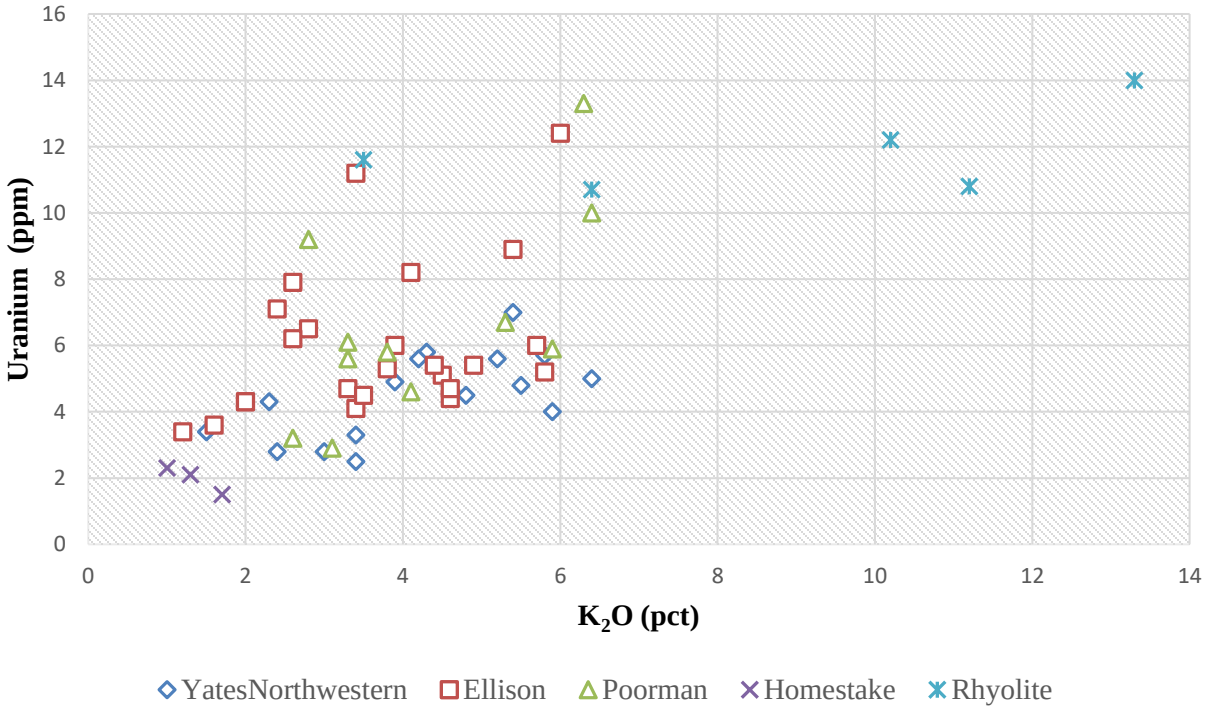

Figure 54C: Homestake Survey 1700 Level Th Vs. K_2O

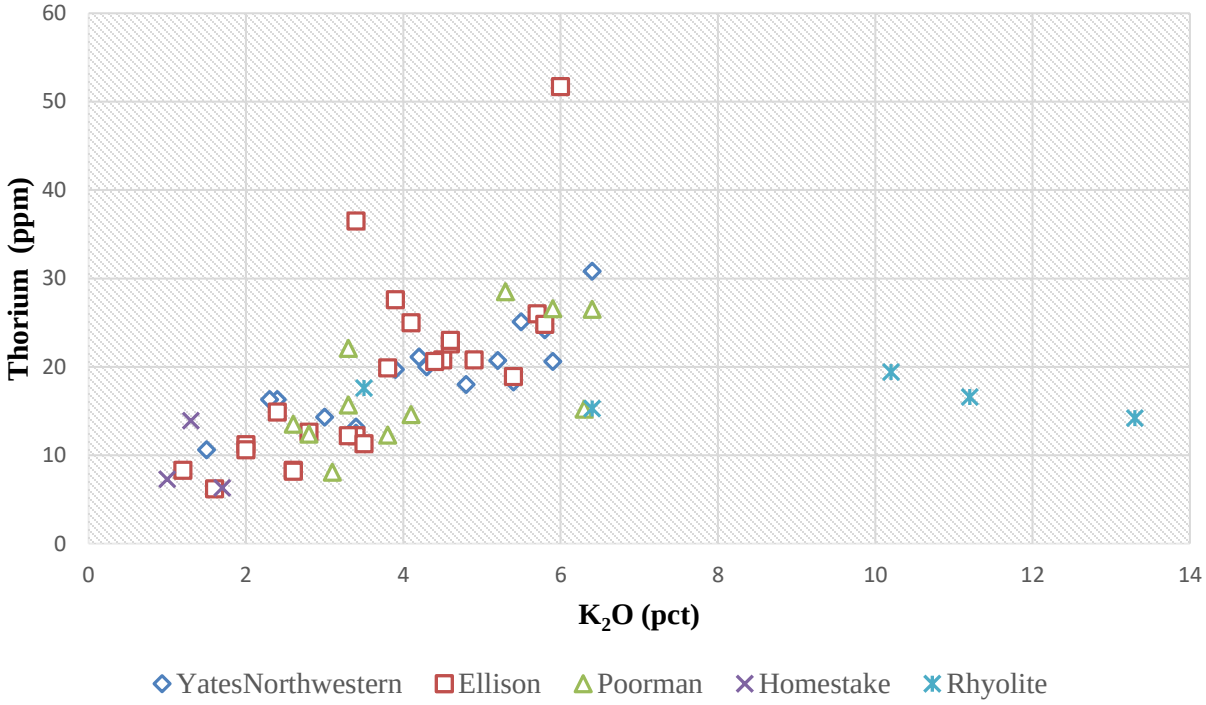

Figure 55A: Homestake Survey 4100 Level Th Vs. U

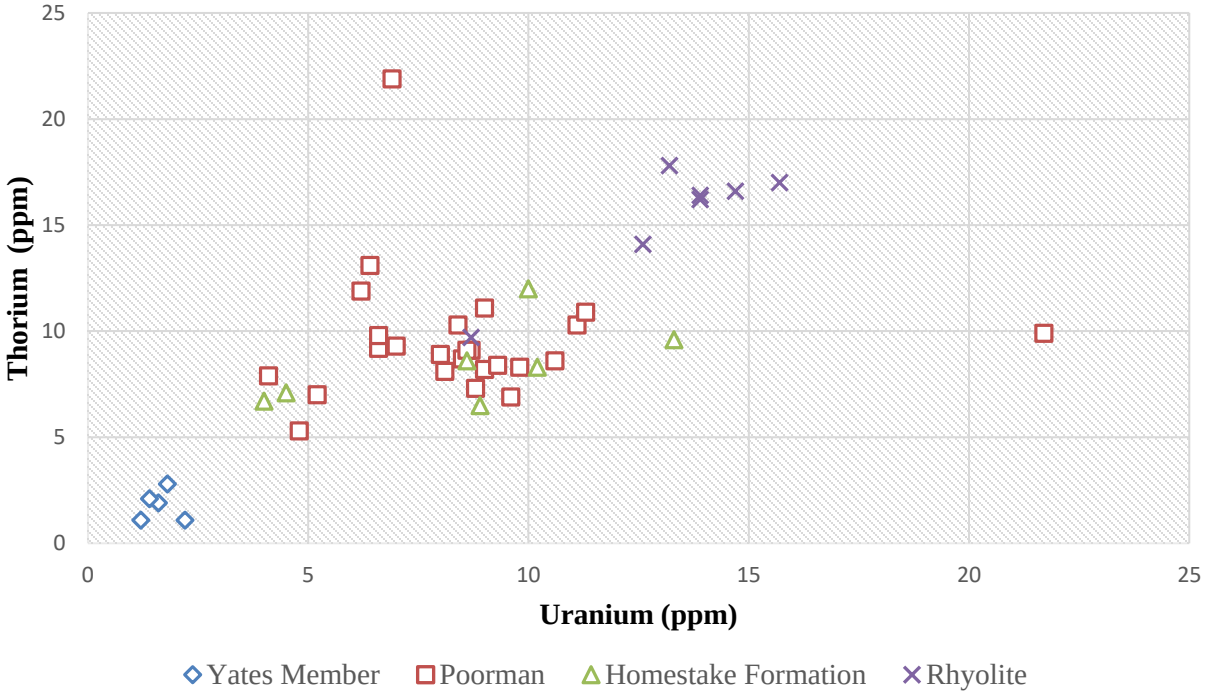

Figure 55B: Homestake Survey 4100 Level U Vs. K_2O

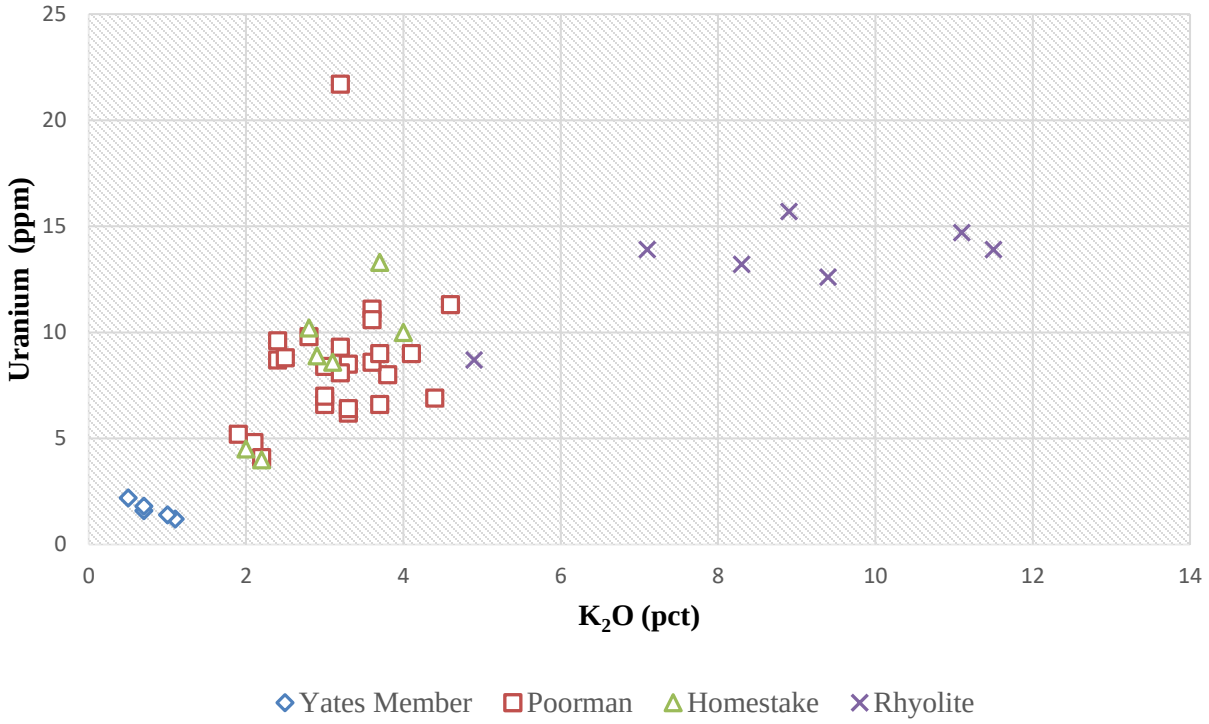

Figure 55C: Homestake Survey 4100 Level Th Vs. K_2O

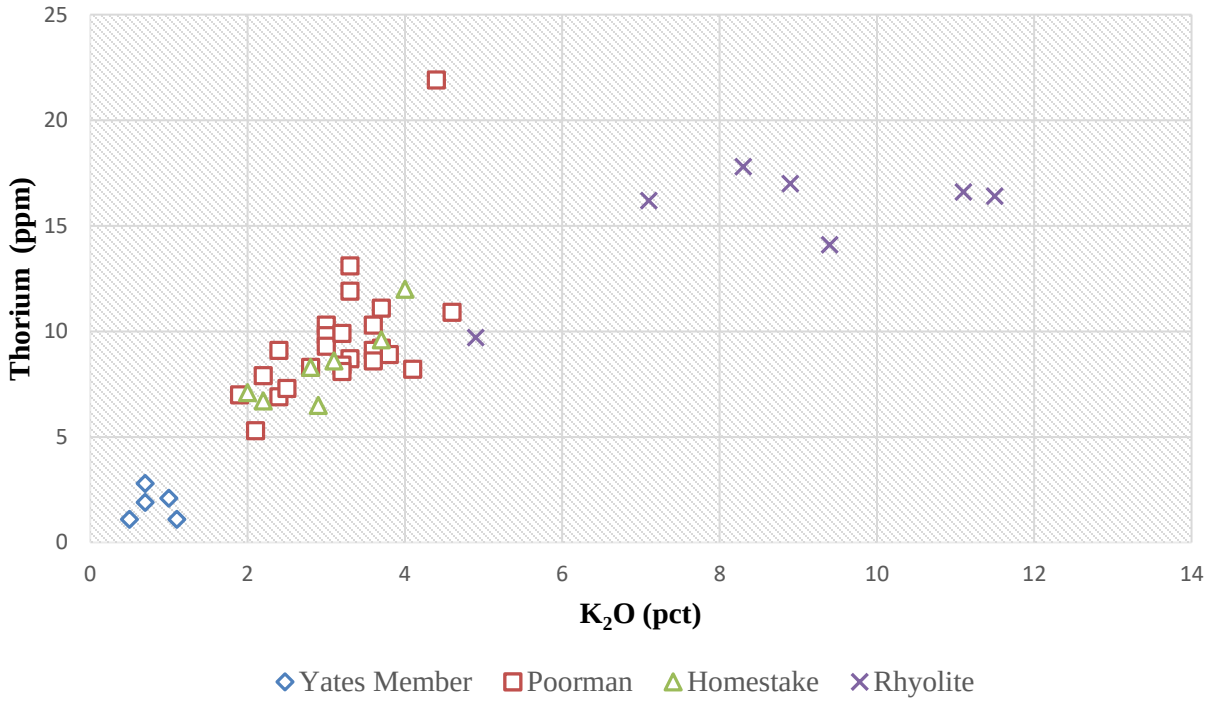

Figure 56A: Homestake Survey 4850 Level Th Vs. U

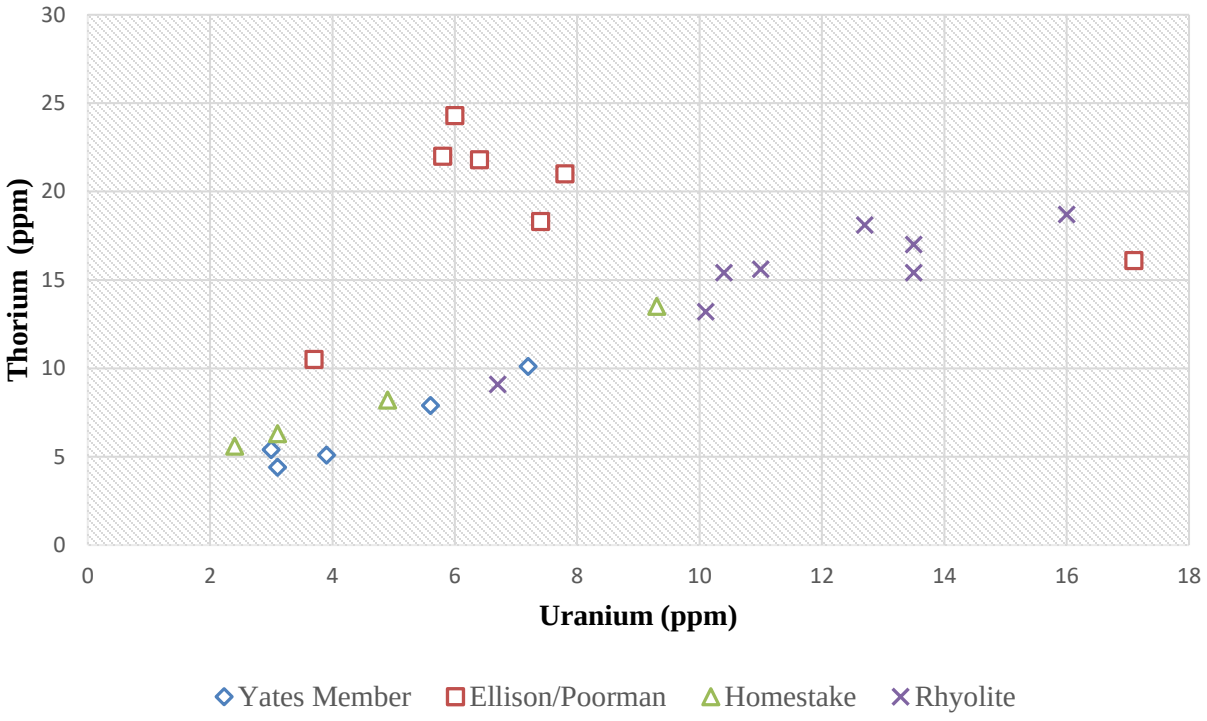

Figure 56B: Homestake Survey 4850 Level U Vs. K_2O

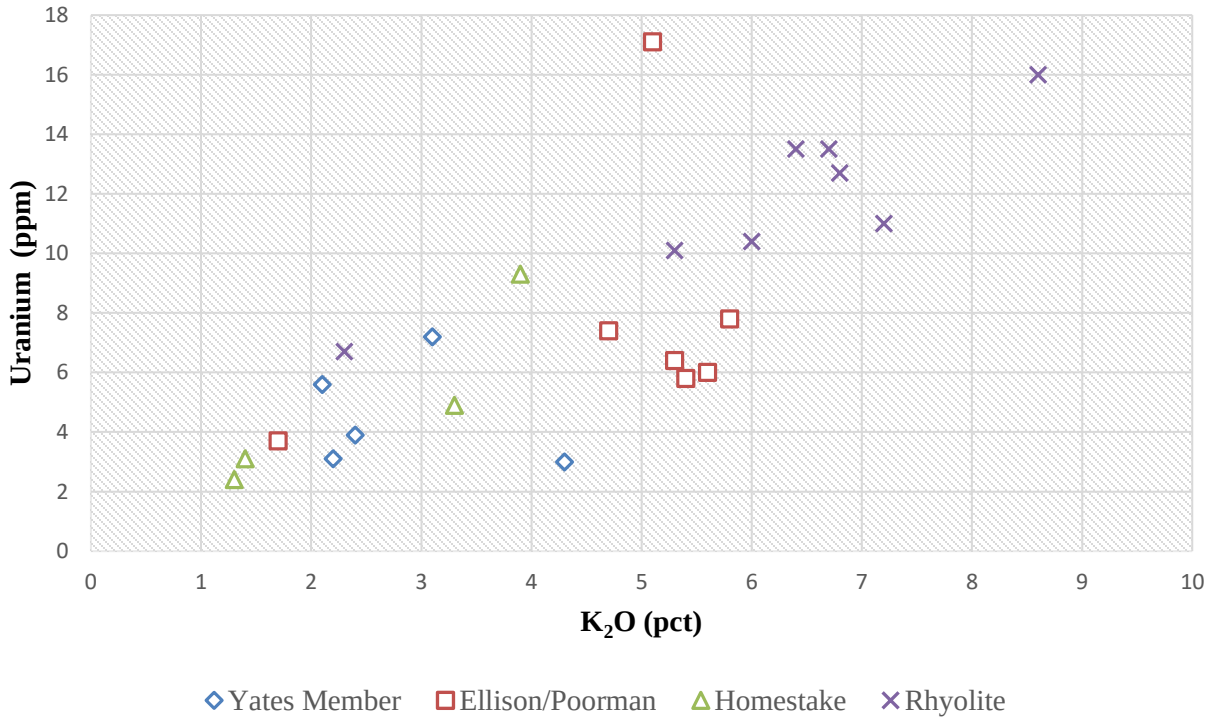

Figure 56C: Homestake Survey 4850 Level Th Vs. K_2O

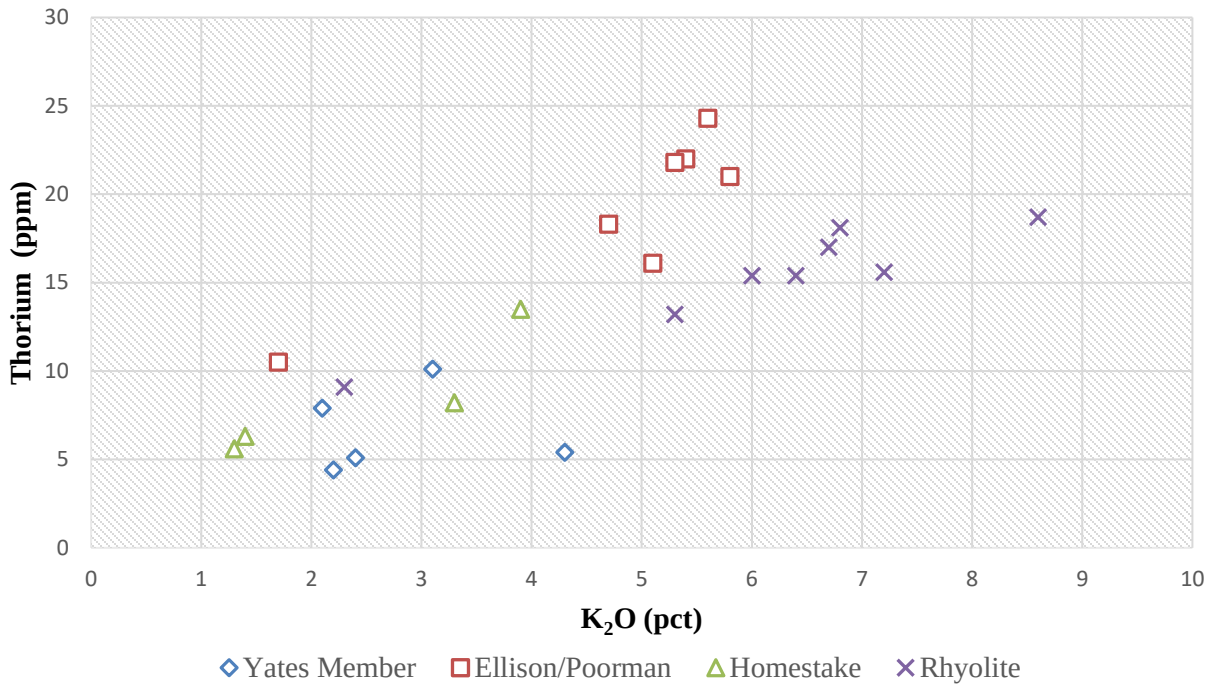

Figure 57A: Homestake Survey Surface Outcrops Th Vs. U

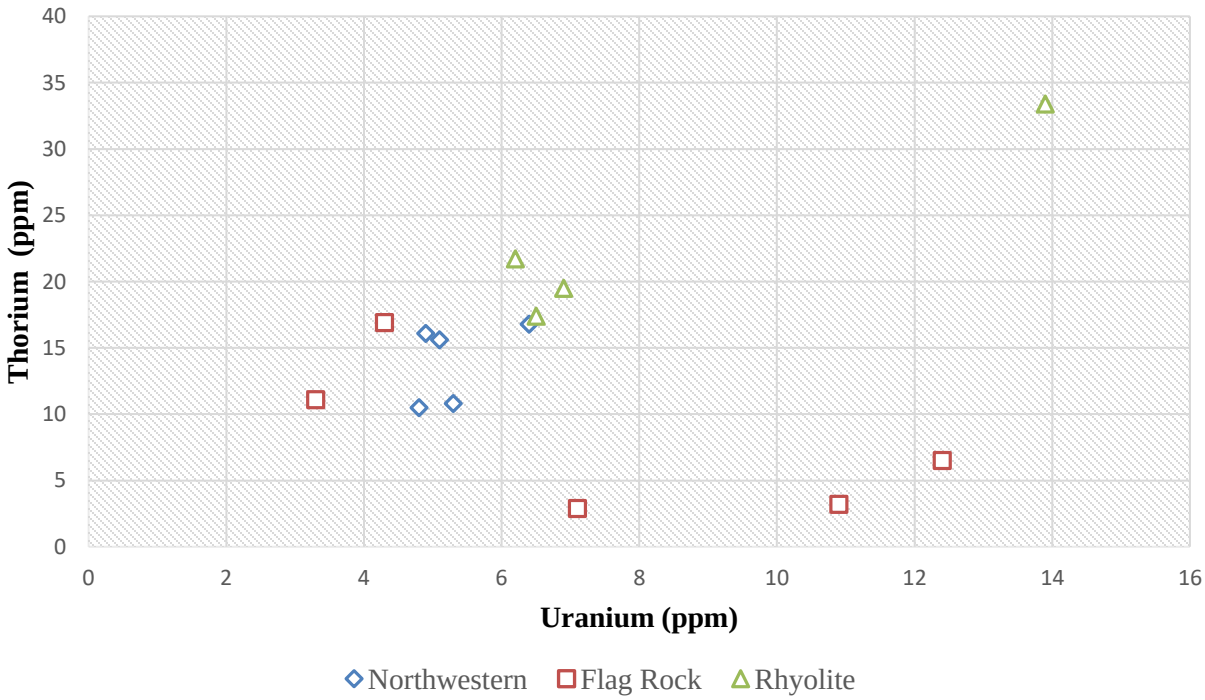

Figure 57B: Homestake Survey Surface Outcrops U Vs. K_2O

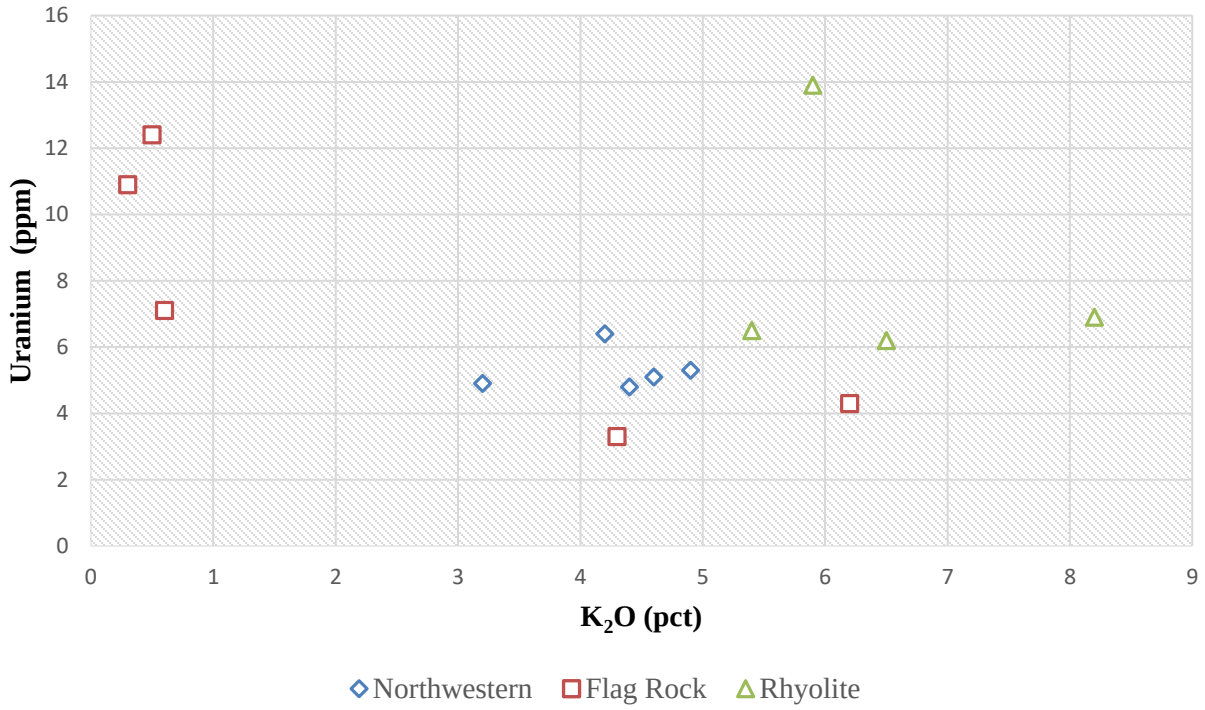

Figure 57C: Homestake Survey Surface Outcrops Th Vs. K_2O

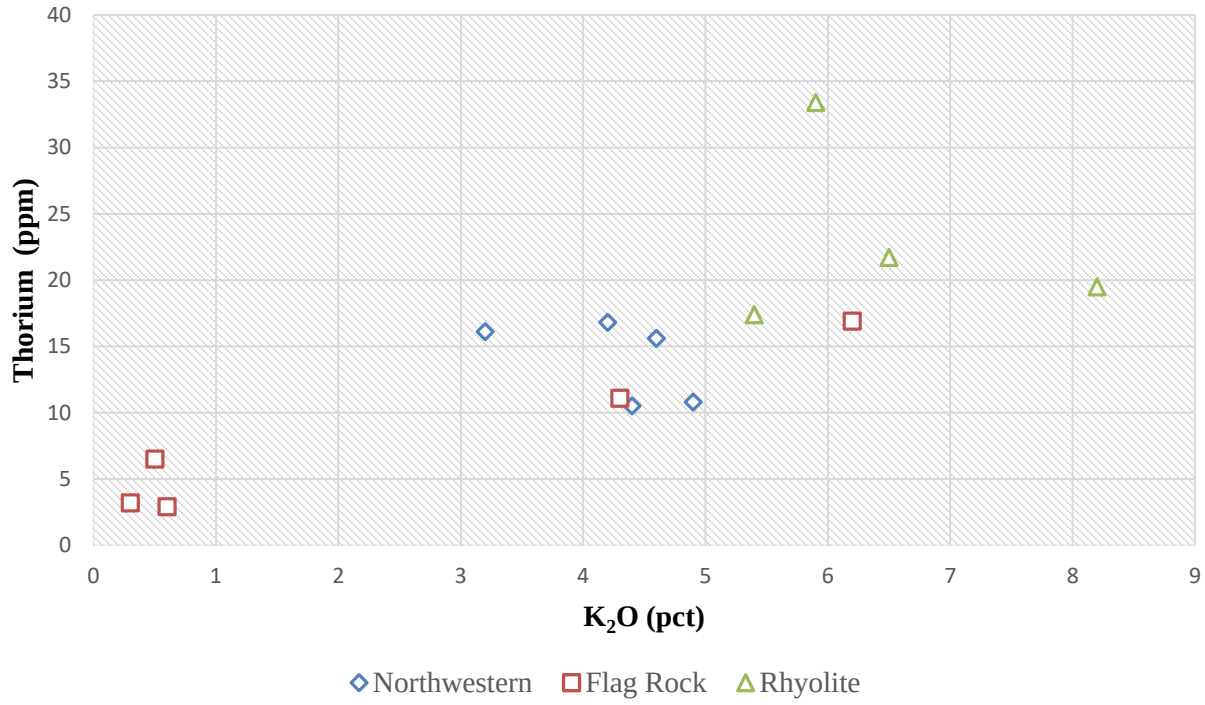

Appendix E

U, Th, and K ratios of rhyolite present on SURF Property and inside the Homestake Gold Mine

Figure 58A: HGM Survey Rhyolite U Vs. Th

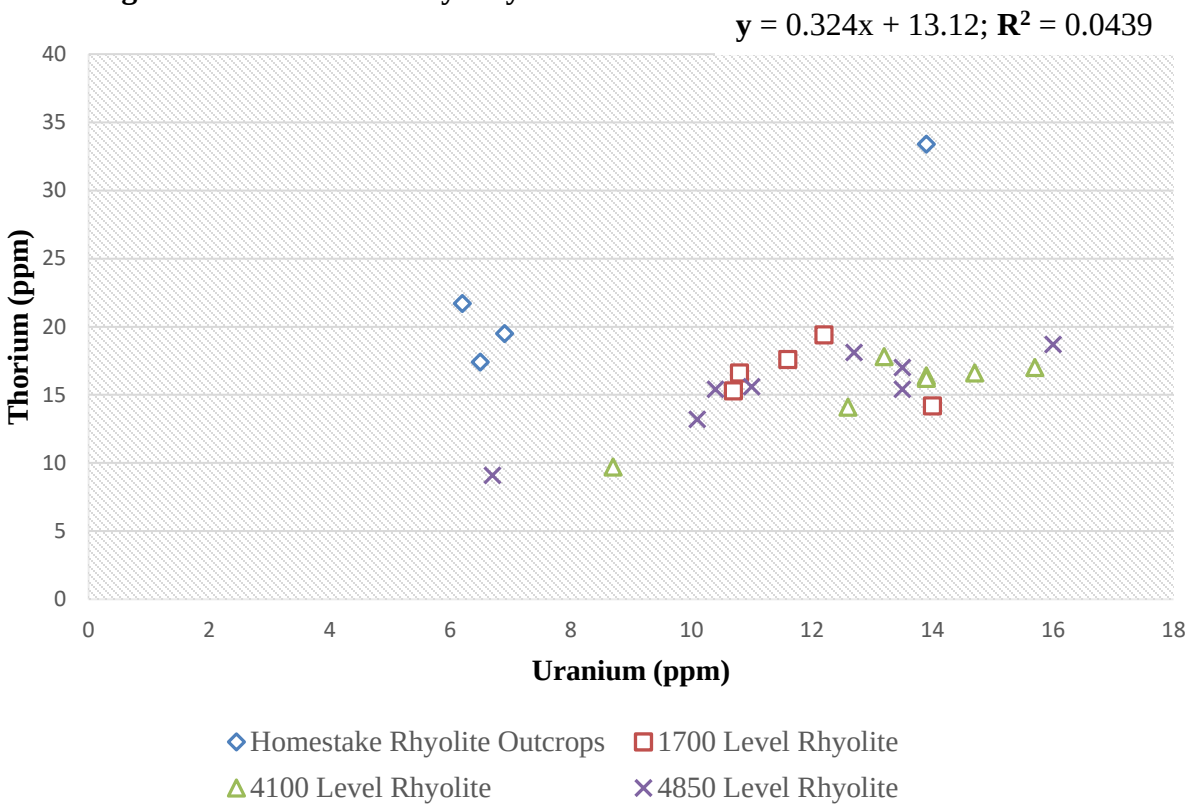

Figure 58B: HGM Survey Rhyolite U Vs. Th

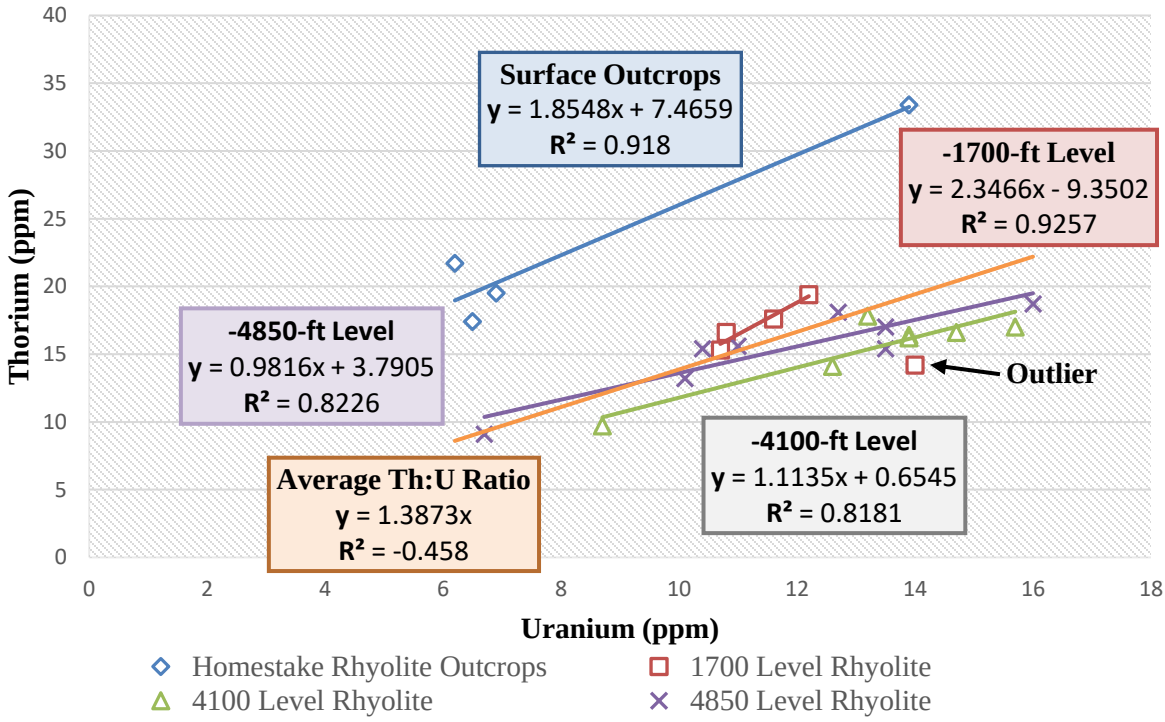

Figure 58C: Homestake Gold Mine Survey Rhyolite

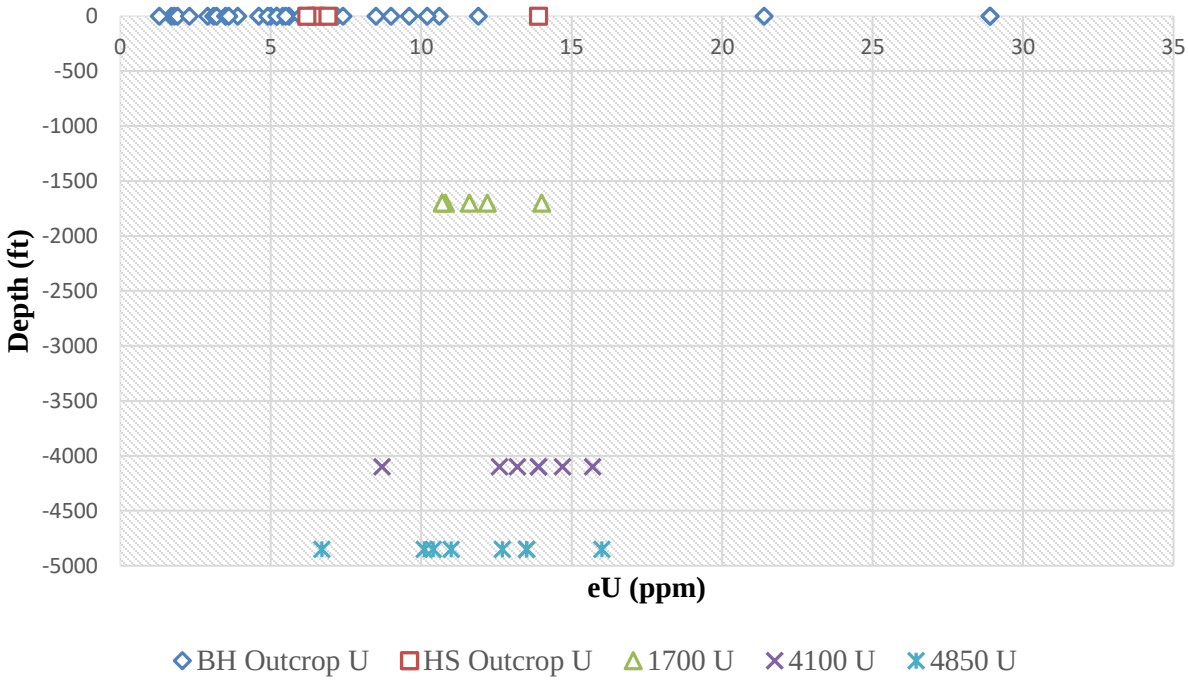

Figure 58D: Homestake Gold Mine Survey Rhyolite

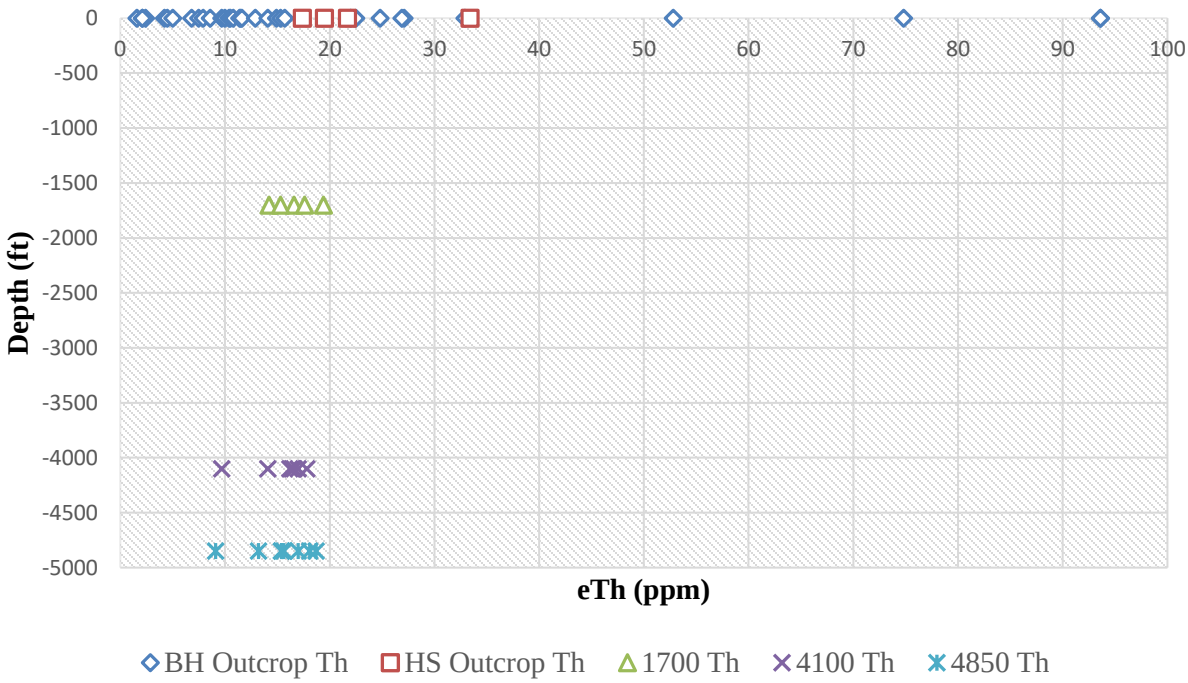

Figure 58E: Homestake Gold Mine Survey: Rhyolite Average eU Per Depth

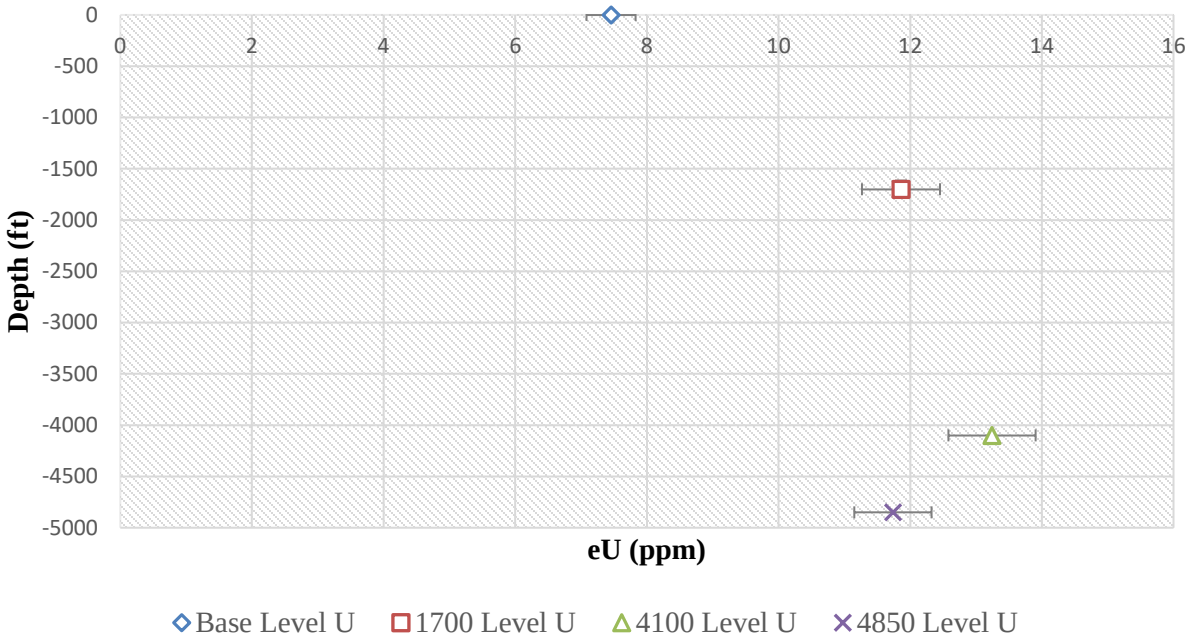

Figure 58F: Homestake Gold Mine Survey: Rhyolite Average eTh Per Depth

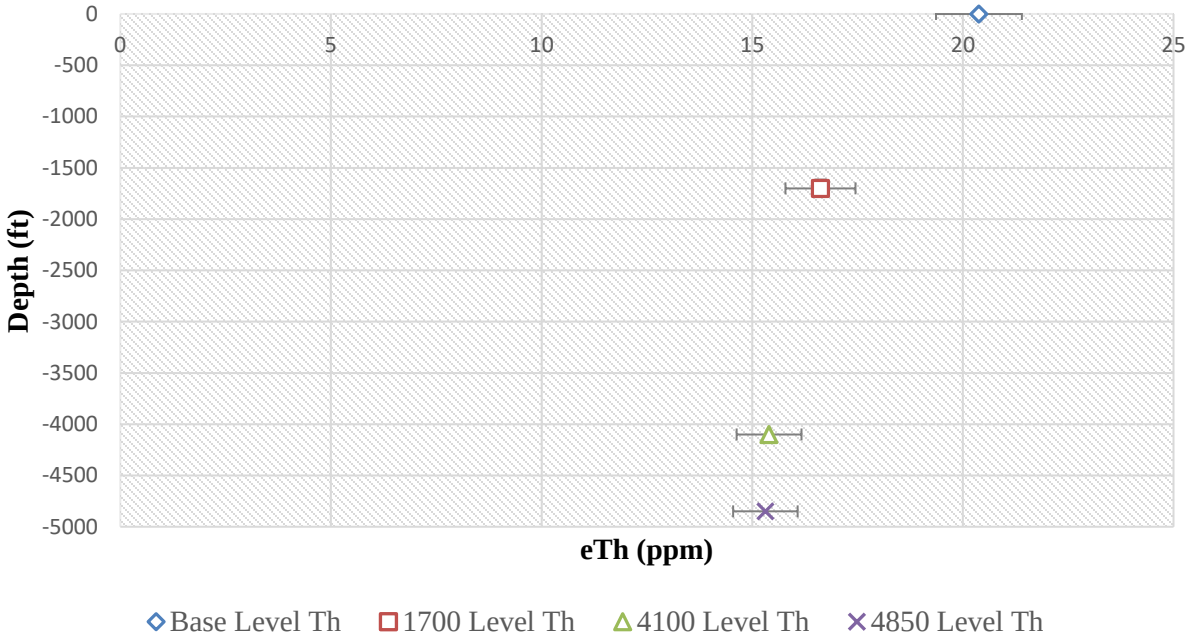

Figure 58G: Homestake Gold Mine Survey: Rhyolite Average eU Per Depth without BH Samples

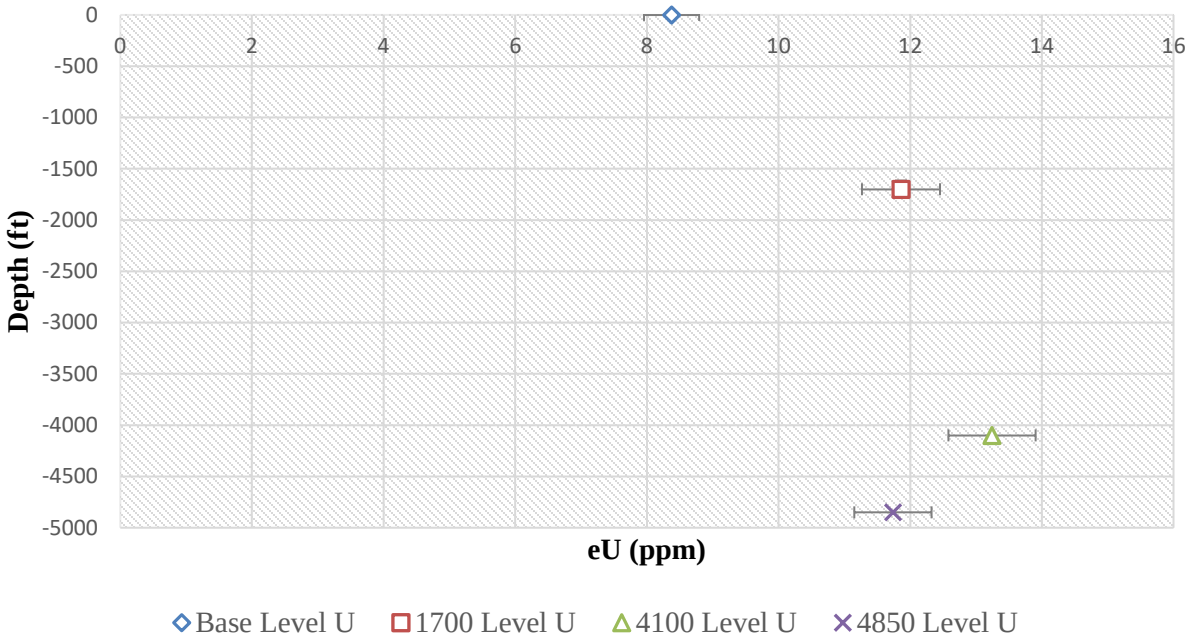

Figure 58H: Homestake Gold Mine Survey: Rhyolite Average eTh Per Depth without BH Samples

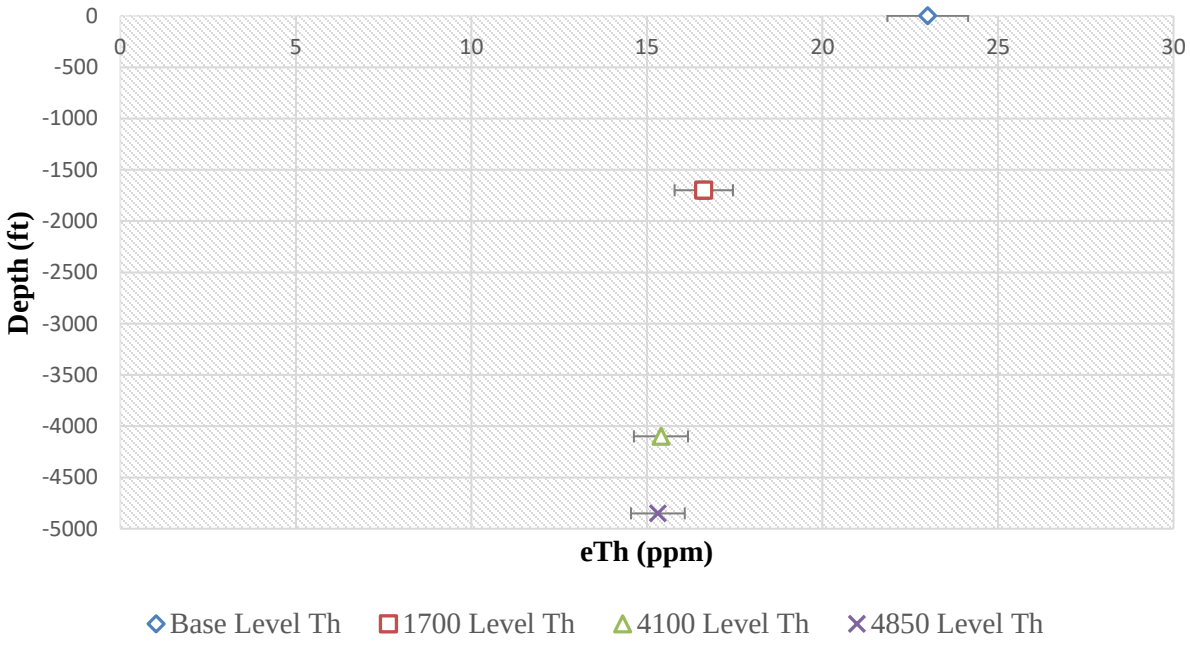

Appendix F

Statistical Analysis of

the Northern Black Hills Samples

Table 39

Black Hills Igneous Rocks Statistics

	U (ppm)	Th (ppm)	K2O (pct)	μWm^{-3}
Minimum	0.00	0.00	0.00	0.00
Maximum	42.80	130.70	13.80	23.92
Average	6.61	19.74	3.13	4.03
Median	4.65	13.76	2.90	3.03
Standard Deviation	6.59	20.92	2.26	3.80
Variance	43.48	437.68	5.09	14.45
Count	215	216	216	216
2 Std Dev Above Avg	19.80	61.58	7.64	11.63

Average Th/U Ratio

2.98

Rhyolite

	U	Th	K	μWm^{-3}
Average	5.33	14.90	3.16	3.23
SD	5.81	19.68	2.50	3.57

*Does Not Include Homestake Samples

Phonolite

	U	Th	K	μWm^{-3}
Average	8.90	29.95	3.60	5.63
SD	5.12	16.93	1.33	2.95

*Does Not Include Homestake Samples

Trachyte

	U	Th	K	μWm^{-3}
Average	5.31	17.92	3.60	3.53
SD	3.89	14.65	3.13	2.46

Latite

	U	Th	K	μWm^{-3}
Average	5.44	12.78	3.46	3.12
SD	5.47	4.70	1.98	2.04

Latitic Andesite

	U	Th	K	μWm^{-3}
Average	4.23	15.77	2.77	2.92
SD	3.49	12.22	1.27	2.19

Table 39: Cont.

Granodiorite

	U	Th	K	μWm^{-3}
Average	11.02	31.78	3.42	6.41
SD	5.25	15.01	1.57	3.00

Volcanic

	U	Th	K	μWm^{-3}
Average	15.39	46.36	3.49	8.97
SD	12.65	42.45	2.28	7.59

Basalt

	U	Th	K	μWm^{-3}
Average	16.14	13.55	0.70	6.14
SD	4.15	8.23	0.76	2.00

Table 40

Black Hills Metamorphic Rocks Statistics

	U (ppm)	Th (ppm)	K2O (pct)	μWm^{-3}
Minimum	0.00	0.00	0.00	0.00
Maximum	65.90	52.20	6.40	21.30
Average	3.87	9.99	2.31	2.28
Median	3.07	8.50	2.24	1.96
Standard Deviation	5.90	8.16	1.62	2.24
Variance	34.80	66.64	2.63	5.01
Count	143	143	143	143
2 Std Dev Above Avg	15.67	26.32	5.55	6.76

Average Th/U Ratio

2.58

Schist

	U	Th	K	μWm^{-3}
Average	4.07	11.30	2.56	2.48
SD	3.11	8.04	1.70	1.67

Phyllite

	U	Th	K	μWm^{-3}
Average	3.77	9.94	2.43	2.26
SD	2.61	6.36	1.70	1.23

Metagreywacke

	U	Th	K	μWm^{-3}
Average	5.07	14.56	2.99	3.10
SD	2.74	3.97	0.37	1.15

Metabasalt

	U	Th	K	μWm^{-3}
Average	14.01	14.43	2.25	5.74
SD	25.74	19.02	1.38	8.14

Quartzite

	U	Th	K	μWm^{-3}
Average	2.82	4.85	1.52	1.44
SD	2.35	4.87	1.44	1.17

Table 40: Cont.

Slate

	U	Th	K	μWm^{-3}
Average	2.80	10.63	2.61	2.04
SD	2.22	6.43	1.53	1.31

Metagabbro-Greenstone

	U	Th	K	μWm^{-3}
Average	0.88	1.63	0.68	0.48
SD	0.91	1.70	0.79	0.49

Table 41

Black Hills Sedimentary Rocks Statistics

	U (ppm)	Th (ppm)	K2O (pct)	μWm^{-3}
Minimum	0.00	0.00	0.00	0.00
Maximum	52.81	51.10	6.90	16.18
Average	2.20	2.60	0.64	0.96
Median	1.50	1.30	0.20	0.67
Standard Deviation	4.17	4.61	1.10	1.45
Variance	17.37	21.22	1.20	2.11
Count	235	235	235	236
2 Std Dev Above Avg	10.54	11.82	2.83	3.86

Average Th/U Ratio

1.18

Sandstone

	U	Th	K	μWm^{-3}
Average	2.27	2.49	0.74	0.99
SD	3.35	3.25	1.07	1.16

Limestone

	U	Th	K	μWm^{-3}
Average	2.07	2.08	0.51	0.87
SD	4.72	2.76	0.97	1.51

Gypsum

	U	Th	K	μWm^{-3}
Average	1.21	1.40	0.25	0.51
SD	1.38	1.69	0.33	0.59

Shale

	U	Th	K	μWm^{-3}
Average	1.52	0.50	0.05	0.51
SD	1.39	0.71	0.07	0.49

Greywacke

	U	Th	K	μWm^{-3}
Average	4.06	17.22	4.99	3.24
SD	0.51	11.48	2.70	0.81

References

Adams, J.A.S., Osmond, K., Rogers, J.J.W. "The Geochemistry of Thorium and Uranium." *Physics and Chemistry of the Earth* 3 (1959): 298-348. Print.

Anderson, D. L., ed. *New Theory of the Earth*. 2nd ed. Cambridge, UK: Cambridge University Press, 2007. Print.

Aswathanarayana, U. *Principles of Nuclear Geology*. New Delhi, India: Oxonian Press Private Limited, 1985. Print.

Arya, A. P. *Fundamentals if Nuclear Physics*. Boston, MA: Allyn & Bacon, 1971, 166. Print.

Atekwana, E. A. "Precambrian Basement Beneath the Central Midcontinent United States as Interpreted from Potential Field Imagery." *Basement and Basins of Eastern North America.* Ed. van der Pluijm, B.A., Catacosinos, P.A. Boulder, Colorado, 1996. 33-44. Print. Geological Society of America Special Paper 308.

Beardsmore, G. R., and J. P. Cull. *Crustal Heat Flow: A Guide to Measure and Modeling*. 1st ed. Cambridge, United Kingdom: Cambridge University Press, 2001. Print.

Bickford, M. E., W. R. Can Schmus, and I. and Zietz. "Proterozoic History of the Mid-Continent Region of North America." *Geology* 14 (1986): 492-6. Print.

Bodorkos, S., et al. "A High-Resolution, Calibrated Airborne Radiometric Dataset Applied to the Estimation of Crustal Heat Production in the Archaean Northern Pilbara Craton, Western Australia." *Precambrian Research*.128 (2004): 57-82. Print.

Boyle, R. W. *Geochemical Prospecting for Thorium and Uranium Deposits*. The Netherlands: Elsevier Scientific Publishing Company, 1982. Print.

Brenner, R. L., 1981, Cretaceous Stratigraphy and Sedimentation in Northwestern Iowa, Northeastern Nebraska, & Southeast South Dakota: Iowa Geological Survey Guidebook Series No. 4.

Burchett, R. R., 1986, Geologic Bedrock Map of Nebraska: Nebraska Geological Survey. Scale 1:1 Million.

Caddey, S. W., et al. "The Homestake Gold Mine, an Early Proterozoic Iron-Formation-Hosted Gold Deposit, Lawrence County, South Dakota." *U.S. Geological Survey Bulletin.* Eds. Daniel J. Shawe, Rodger P. Ashley, and L. M. H. Carter. 1857th Chapter J. Washington, D.C.: United States Government Printing Office, 1991. Print. Geology and Resources of Gold in the United States.

Clayton, Lee, 1980, Geologic Map of North Dakota: U. S. Geological Survey, Scale 1:500K.

Coltori, M., et al. "U and Th Content in the Central Apennine Continental Crust: A Contribution to the to the Determination of the Geo-Neutrinos Flux at LNGS." Geochimica et Cosmochimica Acta 75 (2011): 2271-94. Print.

Connolly, J. P. "Geology and Mineralogy of the Keystone District [Pennington County, S.D.]." *Black Hills Engineer* 13.1 (1925). Print.

---. "The Tertiary Mineralization of the Northern Black Hills." *South Dakota School of Mines Bulletin*.15 (1927). Print.

CRC Handbook of Chemistry and Physics. Ed. William M. Haynes. 97th ed. Boca Raton, FL: CRC Press, Taylor & Francis Group, 2016. Print. CRC Handbook of Chemistry and Physics.

Davies, J. H., and D. R. Davies. "Earth's Surface Heat Flux." *Solid Earth* 1 (2010): 5-24. Print.

Dewitt, E., et al. *Mineral Resources Potential and Geology of the Black Hills National Forest, South Dakota and Wyoming*. 1580th ed. Washington, D.C.: United States Government Printing Office, 1986. Print. U.S. Geological Survey Bulletin.

Dewitt, E., et al. "Mineral Resource Potential and Geology of the Black Hills National Forest, South Dakota and Wyoming." *U.S. Geological Survey Bulletin 1580.* Washington, D.C.: U.S. Geological Survey, 1986. 1-135. Print.

Diffendal, R. F. Jr, 1991, Geologic Map Showing Configuration of Bedrock Surface, North Platte 1x2 Quad. Nebraska: USGS Map I-2277. Scale 1:250K.

Dye, S. T., and E. H. Guillian. *National Academy of Science of the United States* 105.1 (2008): 44-7. Print.

Ehlers, E., and H. Blatt. *Petrology: Igneous, Sedimentary, and Metamorphic*. San Francisco, CA: W. H. Freeman and Company, 1982. Print.

Faul, H. *Nuclear Geology*. New York, N.Y.: John Wiley & Sons, Inc., 1954. Print.

Faure, G., and T. M. Mensing. *Isotopes: Principles and Applications*. 3rd ed. Hoboken, N.J.: Wiley, 2004. Print.

Faure, G. *Principles of Isotope Geology*. 1st ed. New York: John Wiley & Sons, Inc., 1977. Print.

Fermi, E. "Versuch Einer Theorie Der B-Strahlen." *Z. Physik* 88 (1934): 161-77. Print.

Fiorentini, G., M. Lissia, and F. Mantovani. "Geo-Neutrinos and Earth's Interior." Physics Reports 453 (2007): 117-82. Print.

Gosnold, W. D., Jr. "A Model for Uranium and Thorium Assimilation by Intrusive Magmas and Crystallizing Plutons through Interaction with Crustal Fluids." Ph.D. Southern Methodist University, 1976. United States -- Texas: *ProQuest Dissertations & Theses A&I.* Web.

Gosnold, W. D., Jr. "Basin-Scale Groundwater Flow and Advective Heat Flow: An Example from the Northern Great Planes." *Geothermics in Basin Analysis.* Ed. Forster, Andrea, Merriam, Daniel F. New York, N.Y.: Kluwer Academic / Plenum Publishers, 1999. 99-116. Print.

Gosnold, W. D., Jr. "Heat Flow and Ground Water Flow in the Central Great Plains of the United States." *Journal of Geodynamics* 5.1-4 (1985): 247-67. Print.

---. "Heat Flow in the Great Plains of the United States." *Journal of Geophysical Research* B95.1 (1990): 353-74. Print.

---. "Stratabound Geothermal Resources in North Dakota and South Dakota." *Natural Resources Research* 8.3 (1999): 177-92. Print.

Gries, J. P. "Mineral Resources of the Black Hills Area, South Dakota and Wyoming." Preliminary Report 194 ed. United States Department of the Interior, Bureau of Mines, 1974. 60. Print.

Hasterok, D., and D. S. Chapman. "Heat Production and Geotherms for the Continental Lithosphere." *Earth and Planetary Science Letters* 307.1 (2011): 59-70. Print.

Hazen, R. M., R. C. Ewing, and D. A. Sverjensky. "Evolution of Uranium and Thorium." *American Mineralogist* 94 (2009): 1293-311. Print.

Hershey H. G. 1969, Geologic Map of Iowa: Iowa Geological Survey, scale 1:500,000.

Jaupart, C., and J. Mareschal. *Heat Generation and Transport in the Earth*. New York, United States of America: Cambridge University Press, 2011. Print.

Karner, F. R., et al. "Field Trip of the Tertiary Intrusive Province of the Northern Black Hills." *A Field Guide to the Geology of the Black Hills Region, South Dakota.* Ed. F. J. Rich. Logs 2 and 3 Vol. American Geological Institute, 1981. Print.

Karner, F. R. "Geological Framework of the Black Hills-Bear Lodge Mountains Region." *Devils Tower--Black Hills Alkalic Igneous Rocks and General Geology.* Ed. F. R. Karner. 28th International Geological Congress Field Trip Guidebook T131 ed.3-6. Print.

Klasner, J.S., and King, E.R. "Precambrian Basement Geology of North and South Dakota." *Canadian Journal of Earth Science* 23 (1986): 1083-102. Print.

Klasner, J.S., King, E.R., and Van Schmus, W.R. "The pre-Keweenawan History of the Southern Canadian Shield and it Influence on Formation of the Midcontinent Rift." *Geology and Tectonics of the Lake Superior Basin.* Eds. R. J. Wold and W. J. and Hinze. 156th ed. Geological Society of America Memoir, 1982. 27-46. Print.

Lachenbruch, A. H. "Crustal Temperature and Heat Production: Implications of the Linear Heat-Flow Relation." *Journal of Geophysical Research* 75.17 (1970): 3291-300. Print.

Larsen, E.S., Phair, P., Gottfried, D., Smith, W.L. "Uranium in Magmatic Differentiation." *Contributions to the Geology of Uranium and Thorium by the United States Geological Survey and Atomic Energy Commission for the United Nations International Conference on Peaceful used of Atomic Energy, Geneva, Switzerland, 1955.* Washington: Paige, L.R., Stocking, H.E., Smith, H.S., 1956. 65-74. Print. Geological Survey Professional Paper 300.

Lauf, R. J. *Mineralogy of Uranium and Thorium.* Atglen, PA: Schiffer Publishing, Ltd., 2016. Print.

Lesko, K. T. "The Deep Underground Science and Engineering Laboratory at Homestake." *Journal of Physics* Conference Series 136 (2008). Print.

Lilley, J. *Nuclear Physics*. Baffins Lane, Chichester, West Sussex, England: John Wiley & Sons, Ltd, 2001. Print.

Lisenbee, A. "Laramide Structure of the Black Hills Uplift, South Dakota-Wyoming-Montana." *Laramide Faulting in the Western United States.* Ed. V. Matthews. 3rd ed., 1978. 165-196. Print. Geological Society of America Memoir 151.

---. "Studies of the Tertiary Intrusions of the Northern Black Hills Uplift, South Dakota and Wyoming: A Historical Review." *Geology of the Black Hills, South Dakota and Wyoming.* Ed. Fredrick J. Rich. 2nd ed. Alexandria, Virginia: American Geological Institute, 1986. 106-125. Print.

Ludhova, L. "Geoneutrinos: Theory and Phenomenology." *AIP Conference Proceedings* 1560.1 (2013): 171-5. Web.

Martin, J. E., Sawyer, J. F., Fahrenbach, M. D., Tomhave, D. W., and Schulz, L. D., 2004, Geologic Map of South Dakota: South Dakota Geological Survey.

McDonough, W. F., J. G. Learned, and S. T. Dye. "The Many Uses of Electron Antineutrinos." *Physics Today*. March 2012 (2012): 48-51. Print.

McDonough, W. F., and S. S. Sun. *Chemical Geology* Chemical Geology.3-4 (1995): 223-53. Print.

McDonough, W. F. "Ghosts from within." *Nature* 436 (2005). Print.

McLennan, S.M., Taylor, S.R. "Heat Flow and the Chemical Composition of Continental Crust." *The Journal of Geology* 104.4 (1996): 369-77. Print.

Morey, G.B., and Meints, Joyce, 2000, Geologic map of Minnesota - Bedrock Geology: Minnesota Geological Survey, State Map Series, S-20, 3rd edition, scale 1:1,000,000. available online at: http://www.geo.umn.edu/mgs/currentpubs.htm.

Mudrey, M.G., Jr., Brown, B.A., & Greenberg, J.K., 1982, Bedrock Geologic Map of Wisconsin: University of Wisconsin-Extension, Geological and Natural History Survey, scale= 1: 1,000,000.

Norton, J. J. "Gold in the Black Hills, South Dakota and how New Deposits might be found." *U.S. Geological Survey Circular* 699 (1974): 1-26. Print.

Paige, W. M. "Geology of the Region Around Lead, South Dakota, and its Bearing on the Homestake Ore Body." *U.S. Geological Survey Bulletin*.765 (1924). Print.

Pinti, D. "Bulk Silicate Earth." *Encyclopedia of Astrobiology*. Eds. R. Amils, et al.Springer Berlin Heidelberg, 2014. 1. Print. Springer eBook.

Roy, R., Decker, E., Blackwell, D., & Birch, F. "Heat Flow in the United States." *Journal of Geophysical Research* 73.16 (1968): 5207-21. Print.

Roy, R., and D. Blackwell. "Heat Generation of Plutonic Rocks and Continental Heat Flow Provinces." *Earth and Planetary Science Letters* 5.No. 1 (1968): 1-16. Print.

Rudnick, R.L, Gao, S. "Composition on Continental Crust." *Treatise on Geochemistry*. Ed. H. D. H. Turekian. 2nd ed. 3 Vol. Elsevier Science Limited, 2014. Print.

Rudnick, R.L., Fountain, D.M. "Nature and Composition of Continental Crust: A Lower Crustal Perspective." *Reviews of Geophysics* 33.3 (1995): 267-309. Print.

Sanford Underground Research Facility. "Deep science at the frontier of physics." *http://www.sanfordlab.org*. Web. <http://www.sanfordlab.org/about/deep-science-frontier-physics>.

Sims, P. K., and Kisvarsanti, E.B., Morey, G.B. "Geology and Metallogeny of Archean and Proterozoic Basement Terranes in the Northern Midcontinent, U.S.A. - an Overview." *U.S. Geological Survey Bulletin* 1815 (1987): 1-51. Print.

Sramek, A., W. F. McDonough, and J. G. Learnerd. "Geoneutrinos." *Advances in High Energy Physics* (2012): 34. Print.

Stillwell, L. W., "Communication to the Editors Telling of the Finding of Pitchblende and Uranium Mica on Bald Mountain, South Dakota." *American Journal of Science* 30.175 (1885): 82. Print.

Stober, I., and K. Bucher. *Geothermal Energy: From Theoretical Models to Exploration and Development*. Verlag Berlin Heidelberg: Springer Publishing, 2013. Print.

Swinehart, J. B., Souders, V. J., DeGraw, H. M., and Diffendal, R. F., 1985, Cenozoic paleography of the west-central United States, Society of Economic Paleontologist and Mineralogist, RMS, Rocky Mtn. Paleogeography Syp.3, p 209-229.

Tilling, R. I., and D. Gottfried. *Distribution of Thorium, Uranium, and Potassium in Igneous Rocks of the Boulder Batholith Region, Montana, and its Bearing on Radiogenic Heat Production and Heat Flow*. Professional Paper ed. 614 E Vol. United States Geological Survey, 1969. Print.

Usman, S. M., et al. "AGM2015: Antineutrino Global Map 2015." 2015. Web.

Van Schmus, W. R. "Tectonic Setting of the Midcontinent Rift System: " *Tectonophysics* 213 (1992): 1-15. Print.

Vickers, R. C. "Occurrences of Radioactive Minerals in the Bald Mountain Gold-Mining Area, Northern Black Hills, South Dakota." *Geological Survey Circular.* 351st ed. Washington, D.C>: United States Department of Interior Geological Survey, 1954. 1-8. Print.

Waples, D. W. "A New Model for Heat Flow in Extensional Basins: Estimating Radiogenic Heat Production." *Natural Resources Research,* 11.2 (2002): 125-33. Print.

---. "A New Model for Heat Flow in Extensional Basins:
Radiogenic Heat, Asthenospheric Heat,
and the McKenzie Model." *Natural Resources Research* 10.3 (2001): 227-38. Print.

Willman, H.B., and others, (compilers), 1967, Geologic Map of Illinois: Illinois State Geological Survey, scale = 1: 500,000, paper.

Whitefield, J.M., Rogers, J.J.W., Adams, J.A.S. "The Relationship between the Petrology and the Thorium and Uranium Contents of some Granitic Rocks." *Geochimica et Cosmochimica Acta* 17 (1959): 248-71. Print.

Wollenberg, H. A., and A. R. Smith. "Radiogenic Heat Production of Crustal Rocks: An Assessment Based on Geochemical Data." *Geophysical Research Letters* 14.3 (1987): 295-8. Print.

Wollenberg, H. A., and A. R. Smith. "Radiogeologic Studies in the Central Part of the Sierra Nevada Batholith, California." *Journal of Geophysical Research* 73.4 (1968): 1481-95. Print.

Yermolayev, N. P. "Uranium and Thorium in Regional and Contact Metamorphism." *Geochem International* 8 (1973): 599-609. Print.

Zimny, E. G. "Geoneutrino Production of the Northern Black Hills, South Dakota, United States of America." M.S. The University of North Dakota, 2014. United States -- North Dakota: *Dissertations & Theses @ University of North Dakota.* Web.